Synthesis and Characterization of a Lignin Based Thermoplastic

A Thesis
Presented in Partial Fulfillment of the Requirements for the
Degree of Master of Science
with a
Major in Environmental Science
in the
College of Natural Resources
University of Idaho
By

Eric L. Young

Major Professor: Armando McDonald, Ph.D.
Committee Members: Tom Gorman, Ph.D.; Kristopher Waynant, Ph.D.
Department Administrator: J.D. Wulfhorst, Ph.D.

August 2017

Authorization to Submit Thesis

This thesis of Eric L. Young, submitted for the degree of Master of Science with a Major in Environmental Science and titled "**Synthesis and Characterization of a Lignin Based Thermoplastic**," has been reviewed in final form. Permission, as indicated by the signatures and dates below, is now granted to submit final copies to the College of Graduate Studies for approval.

Major Professor: _____ Date: _____
Armando McDonald, Ph.D.

Committee Members: _____ Date: _____
Tom Gorman, Ph.D.

_____ Date: _____
Kristopher Waynant, Ph.D.

Department
Administrator: _____ Date: _____
J.D. Wulfhorst, Ph.D.

Abstract

Lignin based copolymers were synthesized using a single pot, solvent free, melt condensation reaction. The synthesis occurred in two stages. In the first stage a prepolymer consisting of a diol and diacid with varying amounts diamine was heated under vacuum. In the second stage, prepolymer was mixed with kraft lignin and further reacted under vacuum at elevated temperature. Progression of polymerization was monitored using FT-IR and ESI-MS. Polymer properties were characterized using DMA, DSC and TGA techniques. The morphology was analyzed using polarized optical microscopy. Polymer mechanical properties were found to be influenced by the type of diacid, lignin and diamine content, ball milling of lignin and presence of an acid catalyst. The lignin-copolymers were shown to have thermoplastic behavior. Additionally, above 30 wt% lignin the lignin-copolymers did not exhibit melt behavior.

Acknowledgements

I’d like to thank Armando McDonald for all of the guidance and insight he has offered along the way. The Environmental Science Program provided the majority of the funding for my project, for which I am extremely grateful. Also Justin Knox in the Statistics Consulting Center has offered invaluable assistance on statistical analysis and modeling of data.

Dedication

Many thanks to Jeff, my roommate, for his indispensable moral support along the way. Also my parents, Ken and Beckie Young, who have joined me in celebrating the ups and encouraged me through the downs. Also I would like to offer my most sincere thanks to MAMBA and the volunteers who support their work in building and maintaining high quality trails on Moscow Mountain. Without the support of these people and many others this process would have been made considerably more difficult and less enjoyable.

Table of Contents

Table of Figures

List of Tables

1 Introduction

1.1 Thermoplastics

Historically petroleum based polymers have overwhelmingly dominated the commodity polymer market. In recent years, however, it has become increasingly evident that there is a great need for renewably sourced polymers. This is substantiated by two major observations. First, petroleum acquisition and utilization has become associated with environmental degradation and second, petroleum resources are finite (Wool, 2005). In order for polymer materials to continue being used as extensively as they are now there must exist sustainable counterparts either matching or exceeding the structural properties of currently available polymeric materials.

One class of commodity polymers of particular importance are thermoplastics such as polyethylene (PE), poly(vinyl chloride) (PVC) and polystyrene (PS) (Cowie, 2008). These materials have the property of becoming moldable above a certain temperature known as the melt temperature. As the polymer cools below this temperature the material stiffens and maintains the shape in which it was molded in the melt. A defining feature of a thermoplastic is that this melt molding process is repeatable many times with minimal loss of structural properties through processing. The ability to melt process enables thermoplastic materials to be injection molded and extruded into a seemingly infinite variety of shapes and forms which leads to their ubiquitous use in modern infrastructure (Cowie, 2008). It is due to this ubiquity that the urgent need for renewably sourced alternatives to traditional petroleum derived thermoplastics arises.

1.2 Lignin

1.2.1 Lignin in Industry

Lignin has emerged as one of the most promising renewable feed-stocks to this end. Lignin exists naturally as an aromatic hetero-polymer present in all plant tissue where it serves several critical functions such as facilitation of water and nutrient transport, structural support as well as providing resistance to bacterial and environmental deterioration (Sperry, 2002) (Vance, 1980). It is the most abundant naturally occurring aromatic polymer (Lora,

2002). Industrially it is significant in the paper pulping process which largely focuses on the removal of lignin from the cellulose fibers. Consequently, lignin constitutes a major byproduct of the paper pulping industry. For instance, the pulp and paper industry alone produced 50 million tons of extracted lignin in 2004 (Zakzeski, 2010). Additionally, lignin is produced also as a waste product from the cellulosic ethanol production process. Lignin resulting from cellulosic ethanol production is expected to increase as governments adopt legislation mandating the use of renewable, biologically sourced fuel. An example of such legislation in the United States is the Renewable Fuel Standard (RFS) which mandates fuel producers to blend a certain amount of renewable fuels in with transportation fuels. The RFS stipulates 36 billion gallons of renewable fuel will be added in the year 2022 while only 15 billion gallons can be produced from starch based ethanol. This leaves a deficit of 21 billion gallons to be made up elsewhere, likely cellulosic ethanol (Renewable Fuel Standard, 2017). Due to the abundance, availability and low cost lignin stands poised as one of the most viable renewable feed-stocks for thermoplastic production.

1.2.2 Lignin Composition and Treatment

Utilization of lignin to this end does not come without complications. These are namely its relatively high glass transition temperature (T_g) as well as the onset of thermal degradation occurring at temperatures near or even below the T_g, which renders lignin unsuitable for use in conventional thermal processing techniques such as injection molding and extrusion. Additional complications stem from the fact that lignin is itself a heterogeneous polymer and the chemical composition varies dramatically across species. Even within the same individual specimen lignin composition can vary from one tissue sample to the next. For example, it is known that lignin in compression wood of gymnosperms will largely consist of guaiacyl (G) units. Similarly, wood samples taken from the top and bottom of a mature tree will contain different levels of lignin (campbell, 1996).

Another factor having influence on the chemical composition of lignin is the process by which it is extracted. There are many ways of removing lignin from plant tissue. One common method in use today is the kraft pulping process wherein wood chips are subjected to an aqueous cooking liquor containing sodium hydroxide and sodium sulfide at elevated

pressure. The sodium hydroxide cleaves linkages in lignin while the sodium sulfide further generates sodium hydroxide as well as sodium hydrosulfide which aids in solubilizing lignin in the liquor (Shmulsky, 2011). This highly caustic processing has dramatic implications for the chemical structure of the end lignin product, by cleaving ether linkages as well as forming condensed structures (Chakar, 2004). The same is true for any method utilized for removing lignin from biomass whether for pulp production or cellulosic ethanol production. As mentioned before the species that the lignin is derived from also contributes to wide variability in the chemical structure. Native lignin is generated through radical polymerization processes largely involving three distinct hydroxycinnamyl alcohol precursors. These are collectively referred to as monolignols. They are *p*-coumaryl alcohol, coniferyl alcohol and synapyl alcohol. Upon free radical initiated polymerization the structural units they form are known as *p*-hydroxyphenyl (H), guaiacyl (G) and syringyl (S), respectively. Softwood species typically contain lignin composed of more than 95% G units while hardwood species exhibit a mix of G and S units with a small amount of *p*-hydroxyphenyl units. In annual species such as grasses and cereal crops the presence of *p*-hydroxyphenyl units is more prevalent (Dence, 1992). All of this variability leads to significant obstacles for attempting to utilize lignin in the development of a commodity like thermoplastic. This necessitates characterization of the lignin feedstock being used.

1.2.3 Incorporation of Lignin in Polymeric Materials

As a raw material lignin has a relatively high T_g ranging from 90-180°C (Li H. , 2014). This results from extensive intermolecular and intramolecular hydrogen bonding interactions due to the abundance of aromatic and aliphatic hydroxyl groups present in the lignin molecule (Aracri, 2014). As a standalone polymer lignin itself is also a brittle material which tends to impart this undesirable quality as it is incorporated in polymer systems at increasing contents (Feldman, 2003).

1.2.4 Lignin Plasticization

There have been substantial efforts to investigate ways of chemically and physically modifying lignin to alter these undesirable properties. One of the simplest ways to improve thermal processability of lignin is to incorporate plasticizers (Bouajila, Dole, Joly, & Limare,

2006). Plasticizers have found use in many industrially produced thermoplastics such as PVC. As a virgin polymer PVC is a stiff, brittle material susceptible to cracking. The addition of phthalate esters as plasticizing agents endows PVC with flexibility, lower processing temperatures and dramatically improves performance characteristics (Graham, 1973). In a similar manner plasticization of lignin has been demonstrated as an effective technique for lowering the T_g and improving flexibility. One ubiquitous lignin plasticizer which occurs naturally is water. Water has been found to decrease the T_g of kraft lignin from 160 to 60°C as water content is changed from 0 to 30 wt% (Bouajila, 2006). In this article it is also revealed that the mechanisms for plasticizing lignin are highly dependent on the presence of water. Dry lignin tends to be better plasticized by molecules capable of participating in hydrogen bonding while lignin saturated with water is better plasticized by molecules resembling the lignin monomer structure.

1.2.5 Lignin Polymer Blends

Polymer blends are often utilized to generate a product containing the desirable properties of each constituent. Miscibility between the constituents is the major concern with regard to blends. If there is poor miscibility in the polymer blend system, then phase separation will occur. This behavior can be accurately predicted by determining the value of the solubility parameter for the individual constituents (David & Sincock, 1992). This value is an estimate of the attraction the molecules of a given substance have toward one another and in practice is measured through differential scanning calorimetry (DSC) experiments focusing on total heat of vaporization. For a homogenous system to result the value of the solubility parameter for each constituent must be within 1.5 (cal/cm^3) of each other (Banu, 2006). When this is not the case a heterogeneous system occurs. The result is often a product with poor mechanical properties as interfacial failure will usually occur at the boundaries between phases where there is poor mechanical adhesion. Phase separation can be detected through thermal analysis where it is witnessed as the occurrence of two T_g's corresponding to each of the constituents transitioning independently (Wang, 2016). It can also be observed using microscopy where phase separation appears as distinct domains.

Lignin is a difficult polymer to incorporate into blends because of its highly polar chemical structure. This characteristic is in stark contrast to the majority of commodity polymers which are relatively nonpolar (Dehne, 2017). Because of this miscible lignin polymer blends are relatively uncommon (Wang J, 1992). Nevertheless, lignin blends have been studied extensively. In one such study a lignin polylactic acid (PLA) blend was explored for the purpose of producing a filament for use in a 3D printer. The result was a product exhibiting all of the aforementioned negative qualities of lignin polymers blends. The system was observed to be heterogeneous using scanning electron microscopy. This contributed to ineffective stress transfer between the lignin aggregates and PLA matrix which increased PLA's brittleness. It was also observed that viscosity increased as lignin content was increased. Because of this lignin could only be incorporated at 5 wt% in order to produce a filament with appropriate flow characteristics for use in the 3D printer. This material was reported to exhibit an 18% and 6% reduction in the ultimate tensile strength and young's modulus, respectively (Gkartzou, 2016).

Poly-(ethylene oxide) (PEO) has been shown to exhibit miscibility with lignin at all blend ratios (Kelley, 1990). The miscibility of this system was attributed to hydrogen bonding interactions between the hydroxyls in lignin and the oxygen present in the ether linkages of PEO. This was validated through an analysis of the FT-IR spectra of both unaltered lignin blends and methylated lignin blends such that the effect of aliphatic and aromatic hydrogen bonding could be discerned. Poly-(ethylene terephthalate) (PET) has also been shown to be miscible with hardwood kraft lignin however it was reported that the same hydrogen bonding interactions were not observed in FT-IR spectra of the PET lignin system (Kadla, 2004). In the same study it was found that neither Poly-(vinyl acetate) (PVA) nor polypropylene (PP) formed a miscible mixture with the same lignin.

Blends of organosolv lignin with poly-(vinyl pyrrolidone) (PVP) have also shown miscibility as well as acetylated lignin derivatives with PVP independent of the degree of acetylation (Teramoto, 2012). In this study lignin blends with poly-(vinyl acetate-co-vinyl pyrollidone) were also found to be miscible when the vinyl pyrollidone fraction was greater than 30 mol%. Although both the acetylated organosolv lignin as well as the vinyl pyrollidone containing

polymer were soluble in THF, when present concurrently a precipitate was observed. The yield of this precipitate was observed to decrease with increasing degree of acetylation as well as decreasing vinyl pyrollidone fraction in the poly(viny pyrollidone-co-vinyl acetate) copolymer. This suggests heightened intermolecular interactions between unsubstituted organosolv lignin and PVP. Despite these improved interactions and the observance of miscibility in this system the resulting material was still too brittle to be useful in any practical sense. In an attempt to improve the intermolecular attractions in a lignin polymer blend the prospect of forming ionic bonds between constituents has been investigated (Hasegawa, 2008). Lignosulfonic acid was blended with PVP and the sulfonate group served as the anion with the counter cation being the pyridinium group. Both the 2 and the 4 isomers of vinyl pyridine were investigated and it was found that the 4 isomer of pyridine allowed for greater intermolecular attraction as indicated through FT-IR analysis. The bands at 1622 cm^{-1} and 1636 cm^{-1} were attributed to the proton transfer from the lignosulfonic acid group to the pyridine group for poly(2-vinyl pyridine) and poly(4-vinyl pyridine), respectively and can thus be used as an indicator of the extent of ionic interaction. Stronger ionic interactions present in the poly(4-vinyl pyridine)-lignin complex were substantiated by a more pronounced band at 1636 cm^{-1}. Additionally, an increased T_g value was observed for the poly(4-vinyl pyridine)-lignin complex as well. The lignin-PVP system was also tested as a wood adhesive through shear testing. The poly(4-vinyl pyridine) system was found to fail at approximately $1/3^{rd}$ of the stress capable of a commodity type PVA adhesive (1.1 vs 3.3 MPa respectively). The poly(2-vinyl pyridine) isomer was only capable of withstanding 0.3 MPa of stress.

Another area of research has been to blend lignin with polyhydroxybutyrate (PHB). Mousavioun et al (Mousavioun P, 2010) found that by incorporating soda lignin they were able to improve thermal stability over pure PHB but the onset temperature of thermal degradation was reduced compared to PHB. The morphology of the blend was studied using DSC and scanning electron microscopy (SEM) and it was found that up to 40% soda lignin content the blend exhibited favorable intermolecular compatibility. It has also been established that the particle size of the lignin contributes to the end properties of lignin blends with smaller particles allowing for better stress transfer (Miao, 2016).

In another study lignin blends with poly(3-hydroxybutyrate-co-3-hydroxyvalerate) (PHBV) and PP were investigated (Luo, 2017). However, in this study the lignin molecule was first esterified using carboxylic anhydrides from C_2 to C_6 chain length. This chemical modification improved compatibility between the constituents. The tensile strength and elongation at break were shown to increase progressively with increasing ester chain length. In addition, the lignin esters demonstrated improved hydrophobicity. This resulted in less absorption of water and swelling in water soak tests.

1.2.6 Lignin Derivatization

It is believed that the relatively high T_g of lignin is largely the result of extensive hydrogen bonding interactions (Kubo S, 2005) within the lignin molecule. Similar to the above mentioned study where lignin esters were blended with PHBV, another area of research for valorizing lignin has been to derivatize the hydroxyl groups contained within the lignin molecule through esterification reactions to bring the T_g down (Zhao X. , 2017; Kay, 2016). Very early on research was conducted on the effects of esterification and the chain length of the esterifying agent (US Patent No. 2429102, 1947). These efforts revealed that with a chain length shorter than 12 carbon atoms the material characteristics were dominated by lignin. However, above 12 carbon atoms the material began to take on an oilier, greasy texture. It was suggested that the materials generated using acid anhydrides with carbon chains longer than 12 may be effectively utilized as release agents for molds of both thermoplastics and thermosets. In particular, the lignin penta-stearate derivative showed excellent compatibility when utilized in the molding of products containing wood fibers.

Koivu et al found that when fatty acid chloride was present at 130% total molar content of hydroxyls in lignin quantitative esterification was achieved (Koivu, 2016). Additionally, the T_g was reduced from 145°C for unaltered softwood kraft lignin to 45°C for fully substituted kraft lignin using the C_{12} derivative as determined by DSC. Samples containing 10, 30 and 50% molar ratios of fatty acid acyl chloride showed melting peaks where samples containing higher molar ratios of acyl chloride exhibited only glass transitions. All samples exhibited thermal degradation temperatures in the range of 190-210°C by thermogravimetric analysis (TGA). The palmitic derivative was observed to be miscible with PE.

1.2.7 Grafting Lignin Copolymers

Another approach for chemically modifying lignin to improve thermoplastic properties is to covalently link a separate polymer onto the lignin molecule. This method is known as grafting and can be divided into two major categories. These are grafting from and grafting onto. In the grafting from approach the separate polymer is polymerized piecewise from the lignin molecule. In the grafting onto approach the separate polymer is first polymerized independently of the lignin and then in a later stage the polymer is covalently linked to lignin (Cowie et al, 2008). The grafting from approach has been demonstrated in many studies (Janata et al, 2003; Gao et al, 2013; (Zhu, 1999). One such example is a study in which epoxidized soybean oil is reacted with carbon dioxide to generate a carbonated soybean oil (Lee & Deng, 2015). Next the carbonated soybean oil is reacted with 3-aminopropyltriethoxysilane which has the effect of generating a urethane linkage without the use of toxic isocyanates. Finally, the urethane monomer is reacted with lignin. This approach has the benefit of utilizing upwards of 85 wt% biomass. By adjusting the curing temperature as well as the lignin content it was found that material properties such as young's modulus and tensile strength could be adjusted to generate a product ranging from stiff and ridged to highly flexible and capable of significant elongation.

In one study the grafting onto approach was used with a reactive PLA precursor terminated in acyl chloride groups (Kim, 2016). The samples were generated using a solvent based synthesis wherein methanol soluble kraft lignin was dissolved in pyridine. Next acid chloride terminated PLA was solvated in dichloromethane. The solutions were created to give a mass ratio of 3:2 lignin to PLA. This however, is not representative of the final copolymer product as the yields were not 100%. These solutions were mixed and held at 0°C and the unreacted precursors are washed away using a series of solvents and at this point the study states difficulty in determining the final composition and so it remains unknown what the final lignin content is in the finished product. This study found a negative correlation between the molecular weight of the PLA precursor and the molecular weight of the resulting lignin-PLA copolymer. This is likely the result of steric factors. A larger PLA molecule once grafted will sterically hinder the hydroxyl groups in the vicinity which would otherwise be available for

grafting. The result is a less extensively grafted lignin structure exhibiting a lower molecular weight. Mechanical tensile tests demonstrated a tensile strength and young's modulus of 3.80 MPa and 0.45 GPa, respectively. DSC analysis showed a melting endotherm for all samples around 150°C which is promising with regard to use of the material as a thermoplastic.

Another study demonstrates a process wherein PHBV is blended with kraft lignin with a small amount of dicumyl peroxide (DCP) present as a radical initiator (Luo et al, 2016). The mixture is processed through a reactive extrusion technique. At elevated temperature the radical initiated cross linking is enabled. This improves interfacial interactions that would otherwise be unfavorable in a typical blend scenario. The study revealed a decrease in the size of spherulites present in PHBV with a greater nucleation density. The T_g, thermal stability and tensile strength were all enhanced as compared against virgin PHBV.

1.3 Renewable Feed-stocks

In the grafting approach it is common to utilize potentially renewable feedstock for the grafting polymer. The obvious advantage here is a more completely renewably sourced end product. For example, the three examples provided for grafting to and from lignin utilized PLA, a soybean oil derivative as well as PHBV. All of these can be considered renewable resources. Other prospective renewable feed-stocks that have been studied are diols and diacids to form polyesters. Succinic acid has been identified as a likely candidate to be produced from microbial fermentation (Werpy, 2006). There are many biological pathways to produce succinic acid. However, they are not straightforward and have complicating factors such as: 1) microorganisms having a low tolerance of elevated succinic acid concentration which limits yields; 2) cost of growth media; 3) co-products that render the solution incompatible with catalytic upgrading techniques without preliminary purification and 4) narrow pH range tolerance for production which necessitates neutralization of acid products. From succinic acid it is a trivial matter to hydrogenate over a metal catalyst to produce 1,4-butanediol and a variety of other potential building block molecules. Similarly, adipic acid, another prevalent precursor for commodity thermoplastics, has been shown to have potential for biological production (Deng, 2016).

1.4 Current Study

1.4.1 Outline

In the current study softwood kraft lignin is grafted onto a poly(ester-amine) prepolymer in an attempt to generate a bio-based thermoplastic. The synthesis is a single pot, melt condensation reaction in which the reactants act as solvents, thereby eliminating the problem of solvent recovery and/or disposal. The reaction scheme is shown below in Figure 1.1.

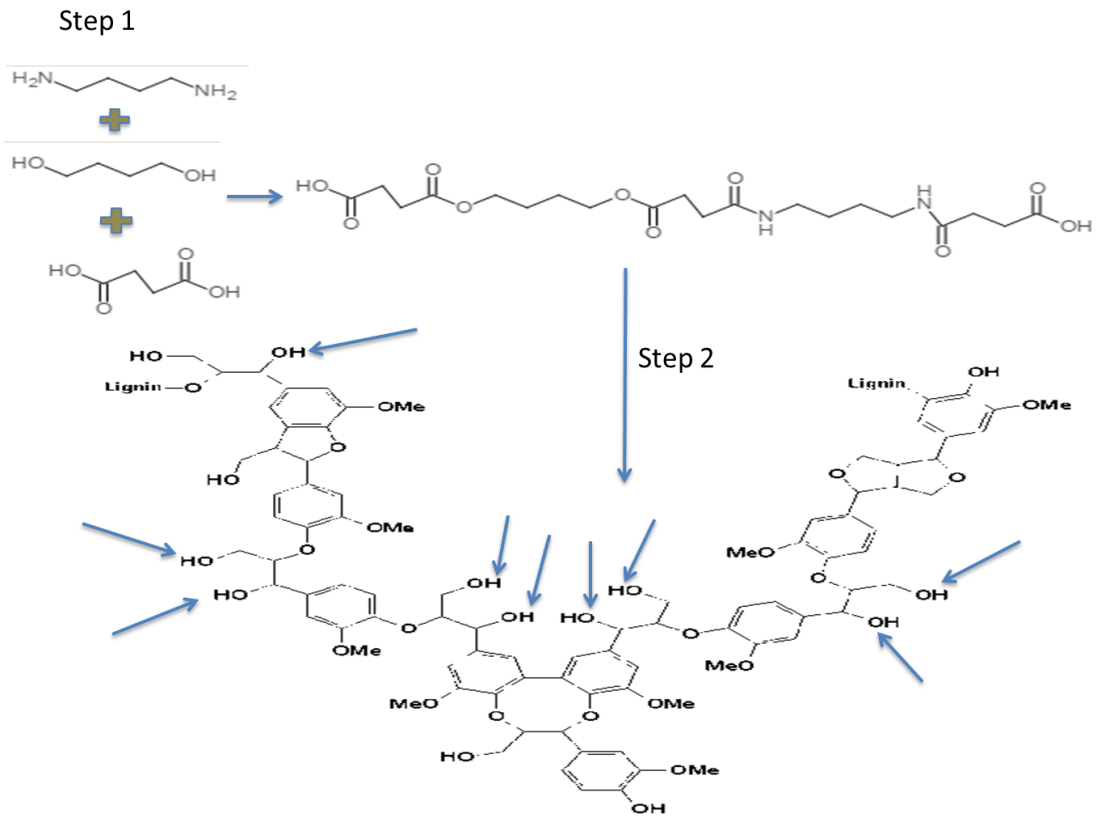

Figure 1.1 Reaction schematic of preparing the prepolymer and lignin-copolymer

It was hypothesized that the resulting material would behave similarly to an elastomer such as styrene butadiene rubber. The amorphous lignin would operate as hard segments while the more crystalline prepolymer would take the place of the soft segments. A diagram illustrating this concept was adopted from Bova, et al. (2016) and is shown in Figure 1.2.

Figure 1.2 Hard and soft segments of lignin copolymers taken from Bova, et al., 2016

1.4.2 Research Objectives

The objective of this study is to explore a "green" synthesis approach to a bio-based thermoplastic. The synthesis will involve a single pot, two step procedure. In the first step a prepolymer will be generated. Three different acids will be tested in the prepolymer synthesis. In addition, varying amounts of diamine will be tested. Evidence of polymerization will be provided through electrospray ionization-mass spectrometry (ESI-MS) analysis as well as FT-IR spectral analysis. After successful polymerization of the prepolymer lignin will be added at varying contents followed by further polymerization. The objective is to generate a series of lignin copolymers having a range of properties. The thermal and mechanical properties of the copolymers will be characterized using dynamic mechanical analysis (DMA), DSC, TGA and tensile testing. The morphology of the copolymers will be studied using polarized optical microscopy as well as x-ray diffraction (XRD)

The progression of this thesis is outlined in Figure 1.3

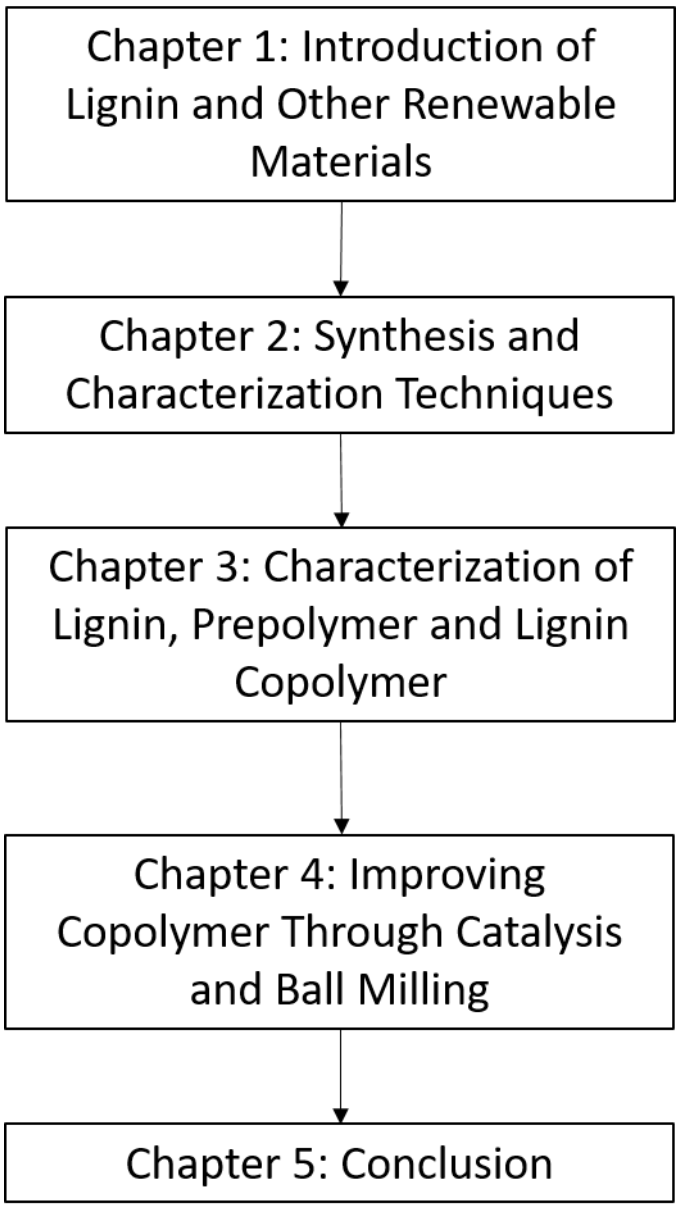

Figure 1.3 Flowchart for thesis outlining the progression of discussion

2 Materials and Methods

2.1 Synthesis

Softwood kraft lignin (Indulin AT) was obtained from Mead Westvaco and used as received. Succinic acid (SA) was obtained from Mallinckrodt Chemical Works. Adipic acid (AA), p-toluenesulfonic acid (TSA) and 1,4 diaminobutane (DAB) were all obtained from Acros Organics and suberic acid (SuA) and 1,4 butanediol (BD) were all obtained from Alfa Aesar. All reagents were used as received.

The prepolymer was prepared by mixing 1.1 molar ratio of diacid together with the desired molar ratio of BD and DAB such that the sum of the molar ratios of BD+DAB was 1 relative to the diacid. The levels of DAB tested were 0, 0.1 and 0.2 molar content. For the 0 wt% lignin samples diacid was present at a molar ratio of 1. The prepolymer mixture was stirred thoroughly and placed in a vacuum oven at -50 KPa and 60°C for 30 minutes. The mixture was then stirred again and placed in the vacuum oven at -50 KPa and 140°C for 3 hours. Lignin was then added to the prepolymer at mass ratios of 10, 20, 30, 40 and 50 wt% and the mixtures were stirred thoroughly and placed in teflon molds. The molds containing the lignin copolymer mixtures were then placed in a vacuum oven at 150°C and -50 KPa for 48 hours. Examples of sample names with their corresponding chemical makeup are provided in Table 2.1

Table 2.1 Prepolymer/lignin-copolymer formulations with monomer composition and sample

Sample Name	Acid	BD Molar Content	DAB Molar Content	Acid Molar Content	Lignin Mass Content (%)
SA BD 0.8 0% lig	Succinic Acid	0.8	0.2	1	0
SA BD 0.8 10% lig	Succinic Acid	0.8	0.2	1.1	10
SA BD 0.8 20% lig	Succinic Acid	0.8	0.2	1.1	20
SA BD 0.9 0% lig	Succinic Acid	0.9	0.1	1	0
SA BD 0.9 10% lig	Succinic Acid	0.9	0.1	1.1	10
SA BD 0.9 20% lig	Succinic Acid	0.9	0.1	1.1	20
SA BD 1 0% lig	Succinic Acid	1.0	0	1	0
SA BD 1 10% lig	Succinic Acid	1.0	0	1.1	10
AA BD 0.8 0% lig	Adipic Acid	0.8	0.2	1	0
AA BD 0.8 10% lig	Adipic Acid	0.8	0.2	1.1	10
AA BD 0.9 0% lig	Adipic Acid	0.9	0.1	1	0
AA BD 0.9 10% lig	Adipic Acid	0.9	0.1	1.1	10
SuA BD 0.8 0% lig	Suberic Acid	0.8	0.2	1	0
SuA BD 0.9 10% lig	Suberic Acid	0.9	0.1	1.1	10
SuA BD 1 20% lig	Suberic Acid	1.0	0	1.1	20

In addition to the samples mentioned above, lignin copolymers were prepared using ball milled lignin. Indulin AT kraft lignin was ball milled in a cylinder of diameter 77 mm and length 80 mm filled with 10 balls of 20.5 mm diameter and 10 balls of 12 mm diameter. Samples were milled for one week. Particle size both before and after ball milling was measured using an Olympus BX51 optical microscope at 400x magnification.

A separate series of copolymers were generated in which an acid catalyst, TSA, was utilized. For the acid catalyzed copolymers the catalyst was added at the same time as the lignin. The amount of catalyst added was 0.5% of the total mass of the sample. The rest of the synthesis was carried out in the same manner as before.

2.2 FT-IR Analysis

FT-IR spectra were acquired using a Thermo-Nicolet iS5 equipped with a ZnSe attenuated total reflection (iD5 ATR) accessory. Peak fitting analysis was performed using Igor Pro version 6.03.

2.3 Mechanical Analysis

Tensile testing was performed on a TA Q800 DMA instrument. Samples were cut to the shape of a dog bone if the sample permitted. For samples that were too brittle for cutting the sample was tested in the shape of a rectangle. Samples dimensions were approximately 7 x 27 mm^2. The sample was equilibrated at 30°C followed by a force ramp of 1 N/min to 18 N.

2.4 Thermal Analysis

2.4.1 DSC Analysis

DSC was performed on a TA instruments Q200 DSC equipped with a refrigeration unit. In order to determine the T_g's, the samples were first annealed at 135°C for 1 minute to erase thermal memory. Samples were then analyzed from -70 to 150°C at a heating rate of 5°C/minute with a temperature modulated (TMDSC) profile overlaid of $\pm$ 0.5°C every 20 seconds. The T_g's were recorded as the temperature associated with the minimum value of the first derivative of the heat flow signal at the steepest point in the inflection found in the thermogram showing heat flow versus temperature.

For determination of activation energies E_a the samples were analyzed at 3 different heating rates (β) overlaid with a $\pm$ 0.5°C/20 second temperature modulation. These were 5, 10 and 15 °C/min. Glass transition temperatures were recorded and a linear regression was applied to the plot of $\ln(\beta)$ against $1/(T*R)$ where R is the ideal gas constant in units of J/(mol*K). According to the Arrhenius equation the slope of the line obtained from the regression analysis was determined to be the activation energy of the transition.
Calibration and response of the instrument was checked by measuring a polystyrene standard which exhibits a glass transition near 100°C.

2.4.2 DMA Analysis

DMA was performed on a Perkin Elmer DMA 7 instrument. Samples were tested in compression mode from -20°C to 140°C at a heating rate of 5°C/min. The static force exerted was 20 mN and the dynamic force 16 mN at a frequency of 1 Hz. The instrument was set to record storage modulus (E'), loss modulus (E'') and the ratio of the two was calculated and

reported as the tan delta signal (E''/E'). The temperature associated with the peak in the tan delta signal is reported as the glass transition temperature (Banu, El-Aghoury, & Feldman, 2006).

Time temperature superposition (TTS) master curves were generated using the following method on a TA Q800 DMA instrument in tensile mode. The sample was first equilibrated at 30°C and held isothermally for 5 minutes. After the isothermal stage a frequency sweep was performed from 0.1 to 100 Hz on a logarithmic scale. The scan was carried out under strain control set at 0.05% strain. Following the frequency sweep the temperature was stepped 2.5 °C and the frequency sweep was performed again. This cycle was repeated until a temperature of 130 °C was reached. Calibrations of both DMA instruments were performed using a zinc and indium standard. The melt temperature was recorded and a correction was applied.

2.4.3 TGA Analysis

TGA was performed on a Perkin Elmer TGA 7 instrument. The instrument was programmed to perform a temperature ramp of 20°C/min starting at 30°C and ending at 900°C. The percent of original weight was recorded versus temperature. Thermal stability was analyzed by comparing the temperatures at which the sample had lost 5% of original mass (T_{d5}). Another method for analysis of thermal stability was to determine the onset of thermal degradation by drawing two tangent lines. The first tangent line is drawn on the flat region before thermal degradation while the second is drawn at the inflection after the first region where thermal degradation is observed. The temperature at the intersection of these tangent lines is determined as the onset temperature (T_{onset}). An example of this analysis is shown in Figure 3.16.

2.4.4 TMA Analysis

TMA was performed on a Perkin Elmer TMA 7 instrument. The instrument was programmed to perform a temperature ramp of 5°C/min from -20°C to 300°C. The softening temperature was determined to be the intersection of the two tangent lines. The first was drawn from the

flat part of the curve before softening and the second tangent line was drawn from the inflection point.

2.5 Electrospray Ionization Mass Spectrometry

Molar masses of prepolymer samples were determined by positive ion ESI-MS obtained from a Finnigan LCQ-Deca instrument. The low molecular weight samples were dissolved in methanol containing 1% acetic acid while more extensively polymerized samples necessitated a solvent system of 1:1 chloroform:methanol. The samples were then introduced to the electrospray at a flow rate of 10 µL/min. The ion source and capillary voltages were 4.48 kV and 47 V respectively, each at a temperature of 275°C. Spectra were obtained by scanning through a mass to charge (z/z) ratio range of 80-2000. The number average molecular weight was calculated as $M_n = \sum N_i M_i / \sum N_i$ and the weight average as $M_w = \sum N_i M_i^2 / \sum N_i M_i$ where N_i is the intensity and M_i is the mass after accounting for the charge. The PDI is calculated as PDI = M_w/M_n.

2.6 Melt Testing

Melt testing was performed in a hydraulic hot press in order to determine if the samples exhibited melt flow behavior. Samples were placed on sheets of parchment paper with a separate sheet placed on top. Then an aluminum plate having a mass of 830 g was placed over the samples. This insured a consistent application of pressure for all samples. The samples were then placed into a hot press heated to 115°C. The hot press was then closed to the point where the aluminum plate was touching the heated platen to facilitate heat transfer but no pressure was introduced by the hydraulic. Samples were heated for 10 minutes and removed. Melting was determined by whether or not the samples had exhibited any flow behavior.

2.7 Polarized Light Microscopy

Samples were analyzed for birefringence using an Olympus BX51 optical microscope at 400x magnification. The microscope was set to operate in transmittance mode where a polarizer first polarized the light from the source before passing through the sample. If crystallinity is present the spherulites will interfere with the polarized light, shifting the

polarization to a new angle. A polarizer before the eye piece is rotated such that when it is in line with the direction of polarization of the light leaving the sample the zones of crystallinity are visible.

2.8 X-Ray Diffraction

X-Ray Diffraction (XRD) was performed on a Siemens D5000 Diffractometer using a Cu Kα source (1.542 Å) running at 40 kV, 30 mA at room temperature. The diffraction patterns were recorded in the 2θ range of 2-50° at increments of 0.5°. The crystallinity index was determined using a diffraction deconvolution method with minor modifications (Terinte, Ibbett, & Schuster, 2011). The peak positions and widths were held constant and the amplitude was allowed to be adjusted. The ratio of crystalline peaks to total peak area including amorphous peaks was used to calculate percent crystallinity. Peak fitting analysis was performed using Igor Pro version 6.03.

2.9 Statistical Analysis and Response Surface Modeling

All statistical analysis were performed in R version 3.3.1 using type III sum of squares. Response surface models were created using the car package.

3 Results and Discussion

3.1 Lignin

It is important to verify the properties of the lignin feedstock. Indulin kraft lignin used in this synthesis has been characterized in a previous paper (Li and McDonald, 2014) and several experiments were conducted in this study to compare against previous characterizations as described below.

3.1.1 Indulin Kraft Lignin TMA Characterization

TMA analysis was employed on Indulin AT kraft lignin to determine the softening temperature of the lignin sample. In the research conducted by Li et al (Li and McDonald, 2014) this softening temperature was equated to the T_g. The results from this analysis are shown in Figure 3.1. The softening temperature of 168°C recorded in this study is comparable from results from the literature which report a softening temperature of 157°C. In another study a T_g value by TMA for Indulin kraft lignin was found to be 132°C (Schorr, Diouf, & Stevanovic, 2014).

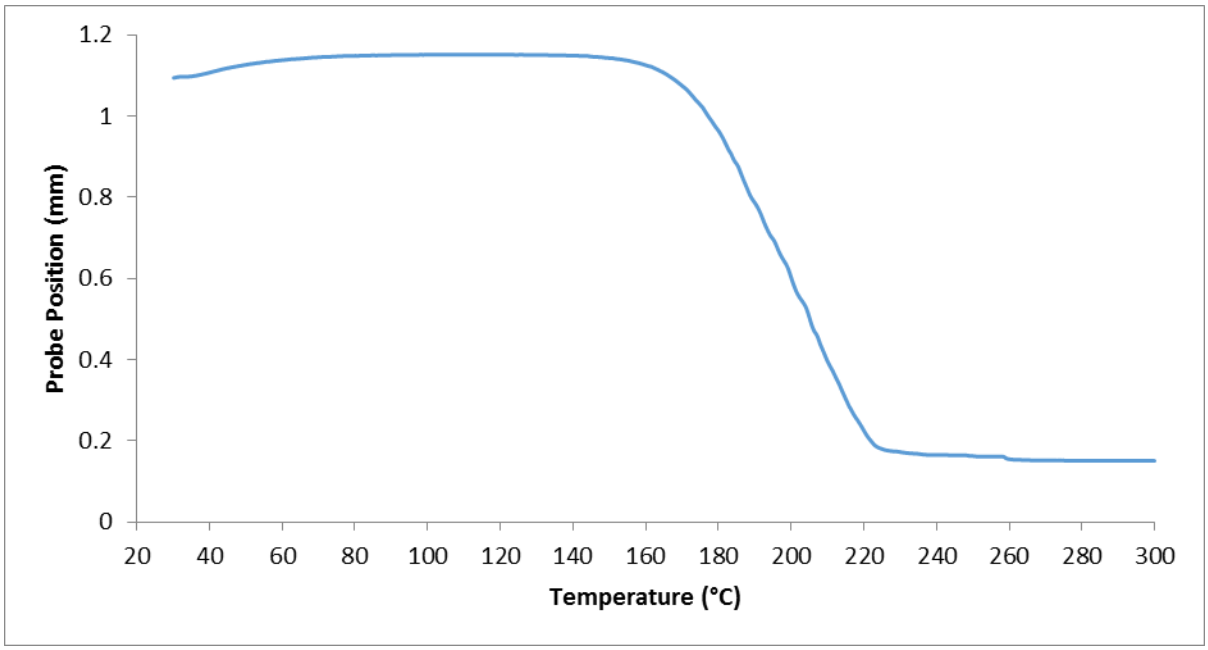

Figure 3.1 TMA thermogram of Indulin AT kraft lignin

3.1.2 Indulin Kraft Lignin DSC Characterization

TMDSC was used to verify thermal characteristics of the lignin used in this study and the results were compared to the literature (Li and McDonald, 2014). Figure 3.2 shows the DSC thermogram for the lignin used in this study. The T_g of 143°C obtained from TMDSC analysis of the lignin used in this study are comparable to the T_g value of 143°C found in the literature for kraft lignin (Li H. , 2014). In another study the T_g temperatures for softwood kraft lignins from two separate mills were evaluated by DSC (Dodd, Kadla, & Straus, 2015). T_g values of 151°C and 122°C were reported. The discrepancies were attributed to minor variations in the pulping process. The T_g value for lignin used in this study agrees well with these literature values.

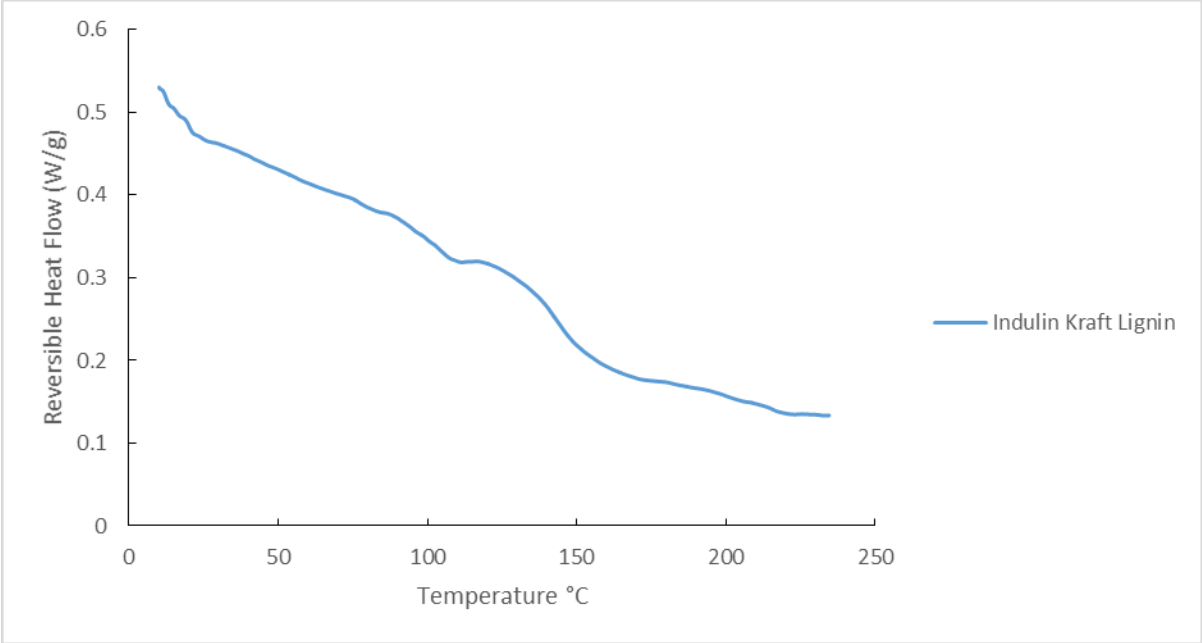

Figure 3.2 DSC thermogram of indulin AT kraft lignin showing T_g at 143°C

3.1.3 Indulin Kraft Lignin FT-IR Characterization

FT-IR was used to verify chemical characteristics of the lignin used in this study and the results were compared to the literature (Li and McDonald, 2014). An FT-IR spectra of the lignin used in this study can be found in Figure 3.3. Each of the characteristic IR band values were able to be correlated with those found in the literature, indicating a high degree of

commonalities between lignins used in each study. Table 3.1 shows these band assignments for Indulin AT kraft lignin.

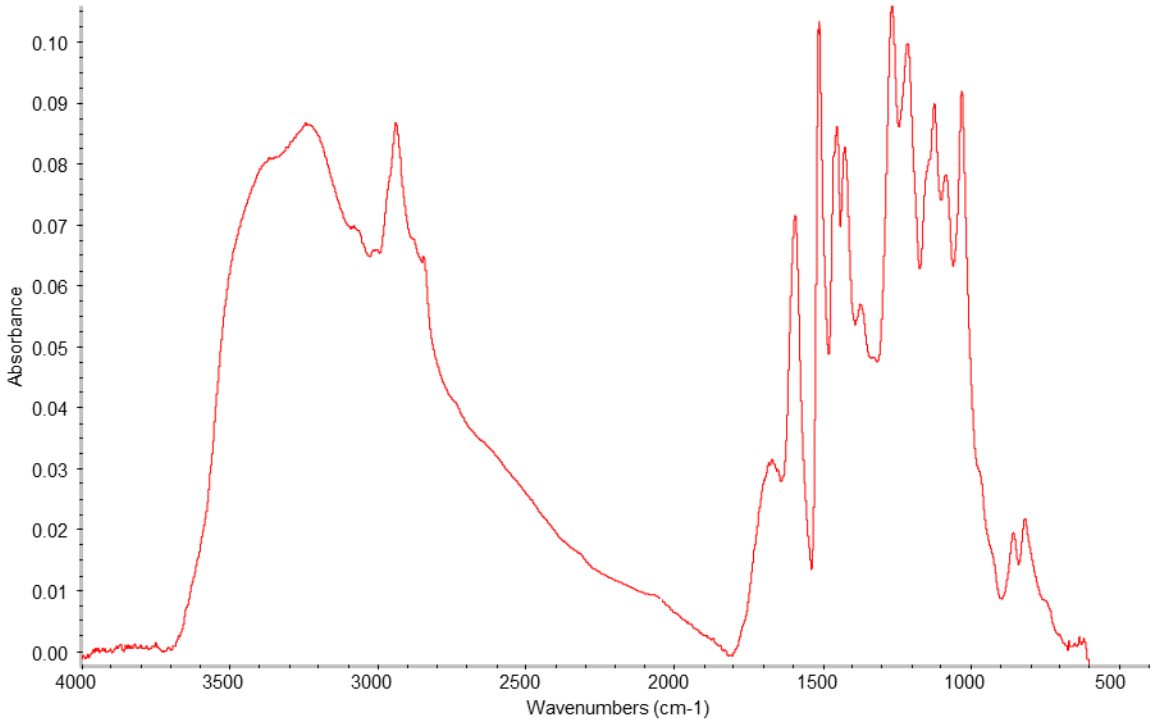

Figure 3.3 FT-IR spectrum Indulin AT kraft lignin

Table 3.1 IR band assignments for Indulin AT kraft lignin

Band (cm^{-1})	Assignment
854	C-H out-of-plane in position 2,5 and 6 of G units
1123	C-O deformation in esterbBond
1214	C-C plus C-O stretch
1264	C-O of guaiacyl ring
1370	symmetric bending deformation of methyl group
1422	C-H in plane deformation with aromatic ring stretching
1454	asymmetric bending deformation of methyl and methylene groups
1507	aromatic skeletal vibrations
1593	aromatic skeletal vibrations
1669	C=O stretching, in conjugation
2847	C-H symmetric stretching
2932	C-H asymmetric stretching
3411	O-H stretching

3.2 Prepolymer

The first step of synthesis is to generate a prepolymer which can then be subsequently reacted with lignin to form the copolymers. This section deals with the characterization of the prepolymer.

3.2.1 FT-IR Analysis of Prepolymers

A range of prepolymers were prepared using a variety of diacids (AA, SA, SuA), BD and DAB and differing compositions, without the addition of catalyst, via a melt condensation reaction (see Table 2.1). To eliminate the use of solvents, following a "green chemistry" approach, BD was used as a reactive solvent. FT-IR spectral analysis was used to monitor the formation of ester and amide functional groups in the prepolymer through the carbonyl absorption band at 1680-1740 cm^{-1} (Figure 3.4). More specifically, the location of the carbonyl stretch can be seen to shift from being centered at 1690 to 1725 cm^{-1} as the carboxylic acid functional group is converted into predominantly esters. The resulting carbonyl band from the polymerized prepolymer IR spectrum can be seen to be composed of two distinct bands for the diacid-diol prepolymer and three separate bands for the diacid-diol-DAB prepolymer. These bands are located at 1690, 1705 and 1725 cm^{-1} for the carboxylic acid, amide and ester carbonyl stretch, respectively. In order to tease out spectral information, the FT-IR spectra were peak fitted. The results from this analysis of AA BD 0.8 prepolymer are shown in Table 3.2 and Figure 3.4.

Table 3.2 FTIR spectral anlaysis of the AA BD 0.8 prepolymer by peak fitting areas and associated percent of total area of carbonyl stretching band

	Peak Areas				Percent of total Area		
	Acid	Amide	Ester		Acid	Amide	Ester
Peak Center (cm^{-1})	1690	1705	1725	total area	1690	1705	1725
width (cm^{-1})	13	13	13		13	13	13
area 0 hr	1.7	0.9	0.4	3.0	56%	30%	14%
area 1 hr	3.3	1.8	1.7	6.8	49%	26%	25%
area 2 hr	2.3	2.2	2.9	7.5	31%	30%	39%
area 3 hr	2.2	2.1	3.6	7.9	28%	26%	46%
area 8 hr	2.7	2.2	4.6	9.5	29%	23%	48%
area 26.5 hr	2.0	2.8	6.2	11.1	18%	25%	56%
area 38 hr	1.4	2.8	5.5	9.7	15%	29%	56%
area 48 hr	1.2	2.5	5.2	8.9	13%	28%	59%

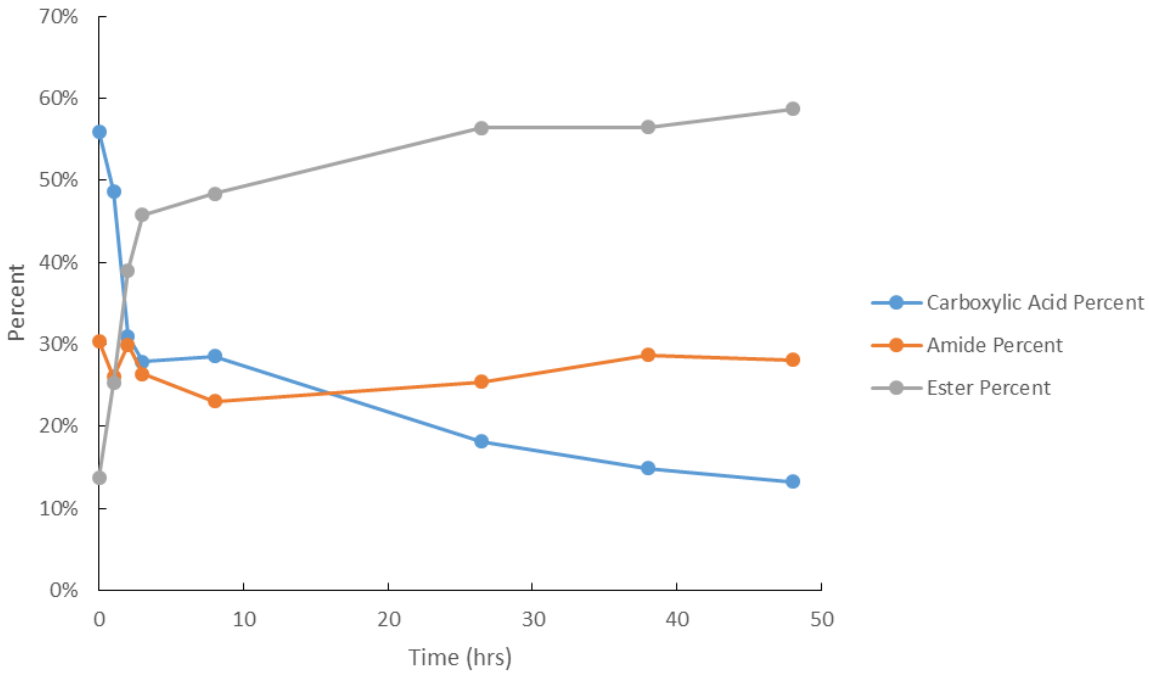

Figure 3.4 Plots showing % of carbonyl (acid, ester, amide) stretch bands with reaction time for the AA BD 0.8 prepolymer

From the results shown in Figure 3.4 it can be seen that as time progresses the band area attributed to the carboxylic acid band at 1690 cm^{-1} decreases, while the band attributed to the

ester at 1725 cm^{-1} increased, again indicating that the reaction proceeded as expected (Li, Sivasankarapillai, & McDonald, 2015). It is interesting to note, however, that the area of the band attributed to the amide remains relatively constant during polymerization. A possible explanation is that the amine group is more reactive than the alcohol and thus the majority of DAB react quickly and early on in the synthesis thus showing little change over time. It has already been discussed that the carboxylic acid band decreases with a concomitant increase in the ester band. Therefore, it may be that the amide band is largely influenced by the tails of bands on either side. The peak fitting that were performed at 0 hr, 8 hr and 48 hr and are shown in Figure 3.5.

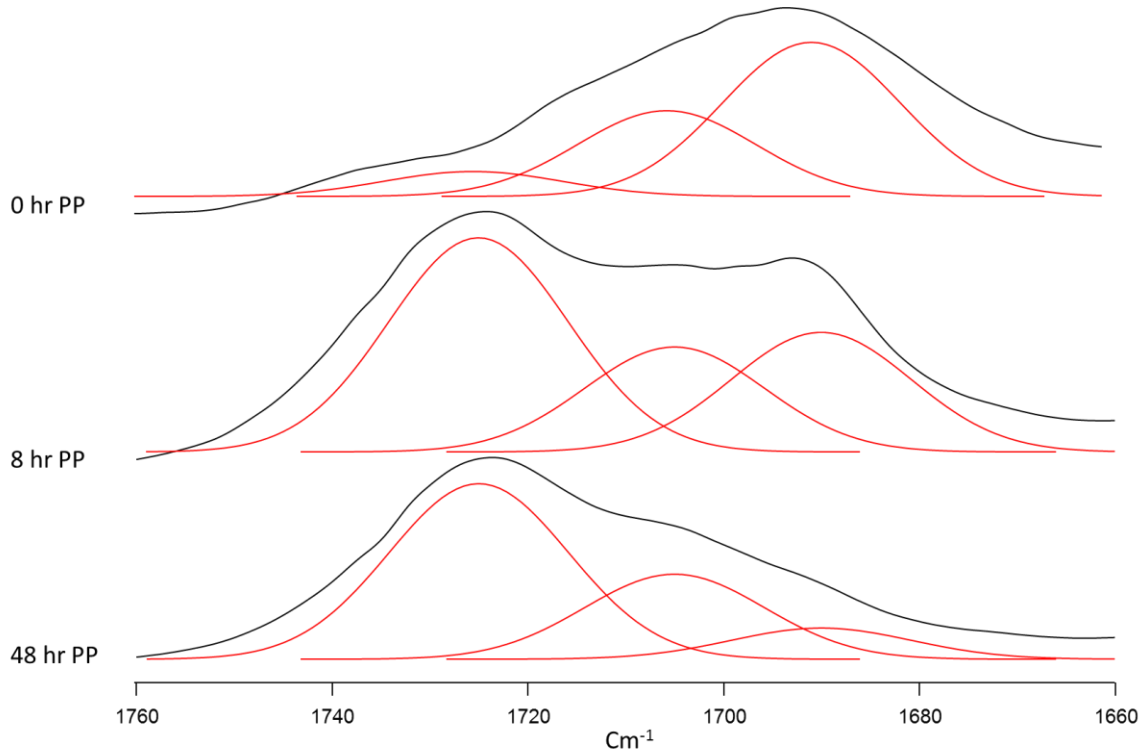

Figure 3.5 Peak fitted FT-IR spectra of prepolymer AA BD 0.8 at 0, 8 and 48 hr

3.2.2 DSC Analysis of prepolymer

3.2.2.1 Interpreting DSC Data for the Prepolymer

Prepolymer thermal properties can be obtained by DSC. Figure 3.6 shows a DSC thermogram of SA BD 0.9 prepolymer in which the glass (-22.96^{o}C) and melt (T_m, 105.44^{o}C) transitions are both clearly identifiable and easy to interpret. The inflection associated with the T_g is obvious and the derivative of heat flow has a peak with a clear minimum that can be

ascribed to the T_g. Similarly, the melt endotherm was readily observed and a melt temperature was assigned to the peak minimum for the heat flow signal.

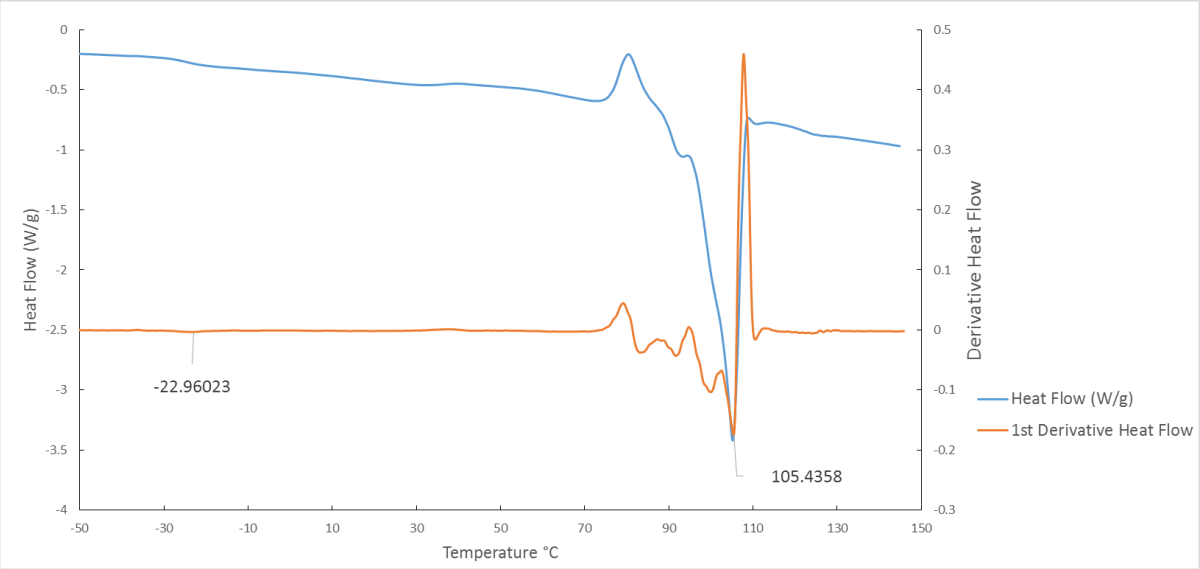

Figure 3.6 DSC thermogram of SA BD 0.9 prepolymer

The DSC thermograms of some of the prepolymers show multiple transitions that overlap, making it difficult to assign a value for any single transition. For instance prepolymer SA BD 1 (Figure 3.7) in which an exothermic transition occurs in the range of the T_g inflection. It is suspected that this exothermic transition is a cold crystallization process. The presence of this exotherm renders the method of assigning the temperature associated with the minimum in the derivative to the T_g inappropriate. The minimum in the derivative for that particular location is associated with the steep, higher temperature side of the exotherm which is not the transition of interest. In some other prepolymer samples it is difficult to distinguish even a single inflection as for the prepolymer SuA BD 0.9 shown in Figure 3.8. In this thermogram a melt endotherm occurring at 40°C is readily apparent. However, in the temperature range leading up to this melt transition there are several subtle changes in the slope of the heat flow signal. There are several local minimums in the first derivative plot that could potentially be interpreted as the transition of interest. Nevertheless, the analysis was carried out by choosing the most probable minimum in the first derivative of the curve obtained by plotting heat flow versus temperature.

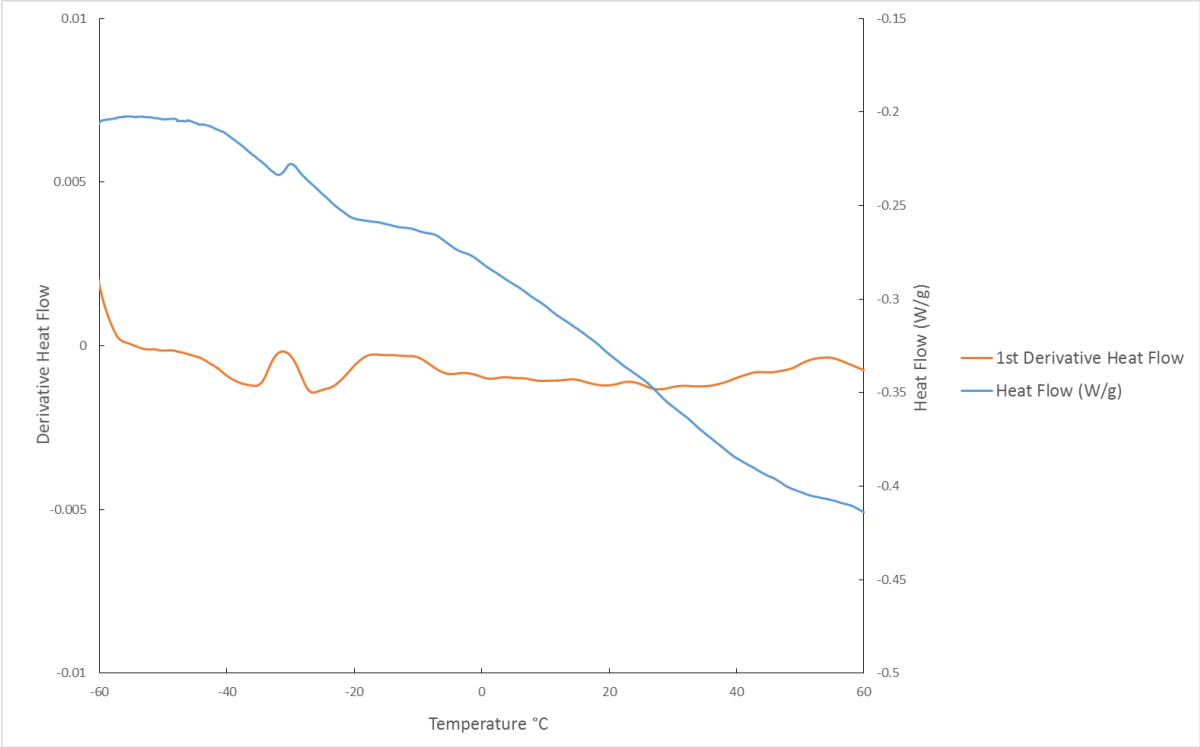

Figure 3.7 DSC thermogram of SA BD 1 prepolymer

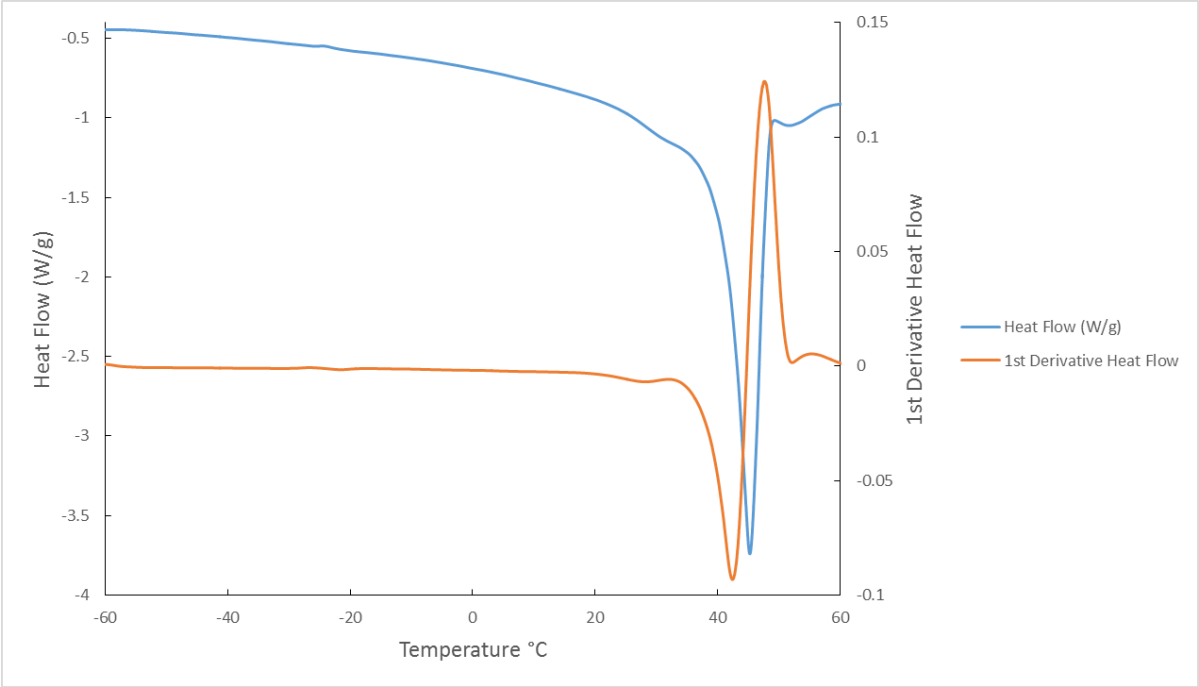

Figure 3.8 DSC thermogram of prepolymer SuA BD 0.9 prepolymer

3.2.2.2 DSC Analysis of Prepolymer Results

The thermal properties of the various prepolymers made with different diacids (SA, AA, SuA), BD and DAB, such as T_g and T_m, were determined by DSC. Figure 3.9 and Figure 3.10 show the T_g and T_m for the prepolymers as a function of DAB content. In addition, the prepolymer T_g was increased by changing the prepolymer diacids from AA (C_6) to SA (C_4) to SuA (C_8). However, the prepolymer T_m increased from AA to SuA to SA. There were no obvious trends between diacid chain length and thermal properties. There was no identifiable T_g at the DAB 0.1 (BD 0.9) level for the AA and SuA prepolymers.

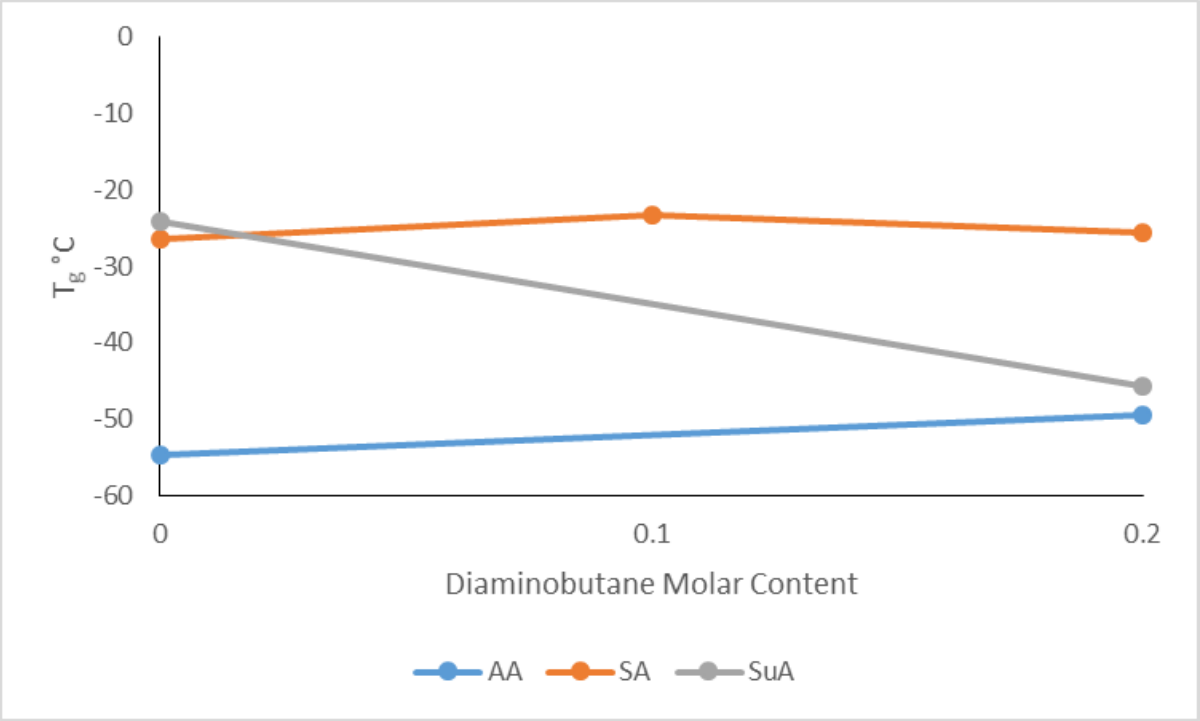

Figure 3.9 Plot showing the T_g of the various prepolymers made with varying molar amounts of DAB

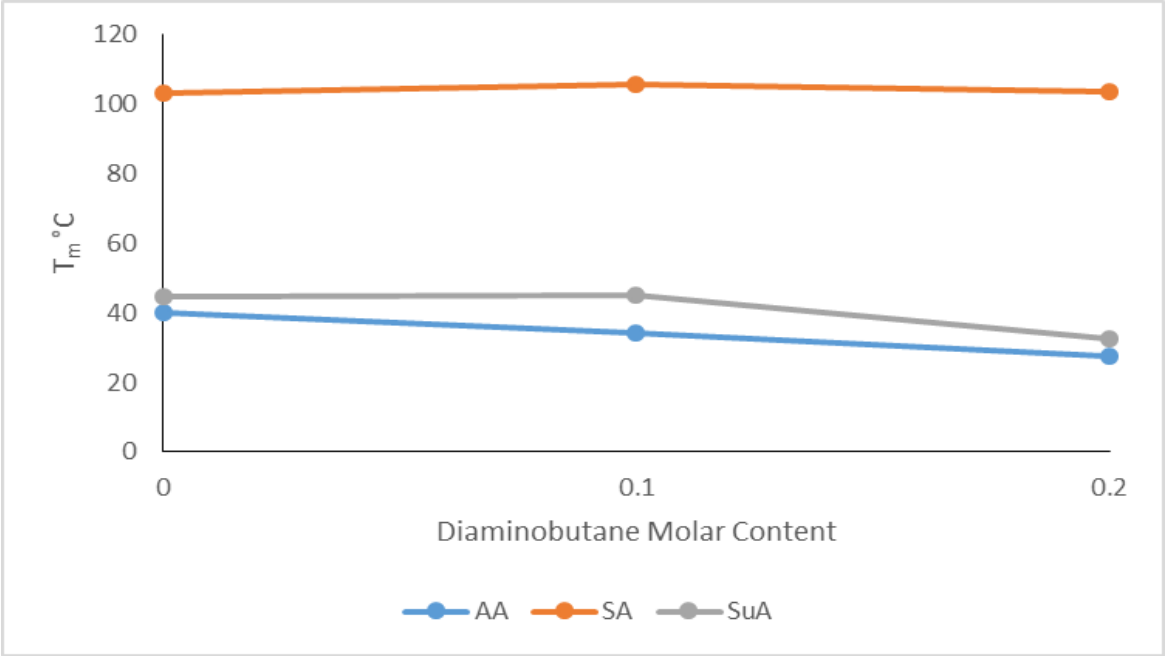

Figure 3.10 Plot showing the change in T_m of the various prepolymers made with varying molar amounts of DAB

Both the T_m and T_g do not show much of a response to the variations in DAB content with the exception of the SuA based prepolymer which drops about 20°C in T_g at the 0.2 mol DAB level. These observations do not agree with previous studies on poly(ester-amide) materials where it has been observed that increasing the proportion of DAB results in higher values for thermal transitions (Wang, et al., 2016).

To confirm that the transition observed in the prepolymer was a T_g, the E_a for the various prepolymer systems were determined. E_a was calculated by plotting the natural log of the heating rate ($\ln(\beta)$) against $1/(T_g*R)$ and given in Table 3.3. An example of this kind of plot can be seen in Figure 3.11.

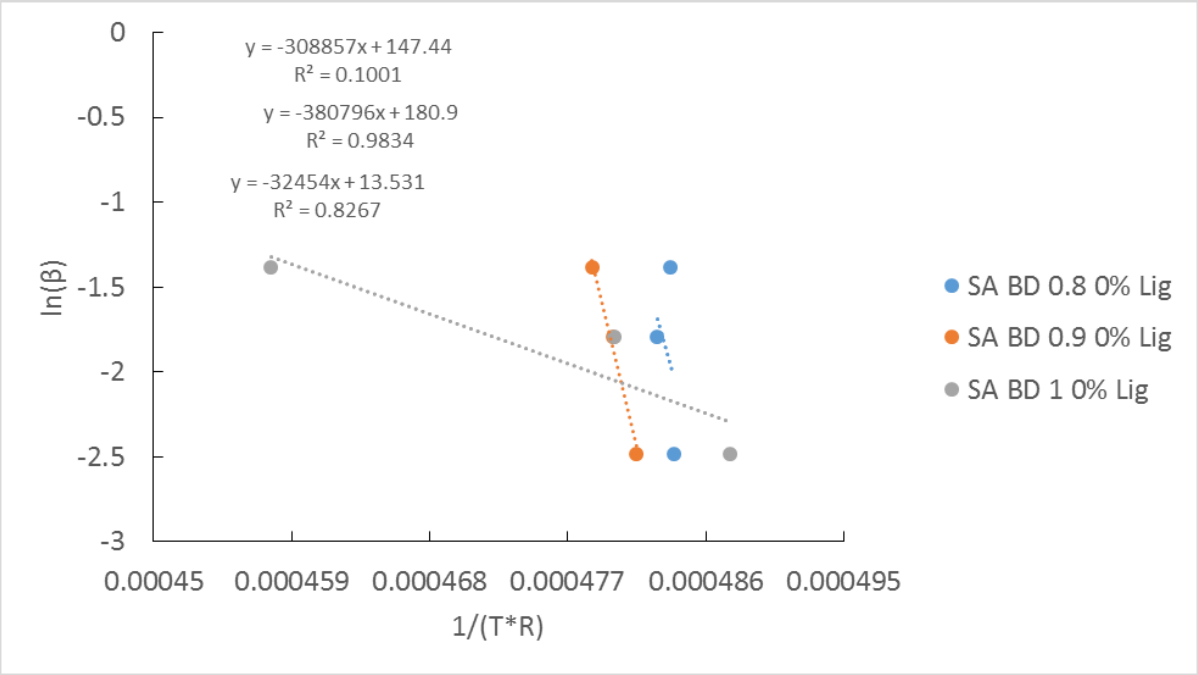

Figure 3.11 Plot of ln(β) versus 1/(T*R) for SA prepolymers to determine E_a of T_g

Table 3.3 E_a values for T_g of prepolymers with regression coefficients

Prepolymer	E_a (KJ/mol)			Regression Coefficient (R^2)		
	SA	AA	SuA	SA	AA	SuA
BD 0.8	309	142	93	0.10	0.81	0.91
BD 0.9	381			0.98		
BD 1	32	189	375	0.83	0.95	1.00

The calculated E_a values for the prepolymer range from 32 to 381 kJ/mol, with two low values of 32 and 93 kJ/mol. The values above 142 kJ/mol suggest that the transition was a glass transition (Vyazovkin, Shirrazzuoli, & Dranca, 2006). The measurement of the associated T_g's in this case were heavily influence by the presence of the cold crystallization peak. The correlation coefficients in these cases were observed to be rather low indicating a lack of linearity between data points. It is likely that the complications aforementioned could be contributing to these discrepancies.

3.2.3 ESI-MS Analysis of Prepolymer

ESI-MS analysis was successfully used to monitor the oligomer formation and molecular weight progression of the prepolymer polymerization. A time study (1, 2, 3 and 38 h) was only performed on the AA BD 0.8 prepolymer by ESI-MS and are shown in Figure 3.12. ESI-MS analysis for the other prepolymers were obtained at 48 h.

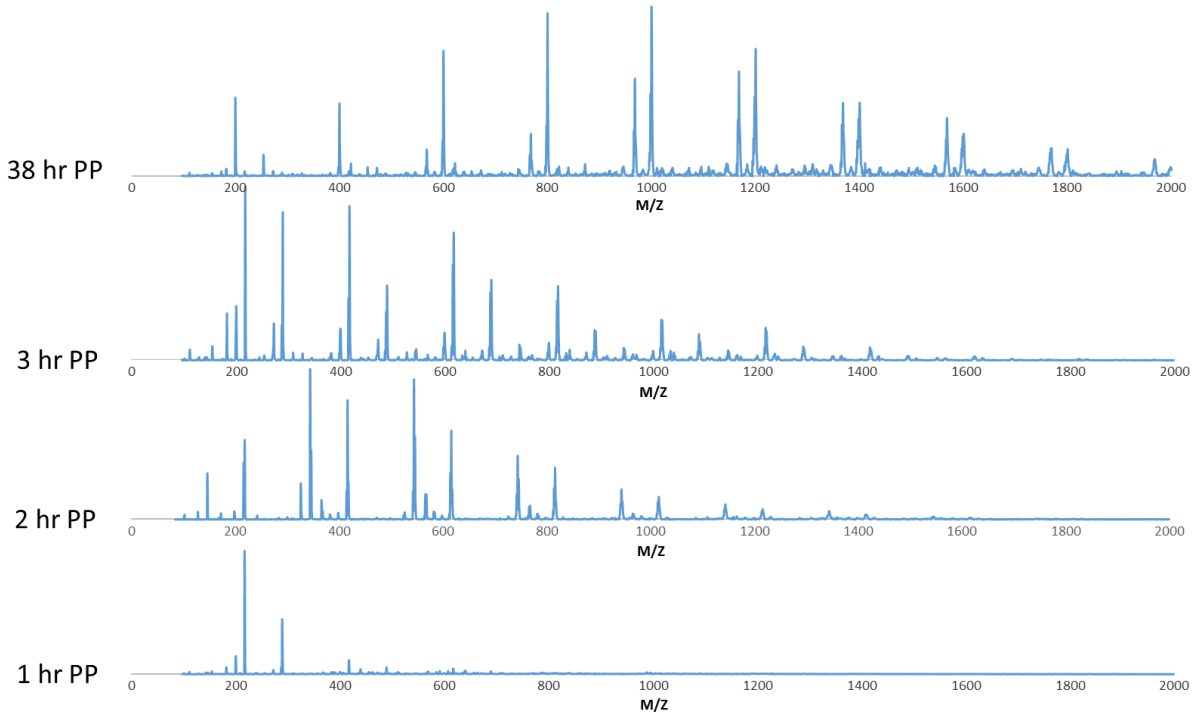

Figure 3.12 ESI-MS of AA BD 0.8 prepolymer at 1, 2, 3 and 38 h of polymerization

The molecular weight (number (M_n) and weight (M_w) average) of the prepolymers were calculated from ESI-MS and the results are shown in Table 3.4. The SA based prepolymers were insoluble in common organic solvents (chloroform, methanol, THF and dichloromethane) and could not be analyzed by ESI-MS. The change in M_n with polymerization time for the prepolymer is shown in Figure 3.13.

Table 3.4 Prepolymer molecular weights and PDI's determined by ESI-MS at 48 h

	M_n (g/mol)		M_w (g/mol)		PDI	
Prepolymer	SuA	AA	SuA	AA	SuA	AA
BD 0.8	998	1061	1209	1271	1.2	1.2
BD 0.9	1062	1203	1287	1338	1.2	1.1
BD 1	924	1171	1173	1339	1.3	1.1

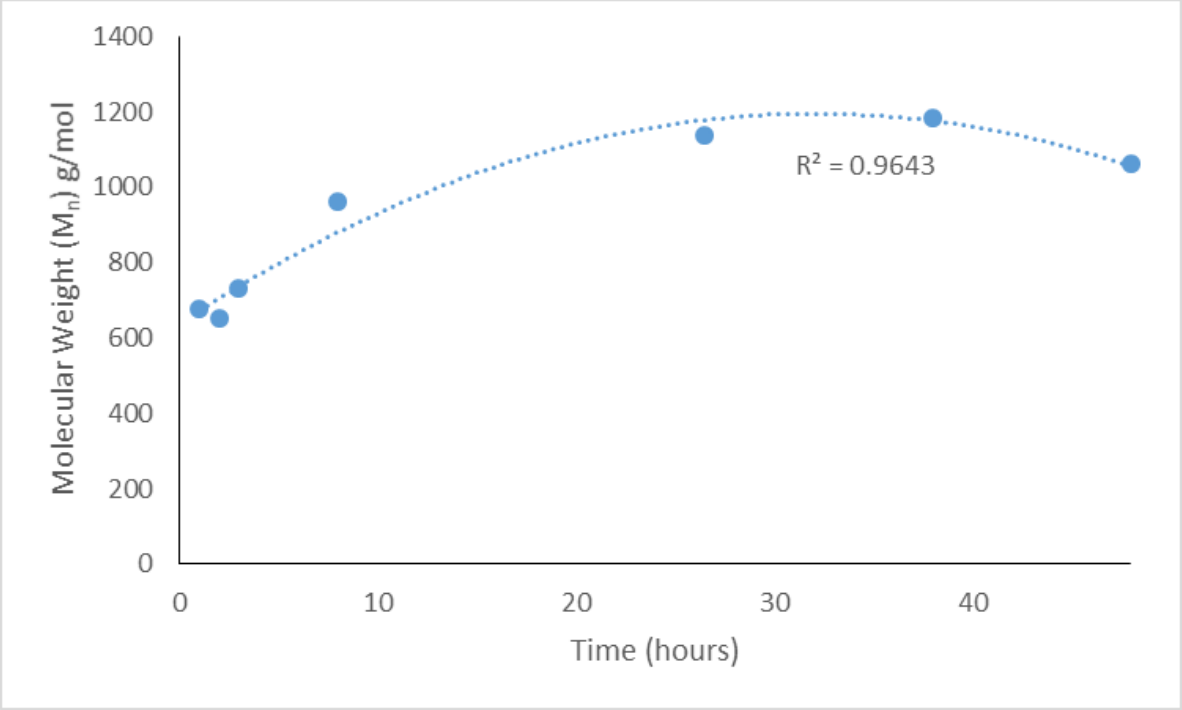

Figure 3.13 Molecular weight (M_n) development with prepolymer (AA BD 0.8) reaction time

The mass spectra shown in Figure 3.12 can be seen to have consistent spacing between prominent peaks. This indicates successive addition of monomer units and implies the possibility of elucidating structural information. A range of possible oligomeric structures, up to a degree of polymerization of 11, were determined and calculated as well as their associated molecular weights. The calculated values were compared against the ESI-MS peaks. The most common ions detected were $[M+H]^+$, $[M+Na]^+$, and $[M-OH]^+$ adducts. Nearly all the peaks were able to be identified through this type of analysis. This provides further evidence for the progression of the polymerization reaction as anticipated. Table 3.5 shows the molecular weights associated with potential oligomer ions for an AA prepolymer.

Figure 3.12 shows the corresponding mass spectrum for a sample of AA BD 0.8 prepolymer at 38 hours of polymerization.

Table 3.5 Molecular ion adducts from ESI-MS data for prepolymer AA BD 0.8.

Units of m/z	AA+DAB	AA+2BD	2AA+1DAB+1BD	3AA+DAB+2BD	
$[M+H]^+$			417.49		
$[M-OH]^+$	199.27	269.4	399.49	599.71	
$[M+Na]^+$					
	3AA+3BD	4AA+DAB+2BD	4AA+2DAB+2BD	5AA+DAB+3BD	6AA+DAB+4BD
$[M+H]^+$					
$[M-OH]^+$		727.83	798.96		
$[M+Na]^+$	618.68			968.03	1168.25

3.2.4 TGA of Prepolymers

The thermal stability of the prepolymers was analyzed using TGA by two methods (5% weight loss and onset temperature). An example of a thermogram resulting from TGA is shown in Figure 3.14.

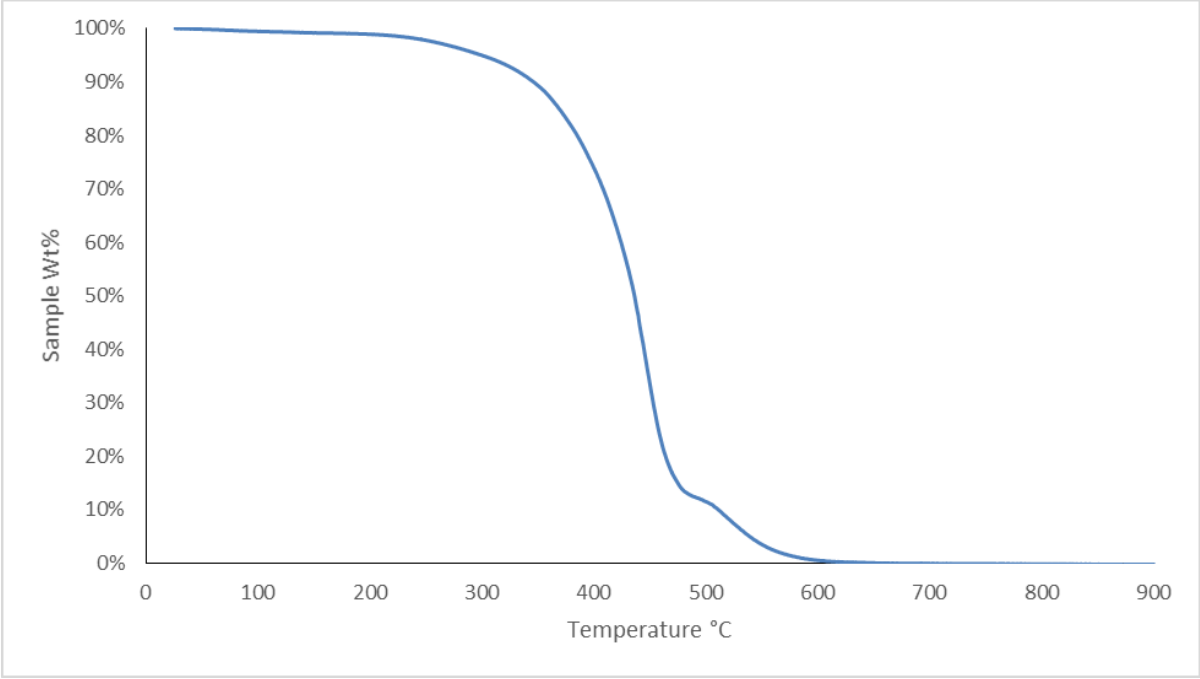

Figure 3.14 TGA thermogram of AA BD 0.8 prepolymer

The thermal stability of the prepolymer is evaluated based on the temperature at which the material has lost 5% of its original mass (T_{d5}). The T_{d5} value for each prepolymer was evaluated for each diacid used (AA, SA, SuA) and are plotted against DAB content in Figure 3.15. For prepolymers containing no DAB, the T_{d5} values decreased from 290 to 280 to 257^{o}C, respectively for the SA, AA and SuA based prepolymers, which followed an increase in diacid chain length. The prepolymer sample exhibiting the greatest T_{d5} value was AA BD 0.9 at a temperature of 333°C. The AA prepolymers exhibited the greatest T_{d5} values at DAB molar contents of 0.1 and 0.2.

Generally, for the prepolymers the T_{d5} value increased with DAB content which agrees with the literature (Ge, Yuan, Luo, & Wang, 2014). However, in another study the onset of thermal degradation for a poly(ester-amide) was found to decrease as amide content was increased from 5% to 25% (Wang, et al., 2016). Futhermore, as the DAB content was increased to 35% the onset temperature increased. This behavior resembles what was observed from the SA based prepolymer series in this study. The values of T_{d5} also show some resemblance to the trend observed in molecular weights from ESI-MS analysis shown in Table 3.4. For the AA and SA series of prepolymers both the molecular weight and T_{d5} temperatures increase to a maximum at the BD 0.9 (DAB 0.1) level and then decrease again at the BD 1 (DAB 0) level.

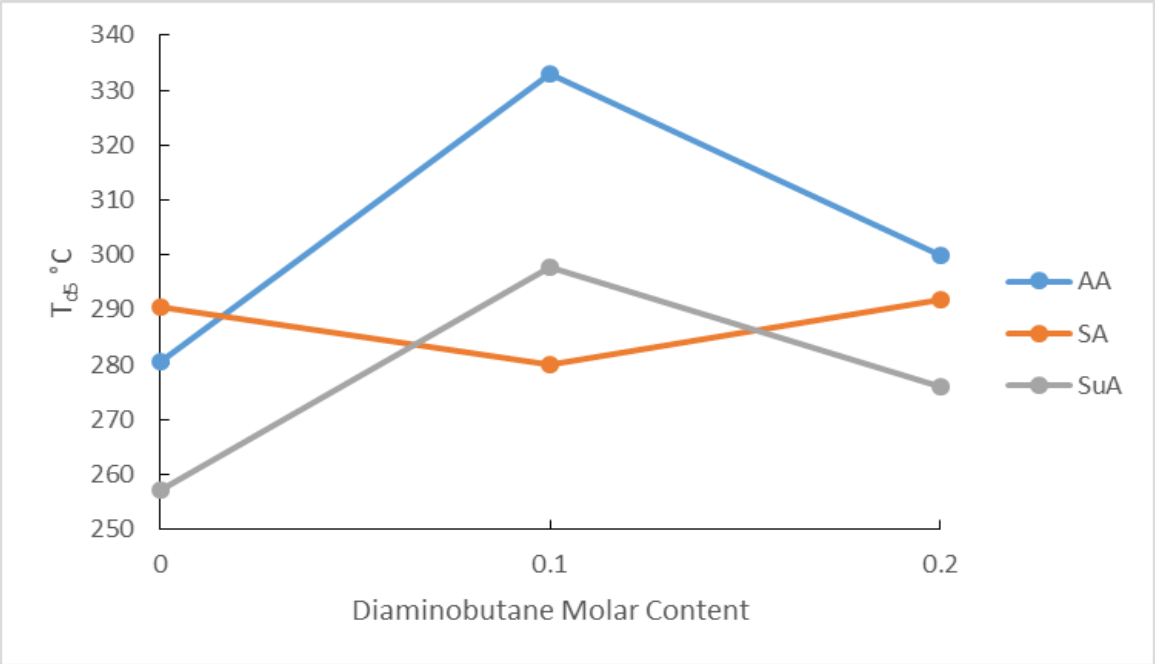

Figure 3.15 Values of T_{d5} obtained from TGA performed on prepolymer samples utilizing AA, SA and SuA diacids

The thermal stability of the prepolymers were also analyzed by their onset temperature (T_{onset}). T_{onset} is defined as the intersection of tangent lines drawn on either side of the onset, as shown in Figure 3.16. The prepolymer T_{onset} values were plotted versus DAB content as shown in Figure 3.17. In the literature comparable onset temperatures greater than 290°C were found for similar polyester materials (Thibaud, Eric, & Luc, 2017). Both the T_{d5} and T_{onset} methods result in similar trends associated with each diacid and the behavior in resopnse to varying DAB. Both the AA and SuA samples increase in T_{onset} as DAB is increased from 0 to 0.1 and then decrease again as DAB is increased from 0.1 to 0.2. The SA T_{onset} remains relatively unchanged as DAB is increased. These behaviors closely resemble what is observed in the T_{d5} method as well. The T_{onset} values however are about 40°C higher than the T_{d5} values. This may be due to the T_{d5} values being subject to influence from the vaporization of volatiles which could lead to a resulting value that is premature relative to the onset of thermal degradation, while the T_{onset} is the start of a degradation transition.

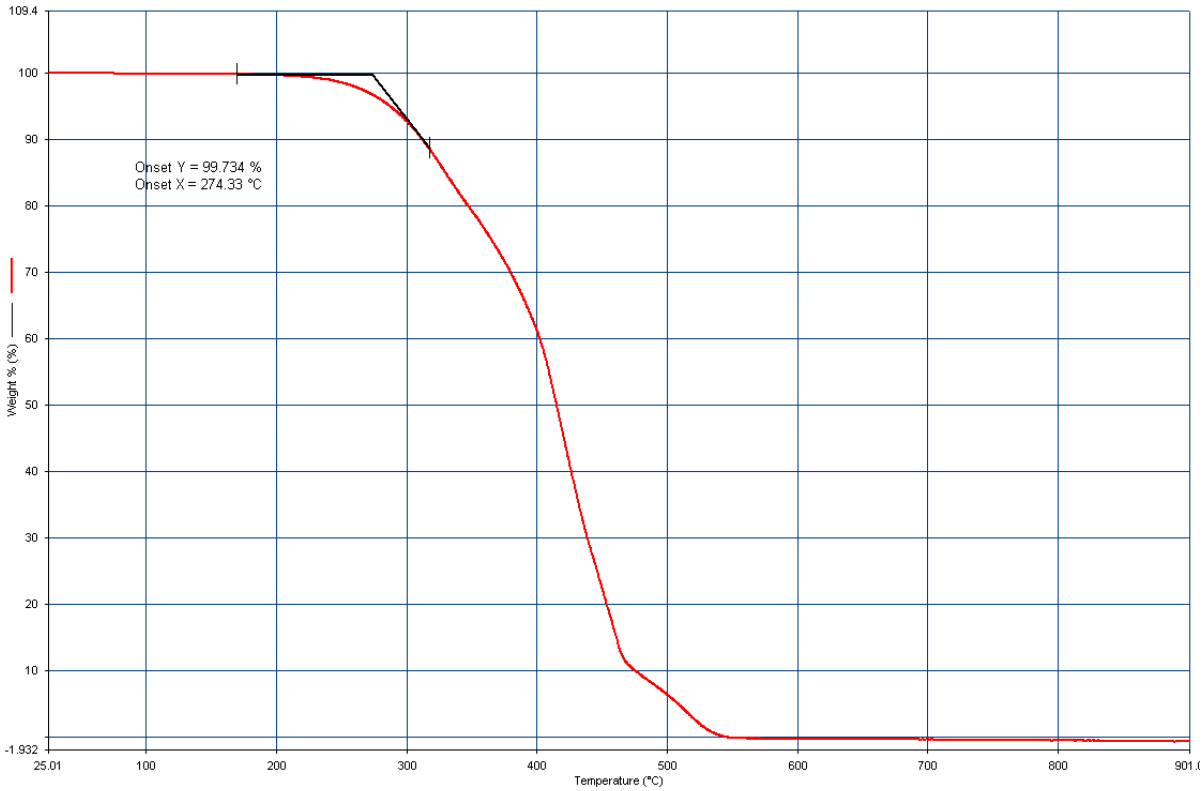

Figure 3.16 TGA Thermogram of prepolymer AA BD 1 prepolymer showing onset evaluation method

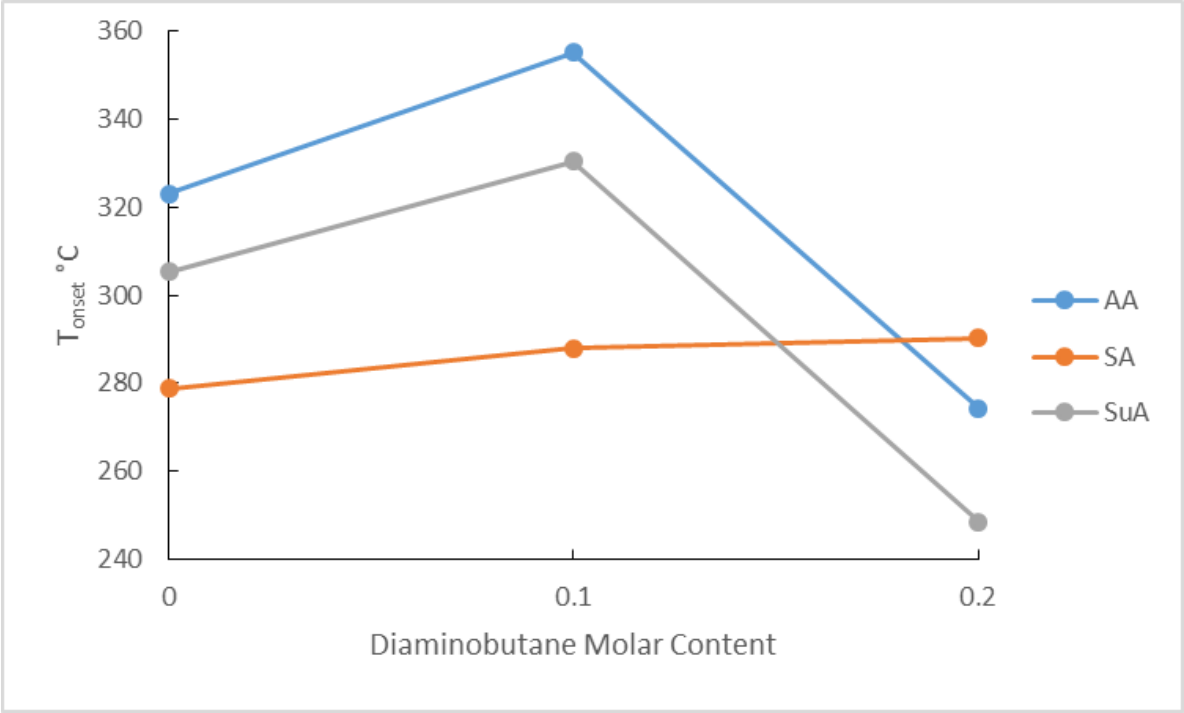

Figure 3.17 Plot of prepolymer T_{onset} against DAB content

3.2.5 DMA Compression Analysis of Prepolymers

DMA in compression mode was employed to determine the thermal transitions of the various prepolymers and establish if there is a correlation between the transitions, such as T_g, and composition. The assumed glass transition (T_g), or melting temperature (T_m), was determined from the peak maxima of the tan δ signal, as shown in Figure 3.18. Generally, DMA is a more sensitive technique to determine T_g than DSC.

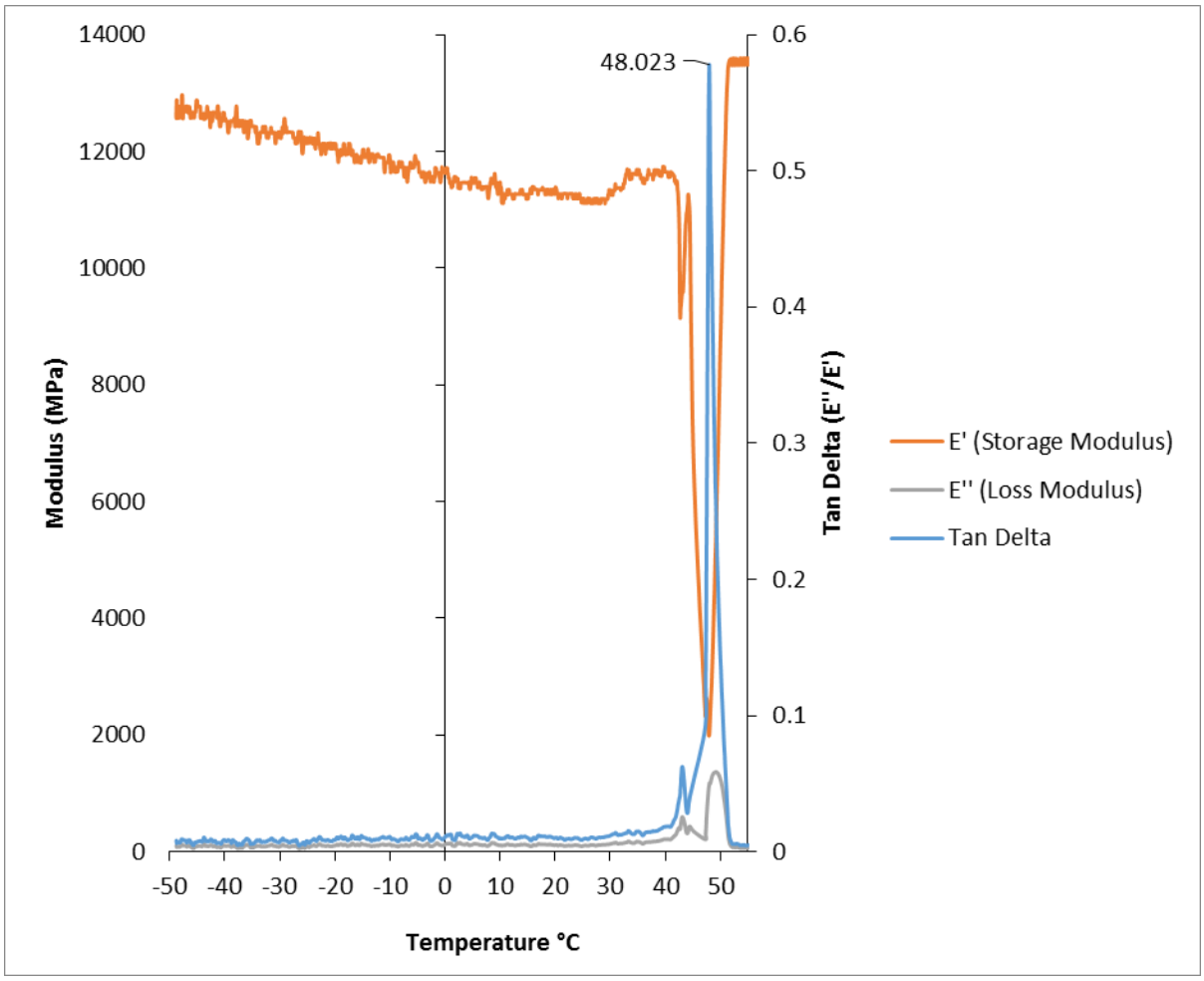

Figure 3.18 DMA thermogram of AA BD 0.8 prepolymer showing storage (E') and loss moduli (E") and, tan δ

The prepolymer transition temperature values from DMA analysis as a function of DAB content are shown in Figure 3.19. The transition temperature values for the polyester prepolymers was about 44°C for the AA and SuA based prepolymers and 100°C for the SA prepolymer. The prepolymer thermal transition values resulting from DMA compression analysis were comparable to the melt temperatures from DSC analysis and therefore assigned as T_m, as shown in Table 3.6. A statistical comparison of the DSC melt temperatures and DMA T_m temperatures will be discussed later. The addition of DAB to the SA and AA based prepolymer slighly increased its T_m, while a greater increase (20°C) was observed for the SuA prepolymers. Work by Wang, et al., (2016) on poly(ester-amines) showed that T_g values determined by DMA decreased as DAB content was increased. The DAB levels in Wang's study were considerably higher than what was used in the current study. This range of prepolymer T_ms will be useful in preparing lignin-copolymers with a span of properties.

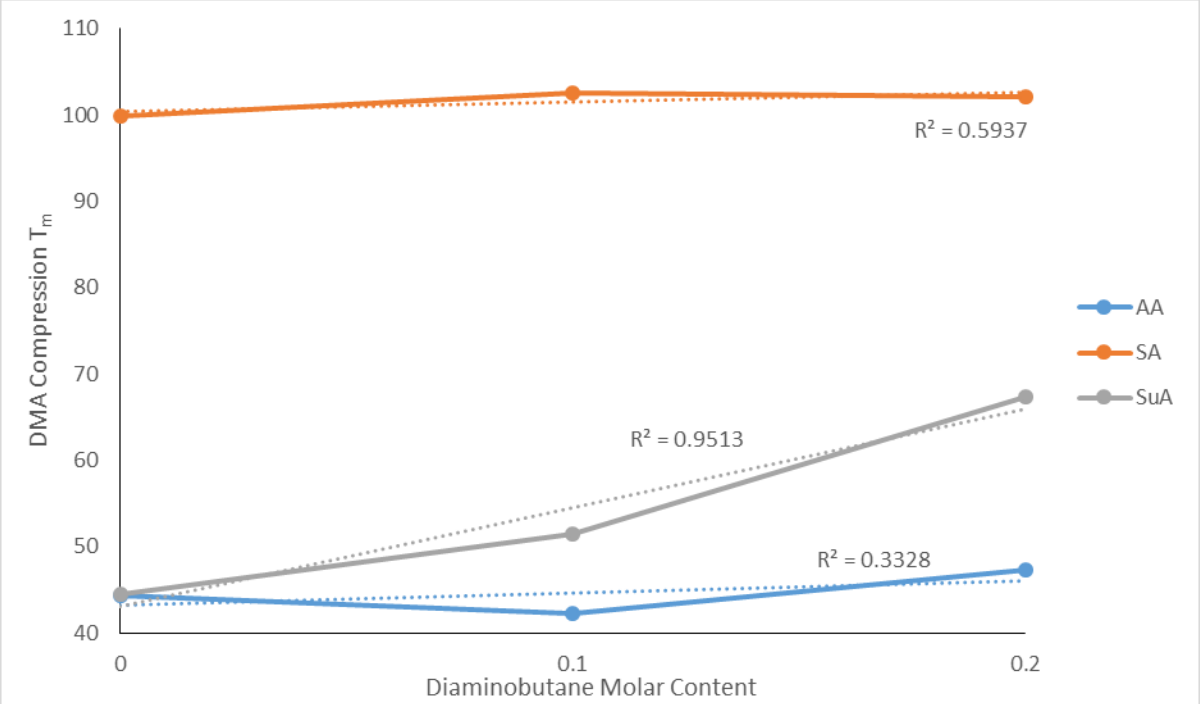

Figure 3.19 Plot showing T_m (determined by DMA) as a function of prepolymer DAB content

Table 3.6 T_m by compression DMA compared with T_m by DSC analysis

Thermal transition	Prepolymer								
	BD 0.8			BD 0.9			BD 1		
	AA	SA	SuA	AA	SA	SuA	AA	SA	SuA
T_m DMA (°C)	47.3	102.0	67.4	42.3	102.5	51.5	44.4	99.9	44.5
T_m DSC (°C)	27.3	103.8	32.5	34.1	105.6	45.3	40.0	103.3	44.7

3.3 Lignin-Copolymers Without Catalyst

To form the lignin-copolymer, lignin as received was added and dispersed in the liquid prepolymer and reacted by melt condensation. The influence of prepolymer composition (diacid type, DAB content) and lignin content on lignin-copolymer properties were examined. The lignin copolymers were formed into sheets ranging from flexible to brittle materials and had a dark brown appearance. The chemical, thermal and mechanical properties of the various lignin-copolymers were determined as discussed below. This section deals with lignin copolymers created without catalyst. Chapter 4 will address copolymers created with catalyst and ball-milled lignin.

3.3.1 FT-IR Analysis of Lignin Copolymers

FT-IR analysis was used to gain evidence on the polymerization reaction between prepolymer and lignin. In particular, an AA series both with and without DAB was monitored so that the differences between formation of ester (1725 cm^{-1}) and amide (1690 cm^{-1}) bands could be evaluated after peak fitting. The percentages of ester, acid and amide bands in a AA BD 0.8 30 wt% lignin copolymer are plotted against reaction time in Figure 3.20. The ester band is seen to increase (up to 70% in 40 h) in conjunction with a decrease in the acid, as was expected. The amide however is observed to remain relatively stable (25-30%) throughout the duration of polymerization, similar to what was observed in the prepolymers. The total amide + ester bands at 40 h reached about 90%. This suggests that the amide reacts very quickly and early on in the polymerization reaction. Figure 3.21 shows the percent of acid and ester plotted against reaction time in a AA BD 1 30 wt% lignin copolymer. Esterification reached about 80% in 30 h.

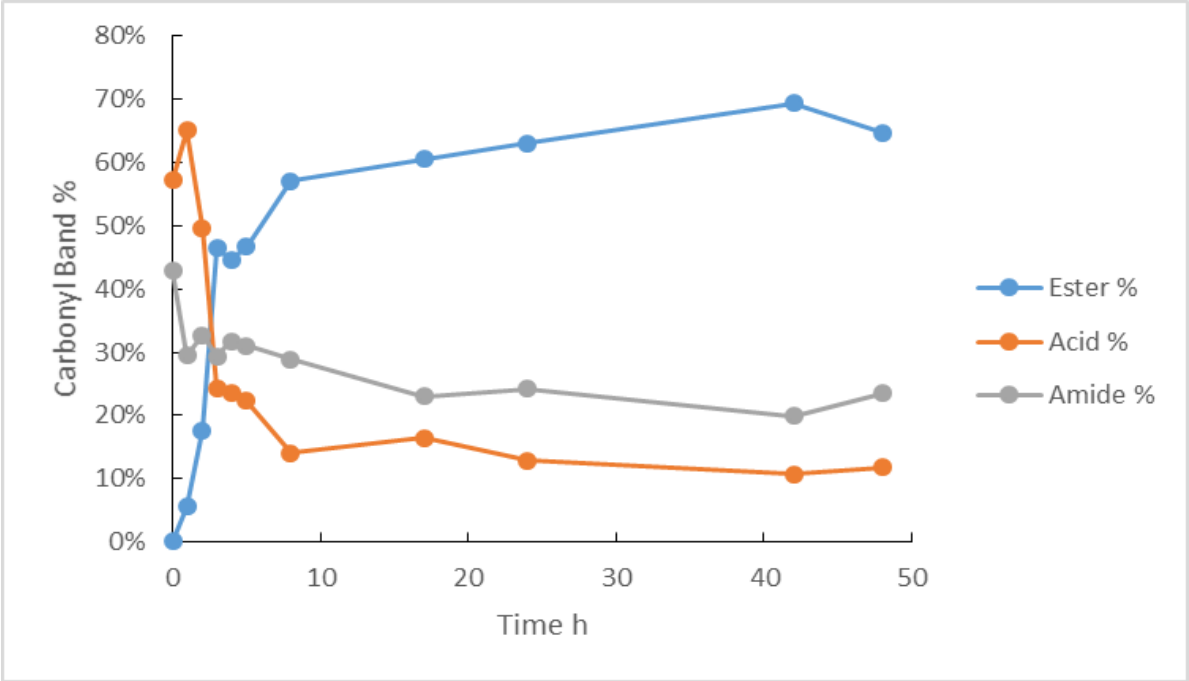

Figure 3.20 Ester, acid and amide % of carbonyl band for AA BD 0.8 30 lignin wt% copolymer

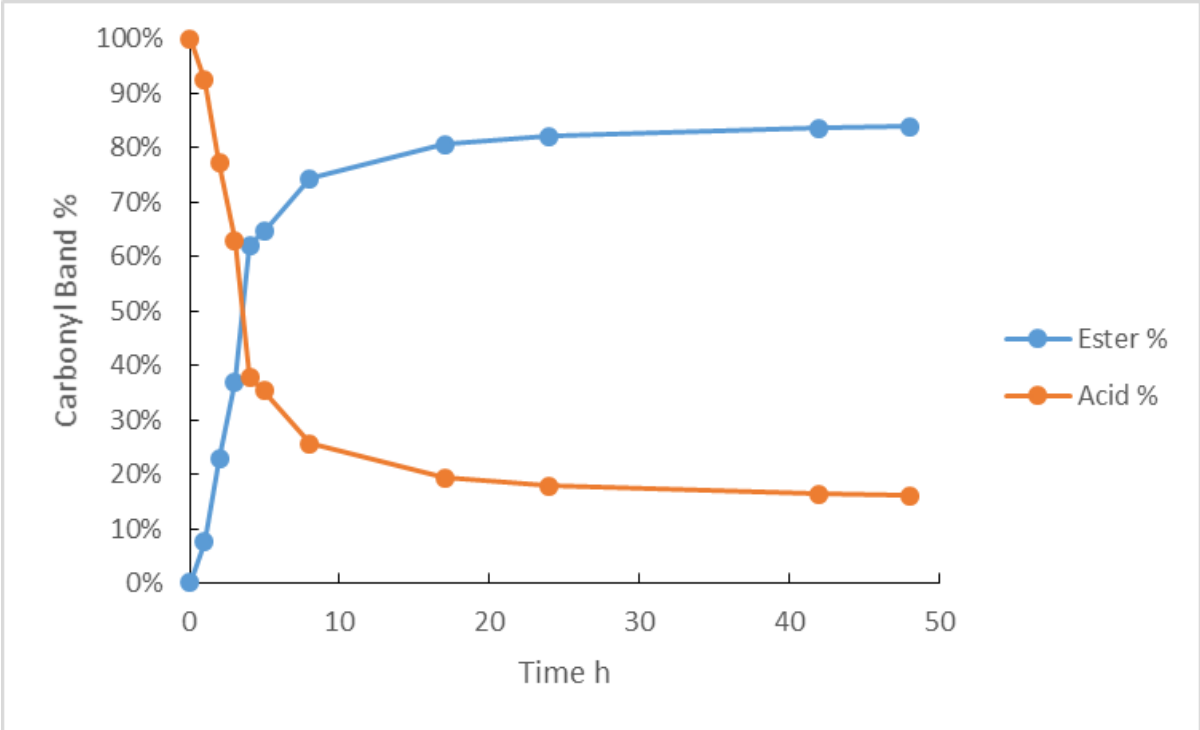

Figure 3.21 Ester and acid % of carbonyl band for AA BD 1 30 lignin wt% copolymer

3.3.2 Thermal Analysis of Lignin Copolymers

The thermal properties of the lignin copolymers were explored using DSC, DMA and TGA.

3.3.2.1 DSC Analysis of Lignin Copolymers

The thermal properties (T_g and T_m) of the various lignin-copolymer formulations were determined by DSC. These were the copolymers containing AA, SA and SuA diacids, each at 10, 20, 30, 40 and 50 wt% lignin and 0, 0.1 and 0.2 molar DAB content. Figure 3.22 through Figure 3.30 show DSC thermograms for the lignin based copolymers ranging from 0 to 50 wt% lignin content. The T_g DSC assignment for the lignin-copolymers still needs to be confirmed and could arise from amorphous polyester/amine zones in the copolymer. The suggested T_gs span a range from -50 to 22 °C. Figure 3.31, Figure 3.32 and Figure 3.33 are graphs of the T_g results plotted against lignin wt% and DAB levels, respectively for AA, SA and SuA based polymers. The T_g's are typically very weak or indiscernible as for the following copolymers: SA BD 0.9 10 wt% lignin sample, AA BD 0.9 0 wt% lignin, AA BD 1 10 and 20 wt% lignin, SuA BD 0.8 10 and 20 wt% lignin, SuA BD 0.9 0, 10, 20 and 30 wt% lignin and SuA BD 1 30 wt% lignin. In almost every case the T_g's that are observed are seen to increase with lignin content. This is especially true upon changing the lignin content from 40 to 50 wt%. The exception is the SuA BD 1 series of copolymers which maintain a consistent T_g around 25°C across all lignin levels where a T_g is observed. Some copolymers appear to decrease T_g before rising again at higher lignin contents. This is the case for AA BD 1 as well as SuA BD 0.8 which exhibit decreasing T_g to 30 wt% lignin at which point the T_g then increases at 40 and 50 wt% lignin. The T_g also appears to broaden as lignin content is increased, especially at the 40 and 50 wt% levels.

The AA series of copolymers span the greatest range in T_g values, ranging from -50°C to 19°C for the AA BD 0.8 copolymers (Figure 3.22 to Figure 3.24). This series demonstrates a strong positive correlation between increasing lignin and T_g. The AA BD 0.8 copolymers had the highest T_g values at the 20 to 50 wt% lignin levels but at the 0 and 10 wt% lignin levels the T_g seems to dip below the copolymers containing less DAB.

For the SA copolymers the values for T_g were around -25°C up to the 20 wt% lignin level (Figure 3.25 to Figure 3.27). At the 30 wt% lignin level the SA BD 0.8 copolymer increases dramatically to around -5°C. All the SA copolymers increase in T_g above 30 wt% lignin from a low of -26°C for both SA BD 0.9 and 1 at 30% to a high of 20°C for SA BD 0.9 at 50%. At the 40 wt% lignin level for SA copolymers a trend is observed where the T_g increases in order of increasing DAB content (-25 to -1^{o}C). This trend does not continue at the 50 wt% lignin level however. At 50 wt% lignin the SA copolymer which exhibited the greatest T_g value (20^{o}C) is the BD 0.9 sample.

The SuA copolymers did not have many samples with a discernable T_g (Figure 3.28 through Figure 3.30). The SuA BD 1 copolymers exhibited an interesting behavior, however, the T_g for these samples appears to respond very little to changing lignin content and the value remains stable around 25°C. This contrasts rather vividly with the SuA BD 0.8 and 0.9 samples which are observed to increase approximately 30°C upon changing the lignin content from 40 to 50 wt%. At the 50 wt% level the order of T_g is also observed to increase with increasing DAB content (from -25 to 8^{o}C).

The presence of cold crystallization exothermic peaks (~-20^{o}C) is also noted in many of the thermograms for the SuA based lignin-copolymers (Figure 3.28 through Figure 3.30). Examples are SuA BD 0.9 30 and 20 wt% lignin as well as SuA BD 0.8 30 and 20 wt% lignin. The exotherm is not unique to the SuA copolymers, however, it is also observed for SA BD 0.9 0, 10, 20 and 30 wt% lignin as well as AA BD 0.9 20% lignin (Figure 3.26 and Figure 3.23). In several series of copolymers the presence of two distinct exotherms is noted. For the AA BD 0.9 20% lignin sample a large exotherm centered near 0°C dwarfs a smaller exotherm located near -25°C. The same features are present in the AA BD 0.8 10% lignin sample. This behavior has been documented in the literature (Rizzuto, et al., 2017).

Melt endotherms were observed in all samples up to 20 wt% lignin. Many of the lignin-copolymers exhibited melt endotherms at the 30 wt% lignin level, with the exception of SuA BD 0.8, SA BD 0.8, AA BD 0.8 and 1 copolymers. The AA copolymers do not appear to

change T_m much in response to lignin content (Figure 3.34). However, the DAB content does affect the T_m such that the AA BD 0.8 sample yields the lowest T_m of 29°C followed by AA BD 0.9 and the AA BD 1 sample yields the highest T_m at 42°C.

The SA copolymers decrease T_m in response to increasing lignin content and amorphous content (Figure 3.35). There is also a well-defined trend in which the copolymers increase in T_m with decreasing DAB content (Figure 3.35). The SA copolymers exhibited considerably higher T_m values as compared against the AA and SuA copolymers. The SA copolymers T_m span a range from 90-106°C compared with 29-41°C for AA copolymers and 31-45°C for SuA copolymers. This clearly shows that the short diacid (SA) had the higher melt temperature in the lignin copolymers.

The SuA copolymers exhibit a similar trend where the T_m decreases with increasing lignin content (Figure 3.36). This is true of the SuA 0.9 and SuA BD 1 copolymers but the SuA BD 0.8 copolymers actually seem to increase in T_m with increasing lignin content. In addition, for many of the samples the melt endotherm appears to decrease in intensity as lignin is increased. This suggests that lignin (an amorphous polymer) inhibits copolymer crystallization by its presence. This observation is supported by the polarized optical microscopy and XRD results in section 3.3.2.5 and 3.3.4 respectively. The results observed through DSC analysis of melt behavior are consistent with the results from melt testing which can be seen in Table 3.15

An additional second order, higher temperature transition can be seen in many of the DSC thermograms around 125°C (Figure 3.22 to Figure 3.30). The temperature where this transition occurs does not change considerably in response to increasing lignin content (Table 3.7). In addition, samples containing 0% lignin do not exhibit this transition. This transition is very close to the lignin T_g of 143°C reported from TMDSC earlier in this study. For these reasons it is hypothesized that this transition can be attributed to the T_g of lignin. The 0 wt% lignin samples were observed to turn to a brown color as the polymerization proceeded and possibly due to degradation. The presence of this separate second order transition suggests

incomplete polymerization, without the use of catalyst, and the presence of a heterogeneous material (Gao, Karaaslan, & Kadla, 2014).

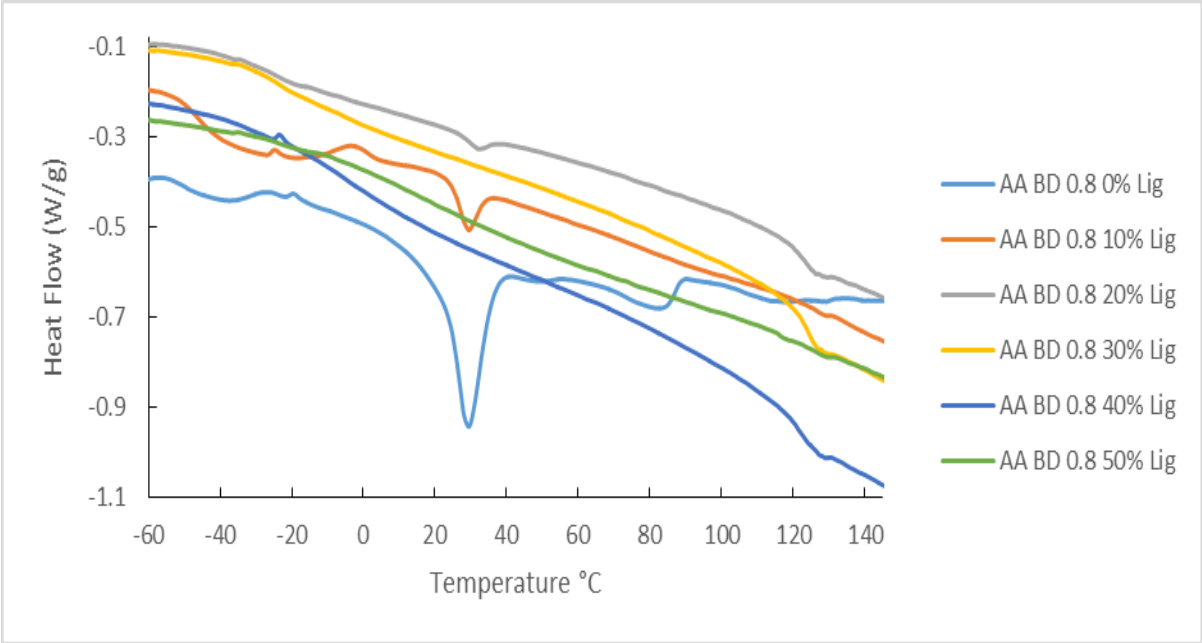

Figure 3.22 DSC thermograms of lignin-copolymer AA BD 0.8 with 0 - 50 wt% lignin

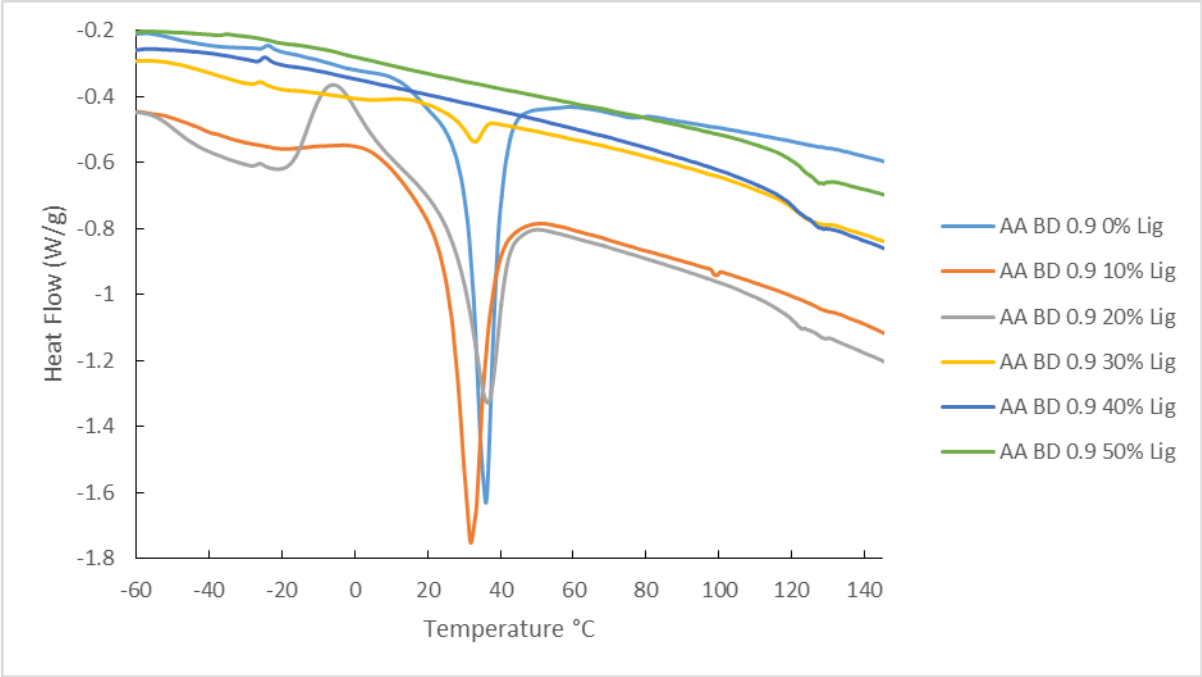

Figure 3.23 DSC thermograms of lignin-copolymer AA BD 0.9 with 0-50 wt% lignin

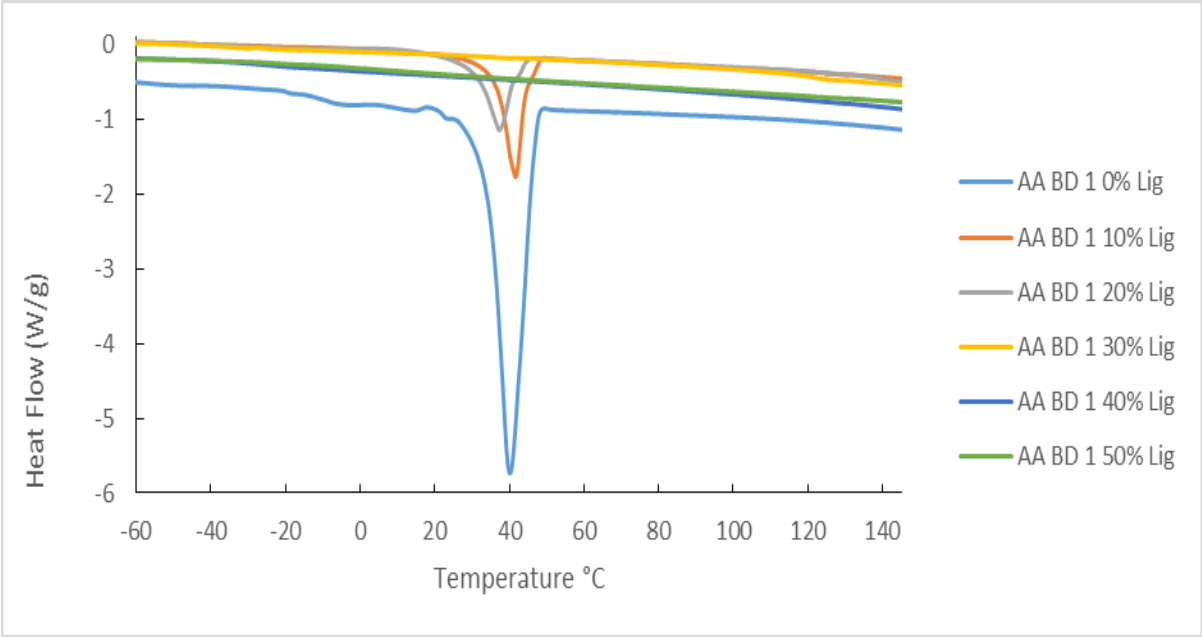

Figure 3.24 DSC thermograms of lignin-copolymer AA BD 1 with 0-50 wt% lignin

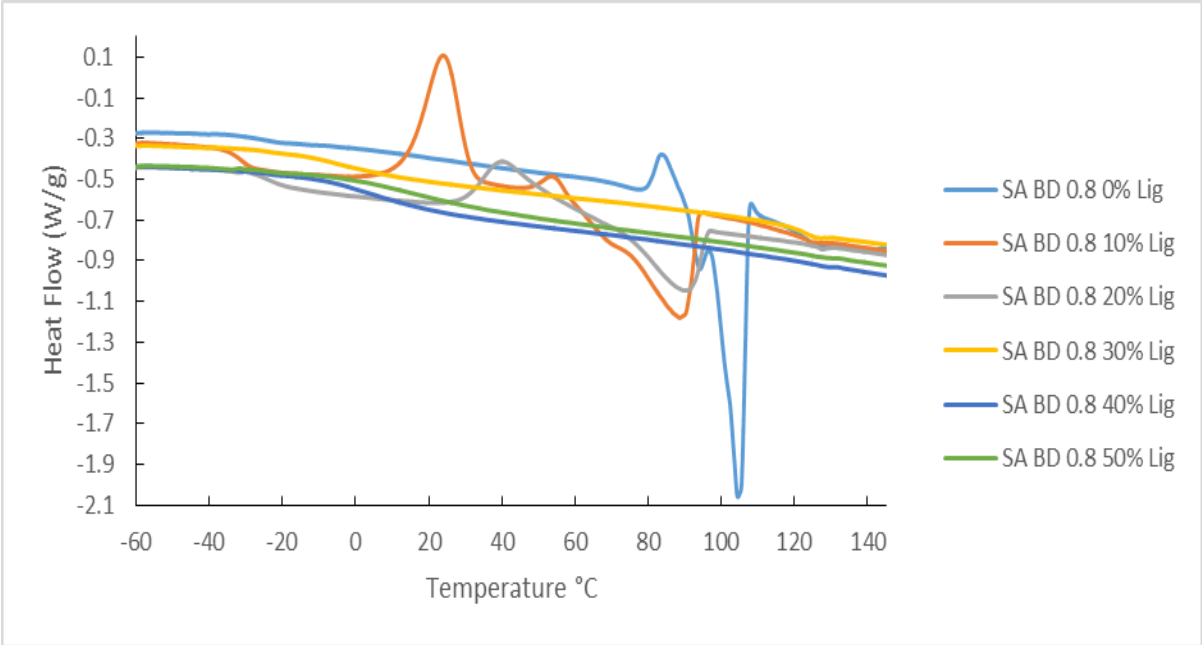

Figure 3.25 DSC thermograms of lignin-copolymer SA BD 0.8 with 0-50 wt% lignin

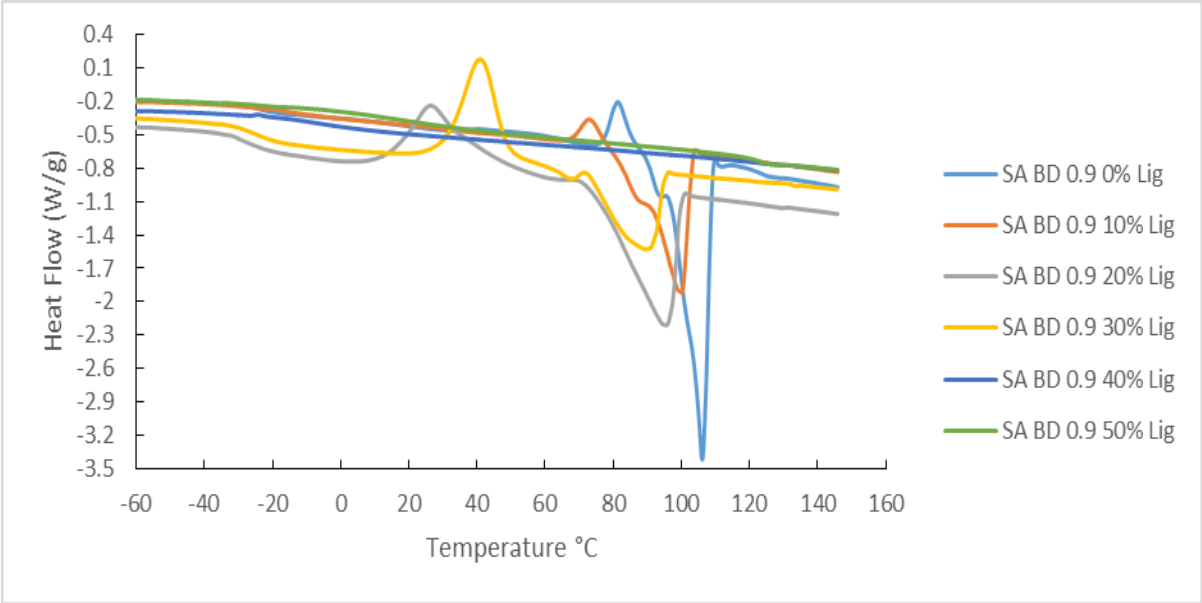

Figure 3.26 DSC thermograms of lignin-copolymer SA BD 0.9 with 0-50 wt% lignin

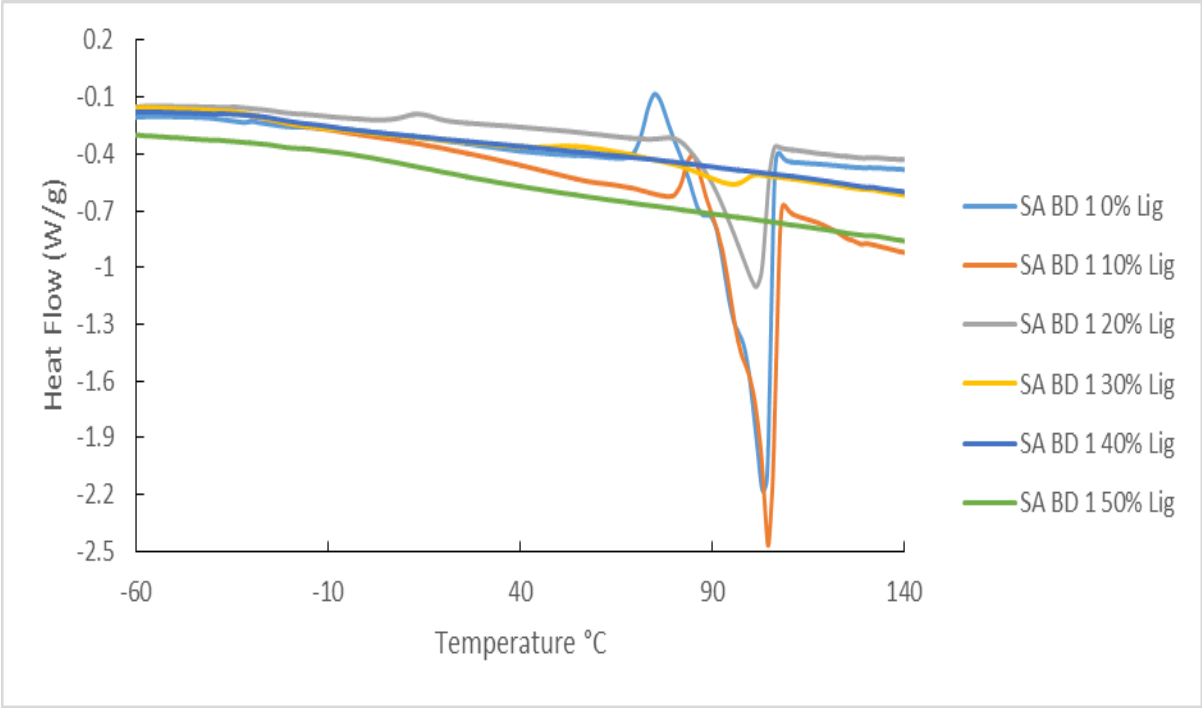

Figure 3.27 DSC thermograms of lignin-copolymer SA BD 1 with 0-50 wt% lignin

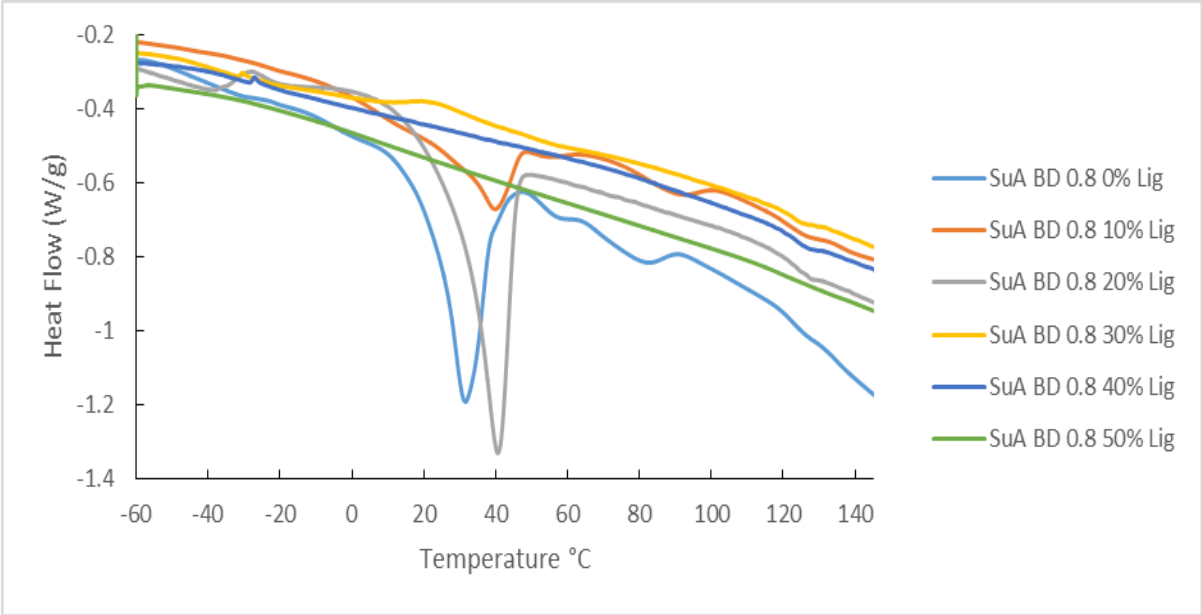

Figure 3.28 DSC thermograms of lignin-copolymer SuA BD 0.8 with 0-50 wt% lignin

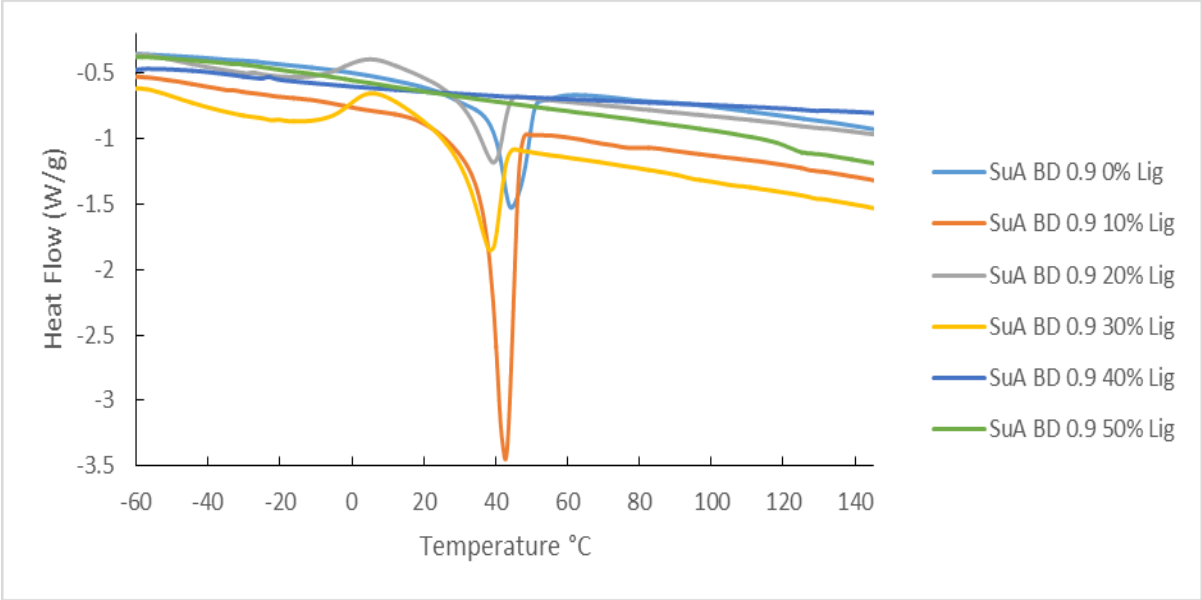

Figure 3.29 DSC thermograms of lignin-copolymer SuA BD 0.9 with 0-50 wt% lignin

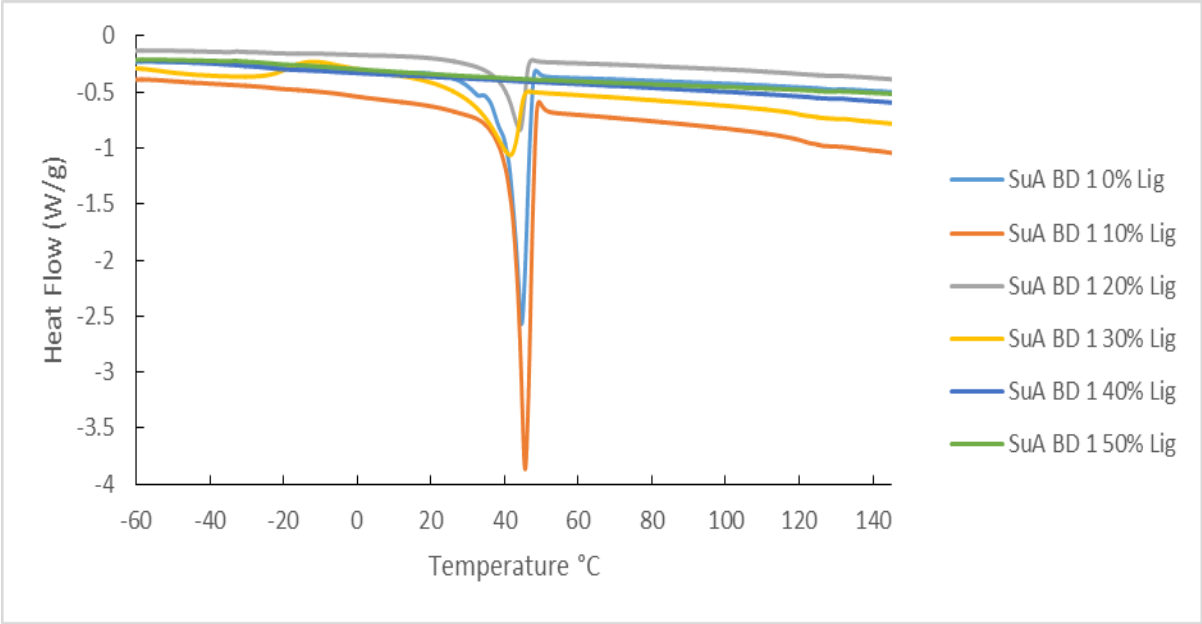

Figure 3.30 DSC thermograms of lignin-copolymer SuA BD 1 with 0-50 wt% lignin

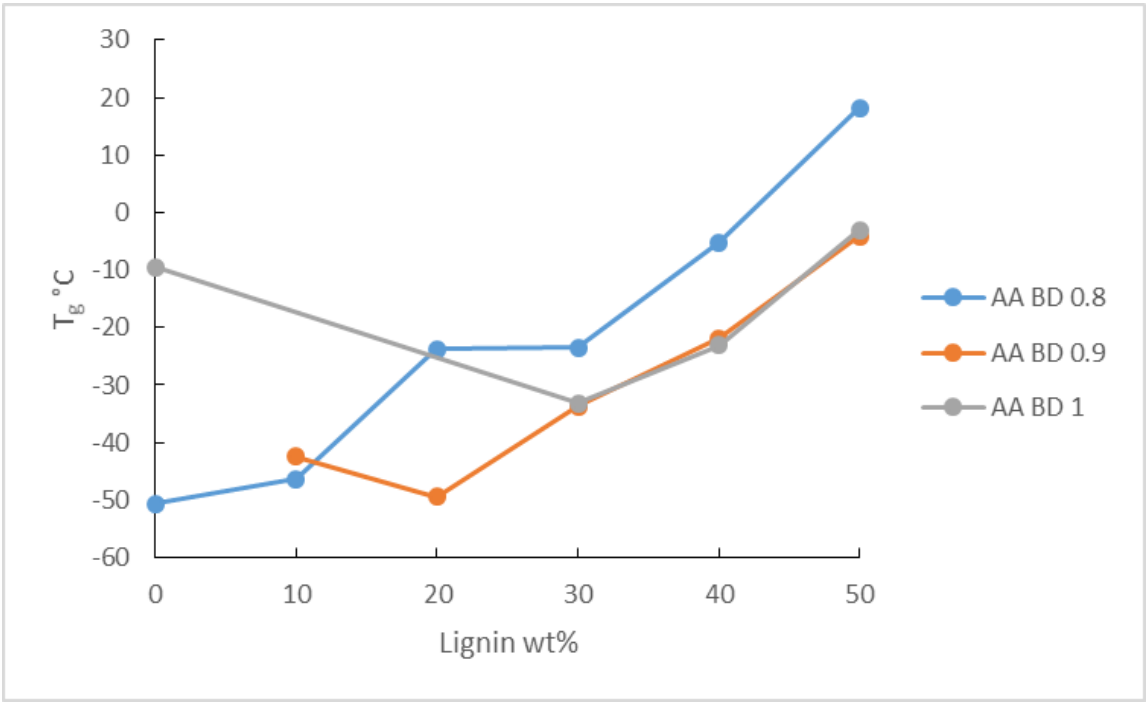

Figure 3.31 Plot of T_g versus lignin wt% of the AA based lignin copolymers at varying DAB levels as determined by DSC.

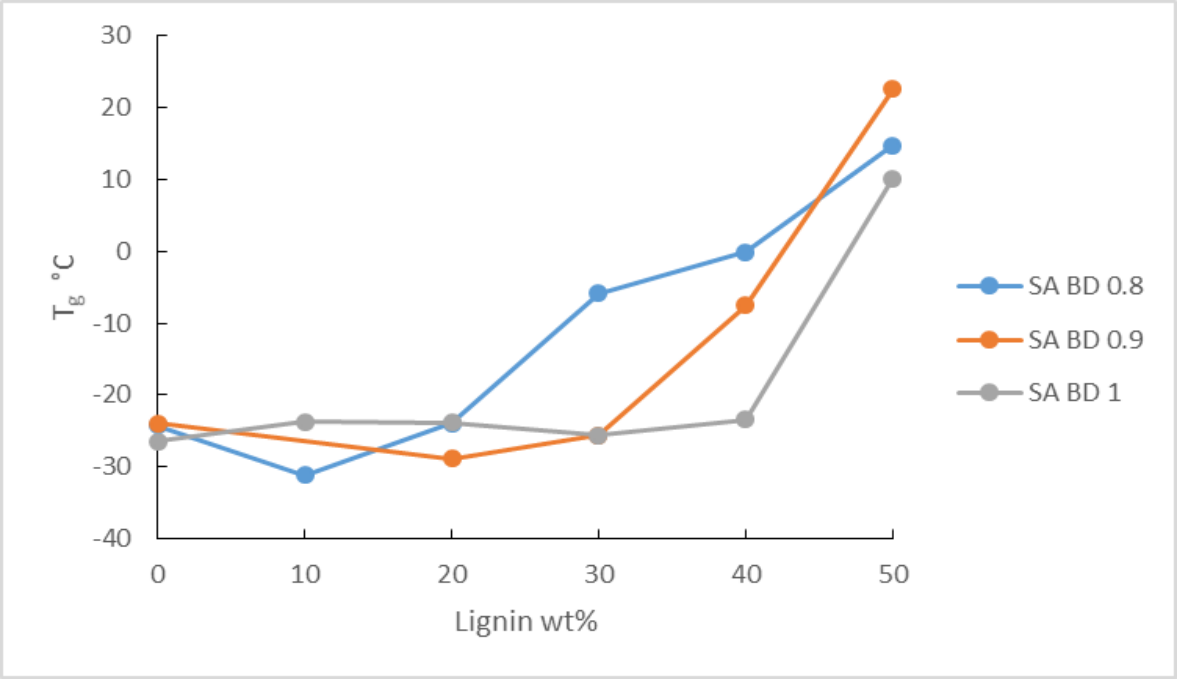

Figure 3.32 Plot of T_g versus lignin wt% of the various SA based lignin copolymers at varying DAB levels as determined by DSC

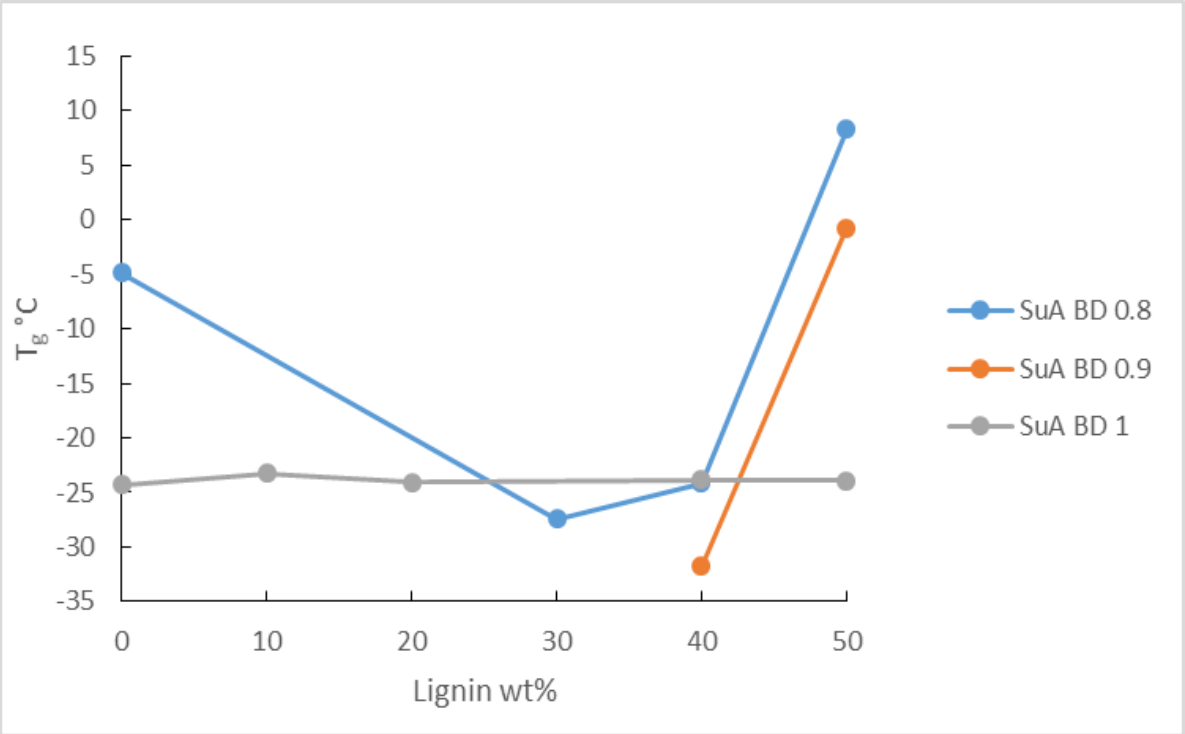

Figure 3.33 Plot of T_g versus lignin wt% of the SuA based lignin copolymers at varying DAB levels as determined by DSC

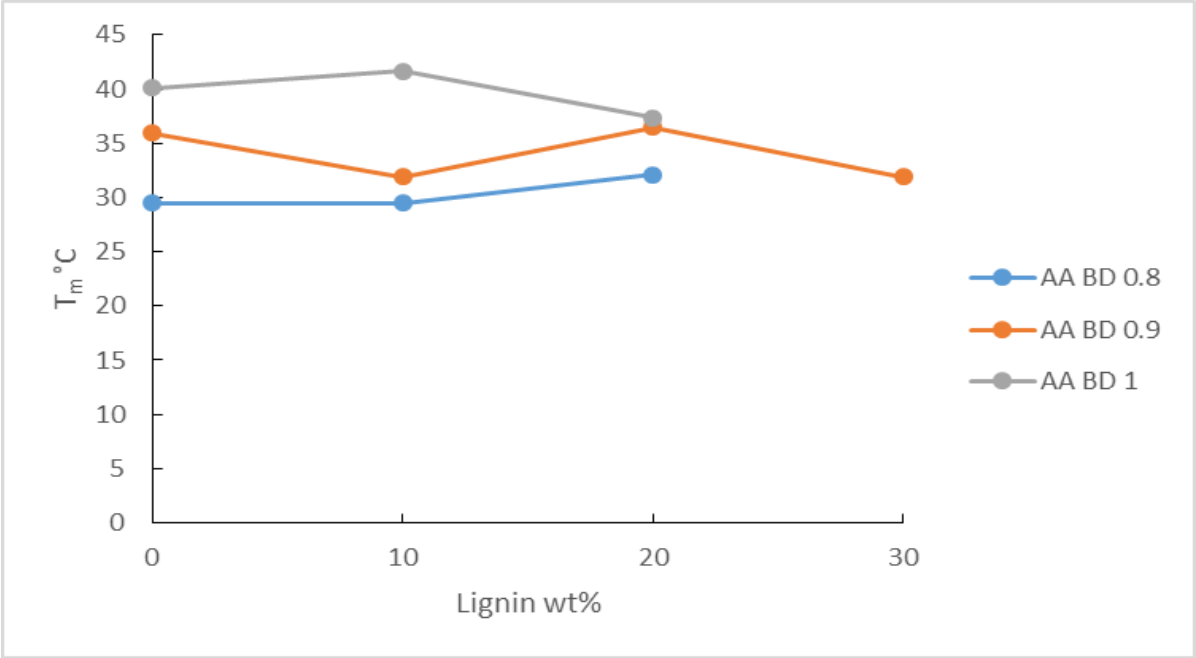

Figure 3.34 Plot of T_m versus lignin wt% for AA lignin copolymers as determind by DSC

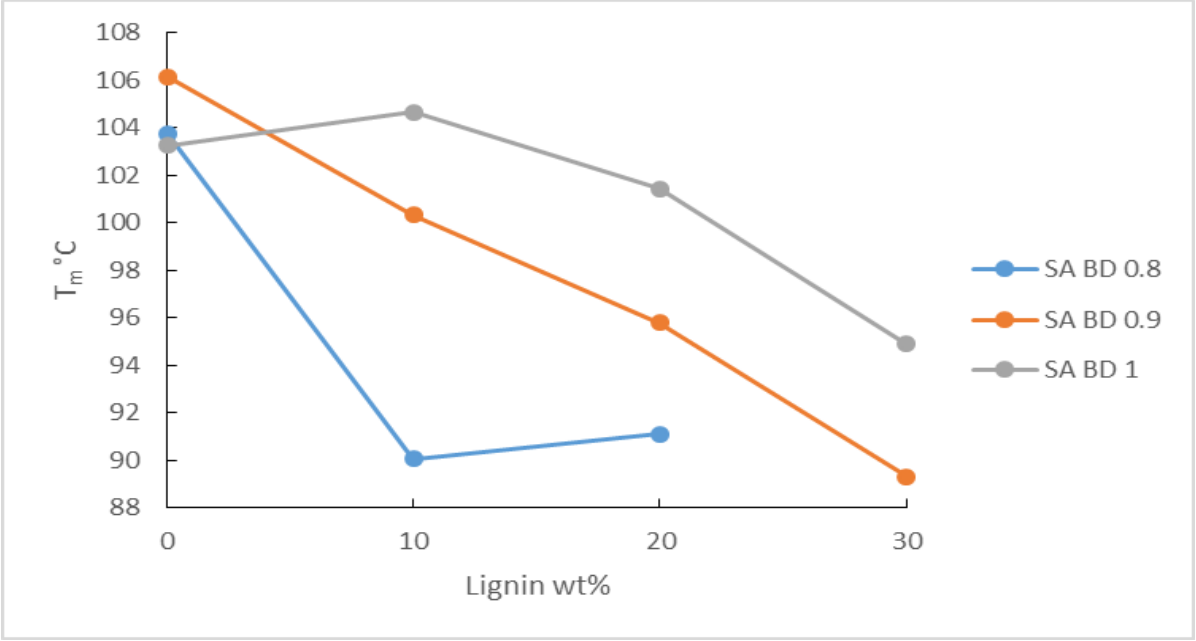

Figure 3.35 Plot of T_m versus lignin wt% for SA lignin copolymers as determind by DSC

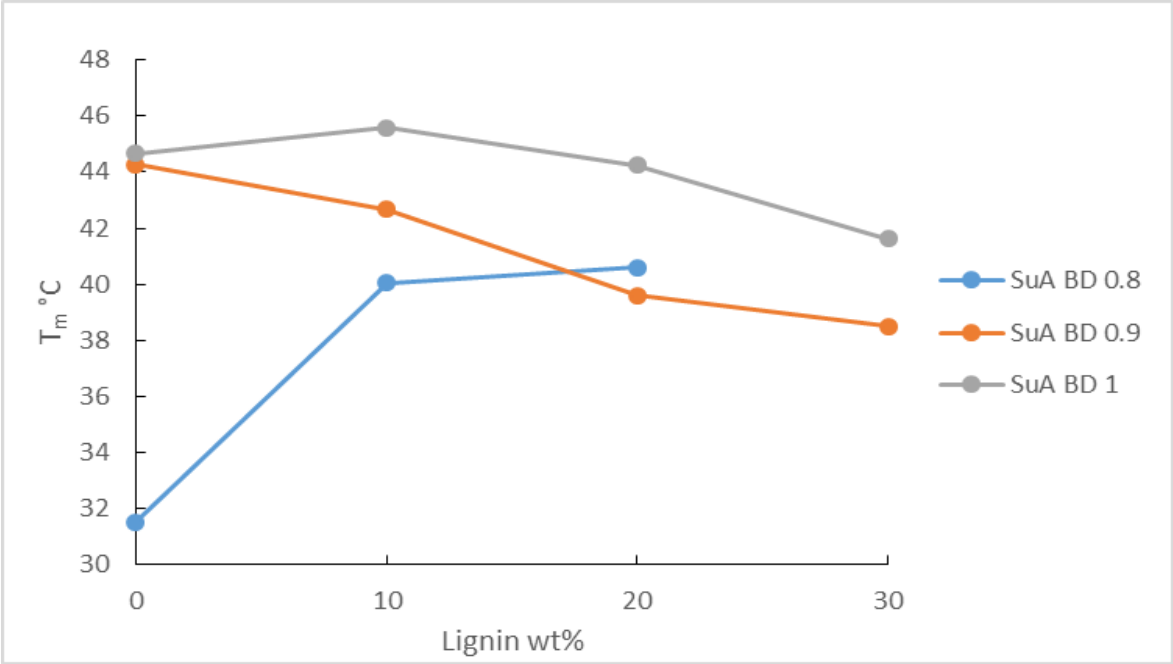

Figure 3.36 Plot of T_m versus lignin wt% for SuA lignin copolymers as determind by DSC

Table 3.7 High temperature second order transition temperature (°C) for the various lignin-copolymers determined by DSC

Lignin content	AA BD 0.8	AA BD 0.9	AA BD 1	SA BD 0.8	SA BD 0.9	SA BD 1	SuA BD 0.8	SuA BD 0.9	SuA BD 1
					Transition temperature (°C)				
0%					122.39			124.32	126.24
10%	125.98	124.97		122.88		128.46	121.25	125.32	120.69
20%	122.92	119.74	127.21	125.21			124.39	120.26	118.44
30%	123.63	121.36	121.43	122.7	130.98	124.59	122.02	126.42	119.18
40%	121.99	120.58		125.85	123.32	126.43	123.77	125.75	123.64
50%	116.09	123.68		124.86	123.02	123.44	126.63	121.86	124.43

3.3.2.2 DMA of Lignin Copolymers

The thermal properties (T_g or T_m) of the various lignin-copolymer formulations were also determined by DMA in compression mode, using the tan δ signal, which is a more sensitive technique than DSC. It is believed that the transition observed by DMA at 40°C is a softening temperature (T_s) or T_m and correlates with the T_m determined by DSC at 31°C for AA BD 0.9 10% lignin copolymer (Figure 3.37). The T_m's ranged from 38 to 103°C depending on composition. Plots of T_m versus lignin content at 0, 0.1 and 0.2 DAB levels for AA, SuA and

SA based lignin copolymers are shown in, Figure 3.38, Figure 3.39 and Figure 3.40, respectively.

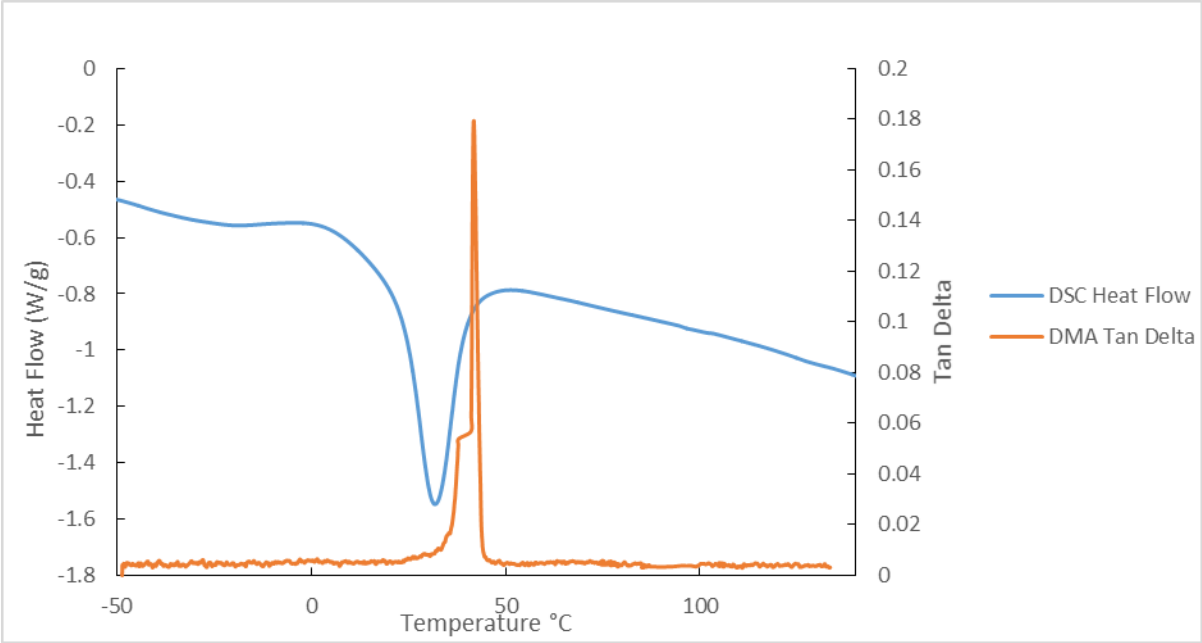

Figure 3.37 DMA tan delta signal w/ DSC heat flow signal for AA BD 0.9 10% lignin copolymer

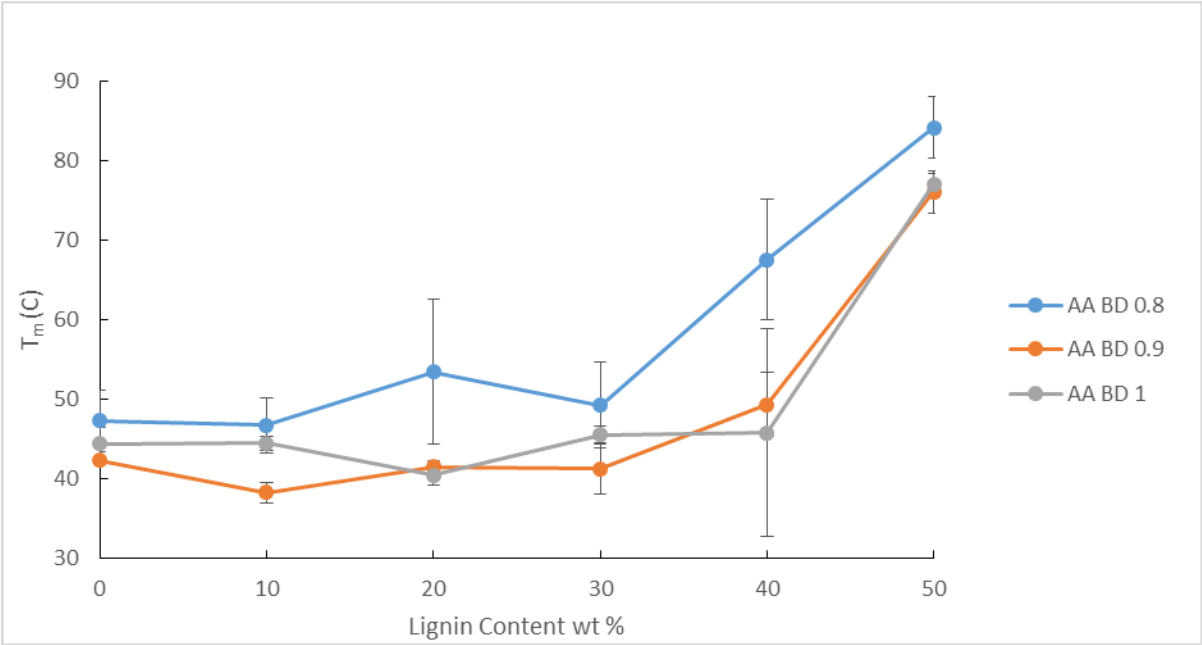

Figure 3.38 Plot of T_m (by DMA) versus lignin content for the AA based lignin-copolymers

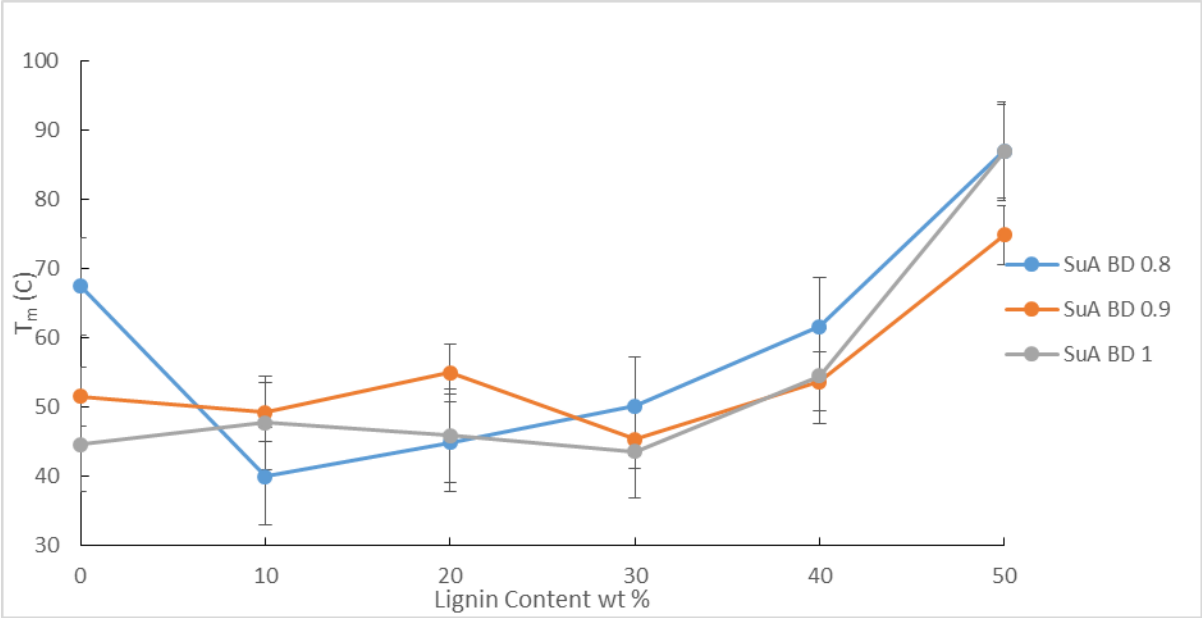

Figure 3.39 Plot of T_m (by DMA) versus lignin content for the SuA based lignin-copolymers

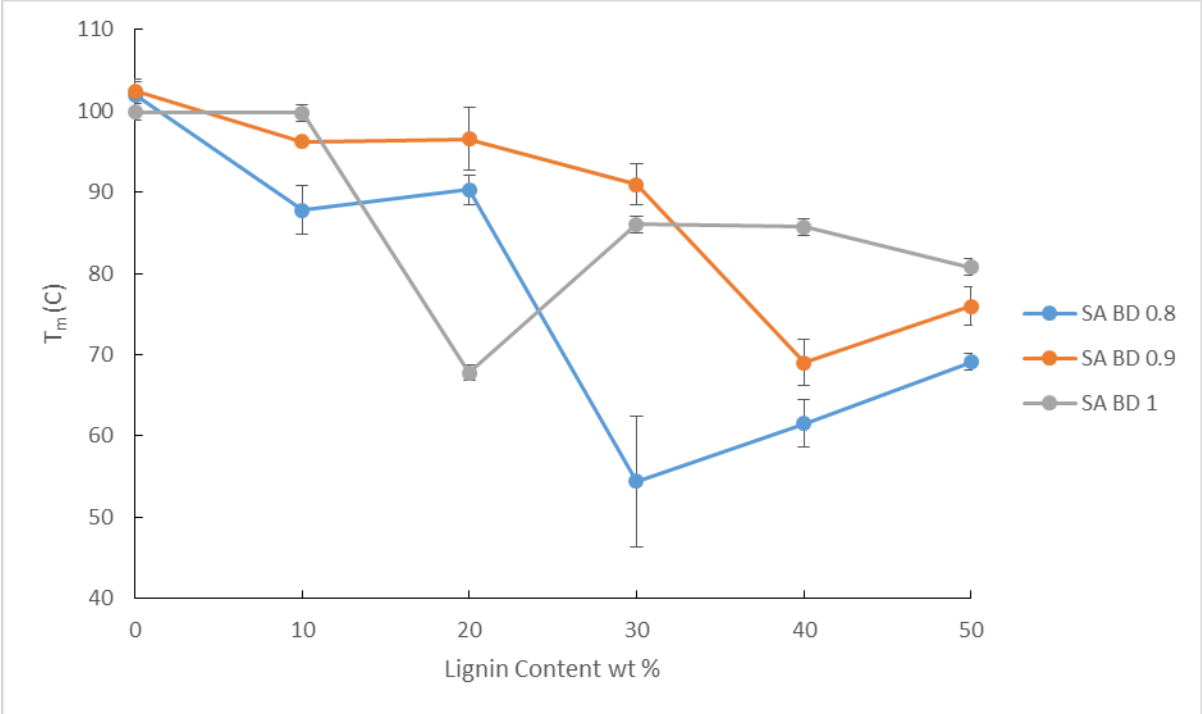

Figure 3.40 Plot of T_m (by DMA) versus lignin content for the SA based lignin-copolymers

The T_m values for the AA copolymers span a range from 38-82°C. Most of the increase occurs at lignin contents greater than 30 wt%. At lignin contents lower than 30 wt% the values for T_m are relatively stable at around 45^{o}C (Figure 3.38). The addition of DAB to the AA based lignin copolymer generally increased its T_m with DAB at 0.2 mole ratio gave the best performing lignin copolymers and the T_m could be tuned from 38 to 82^{o}C by varying the amount of lignin added (0 to 50%).

The T_m values for the SuA copolymers follow a similar trend to the AA based copolymers (Figure 3.40 and Figure 3.39). They span a range from 40-86°C. In the case of the SuA copolymers, as was observed for the AA copolymers, the majority of the T_m increase occurs at lignin contents greater than 30 wt%. In the case of the SuA BD 0.8 copolymer samples the T_m is seen to decrease from 68 to 40^{o}C upon increasing the lignin from 0 to 10 wt%. At the 0, 30 and 40 wt% lignin levels the DAB 0.2 copolymers exhibited the highest T_m values where at the 10 and 20 wt% levels it was the DAB 0.1 samples which gave the highest T_m values. At the 50 wt% lignin level the DAB 0 and 0.2 samples both yielded the maximum T_m value of 86°C for the SuA series of copolymers.

The SA copolymers seem to exhibit a decreasing T_m in response to increasing lignin content (Figure 3.40), in contrast to the AA and SuA copolymers. The SA copolymers T_m span a range from 55-103°C with the highest reported T_m value arising from the SA BD 0.9 0 wt% lignin-copolymer, whereas the AA and SuA copolymers exhibit the highest T_m at the 50 wt% lignin level. Also in contrast to the AA and SuA copolymers, is the observation that at the 10 to 50 wt% lignin the DAB 0.2 samples yield the lowest T_m. In the case of the AA and SuA copolymers the high level of DAB often yields the highest T_m. The SA BD 0.8 30 wt% lignin sample exhibited the lowest T_m value which was 55°C. The SA based polymer at the 0 wt% lignin had a T_m of 102°C which is considerably greater than T_m's for the SuA (55°C) and AA (45°C) based polymers. This demonstrates that the SA prepolymer molecules experience greater intermolecular attractive forces than do the SuA and AA based polymers. The reduced molecular mobility also reduces the dampening effect which can be seen by comparing the height of the tan δ signals for the 0 wt% lignin AA, SA and SuA based

polymers as shown in Figure 3.41. The tan δ signal for the SA sample is less intense than what is observed for the AA and SuA polymers which supports the hypothesis of reduced molecular mobility in SA based polymer (Sivasankarapillai & McDonald, 2010). This effect also has implications for the mechanical properties which will be discussed in section 3.3.5.

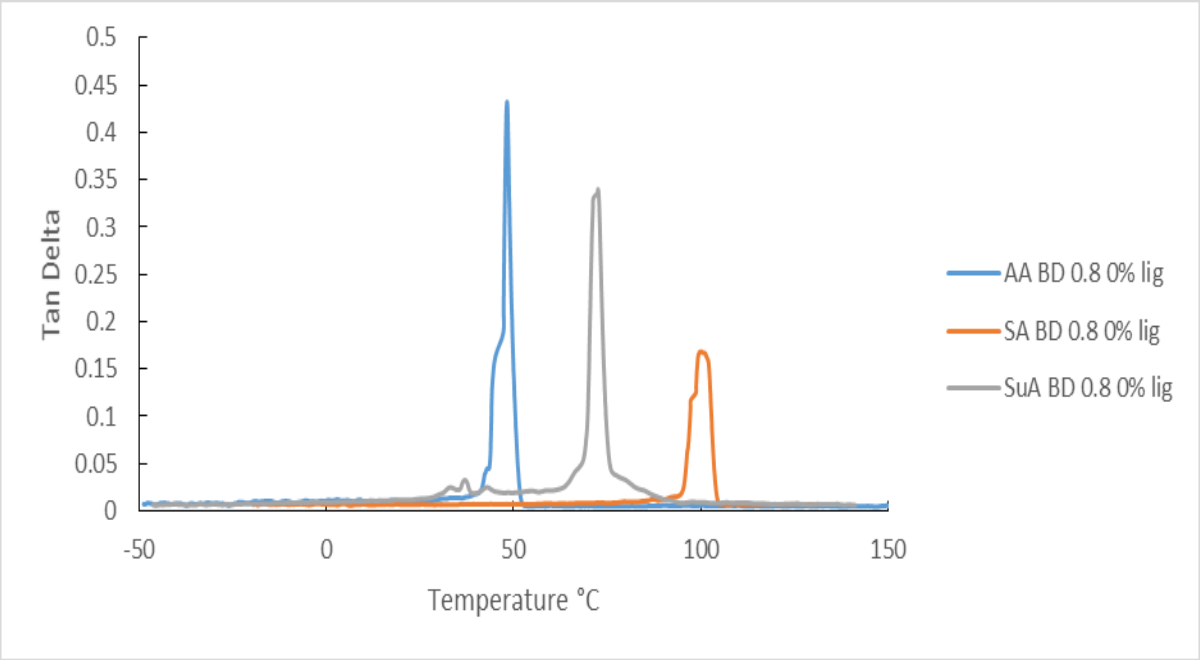

Figure 3.41 Tan δ signals for 0 wt% samples of AA, SA and SuA

In previous studies it has been reported that blends as well as copolymers containing lignin exhibit an increase in the T_g or T_s as lignin content is increased (Sallem-Idrissi, Sclavons, & Debecker, 2015) (Sivasankarapillai & McDonald, 2010). The AA and SuA copolymers from this study fit this trend. However, the SA copolymers do not follow this trend.

Table 3.8 Results from DMA T_m, DSC T_g and DSC T_m transition values for the various lignin-copolymers

DMA T_m (°C)									
Copolymer	SA			AA			SuA		
lignin wt%	BD 0.8	BD 0.9	BD 1	BD 0.8	BD 0.9	BD 1	BD 0.8	BD 0.9	BD 1
0	102.0	102.5	99.9	47.3	42.3	44.4	67.4	51.5	44.5
10	87.8	96.3	99.8	46.7	38.2	44.4	39.9	49.2	47.7
20	90.3	96.6	67.8	53.5	41.4	40.5	44.8	54.9	45.8
30	54.4	91.0	86.0	49.3	41.2	45.5	50.1	45.2	43.6
40	61.5	69.0	85.7	67.5	49.3	45.8	61.5	53.6	54.4
50	69.1	76.0	80.8	84.2	76.1	77.0	86.9	74.8	86.9
DSC T_g (°C)									
Copolymer	SA			AA			SuA		
lignin wt%	BD 0.8	BD 0.9	BD 1	BD 0.8	BD 0.9	BD 1	BD 0.8	BD 0.9	BD 1
0	-24.3	-23.9	-26.5	-50.6	n/a	-9.5	-4.9	n/a	-24.3
10	-31.1	n/a	-23.7	-46.3	-42.5	n/a	n/a	n/a	-23.2
20	-24.0	-28.9	-23.8	-23.8	-49.5	n/a	n/a	n/a	-24.1
30	-5.9	-25.6	-25.6	-23.5	-33.7	-33.2	-27.5	n/a	n/a
40	-0.1	-7.6	-23.5	-5.1	-21.9	-23.0	-24.2	-31.7	-23.8
50	14.7	22.7	10.2	18.2	-4.1	-3.1	8.3	-0.8	-23.9
DSC T_m (°C)									
Copolymer	SA			AA			SuA		
lignin wt%	BD 0.8	BD 0.9	BD 1	BD 0.8	BD 0.9	BD 1	BD 0.8	BD 0.9	BD 1
0	103.8	106.2	103.3	29.5	36.0	40.1	31.5	44.3	44.7
10	90.1	100.3	104.7	29.5	31.9	41.7	40.0	42.7	45.6
20	91.1	95.8	101.4	32.1	36.5	37.3	40.6	39.6	44.2
30	n/a	89.3	94.9	n/a	31.9	n/a	n/a	38.5	41.6
40	n/a	n/a	n/a	n/a	n/a	n/a	n/a	n/a	n/a
50	n/a	n/a	n/a	n/a	n/a	n/a	n/a	n/a	n/a

3.3.2.3 Statistical Analysis Comparing DSC T_m against DMA T_m

A statistical analysis comparing the DSC T_m against the DMA T_m temperatures was conducted A factorial design was used with unbalanced data with four factors which are considered random effects. These are 1) Lignin content, 2) DAB content, 3) Method used for T_g and T_m determination and 4) Type of acid. The generalized linear model for this experiment is shown below.

$$y_{ijklm} = \mu + a_i + b_j + g_k + d_l + ab_{ij} + ag_{ik} + ad_{il} + bg_{jk} + bd_{jl} + gd_{kl} + abg_{ijk} + abd_{ijl} + agd_{ikl} + bgd_{jkl} + abgd_{ijkl} + e_{ijklm}$$

In this model y represents the response, μ the grand mean, a_i b_j g_k d_l represent the effect of the 4 variables, the ab_{ij} terms represent the two way interactions between the variables, abg_{ijk} terms represent the three way interactions, $abgd_{ijkl}$ represents the four-way interaction and e_{ijklm} represents the error. In the application of this model we are testing the null hypothesis to determine the significance of variables. The null hypothesis is shown below and states that the variances between treatments are equal to 0.

$$H_o: \sigma_t^2 = 0$$

The alternative hypothesis is shown below and states that the variances are greater than 0.

$$H_a: \sigma_t^2 > 0$$

In this study the criteria for significance was set at a 95% confidence level. The results from this analysis of variance are shown below in Table 3.9.

Table 3.9 Analysis of variance DSC T_m vs DMA T_m

	Sum Sq	Df	F value	Pr(>F)
(Intercept)	8944.904	1	229.728	1.61E-30
method	318.6814	1	8.184554	0.004925
Acid	5157.377	2	66.22733	1.47E-20
Diamine	43.61201	2	0.560034	0.572561
Lignin	3897.428	5	20.01919	9.14E-15
method:Acid	509.09	2	6.537368	0.001971
method:Diamine	102.8976	2	1.321337	0.270337
method:Lignin	13.42786	3	0.114954	0.951211
Acid:Diamine	462.6937	4	2.97079	0.021876
Acid:Lignin	9548.776	10	24.5237	1.94E-25
Diamine:Lignin	582.0895	10	1.494955	0.148186
method:Acid:Diamine	240.0729	4	1.541422	0.193987
method:Acid:Lignin	550.5827	6	2.356729	0.034097
method:Diamine:Lignin	5.369464	5	0.02758	0.999633
Acid:Diamine:Lignin	4146.922	20	5.325178	1.29E-09
method:Acid:Diamine:Lignin	766.0808	10	1.967492	0.041893
Residuals	5061.8	130		

Many of the p-values for the various interactions are below 0.05, indicating their significance. In the presence of significant interactions between treatments it is inadvisable to conclude anything about the main effects of treatments. However, the p-value of 0.005 obtained for the method treatment is quite close to the 0.05 cutoff for significance which suggests that there is not much difference in the resulting temperatures from each method. In other words, the DMA response could be the same as the melt temperatures obtained through DSC. As mentioned before the problem with this conclusion is that DMA analysis continues to provide a peak in the tan delta signal for the 40 wt% and 50 wt% lignin samples even when DSC analysis does not indicate a melt endotherm for these same samples. This observation refutes the results of the statistical analysis conducted.

3.3.2.4 TGA Analysis of Lignin Copolymers

TGA analysis was employed to explore the thermal stability of the lignin copolymers. The TGA thermograms for the lignin copolymer AA BD 0.8 series plus lignin samples are shown in Figure 3.42.

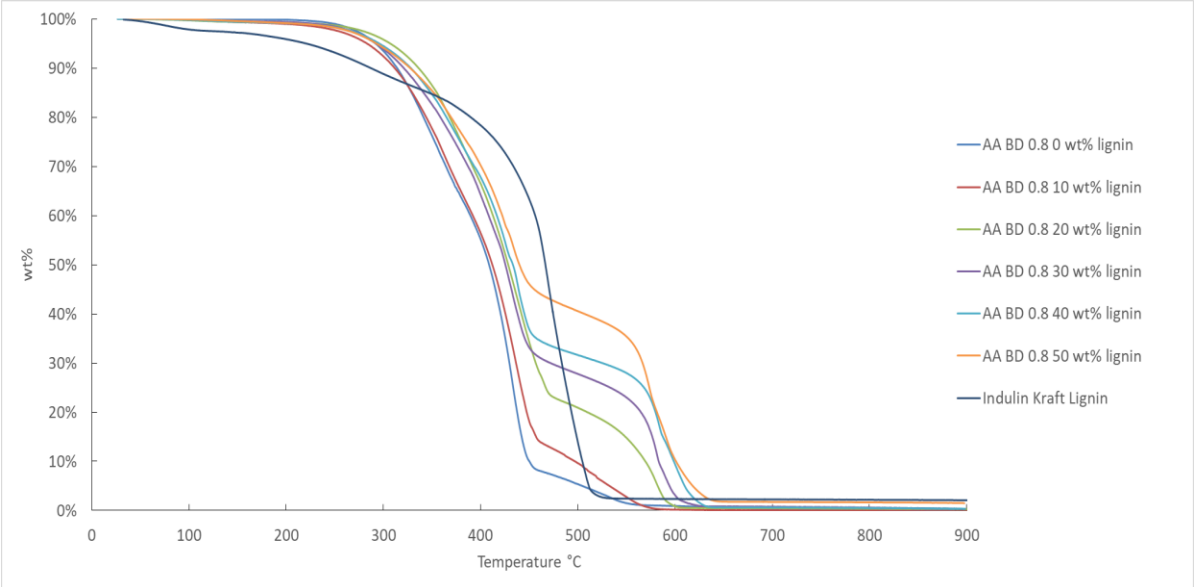

Figure 3.42 TGA thermograms of lignin-copolymer AA BD 0.8 wt% at varying lignin contents

Lignin degradation occurs in 3 stages of weight loss (Figure 3.42). The first stage occurs near 100°C and can be attributed to vaporization of moisture present in the lignin (Watkins, Nuruddin, Hosur, Narteh, & Jeelani, 2015). In the second stage with onset near 210°C the weight loss is attributed to degradation of residual carbohydrate compounds. The final stage

exhibiting an onset near 420°C results in the majority of weight loss and can be attributed to the degradation of the major lignin structure. This stage results in loss of volatile lignin products such as phenolics and alcohols.

The AA BD 0.8 polymer containing no lignin exhibits two degradation stages. The onset of the first stage occurs at 360°C. This degradation stage is attributed to the breakdown of ester linkages present in the prepolymer as these are relatively labile (Li H., 2016) and require less energy for bond disruption as compared to the more stable amide linkages. The second subtle onset can be seen at about 420°C and occurs as a result of the breakdown of the amide linkages.

The degradation behavior of the lignin-copolymers can be described as consisting of the same three major stages. The first two stages of thermal degradation occur in the same manner as the neat prepolymer. The third stage of degradation begins near 480°C and ends at 640°C. This phase is attributed to lignin decomposition. The mass remaining after the first degradation phase can be seen to increase in perfect correlation with the increasing lignin content. Additionally, the wt% remaining after the first and second degradation steps can be seen to correlate well with the lignin content. This behavior is consistent with observations in a previous study (Li, Sivasankarapillai, & McDonald, 2014) and provides strong evidence supporting the hypothesis that the third and final degradation phase results from the thermal breakdown of the lignin component.

Figure 3.43 through Figure 3.45 show the primary onset temperatures for each of the AA, SA and SuA lignin copolymers plotted against lignin content. These results demonstrate that the presence of lignin serves to improve the thermal stability of the prepolymer. In all cases the onset temperatures increase from the neat prepolymer to the 10 wt% lignin level. This contrasts with lignin copolymers in a previous study which exhibited diminished onset values upon the addition of lignin to the prepolymer (Li, Sivasankarapillai, & McDonald, 2014). In the current study however, it is observed that the onset temperatures decrease again as lignin approaches the 50 wt% level and this behavior is consistent with cited research (Li, Sivasankarapillai, & McDonald, 2014). An interesting observation from the onset

temperatures is that the lowest values are in many cases attributed to the highest level of DAB. It was hypothesized that the thermal stability of the lignin copolymers would be enhanced upon addition of amide hydrogen bond donating groups. In the case of the SA copolymers at the 30 wt% lignin level the onset temperatures are observed to decrease from 310°C to 298°C and finally to 289°C in order of increasing DAB content from 0 to 0.1 to 0.2 mole ratio, respectively. Depending on the copolymer formulation with respect to lignin and DAB content the thermal degradation onset temperatures can be adjusted through a range from 249°C to 382°C.

Figure 3.46 is a plot showing onset temperatures for the various diacids with no DAB plotted against lignin content. This graph shows that at the 10, 20 and 30 wt% lignin the copolymers increase in thermal stability with increasing chain length of the diacid. It is interesting to note however that at the 0 wt% level the opposite is true. That is the thermal stability decreases with increasing diacid chain length.

In all cases it is evident that the thermal stability of the lignin-copolymers is enhanced as compared to the native, unaltered lignin which exhibits an onset temperature of 220°C. However, as mentioned before this onset is the result of residual carbohydrate present (< 5%) in the lignin. If the major onset located at 420°C related to the breakdown of the lignin structure is considered the thermal stability of the copolymers are reduced by comparison to lignin.

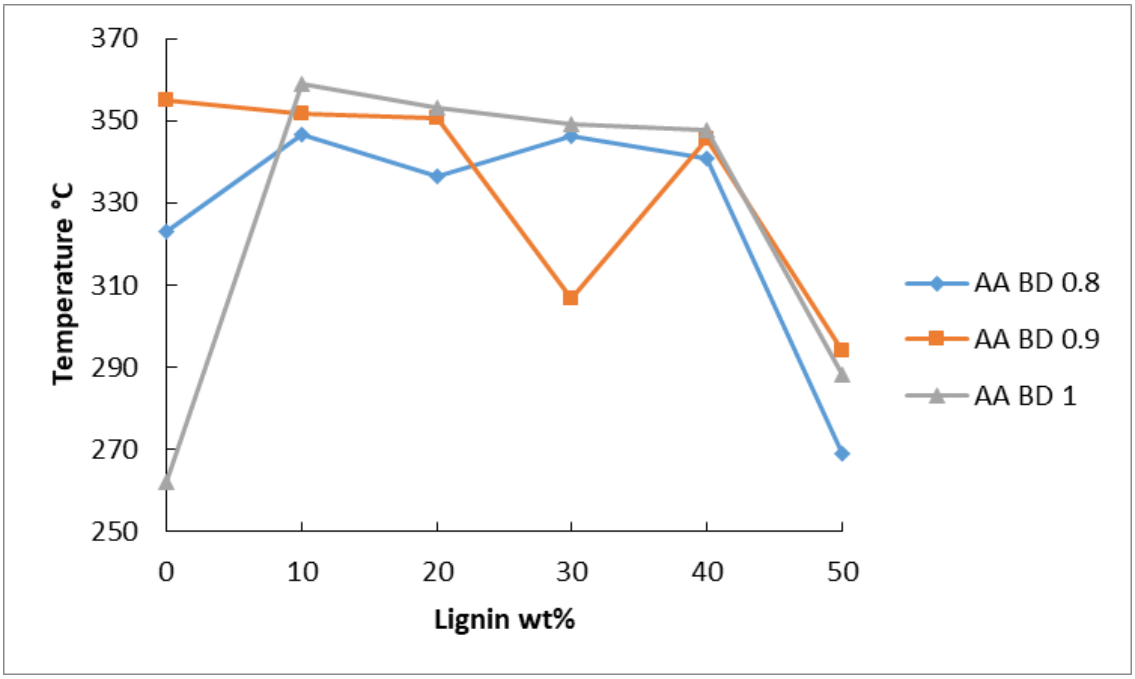

Figure 3.43 Plot of T_{onset} versus lignin content for AA based lignin copolymers

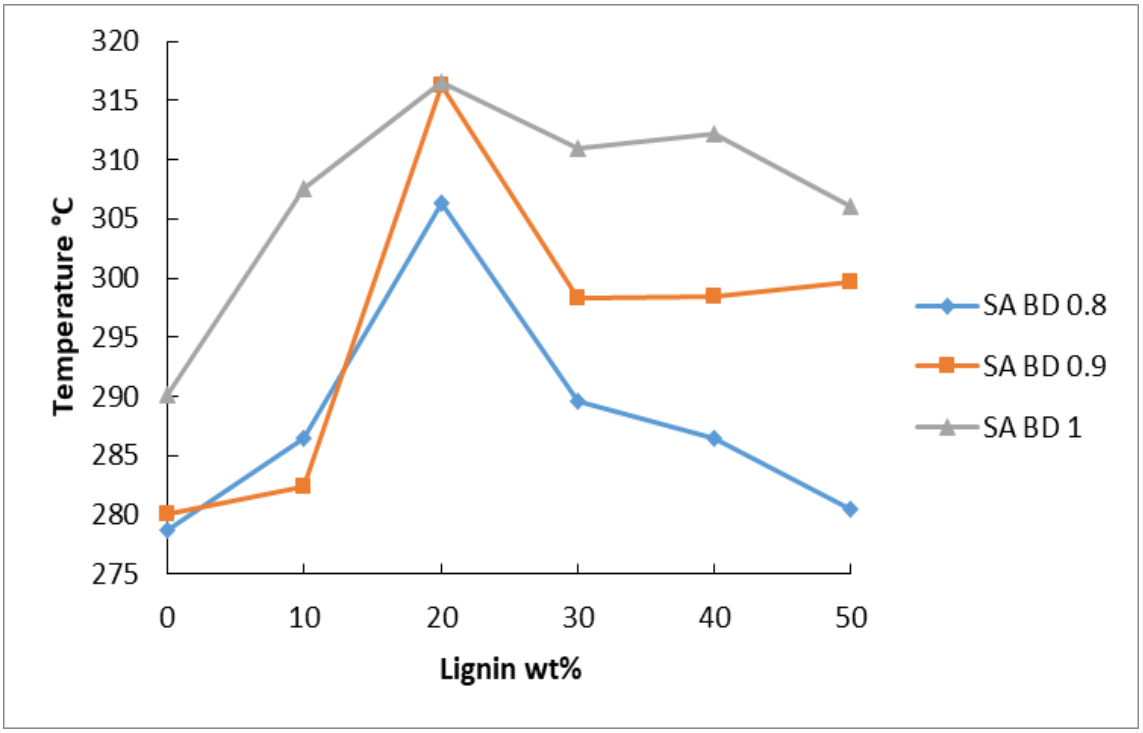

Figure 3.44 Plot of T_{onset} versus lignin content for SA based lignin copolymers

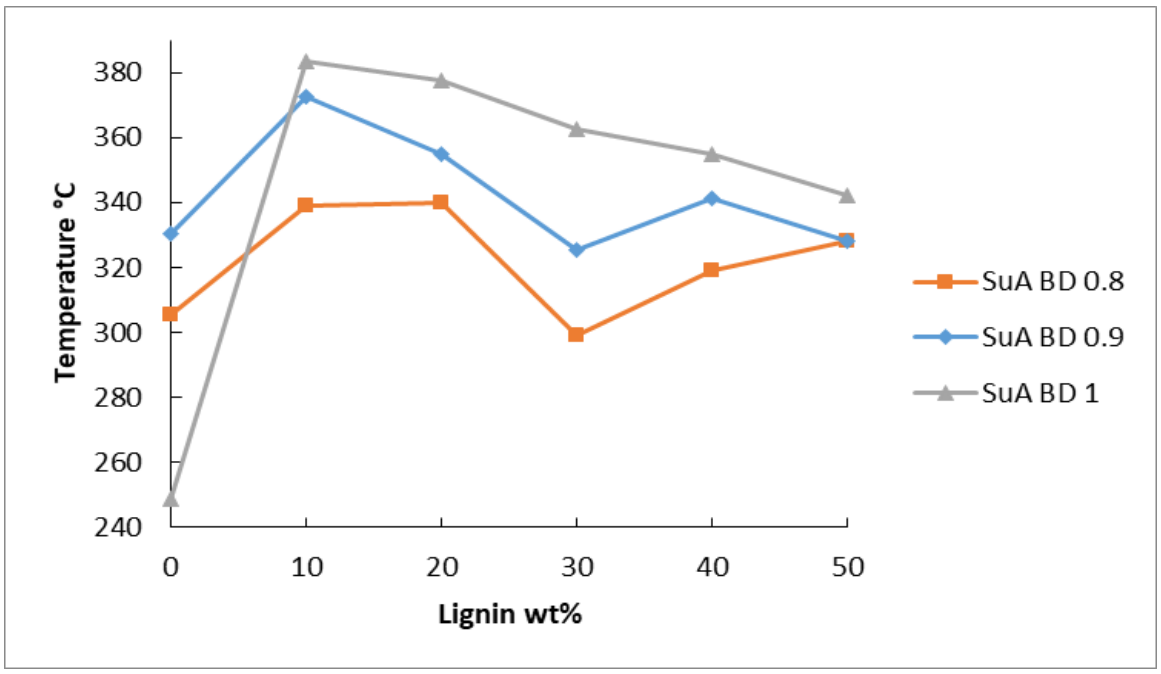

Figure 3.45 Plot of T_{onset} versus lignin content for SuA based lignin copolymers

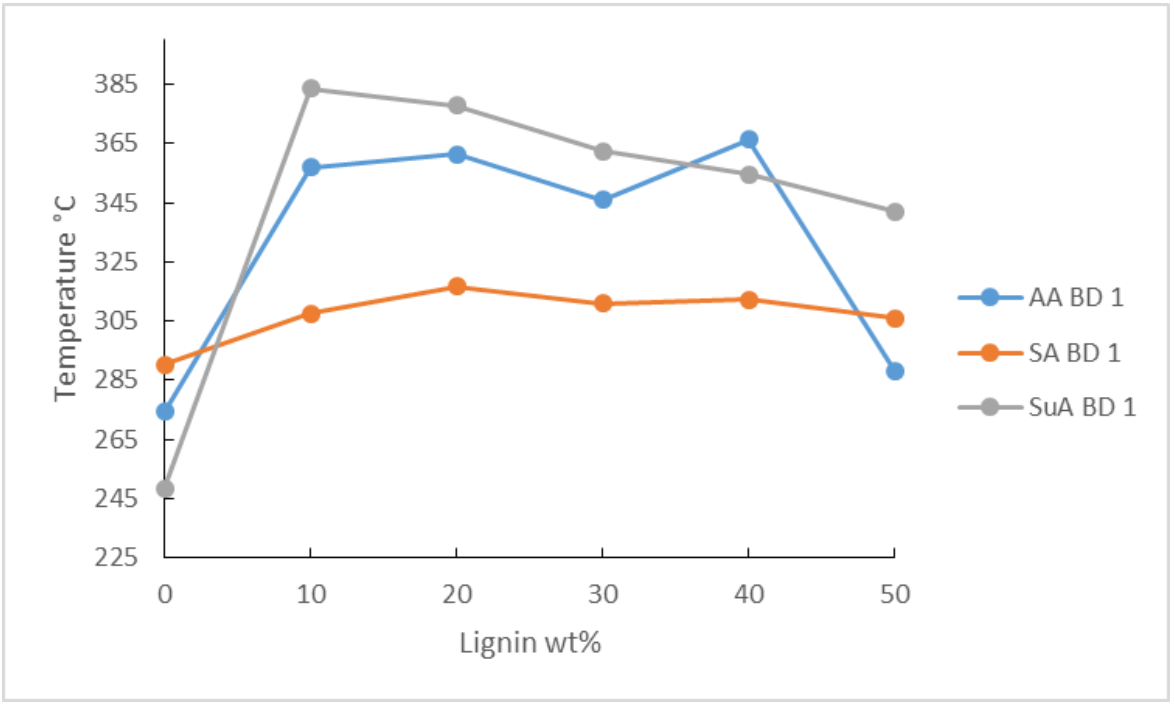

Figure 3.46 Plot of T_{onset} versus lignin content for SuA, AA and SA lignin copolyers with no DAB

3.3.2.5 TMA of Lignin Copolymers

In order to gain a better understanding of the thermal transitions observed through DSC and DMA, TMA was performed on an AA BD 0.8 series of copolymers. In Figure 3.47 the TMA onset temperature for softening (T_s) are plotted against lignin content in addition to the DSC T_g, DSC T_m and DMA T_m. From this figure it can be seen that the T_s from TMA very closely match the T_m from DSC at the 10 and 20 wt% lignin levels. At the 30, 40 and 50 wt% lignin levels the TMA T_s is observed to closely parallel the DSC T_g while remaining about 10°C higher. The DMA T_m values also exhibit similar behavior at the 30, 40 and 50 wt% lignin levels. This suggests that the DMA is responding to a combination of melt behavior within the crystalline zones and glass transition softening within the amorphous zones.

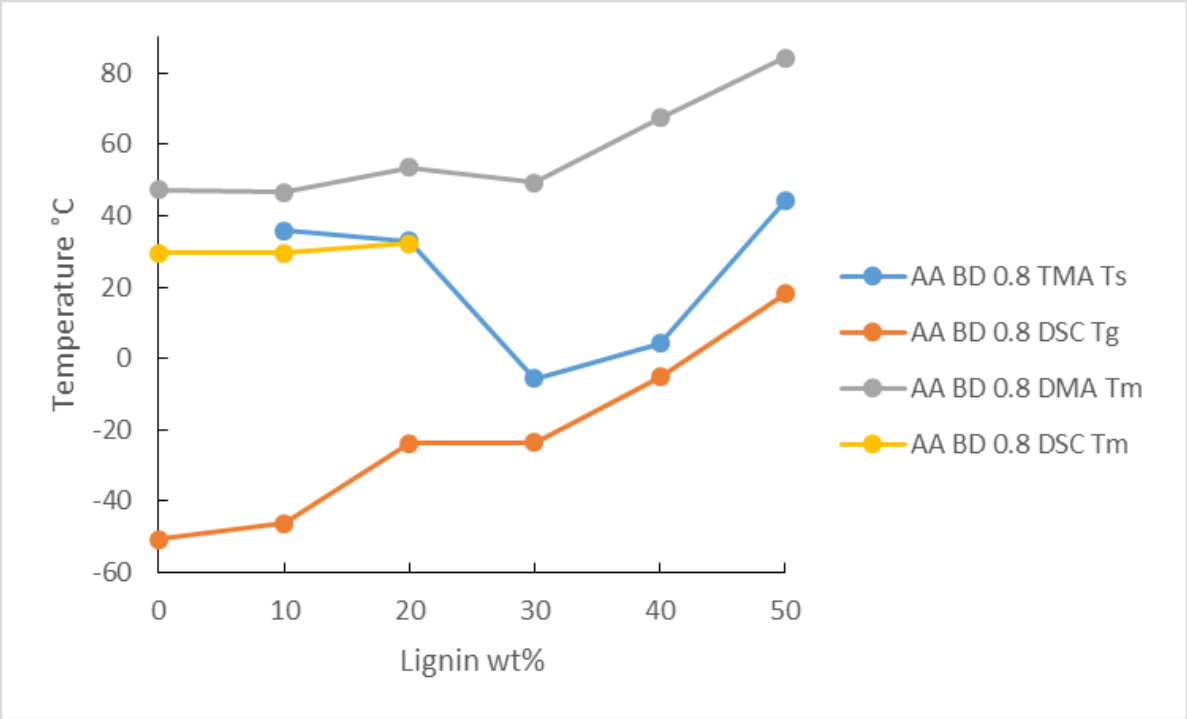

Figure 3.47 AA BD 0.8 TMA T_s, DSC T_g, DMA T_m and DSC T_m plotted versus lignin wt%

3.3.2.6 Molecular Structure Correlation with Thermal Analysis

At low lignin contents (0, 10 and 20 wt%) the TMA and DMA response are attributed to the melting of the crystalline regions of the prepolymer. However, at the 30 wt% lignin level the melting behavior ceases and the TMA responds to the T_g (T_{g1}) associated with the amorphous regions of the prepolymer as well as the amorphous regions between the lignin and

prepolymer interface (T_{g2}). This is why the T_s by TMA and DSC is observed to increase as lignin content increases in close proximity with one another. The system behaves as a blend where the observed T_s is a weighted average of the T_g's of both constituent polymers. It is postulated that the DMA response beginning at 30 wt% lignin is the result of the T_{11} transition. This T_{11} transition is observed in amorphous materials and can be attributed to the breakdown of segment-segment associations which increases segment mobility (Menard, 1999). These segments are the lignin aggregates shown as brown circles in Figure 3.49 with the association regions being represented by the red squiggly line surrounding the lignin aggregates. It can be seen that in the case of the 10 wt% lignin representation (Figure 3.48) the red zone associated with the amorphous T_{11} is not in close enough proximity to the other lignin aggregates to develop interactions. However as lignin content is increased these interactions become the dominant attractive force as shown in the representation of the 50 wt% lignin (Figure 3.49)

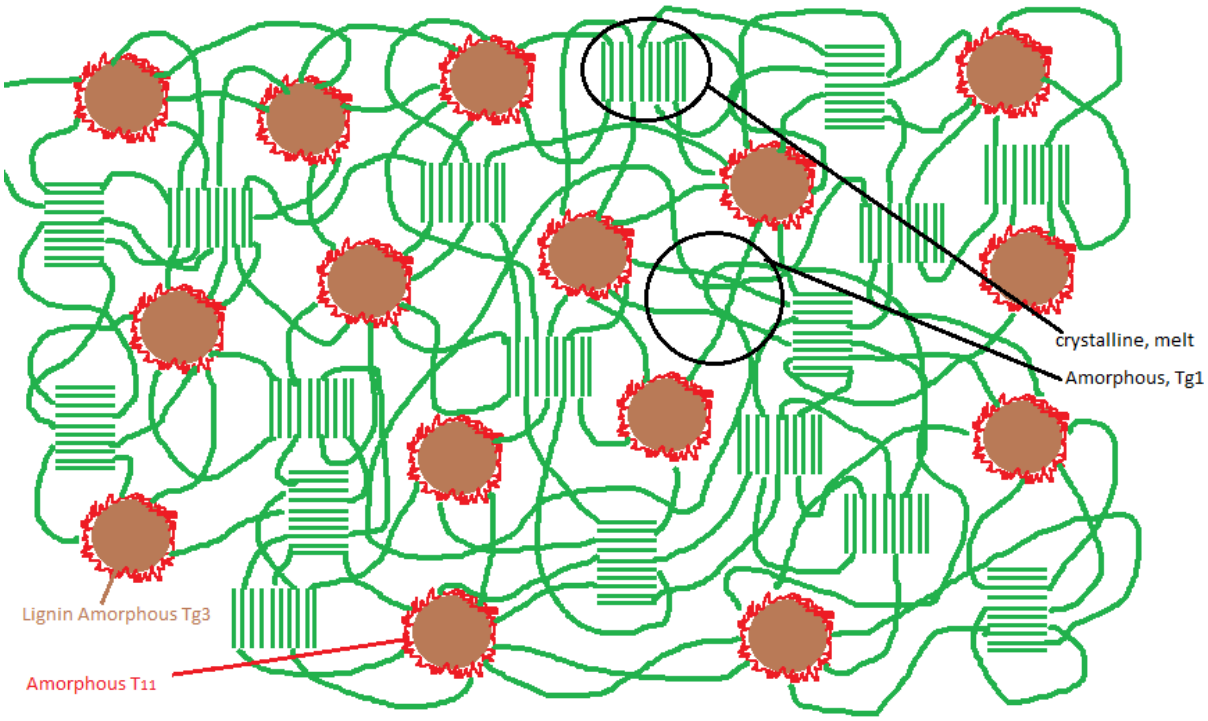

Figure 3.48 Proposed rendition of molecular structure of 10 wt% lignin copolymer

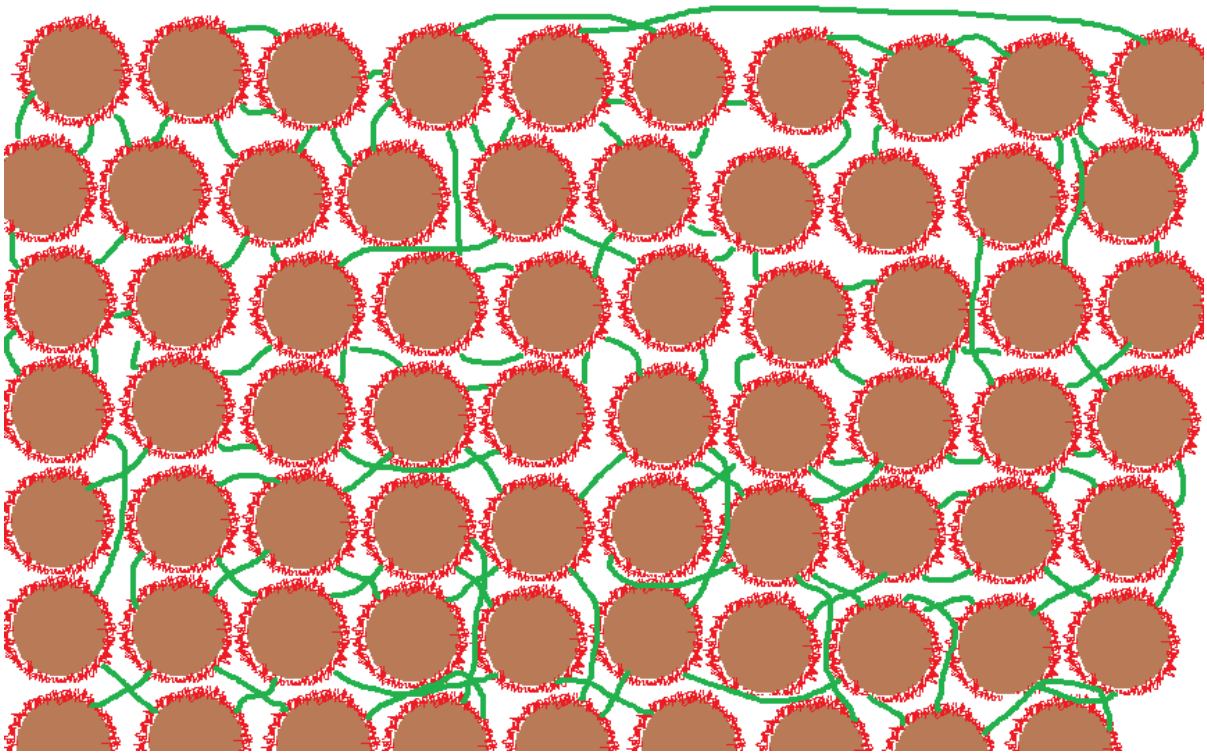

Figure 3.49 Proposed rendition of molecular structure of 50 wt% lignin copolymer

3.3.3 Polarized Optical Microscopy of Lignin Copolymers

Samples were analyzed using polarized optical microscopy in an effort to confirm and characterize the crystalline nature of the lignin-copolymer. Birefringence was observed in all samples, although in the 50% lignin sample it was difficult to observe. Figure 3.50 and Figure 3.51 are polarized optical micrographs of lignin-copolymers AA BD 1 40 wt% and 50 wt% lignin, respectively. These observations are supportive of the crystalline nature of the lignin-copolymers and their crystallinity is reduced with lignin content.

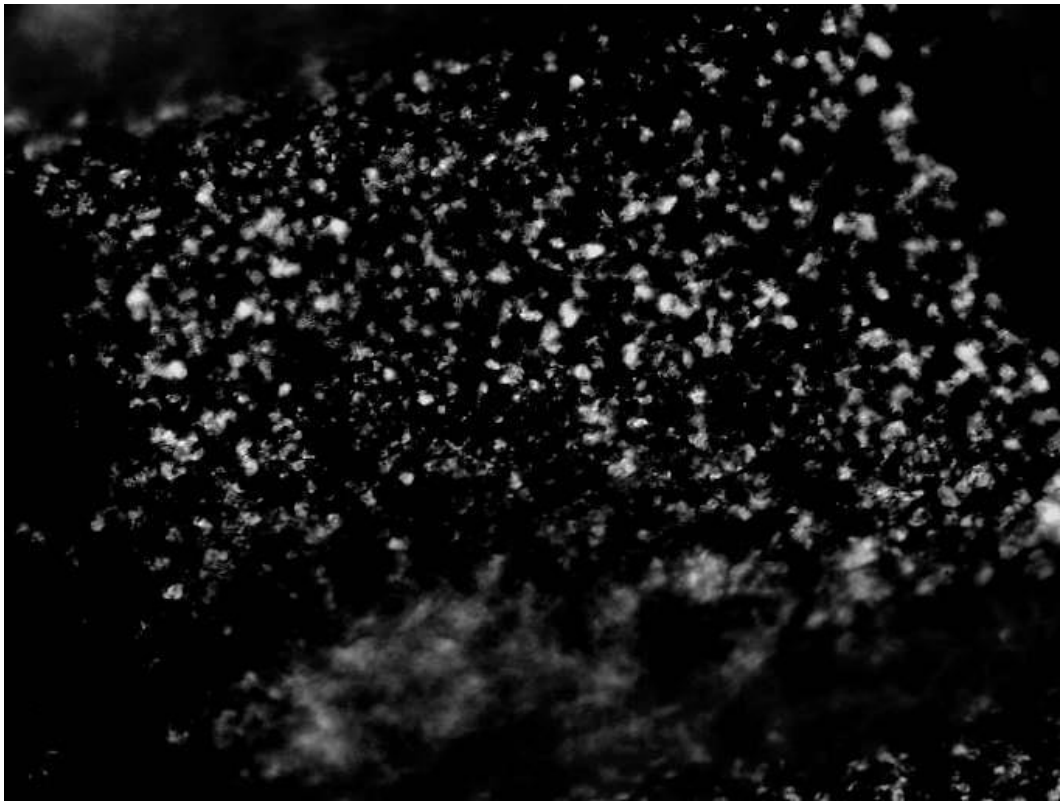

Figure 3.50 Polarized optical micrograph of lignin-copolymer AA BD 1 (40% lignin) at 400x magnification

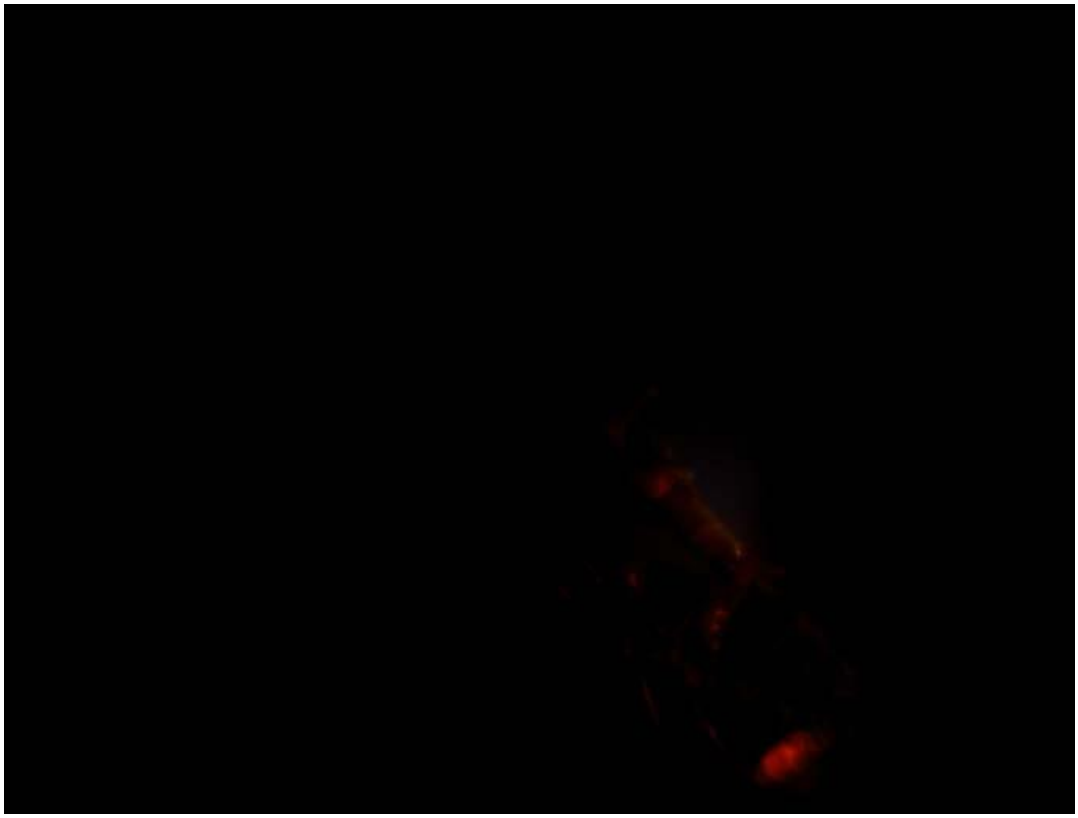

Figure 3.51 Polarized optical micrograph of lignin-copolymer AA BD 1 (50% lignin) at 400x magnification

3.3.4 X-Ray Diffraction Analysis of Copolymers

XRD was used as a tool to analyze the crystalline nature of the SA-ester based lignin-copolymers. Shown in Figure 3.52 are diffractograms obtained from the lignin-copolymer SA BD 1 with increasing lignin content as well as the percent crystallinity results obtained after peak fitting and data analysis (Figure 3.53). It can be seen in the diffractograms of the lignin-copolymers that as lignin content increases the amorphous nature of the material also increases. The calculated crystallinity results from XRD diffractograms are given in Table 3.10. At 0 wt% lignin the polymer crystallinity was determined to be 45.9%. At successive levels of increasing lignin content, the crystallinity is seen to decrease to 3.2% at 50% lignin content. This behavior is partly attributed to the amorphous nature of lignin and disruption of crystal formation within the lignin-copolymer structure (Pan, Gan, Mei, & Liang, 2017). However, this alone does not explain the very low levels of crystallinity observed at the 40 and 50 wt% lignin levels. It is hypothesized that the lignin structure also effects a decrease in

crystallinity by actually interrupting the crystalline nature of the polyester/amine zones within the copolymer. Similar results have been demonstrated in a previous paper on copolymers (Chung, et al., 2013). We assume that a similar trend (decrease in crystallinity with lignin content) would also be observed in the other lignin-copolymers.

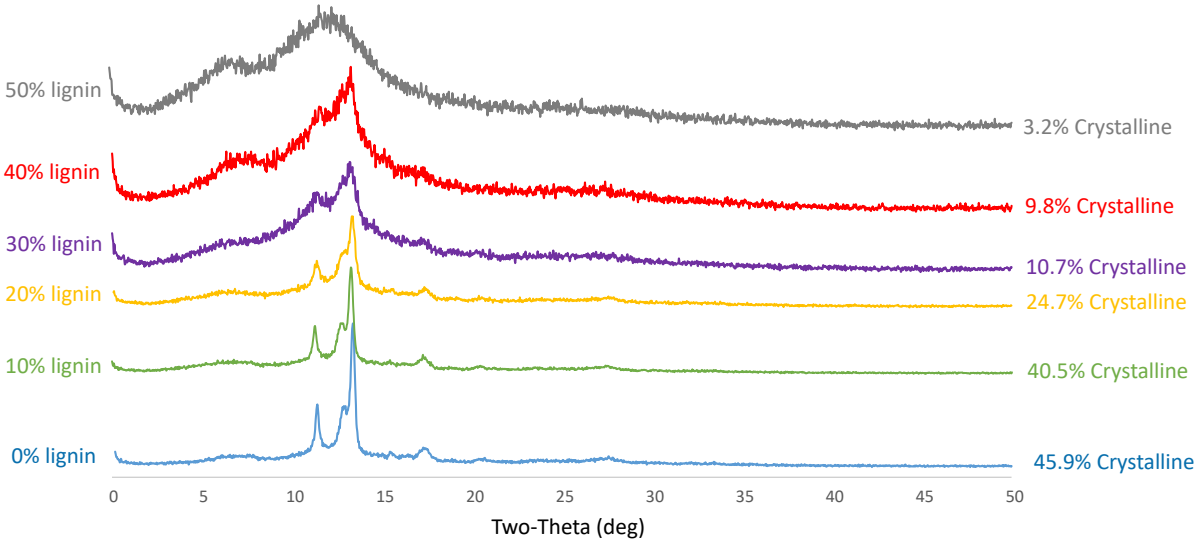

Figure 3.52 XRD diffractograms of SA BD 1 samples with increasing lignin content

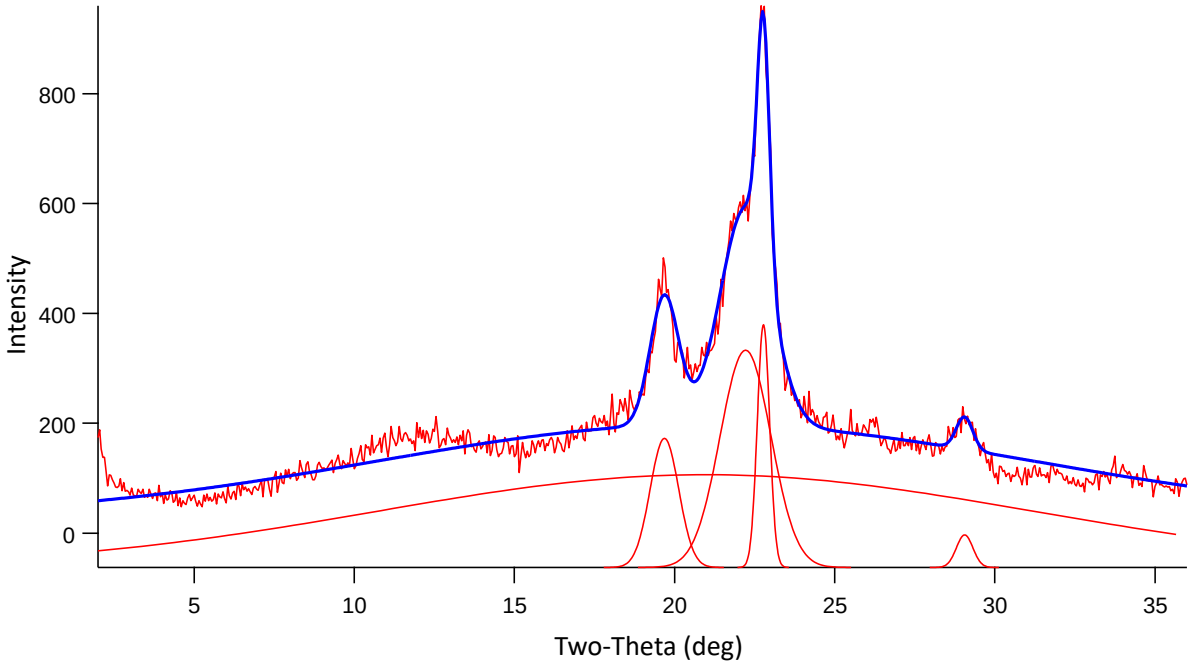

Figure 3.53 XRD of lignin-copolymer SA BD 1 20% lignin with peak fitting analysis

Table 3.10 Percent crystallinity of SA BD 1 copolymers obtained from peak fitting of XRD diffractograms

Lignin wt%	0%	10%	20%	30%	40%	50%
% Crystallinity	45.9	40.5	24.7	10.7	9.8	3.2

3.3.5 Tensile Testing of Lignin Copolymers

A fundamental property of any polymeric material is its ability to resist failure under stress. Knowledge and understanding of this parameter helps the engineer to determine what applications a given material may be suited for and the corresponding design specifications necessary to achieve a desired level of performance. Therefore the strain at break, tensile strength and Young's modulus were determined for the produced lignin-copolymers. Figure 3.54 shows an example of stress strain curves resulting from tensile testing of the AA BD 0.9 based lignin-copolymers with varying lignin contents. All the data with associated standard deviations from tensile testing of lignin copolymers can be found in Table 3.11.

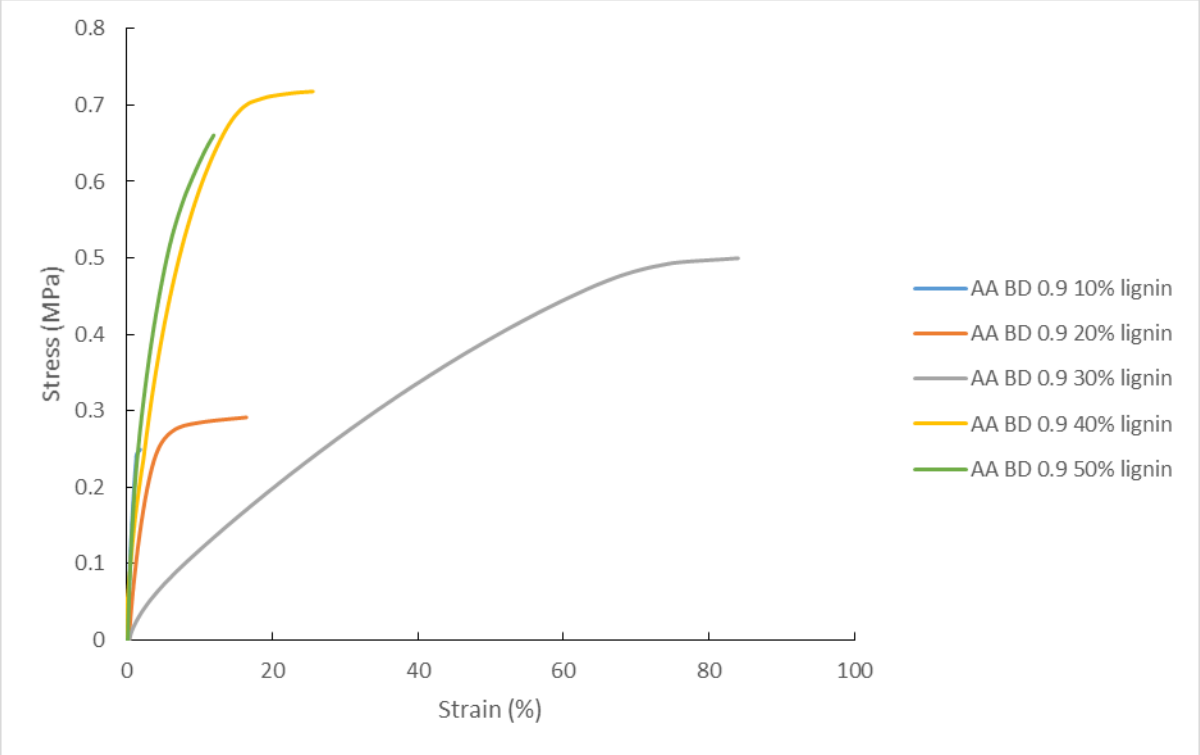

Figure 3.54 Tensile stress-strain plots for lignin-copolymer AA BD 0.9 with varying lignin contents

Young's modulus, tensile strength and strain at break results for AA based lignin-copolymers are shown in Figure 3.58, Figure 3.59 and Figure 3.60, respectively. The Young's modulus values for the AA copolymers span a range from 2 to 70 MPa (Table 3.11). The Young's modulus tends to decrease with increasing lignin content up to the 30 wt% lignin level where the minimum value of 2 MPa is found for the AA BD 1 copolymer. At 40% lignin and above, the Youngs modulus increases to 70 MPa for the lignin-copolymer AA BD 0.9 at 50 wt% lignin.

One possible explanation for this behavior arises from the morphological characteristics of the copolymer. At low lignin loading the crystalline nature of the prepolymer is the dominant contributor to the morphology which endows a high modulus and a low capacity for strain. At 30 wt% lignin the lignin-copolymer is more ductile thus increasing free volume in the matrix and allowing for more deformation with less stress than at lower and higher lignin loadings. This phenomenon is yet to be explained. At 40-50 wt% lignin the brittle and stiff nature of the lignin (highly packed) begins to dominate the polymer characteristics. The exception is the case of the AA BD 0.8 50 wt% lignin sample which displays a decrease from 40 to 30 MPa as lignin content is increased from 40 to 50 wt%, respectively. Similar results have been observed by Kadla et al in which incorporation of a chain-extended hydroypropyl lignin into a polymethyl methacrylate prepolymer matrix at increasing lignin contents led to a lower modulus while incorporation of a crosslinked lignin derivative raised the modulus (Kadla, 2003).

Originally it was hypothesized that by increasing the DAB content in the prepolymer would result in a stiffer polymer due to an increase in hydrogen bond donor groups. This behavior is observed for the 20, 30 and 40 lignin wt% samples but at the 10 and 50 wt% levels the opposite effect is true. That is the stiffest material is the copolymer containing no DAB. This behavior is counterintuitive and an explanation is not immediately apparent. A regressional analysis was performed in order to plot a fitted model of the Young's modulus as a response to lignin and DAB content (Figure 3.55). In the regression model the maximum Youngs modulus for the AA copolymers was about 50 MPa at 50 wt% lignin content with no DAB.

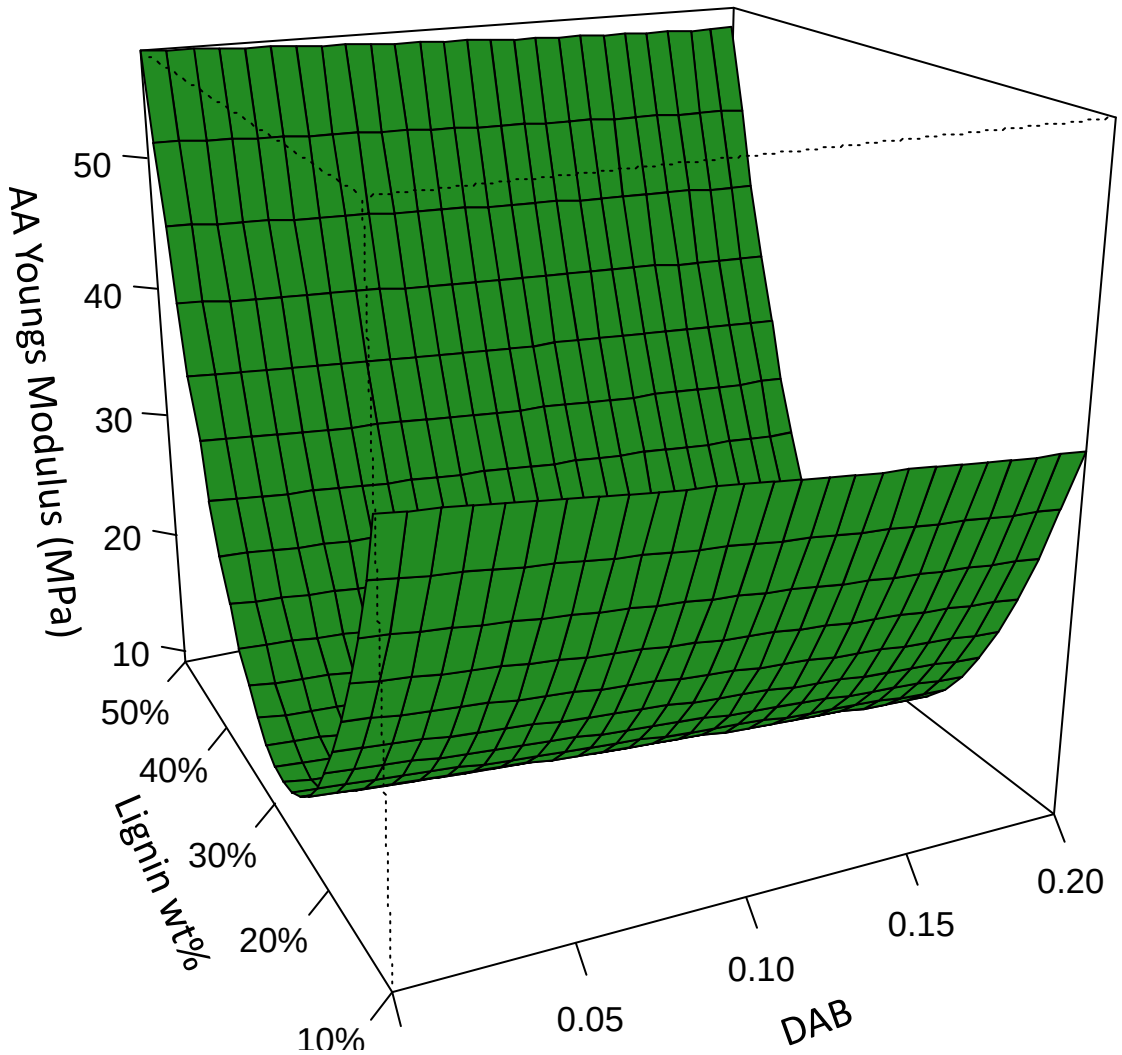

Figure 3.55 Response model plot of Young's modulus versus lignin wt% and DAB content for AA based lignin-copolymer

The tensile strengths (Table 3.12) for the AA series of lignin-copolymers span a range from 0.1 MPa for the lignin-copolymer AA BD 0.8 at 10 wt% lignin to 1.1 MPa for the for the lignin-copolymer AA BD 0.8 sample at 40 wt% lignin. The effects of amine content on Youngs modulus are mirrored in the tensile strength data as well. At both the 10 and 50 wt% lignin levels the lignin-copolymer BD 0.8 shows a diminished tensile strength as compared to their counterparts having lower amine contents. At the 20, 30 and 40 wt% lignin levels, however, the tensile strength values are observed to reverse this trend with the highest tensile strength value belonging to the lignin-copolymer BD 0.8 and the lowest tensile strength value attributed to the BD 1 sample. In every case the tensile strength exhibits a trend where the

values generally increase with increasing lignin content. A regressional analysis was performed in order to plot a fitted model of the tensile strength as a response to lignin and DAB content (Figure 3.56). The maximum tensile strength value for AA copolymers resulting from the regression model was about 0.9 MPa at 50 wt% lignin content and 0.2 molar ratio of DAB.

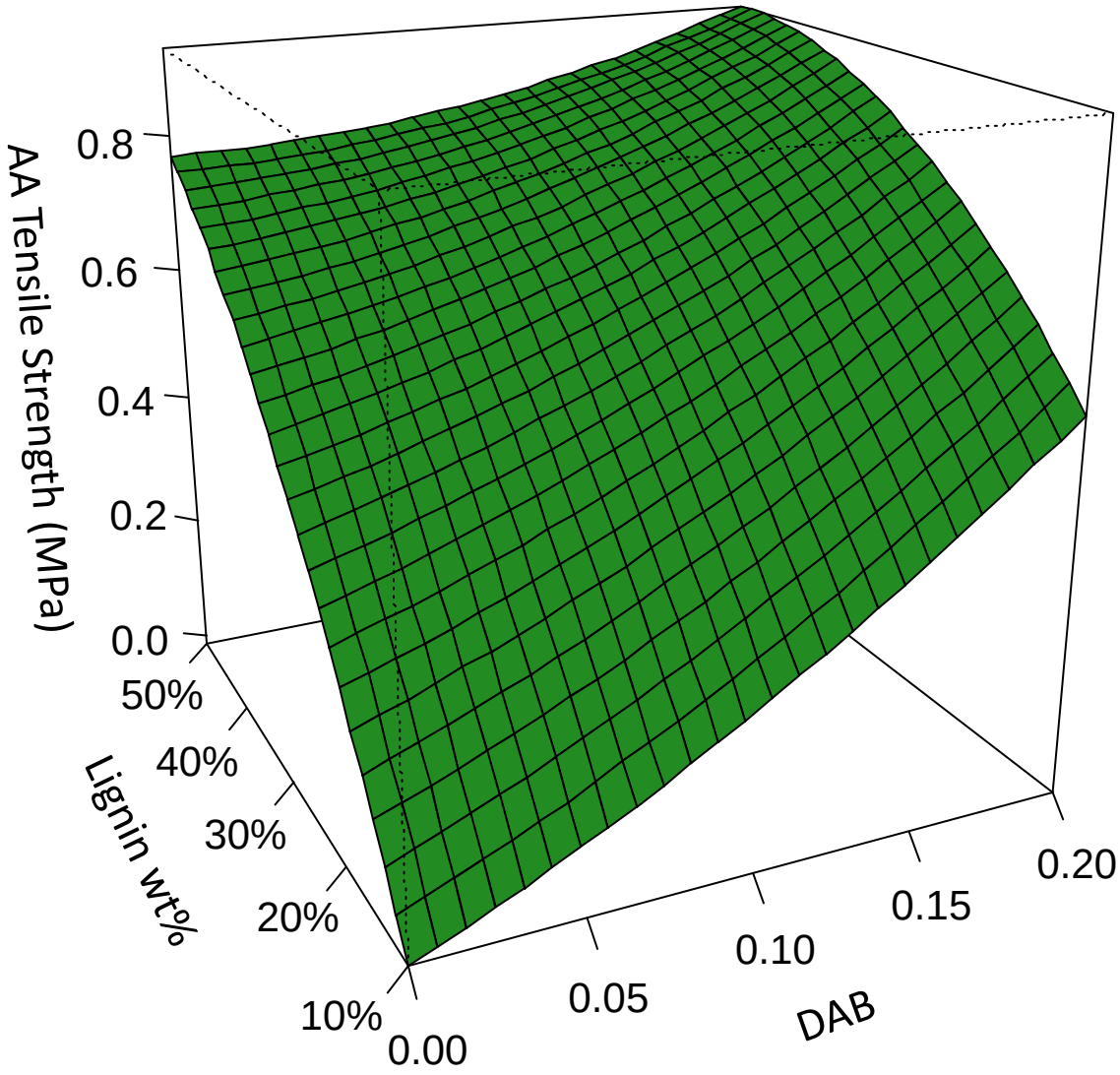

Figure 3.56 Response model plot of tensile strength versus lignin wt% and DAB content for AA based lignin-copolymer.

Tensile strain at break results are given in Figure 3.60 and Table 3.12. It was suspected that increasing the amine content in the copolymer would reduce the amount of chain slippage

and reduce the strain at break. The strain at break results suggest that the opposite is true. At the 10-50 wt% lignin the lowest strain at break values (1%) resulted from the samples containing no DAB. At these lignin levels the strain at break values increase with increasing DAB content with the exception of the 30 wt% lignin. At this level the BD 0.9 sample exhibited a striking increase in capacity for elongation over the other AA lignin-copolymers at 30 wt% lignin. This increase is far beyond the error associated with the measurements which indicates that the value is truly significantly greater than the 30 wt% lignin counterparts. A regressional analysis was performed in order to plot a fitted model of the strain at break as a response to lignin and DAB content and is shown in Figure 3.57. The maximum value for strain at break of AA copolymers resulting from the regression model was 45% at the 30 wt% lignin with a 0.1 molar ratio of DAB.

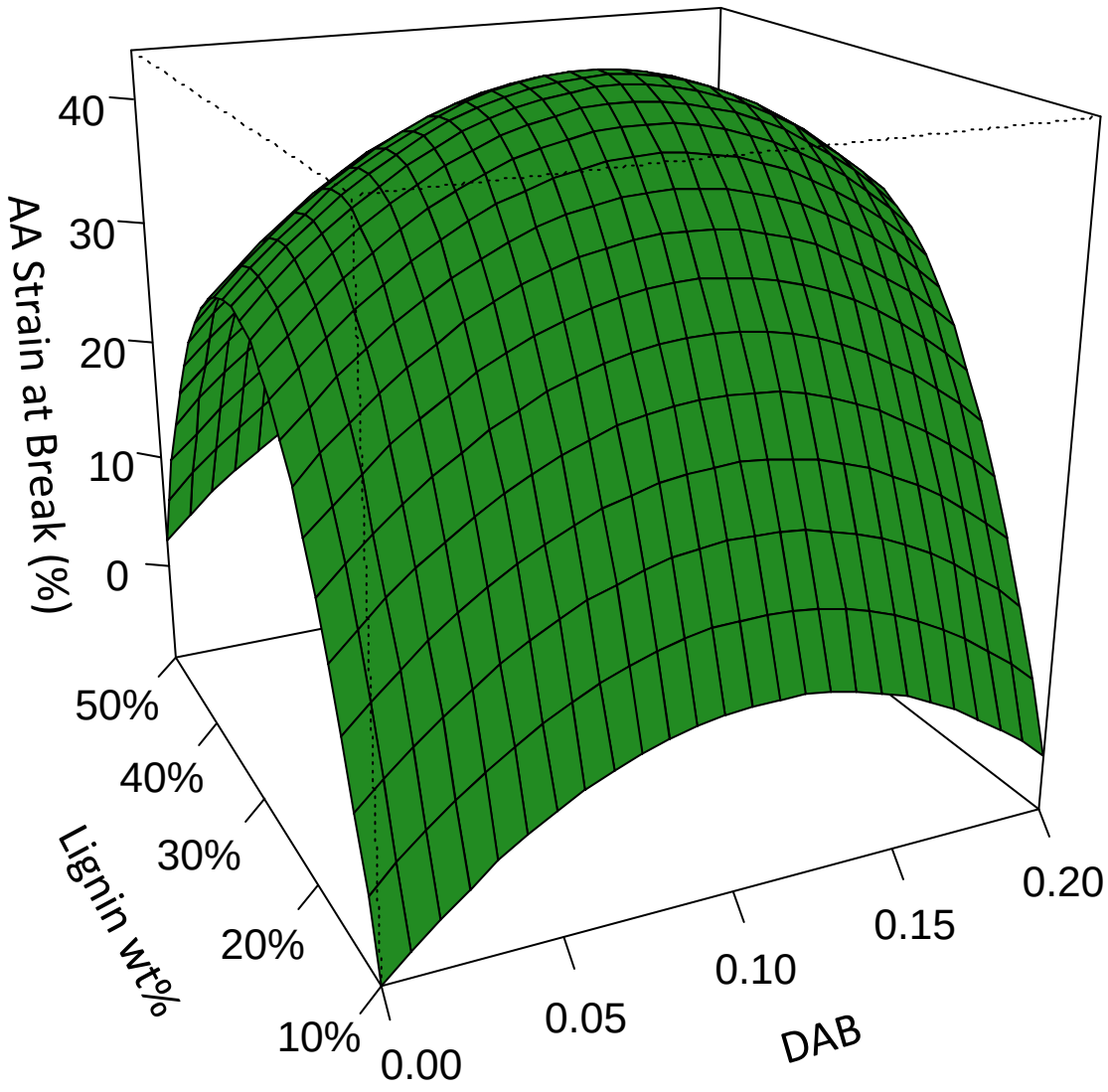
AA Strain at Break (%)
40
30
20
10
0
Lignin wt%
50%
40%
30%
20%
10%
DAB
0.00
0.05
0.10
0.15
0.20

Figure 3.57 Response model plot of strain at break versus lignin wt% and DAB content for AA based lignin-copolymer.

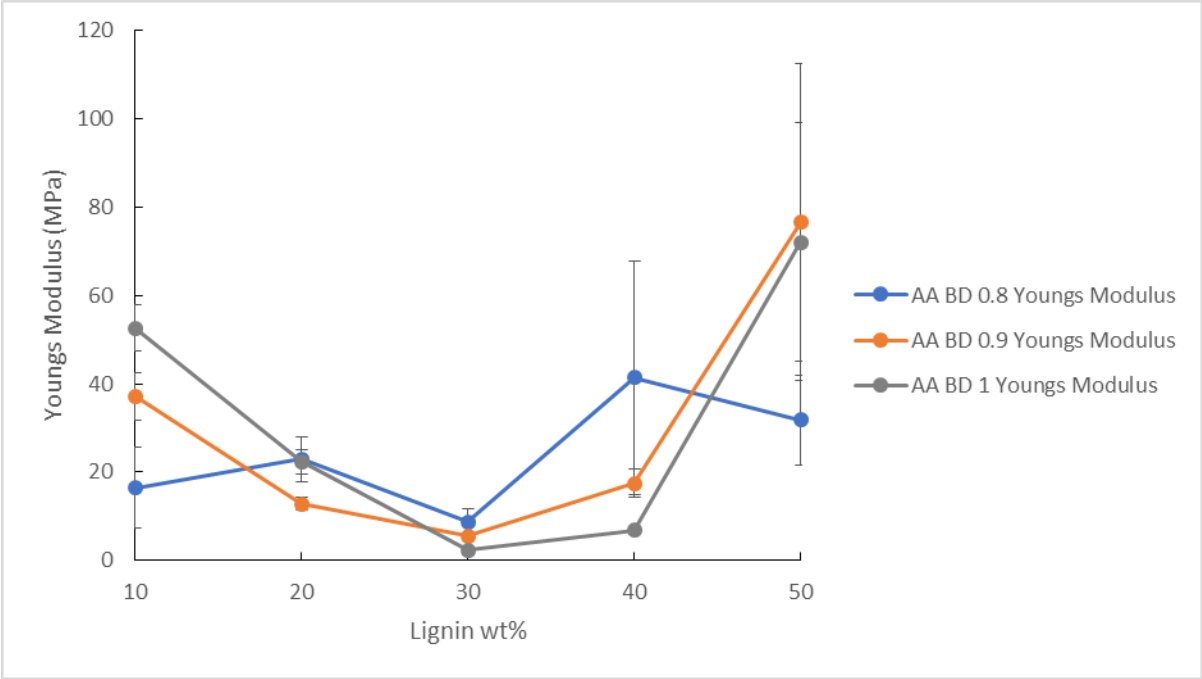

Figure 3.58 Plot of young's modulus of AA based lignin-copolymers plotted against lignin wt% for various DAB levels

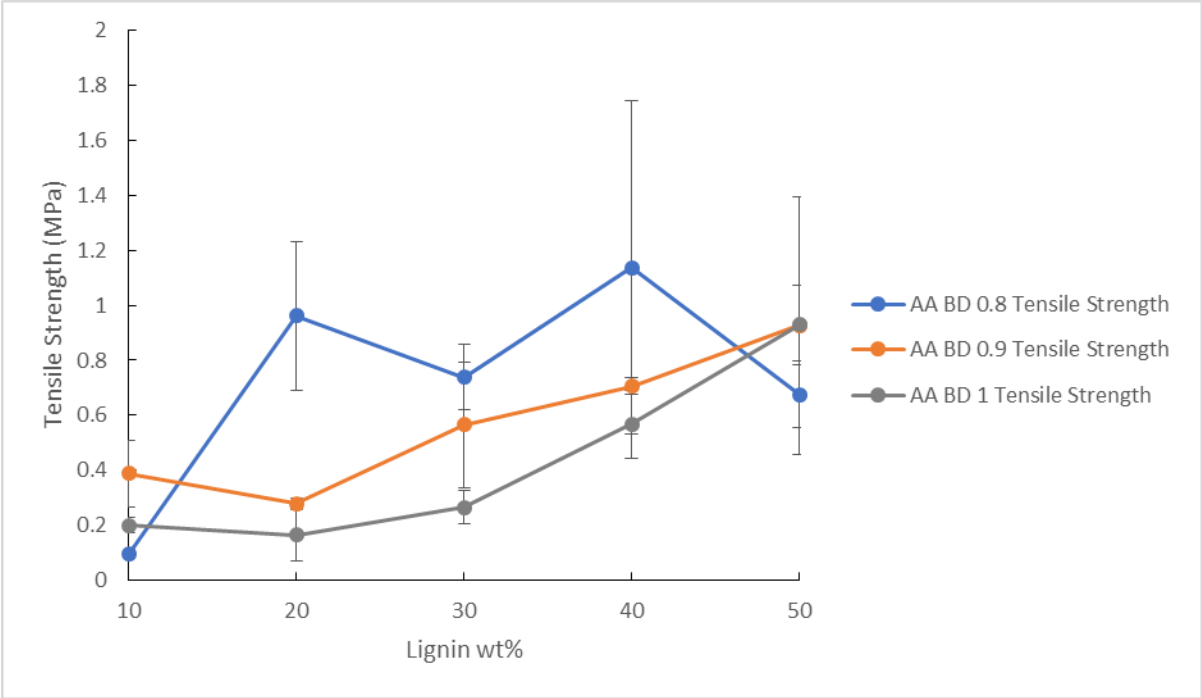

Figure 3.59 Plot of tensile strength of AA lignin copolymers plotted against lignin wt% for various DAB levels

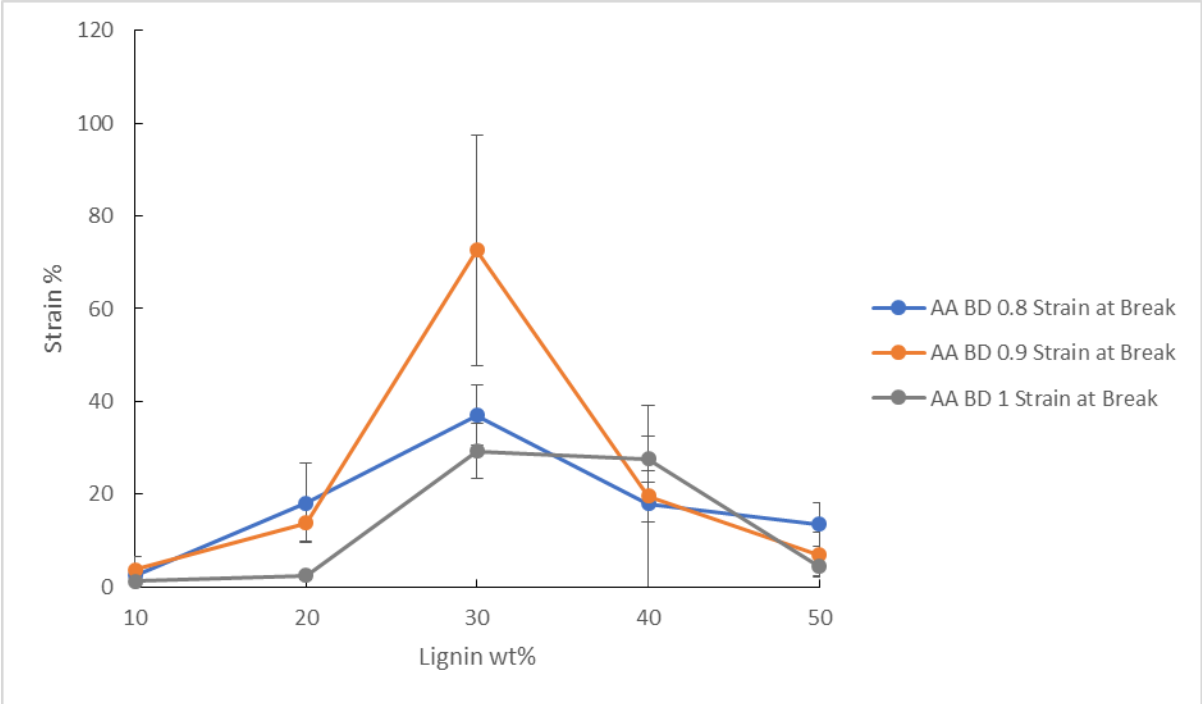

Figure 3.60 Strain at break of AA lignin copolymers plotted against lignin wt% for various DAB levels

The tensile properties of the SA based copolymers were determined (Table 3.11). Figure 3.64, Figure 3.65 and Figure 3.66 show the Young's modulus, tensile strength and strain at break respectively for the SA series of lignin-copolymers. The SA copolymers demonstrate a slightly different trend than the AA series of copolymers with regard to young's modulus. First, the values span a range from 30 MPa for the SA BD 0.8 30 wt% lignin copolymer up to 340 MPa for the SA BD 0.9 10 wt% lignin copolymer. The maximum Young's modulus obtained from the SA copolymers is around 300% greater than that of the AA copolymers and this could be attributable to the shorter diacid chain length. Additionally, the 40 wt% lignin SA samples at the BD 1 and 0.9 level resulted in the lowest stiffness (30 MPa) whereas the 30 wt% lignin samples had the lowest stiffness in the AA copolymers. However, the overall trend of high stiffness at lower lignin decreasing to a minimum and then increasing again as lignin increases toward 50 wt% remains the same. Although in contrast to the AA copolymers the modulus values at 50 wt% lignin never rise above the values obtained at the 10 wt% lignin level. At every level of lignin content except the 50 wt% level the samples

containing no DAB were observed to yield the lowest Young's modulus. A regressional analysis was performed in order to plot a fitted model of the Young's modulus as a response to lignin and DAB content as shown in Figure 3.61. The maximum Young's modulus value of 275 MPa for SA copolymers obtained from the regression model was observed at 10 wt% lignin and no DAB.

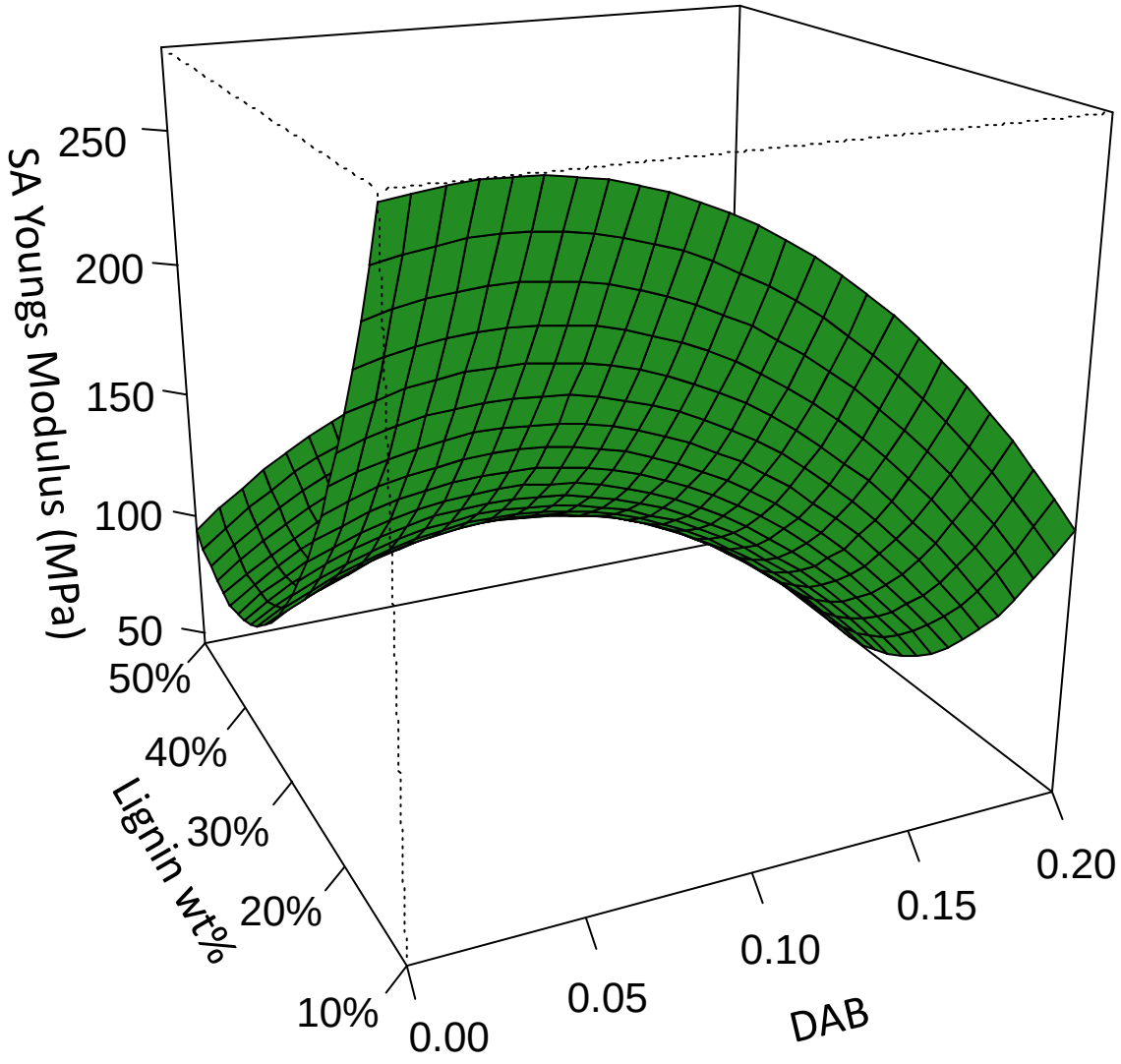

Figure 3.61 Response model plot of Young's modulus versus lignin wt% and DAB content for SA based lignin-copolymers

The tensile strength of the SA copolymers span from 0.3 MPa for the SA BD 0.8 at 10 wt% lignin to 2.8 MPa for the SA BD 1 at 30 wt% lignin. The maximum tensile strength value for the SA copolymers is 100% greater than what was observed for the AA copolymers. In

addition, the highest tensile strength values for the SA copolymers are observed in the samples containing no DAB which is contrary to the AA series of copolymers which exhibited the highest values in the copolymers containing the highest amount of DAB. A regressional analysis was performed in order to plot a fitted model of the tensile strength as a response to lignin and DAB content as shown in Figure 3.62. This graph demonstrates the diminished tensile strength in response to increasing DAB content. The maximum tensile strength value of 1.6 MPa for SA copolymers obtained from the regression model was observed at 40 wt% lignin and no DAB.

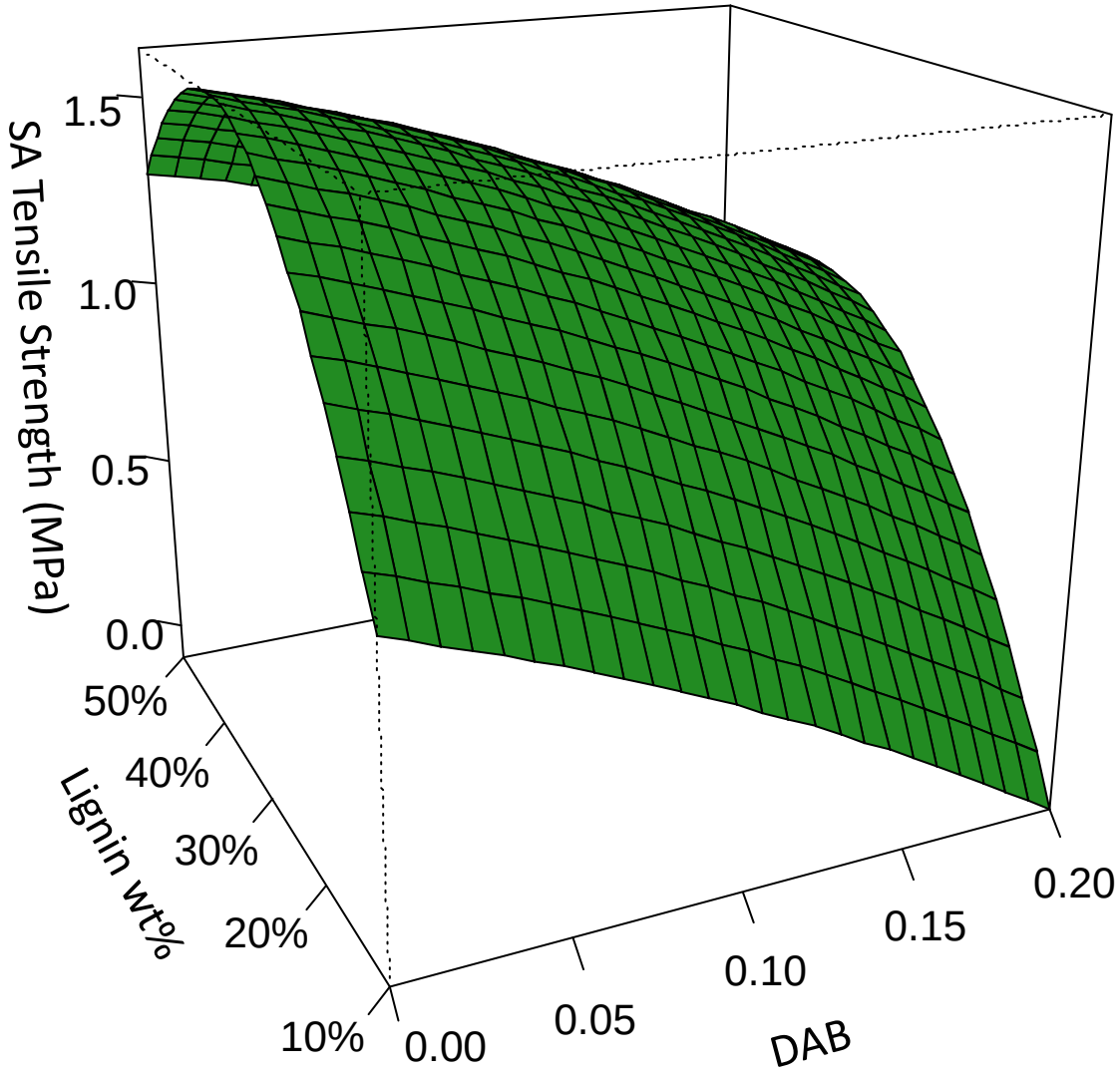

Figure 3.62 Response model plot of tensile strength versus lignin wt% and DAB content for SA based lignin-copolymers

The SA based lignin-copolymer strain at break values span a range from 1% at the 10 wt% lignin level up to 21% for the SA BD 0.9 40 wt% lignin sample. The SA copolymers demonstrated a significantly reduced capacity for elongation as compared to the AA copolymers (max ~40%). There also appears to be a trend where DAB content effects an enhanced ability to elongate in the SA copolymers as demonstrated by the 30 and 40 lignin wt% levels. At the 30 wt% lignin level in particular the strain at break is seen to increase with increasing DAB content. It is interesting that the BD 0.8 sample reaches a maximum value of 20% strain at the 30 lignin wt% level while the BD 0.9 sample reaches a maximum of 21% strain at the 40 lignin wt% level. It is clear that the presence of DAB serves to improve the capacity for strain of the SA copolymers. A regressional analysis was performed in order to plot a fitted model of the strain at break as a response to lignin and DAB content as shown in Figure 3.63. In this graph it can clearly be seen that increasing the DAB content improves the capacity for elongation. The maximum strain at break value of 12% for SA copolymers obtained from the regression model was observed at 30 wt% lignin and a 0.2 molar ratio of DAB.

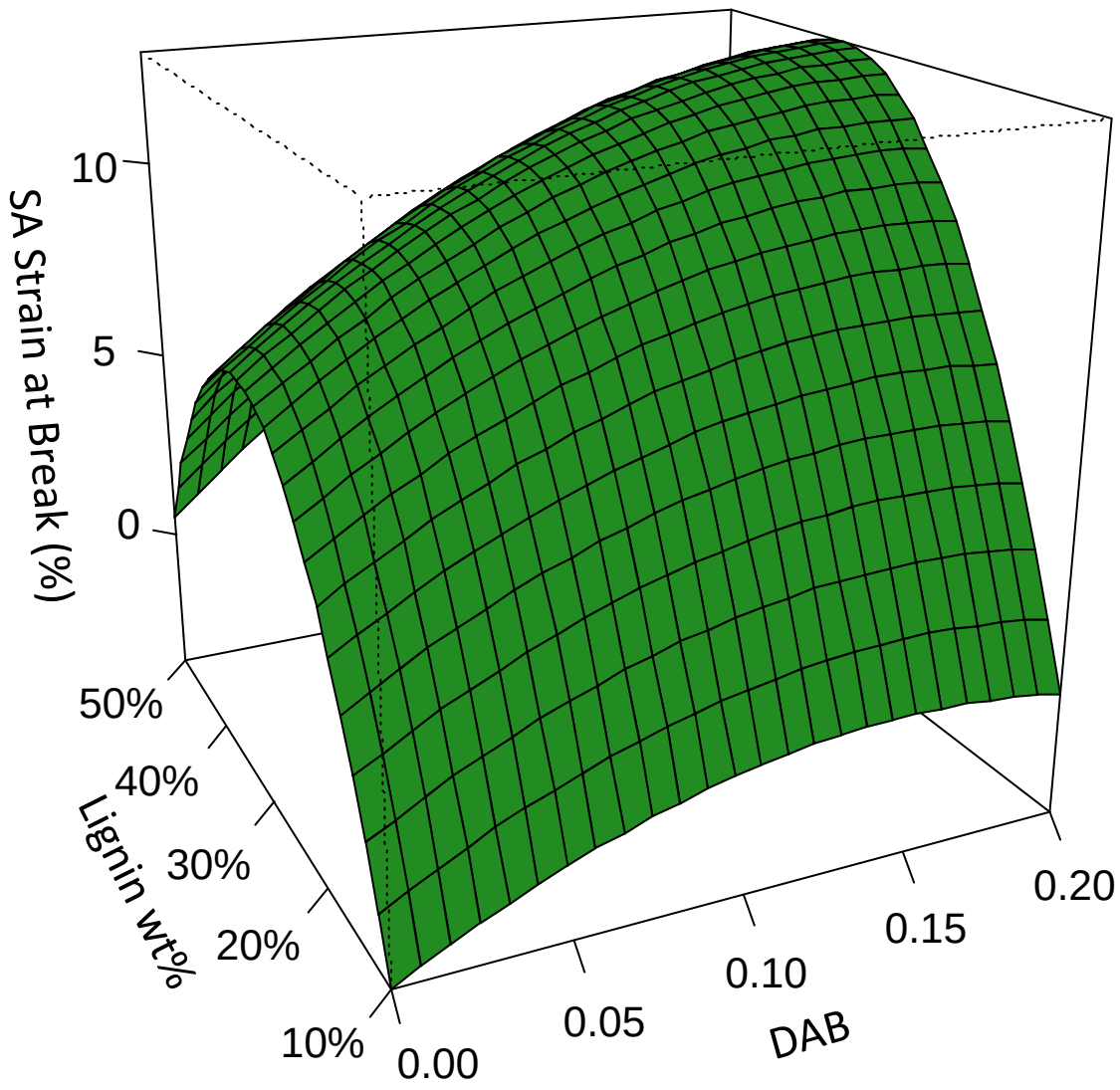

Figure 3.63 Response model plot of strain at break versus lignin wt% and DAB content for SA based lignin-copolymers

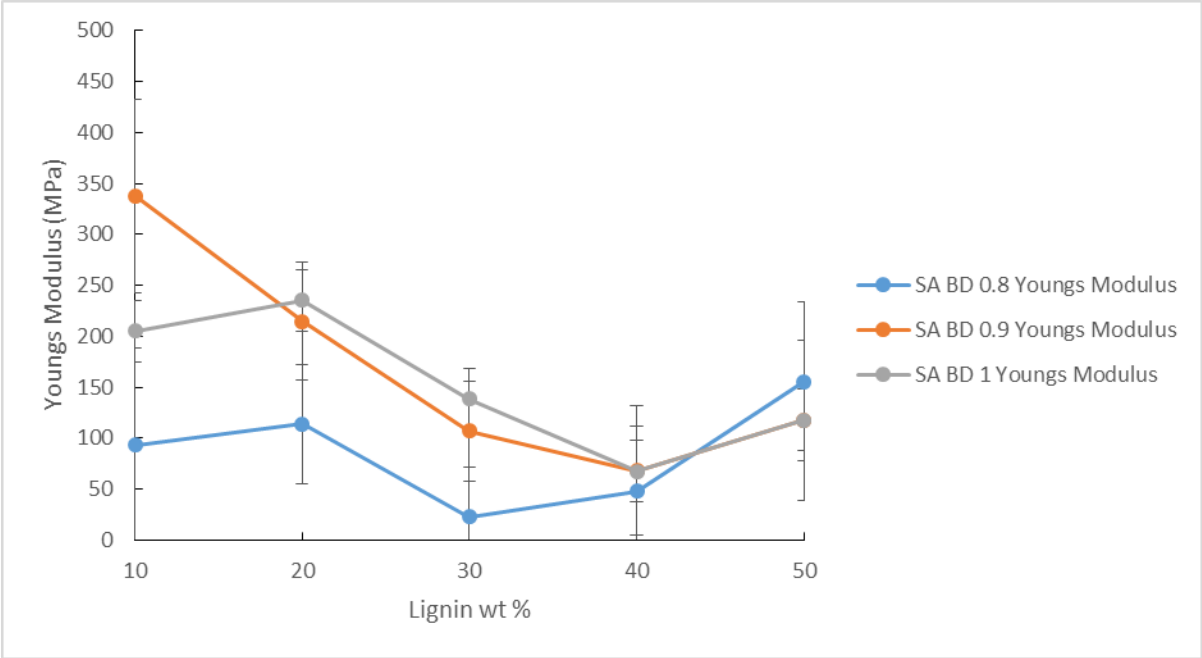

Figure 3.64 Youngs modulus of SA lignin copolymers plotted against lignin wt% for various DAB levels

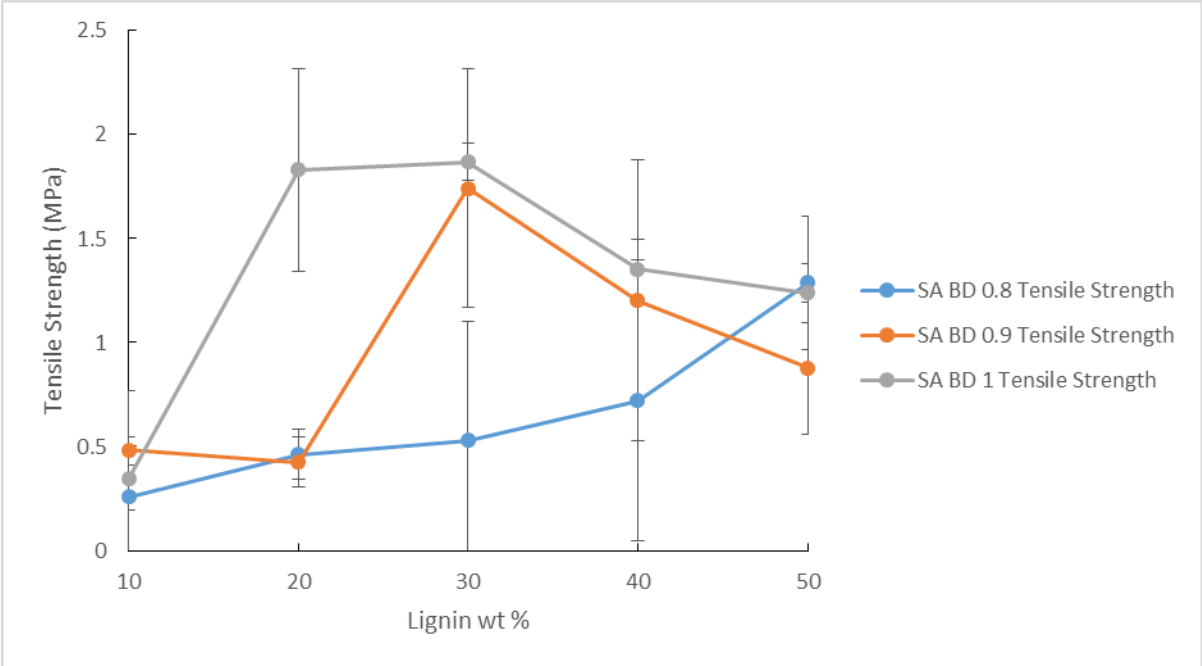

Figure 3.65 Tensile strength of SA lignin-copolymers plotted against lignin wt% for various DAB levels

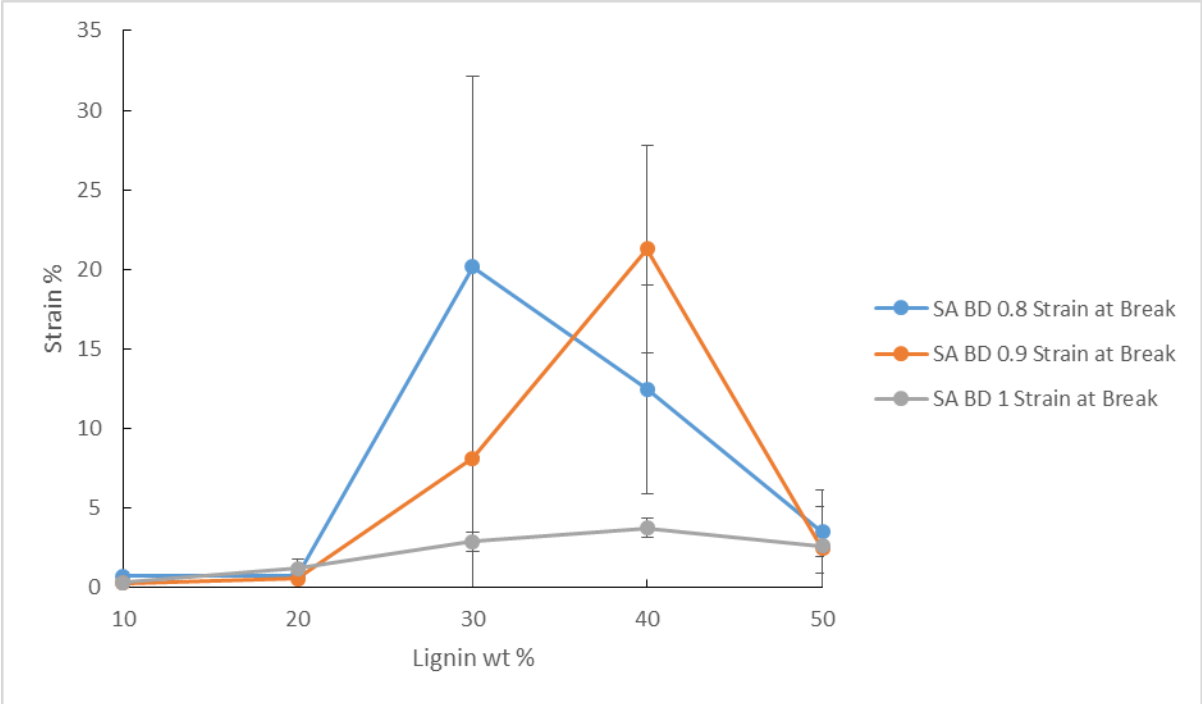

Figure 3.66 Strain at break of SA lignin-copolymers plotted against lignin wt% for various DAB levels

The tensile properties of the SuA based copolymer were determined (Table 3.11). Figure 3.70, Figure 3.71 and Figure 3.72 show stress strain results for the SuA based lignin-copolymers. The Young's modulus values for SuA copolymers span from 20 MPa for the SuA BD 0.8 30 wt% lignin sample to 255 MPa for the SuA BD 1 10 wt% lignin sample. The Young's modulus values obtained from the SuA copolymers demonstrate the same overall trend as the aforementioned samples. At low lignin levels the stiffness is greater and decreases to a minimum before rising again at higher lignin levels. The minimum Young's modulus values for the lignin-copolymers BD 0.9 and 1 are observed at 40 wt% lignin and the BD 0.8 minimum occurs at 30 wt% lignin. This is in contrast to the minimum in young's modulus values for all DAB levels at 30 wt% lignin for the AA copolymers. It is also noted that in the case of the BD 0.9 and 1 copolymers the Young's modulus at the 50 wt% lignin do not surpass the maximum values observed at the 10 wt% lignin level. The Young's moduli increase with decreasing DAB content at the 10 and 20 wt% lignin level. A regressional analysis was performed in order to plot a fitted model of Young's modulus as a response to lignin and DAB content as shown in Figure 3.67. The maximum Young's modulus value of

225 MPa for SuA copolymers obtained from the regression model was observed at 10 wt% lignin and 0 DAB.

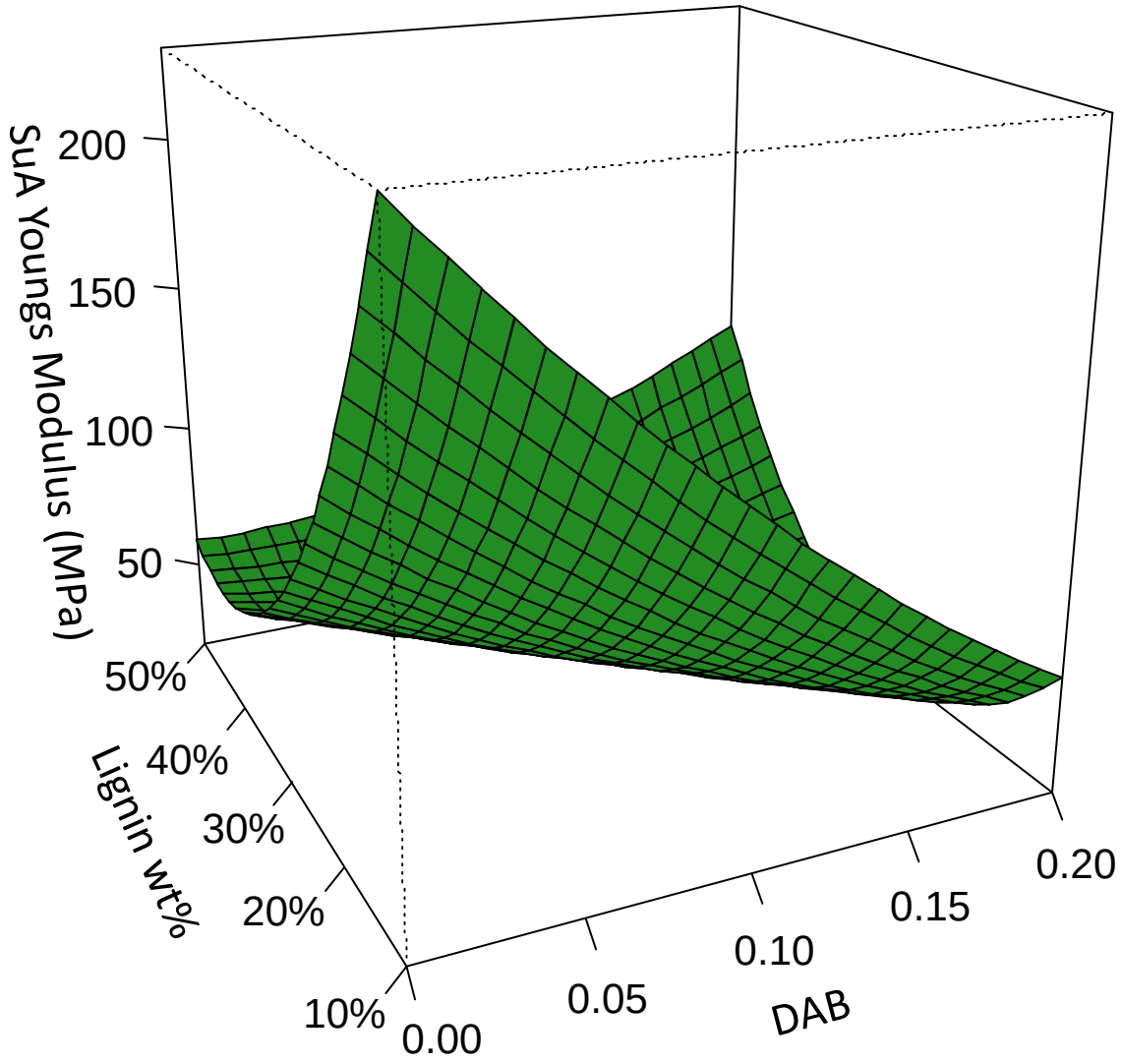

Figure 3.67 Response model plot of Youngs modulus versus lignin wt% and DAB content for SuA based lignin-copolymers

The tensile strength values for SuA copolymers range from 0.3 MPa for the SuA BD 0.8 10 wt% lignin sample up to 1.5 MPa for the SuA BD 1 30 wt% lignin sample. There appears to be a trend of increasing tensile strength up to 30-40 wt% lignin followed by a decrease as lignin approaches 50 wt%. Both the SuA and SA copolymerss follow this trend. At the 30 wt% lignin level the SuA copolymers can be seen to increase in tensile strength in order of decreasing DAB content. This trend is reversed at the 40 wt% lignin level however. A

regressional analysis was performed in order to plot a fitted model of tensile strength as a response to lignin and DAB content as shown in Figure 3.68. The maximum tensile strength value of 1.1 MPa for SuA copolymers obtained from the regression model was observed at 40 wt% lignin and no DAB.

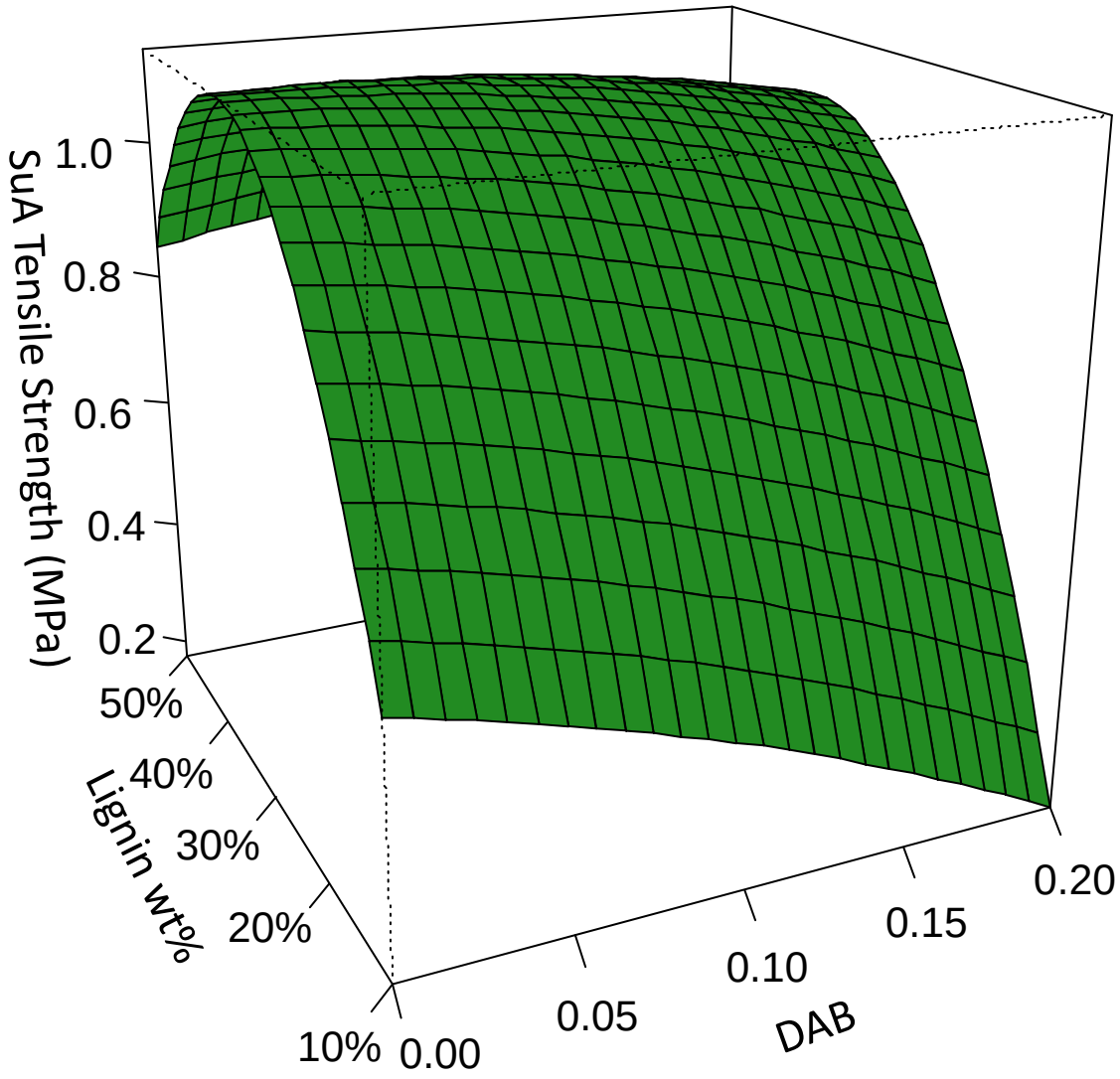

Figure 3.68 Response model plot of ensile strength versus lignin wt% and DAB content for SuA based lignin-copolymers

The strain at break values for SuA based lignin-copolymers span a range from 1% to 35%. The maximum strain at break is only about 50% of that observed from the AA copolymers. The greatest strain at break value for the SuA copolymers resulted from the samples

containing 40 wt% lignin and the intermediate BD level of 0.9. This deviates from both the AA and SA copolymers which gave a maximum strain at break value for the 30 wt% lignin samples. However, the maximum strain at break value for all copolymers resulted from a sample with formulation BD 0.9. A regressional analysis was performed in order to plot a fitted model of tensile strength as a response to lignin and DAB content as shown in Figure 3.69. The maximum strain at break value of 15% for SuA copolymers obtained from the regression model was observed at 30 wt% lignin and 0.1 DAB.

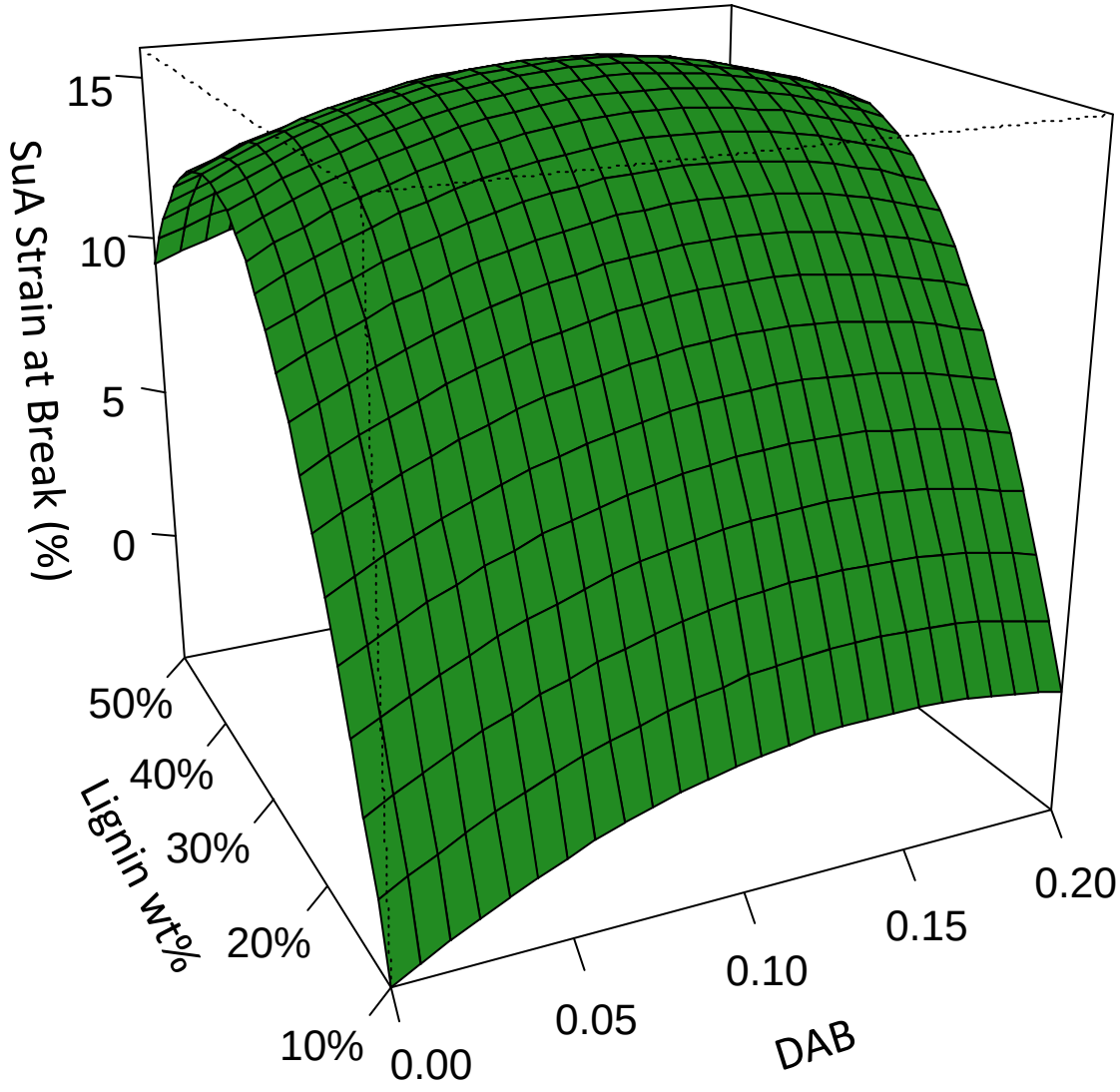

Figure 3.69 Response model plot of strain at break versus lignin wt% and DAB content for SuA based lignin-copolymers

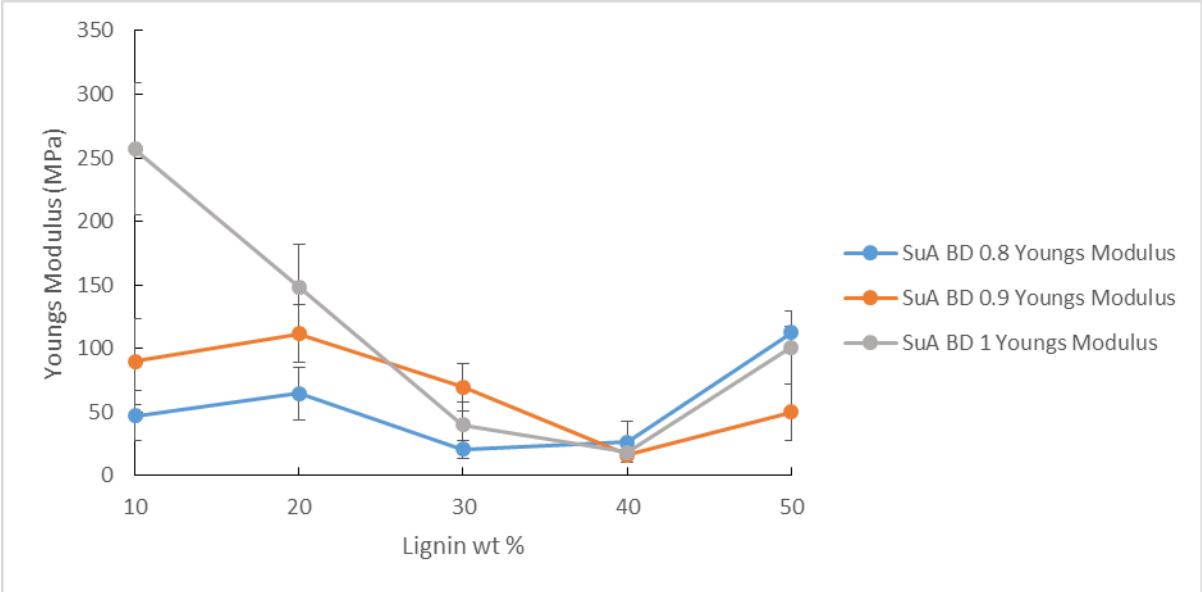

Figure 3.70 Youngs Modulus of SuA lignin copolymers plotted against lignin wt% for various DAB levels

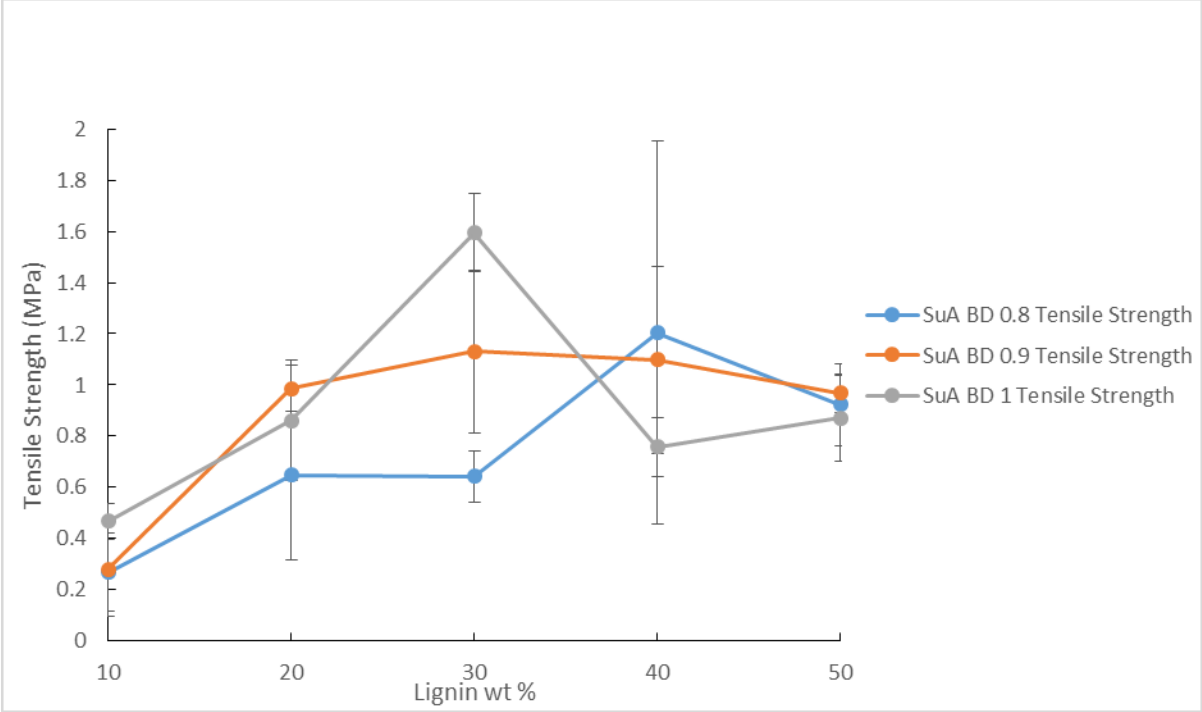

Figure 3.71 Tensile strength of SuA lignin copolymers plotted against lignin wt% for various DAB levels

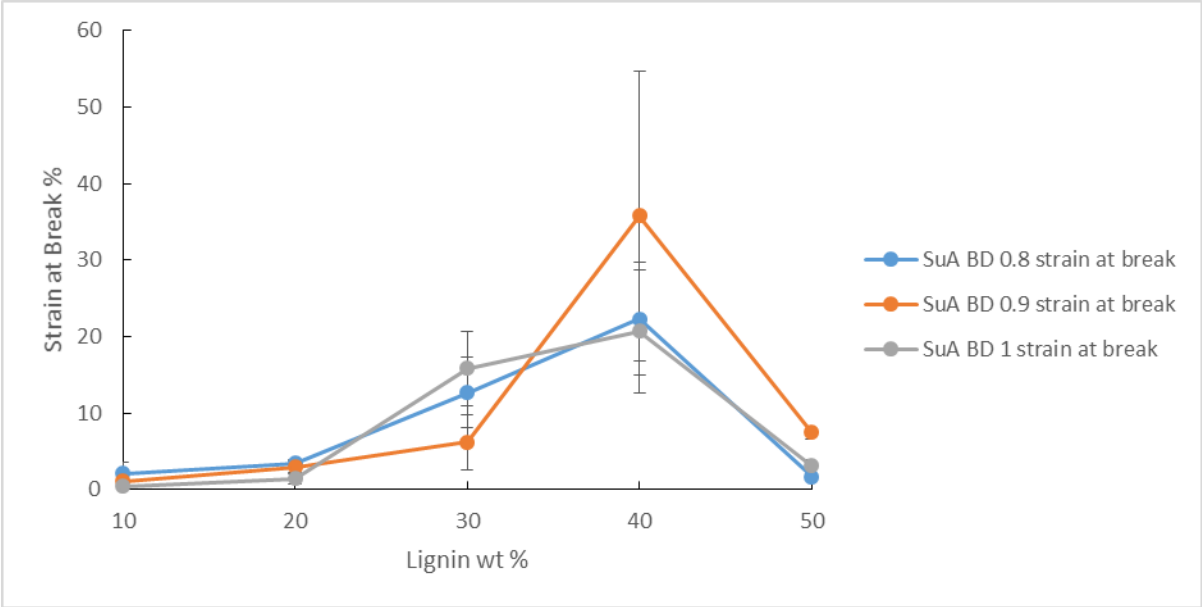

Figure 3.72 Strain at break of SuA lignin copolymers plotted against lignin wt% for various DAB levels

For the purpose of comparing diacid effect on tensile properties Figure 3.73, Figure 3.74 and Figure 3.75 show Young's modulus, tensile strength and strain at break respectively, for the AA, SA and SuA ester copolymers. The Young's modulus values increase in in the following order of AA < SuA < SA of copolymers. With only a few exceptions this is true at every DAB level. The type of diacid used in the synthesis has a large impact on the tensile strength of the resulting copolymer. The SA copolymers exhibit the greatest tensile strength (1.8 MPa) and the AA copolymers the lowest (0.1 MPa). This is true at the BD 1 and BD 0.9 levels, however, at the BD 0.8 level the AA copolymers surpass the SA and SuA copolymers in tensile strength at the 20, 30 and 40 wt% level. This is an interesting observation, especially when taken in consideration of the fact that at the BD 0.8 level the AA copolymers also exhibit the lowest Young's modulus and the highest capacity for elongation. The maximum strain at break values always result from the AA copolymers except at the 40 wt% lignin level for the BD 0.8 and 0.9 samples. Here the SuA copolymers slightly exceed the AA in maximum strain.

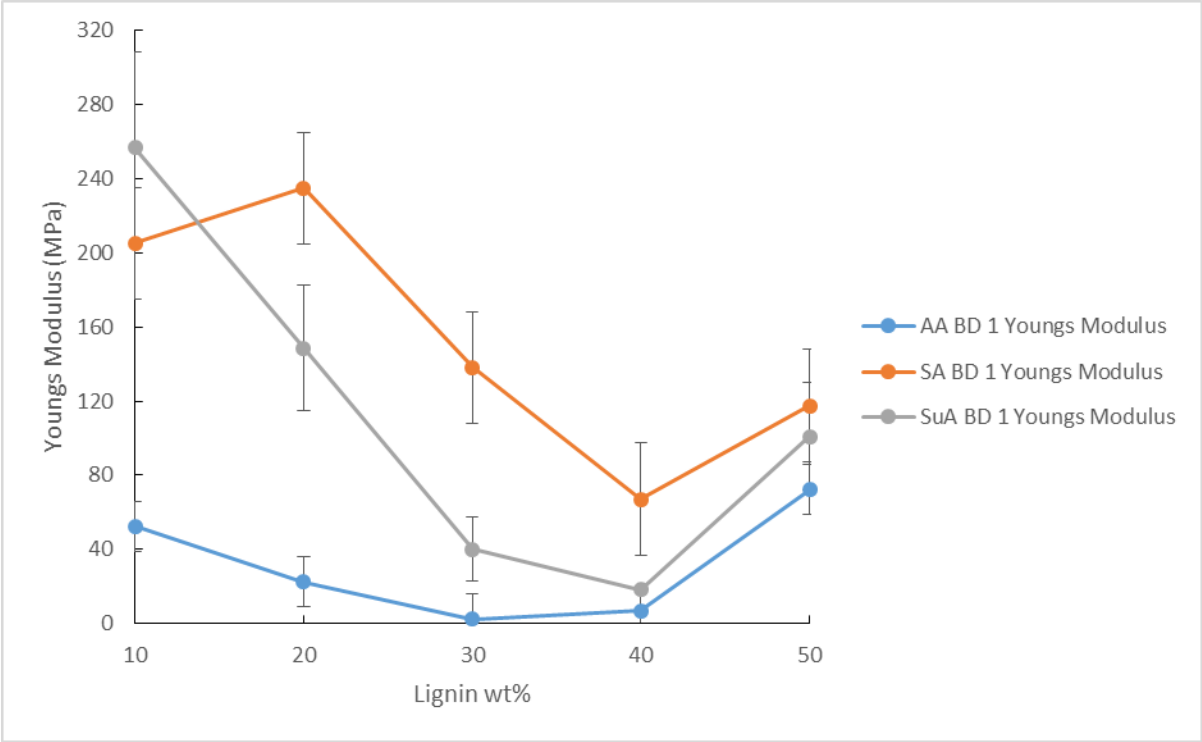

Figure 3.73 Plot of Young's modulus against lignin content for AA, SA and SuA BD 1 lignin-copolymers

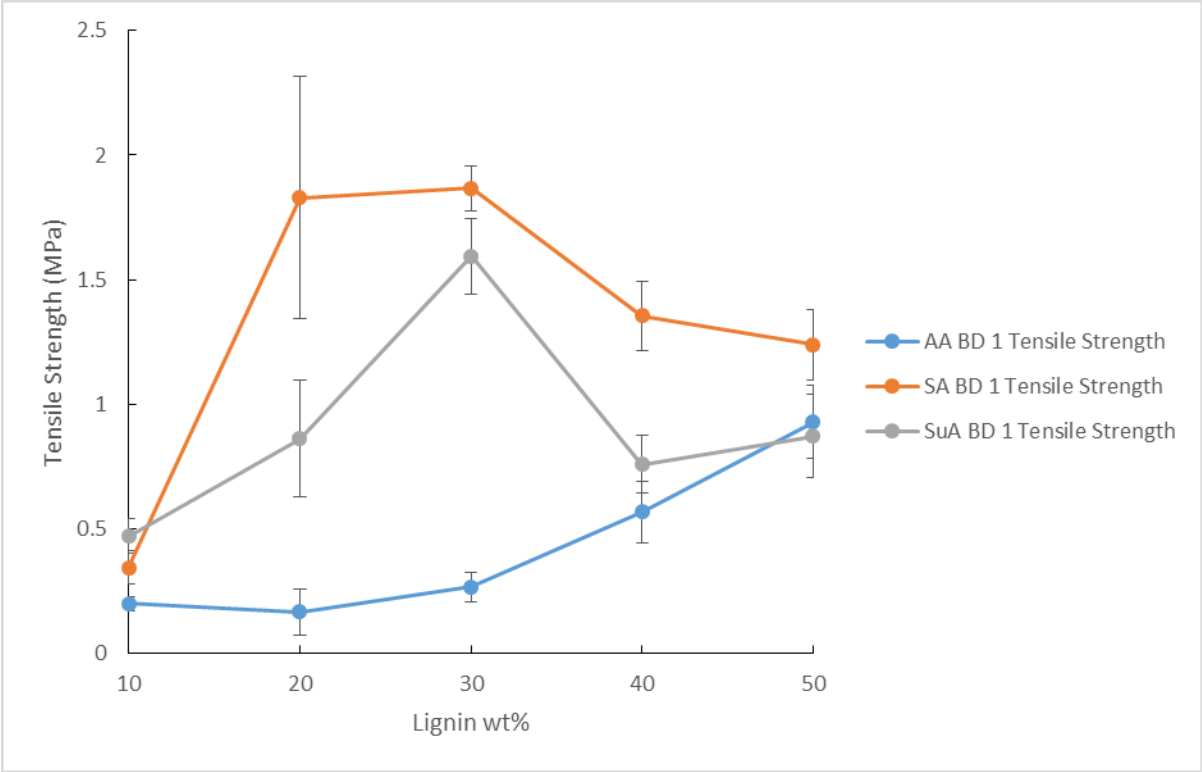

Figure 3.74 Plot of tensile strength against lignin content for AA, SA and SuA BD 1 lignin-copolymers

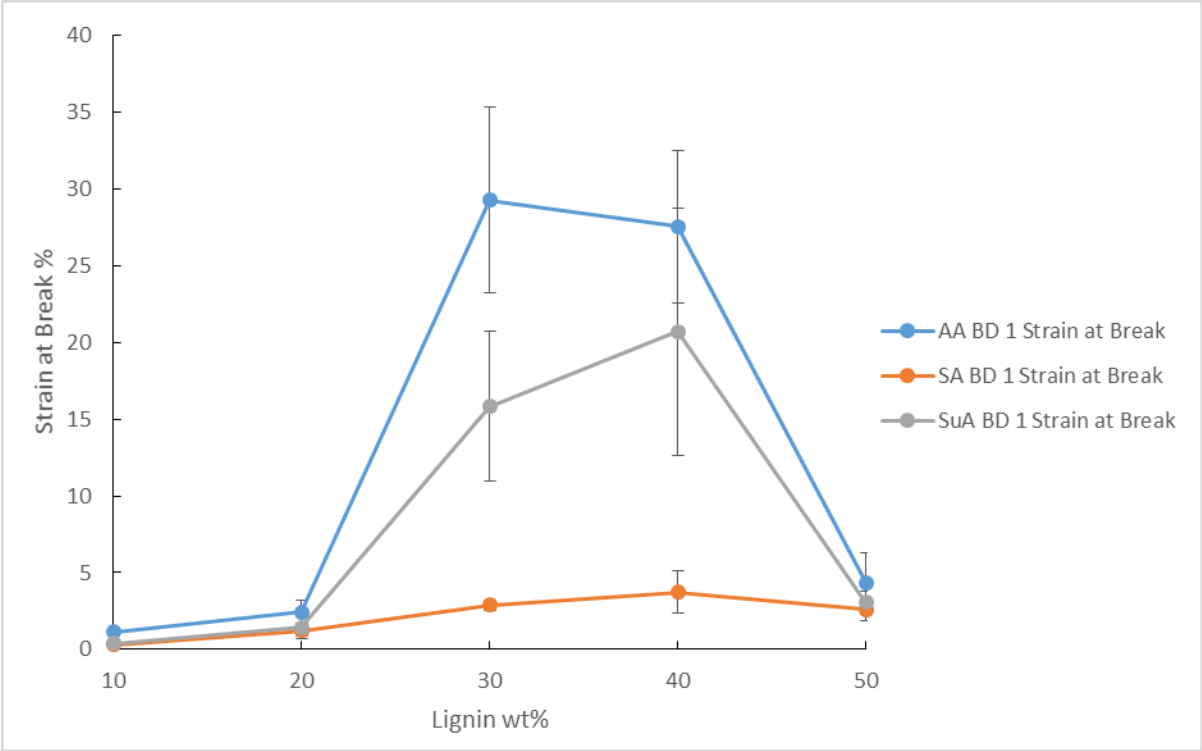

Figure 3.75 Plot of strain at break against lignin content for AA, SA and SuA BD 1 lignin-copolymers

In a study by Chung et al (2013) it was found that incorporation of 10 wt% lignin-graft-PLA into neat PLA resulted in a copolymer with slightly enhanced tensile strength (16%) and strain (9%) as compared to neat PLA. However, the tensile strength and strain were found to decrease upon incorporation of the PLA grafted lignin at the 40 wt% level. At both the high and low wt% of lignin-g-PLA the Young's modulus remained unaffected (Chung Y.-L. , et al., 2013). The samples in this study exhibited Young's modulus and tensile strength values nearly 10 times greater, due to using a stiff bioplastic, than the elastomeric copolymers from the current study. However, the maximum strain at break value of 72% percent from the current study greatly surpassed the maximum value achieved by Chung et al. (2013) which was 2.8%.

In another study by Kim et al the tensile strength and Young's modulus were found to increase substantially upon grafting of PLA onto lignin at a 10:15 mass ratio. The resulting

tensile properties were found to be dependent on the molecular weight of PLA. In the case of tensile strength nearly a 300% increase from 0.83 MPa to 3.80 MPa was observed over the neat PLA. The Young's modulus was found to increase from 40 MPa for neat PLA to 450 MPa upon incorporation of lignin (Kim, Kim, Lee, & Ahn, 2016). Futhermore, these values are on the same order as those observed in the current study. The maximum tensile strength of 3.80 MPa (Kim et al. 2016) is about double the maximum tensile strength of 1.74 MPa from copolymers in this study. Moreover, the maximum Young's modulus of 450 MPa is greater than the 338 MPa from this study.

Youngs Modulus (MPa)																		
	BD 0.8						BD 0.9						BD 1					
	AA		SA		SuA		AA		SA		SuA		AA		SA		SuA	
lignin wt%	response	stdev	response	stdev	response	stdev	response	stdev	response	stdev	response	stdev	response	stdev	response	stdev	response	stdev
10%	16.47	9.14	93.28	36.03	47.12	19.87	37.25	5.38	337.90	94.91	89.75	33.57	52.61	5.30	205.25	51.30	256.80	51.93
20%	22.92	5.16	113.53	63.75	64.68	20.85	12.78	1.47	214.80	58.16	111.54	22.57	22.30	2.71	235.03	83.98	148.50	33.92
30%	8.66	2.97	22.33	6.05	20.71	6.81	5.52	4.18	106.68	49.54	69.68	18.96	2.32	0.32	138.10	28.88	40.14	17.36
40%	41.37	26.42	47.86	22.32	26.41	16.40	17.45	3.28	68.16	64.05	16.45	1.70	6.78	0.83	67.13	45.68	18.08	1.29
50%	31.78	10.08	155.64	78.13	112.73	4.39	76.56	35.87	117.44	78.56	49.95	22.33	72.13	26.94	117.57	8.75	100.80	29.05
Tensile Strength (MPa)																		
	BD 0.8						BD 0.9						BD 1					
	AA		SA		SuA		AA		SA		SuA		AA		SA		SuA	
lignin wt%	response	stdev	response	stdev	response	stdev	response	stdev	response	stdev	response	stdev	response	stdev	response	stdev	response	stdev
10%	0.09	0.02	0.26	0.04	0.27	0.15	0.39	0.12	0.48	0.29	0.28	0.18	0.20	0.03	0.34	0.07	0.47	0.07
20%	0.96	0.27	0.46	0.50	0.65	0.33	0.28	0.02	0.43	0.12	0.99	0.09	0.16	0.09	1.83	0.49	0.86	0.23
30%	0.74	0.12	0.53	0.18	0.64	0.10	0.56	0.23	1.74	0.57	1.13	0.32	0.26	0.06	1.87	0.09	1.59	0.15
40%	1.14	0.61	0.72	0.28	1.20	0.75	0.71	0.03	1.20	0.68	1.10	0.36	0.57	0.12	1.35	0.14	0.76	0.12
50%	0.68	0.12	1.29	0.65	0.92	0.16	0.93	0.47	0.88	0.32	0.97	0.07	0.93	0.15	1.24	0.14	0.87	0.17
Strain at Break (%)																		
	BD 0.8						BD 0.9						BD 1					
	AA		SA		SuA		AA		SA		SuA		AA		SA		SuA	
lignin wt%	response	stdev	response	stdev	response	stdev	response	stdev	response	stdev	response	stdev	response	stdev	response	stdev	response	stdev
10%	2.46	0.31	0.71	0.27	2.08	1.41	3.74	2.65	0.29	0.14	1.07	0.30	1.13	0.19	0.30	0.03	0.39	0.03
20%	18.10	8.49	0.76	0.20	3.42	0.49	13.73	4.02	0.58	0.33	2.91	0.81	2.43	0.77	1.21	0.31	1.44	0.73
30%	37.04	6.50	20.17	11.94	12.69	4.58	72.61	24.93	8.14	4.85	6.20	3.61	29.30	6.05	2.88	0.33	15.85	4.89
40%	17.93	21.12	12.48	6.55	22.32	7.42	19.55	5.48	21.27	24.90	35.83	18.95	27.57	4.95	3.74	1.39	20.71	8.05
50%	13.44	4.72	3.49	2.61	1.71	0.36	6.80	4.84	2.46	0.60	7.45	0.81	4.33	1.95	2.60	0.74	3.06	0.75

Table 3.11 Tensile testing results and standard deviations for all diacids at all DAB levels across all lignin contents

3.3.5.1 Analysis of Variance on Mechanical Properties

In order to determine the significance of the lignin, DAB and acid variables an analysis of variance was conducted on the young's modulus, tensile strength and strain at break responses (Table 3.12).

Table 3.12 Analysis of variance strain at break

	Sum Sq	Df	F value	Pr(>F)
(Intercept)	16367.72	1	230.0333	4.07E-30
Lignin	11321.01	4	39.7766	1.86E-21
DAB	660.811	2	4.643546	0.011343
Acid	4762.921	2	33.46924	2.29E-12
Lignin:DAB	644.5826	8	1.132377	0.346267
Lignin:Acid	6659.78	8	11.69964	2.52E-12
DAB:Acid	444.1672	4	1.560591	0.188946
Lignin:DAB:Acid	4640.107	16	4.075778	3.20E-06
Residuals	8894.214	125		

These results indicate that the lignin content, DAB content as well as the type of acid used are significant at a 95% confidence level. The lignin and acid treatments are highly significant while the DAB treatment is considerably closer to the p-value cutoff for significance at 0.01134. This analysis also reveals that there are significant interactions between the lignin and acid as well as a three-way interaction between lignin, DAB and acid so the interpretation of the main effects of treatments may not be appropriate. Table 3.13 shows the analysis of variance performed on tensile strength response.

Table 3.13 Analysis of variance for lignin-copolymer tensile strength

	Sum Sq	Df	F value	Pr(>F)
(Intercept)	94.09411	1	1042.975	1.66E-62
Lignin	10.63072	4	29.45874	2.96E-17
DAB	0.884239	2	4.900622	0.008933
Acid	4.533856	2	25.12749	6.72E-10
Lignin:DAB	2.541258	8	3.521033	0.001051
Lignin:Acid	2.033239	8	2.817149	0.006615
DAB:Acid	4.371134	4	12.11283	2.37E-08
Lignin:DAB:Acid	7.242221	16	5.01722	6.55E-08
Residuals	11.27713	125		

All two way interactions and the three way interactions resulted in p-values less than 0.05 which indicates that they are significant. Because of the presence of interactions between variables making conclusions about the main effects is not possible. Table 3.14 shows the results from an analysis of variance conducted for the Young's modulus response. These results also indicate the significance of all two-way and three way interactions, therefore it is not appropriate to conclude anything about main effects.

Table 3.14 Analysis of variance for lignin-copolymer young's modulus

	Sum Sq	Df	F value	Pr(>F)
(Intercept)	976010.8	1	848.2376	1.50E-57
Lignin	190930.1	4	41.48369	4.30E-22
DAB	56852.31	2	24.70478	9.09E-10
Acid	306803.8	2	133.3195	1.00E-31
Lignin:DAB	69322.91	8	7.53095	3.57E-08
Lignin:Acid	81597.01	8	8.864357	1.46E-09
DAB:Acid	42838.14	4	9.307512	1.29E-06
Lignin:DAB:Acid	107747.4	16	5.852613	2.34E-09
Residuals	143829.2	125		

3.3.6 Melt Testing of Lignin Copolymers

Melt testing was performed to investigate whether lignin copolymers had potential as a true thermoplastic material that could be melt reprocessed (Table 3.15). The results demonstrate that the lignin-copolymers with a lignin content above 30 wt% exhibited no melting behavior. This observation supports the DSC results in which no melting endotherms are observed for copolymers with 40 and 50% lignin. In addition, melting behavior is always observed for polymers with 0 and 10 lignin %. These results suggest that lignin has the effect of reducing the mobility of the copolymer molecules until at a high enough content the lignin ultimately leads to a material that is incapable of melting. For the SuA, AA and SA BD 0.1 samples at the 30 wt% lignin level the copolymers were observed to become sticky or tacky. Separate pieces of copolymer would stick to one another but would not flow to create a single piece of copolymer. It is likely that melt behavior is occurring under these circumstances but the

viscosity of the polymer in the melt is sufficiently high to resist flow under the conditions at which the experiments were ran.

Table 3.15 Melt testing data for the various lignin-copolymer formulations

	SuA			AA			SA		
Lignin wt%	BD 0.8	BD 0.9	BD 1	BD 0.8	BD 0.9	BD 1	BD 0.8	BD 0.9	BD 1
0	yes	yes	yes	yes	yes	yes	yes	yes	yes
10	yes	yes	yse	yes	yes	yes	yes	yes	yes
20	tacky	tacky	tacky	tacky	tacky	yes	tacky	yes	no
30	no	no	no	no	no	no	no	yes	no
40	no	no	no	no	no	no	no	no	no
50	no	no	no	no	no	no	no	no	no

3.3.6.1 Tensile Testing of Re-Melt Samples

To test the re-melting behavior of the lignin-copolymers only the AA BD 0.8 based lignin-copolymer with 20% lignin was evaluated for their tensile properties. The tensile modulus, strength and strain at break properties before and after remelting for the lignin-copolymer AA BD 0.8 20 wt% samples are respectively shown in Figure 3.76, Figure 3.77 and Figure 3.78. From these results it can be seen that the mechanical properties of the copolymer do appear to be affected by a melt cycle with a clear degradation of both the Young's modulus and tensile strength. It is hypothesized that this results from changes in morphology of the copolymer upon heat treatment. Because the re-melt samples were subjected to pressure the result was a sample with considerably reduced thickness as compared to the unprocessed copolymer counterpart. This would have allowed for much more rapid cooling of the sample and less time for crystallization of the prepolymer matrix leading to a diminished Youngs modulus and tensile strength (Perego, 1996). A separate contributing factor to this observed behavior may be chain degradation of the prepolymer due to hydrolytic action (Migliaresi, 1991). Cleavage of prepolymer chains would also lead to the observation of diminished mechanical properties (Vieira, 2011). The Young's modulus was observed to decrease to 17% of its original value, from 23 MPa to 4 MPa, after the sample had been melted. The tensile strength decreased to about 30% of its original value, from 1 to 0.3 MPa, after melting. The strain at break remained unchanged within the bounds of experimental error. Because thermoplastic materials rely on the ability to be melt processed with minimal loss of mechanical properties these results offer evidence for the need of further investigation of the impact of melting on properties. Additionally it would be appropriate to conduct melt testing on samples generated from an extruder as this would more closely replicate the conditions the material is likely to experience in a commercial setting.

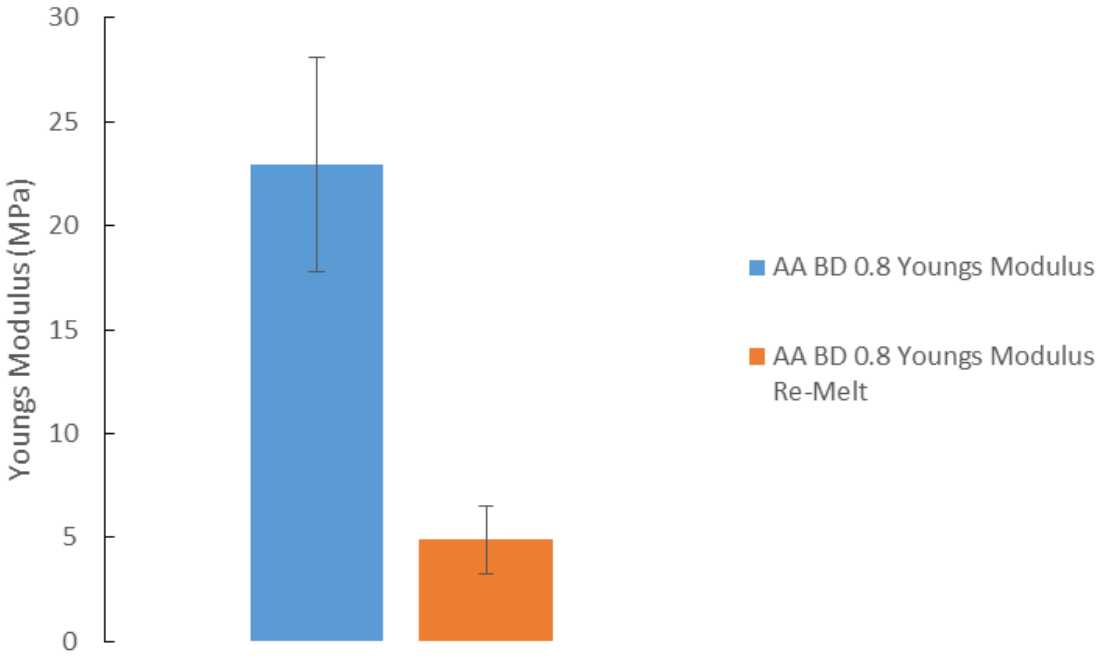

Figure 3.76 Plot of Young's modulus for lignin-copolymer AA BD 0.8 at 20 wt% lignin before and after melting

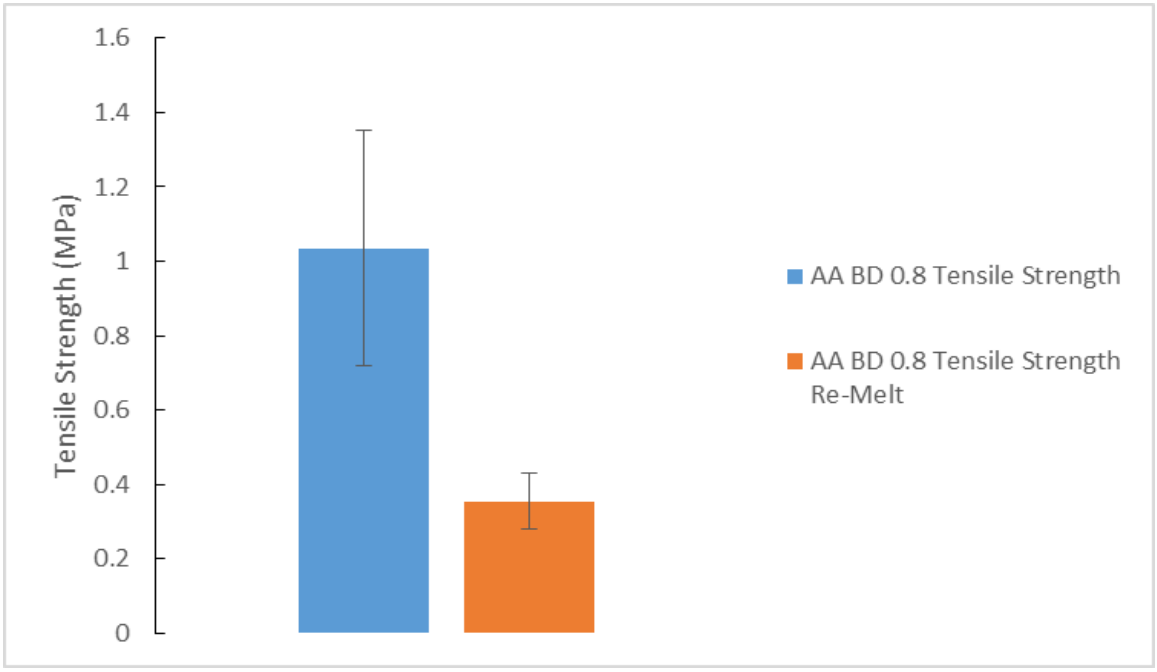

Figure 3.77 Plot of tensile strength for lignin-copolymer AA BD 0.8 20 wt% lignin before and after melting

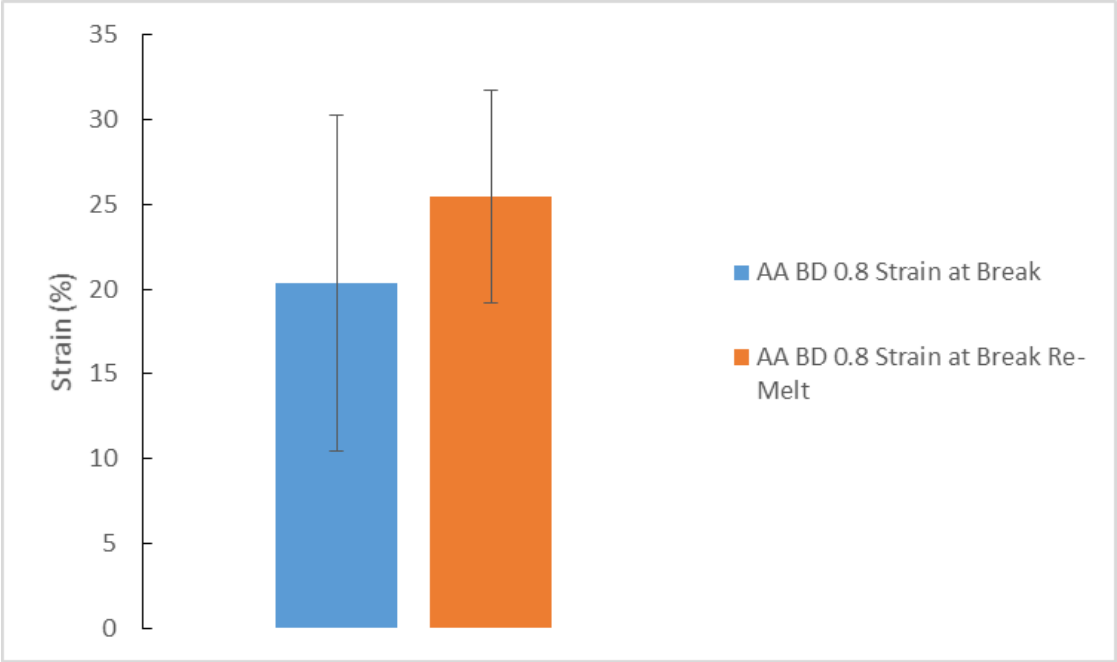

Figure 3.78 Plot of strain at break for lignin-copolymer AA BD 0.8 20 wt% lignin before and after melting

3.3.6.2 Material Defects

To help interpret the mechanical property data morphological analysis by optical microscopy was performed to detect any material defects. The types of defects expected were the presence of air bubbles, as shown in Figure 3.79. Samples which exhibited significant melt flow behavior after polymerization tended to have less of these defects. Table 3.16 shows which samples exhibited defects.

Table 3.16 Shows which samples exhibited defects

	AA			SA			SuA		
lignin wt%	BD 0.8	BD 0.9	BD 1	BD 0.8	BD 0.9	BD 1	BD 0.8	BD 0.9	BD 1
10	no	no	no	no	no	no	no	no	no
20	no	no	no	no	no	no	no	no	no
30	no	yes	yes	yes	yes	yes	yes	no	yes
40	yes	yes	yes	yes	yes	yes	yes	yes	yes
50	yes	yes	yes	yes	yes	yes	yes	yes	yes

Figure 3.79 Lignin copolymer with defects

It is hypothesized that these defects resulted from the generation of water vapor resulting from the condensation reaction forming the amide and ester linkages. The presence of defects can be seen to follow the trend of melt behavior shown in Table 3.15. Samples which did not exhibit melt behavior were observed to contain defects. Particularly, many of the samples at the 30 wt% lignin level and all the samples with lignin greater than 30 wt% had defects present. Furthermore, it is likely that the presence of these defects contributed to larger standard deviations in tensile testing.

3.3.6.3 Analysis of Variance of Mechanical Properties after Melt Processing

In order to determine if there were significant differences in tensile properties as a result of melt processing an analysis of variance was conducted between samples which did and did not undergo a melt cycle. These results are shown in Table 3.17, Table 3.18 and Table 3.19.

Table 3.17 Analysis of variance melt processing strain at break

	Sum Sq	Df	F value	Pr(>F)
(Intercept)	6398.933	1	112.9289	3.48E-09
Processed	363.3894	1	6.413127	0.020852
Residuals	1019.941	18		

Table 3.18 Analysis of variance melt processing tensile strength

	Sum Sq	Df	F value	Pr(>F)
(Intercept)	1.135077	1	26.55874	6.67E-05
Processed	1.820128	1	42.58768	3.91E-06
Residuals	0.769291	18		

Table 3.19 Analysis of variance melt processing Youngs modulus

	Sum Sq	Df	F value	Pr(>F)
(Intercept)	213.5398	1	13.35514	0.001814
Processed	1611.894	1	100.8106	8.39E-09
Residuals	287.808	18		

The statistical analysis performed on melt processed tensile testing data indicates that the tensile strength, Young's modulus and strain at break are significantly impacted as a result of melt processing although the strain at break p-value of 0.02 was near the cutoff for significance which was a p-value of 0.05.

4 Improving Lignin Copolymer Properties by using a Catalyst and Micronized Lignin

This chapter is focused on improving the lignin-copolymer properties by two approaches: (i) using micronized lignin by ball milling to minimize air-bubble defects in the lignin copolymer and (ii) improving the polymerizing of the lignin-copolymer by addition of TSA catalyst. Only a limited number of the AA based lignin-copolymers were prepared and characterized in this chapter.

4.1 Ball Milled Lignin in Copolymers

As mentioned before, the majority of lignin-copolymer samples generated had defects in the form of air bubbles that were created by vapor evolved as a result of the condensation reaction occurring both within the prepolymer and between prepolymer and lignin. By decreasing the lignin particle size and increasing the available surface area of the lignin, by ball milling, would improve the reactivity between lignin and the prepolymer and improve packing of the lignin within the copolymer. Furthermore, it was thought that these voids might be initiating at kraft lignin particles which were acting as nucleation points for the formation of the void or bubble. Therefore, an attempt was made at reducing the particle size of the lignin in an effort to inhibit gas bubble formation and improve the reaction between lignin and prepolymer and thus improve polymer properties.

4.1.1 Ball Milling

Lignin was ball milled for a week and the particle size both before and after ball milling was measured using optical microscopy. Optical micrographs of original and ball milled Indulin kraft lignin are shown respectively in Figure 4.1 and Figure 4.2. Ball milling reduced the lignin particle size from about 10 to <1 μm.

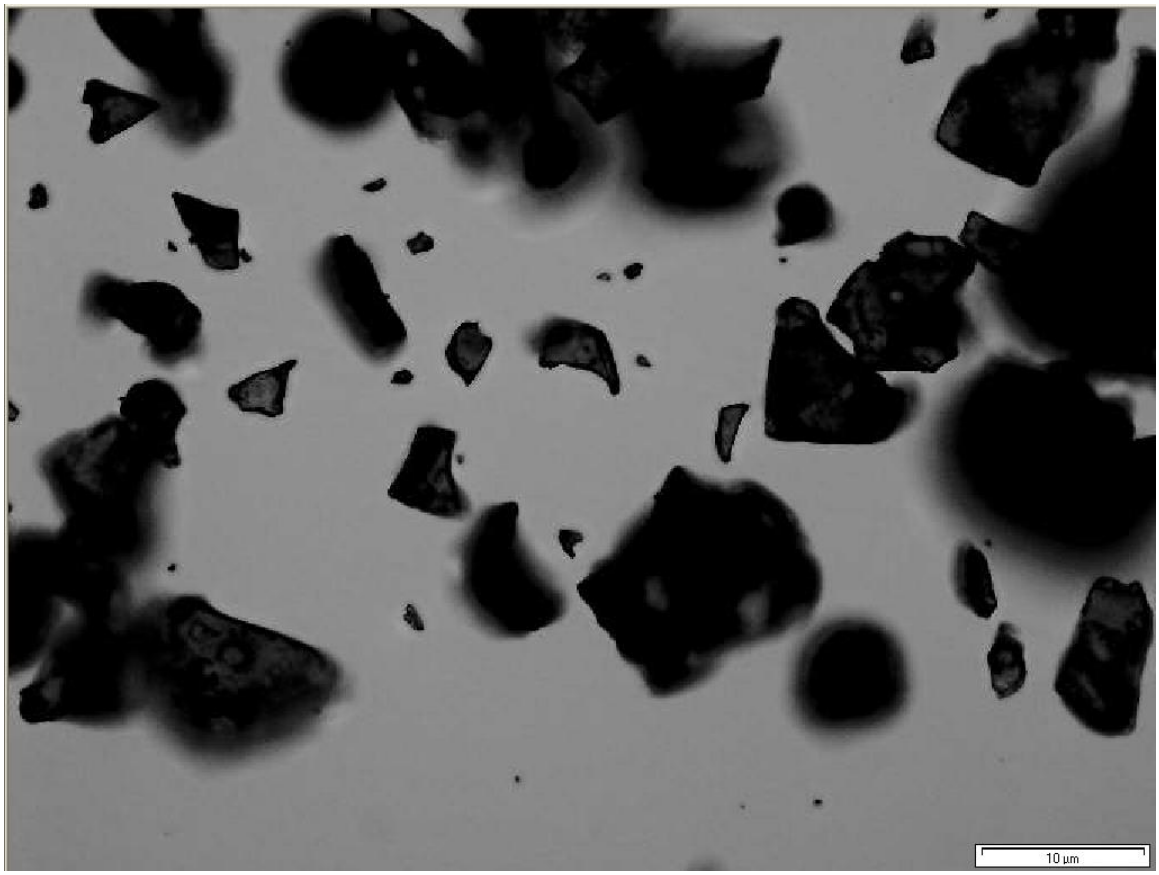

Figure 4.1 Light micrograph of Indulin AT kraft lignin

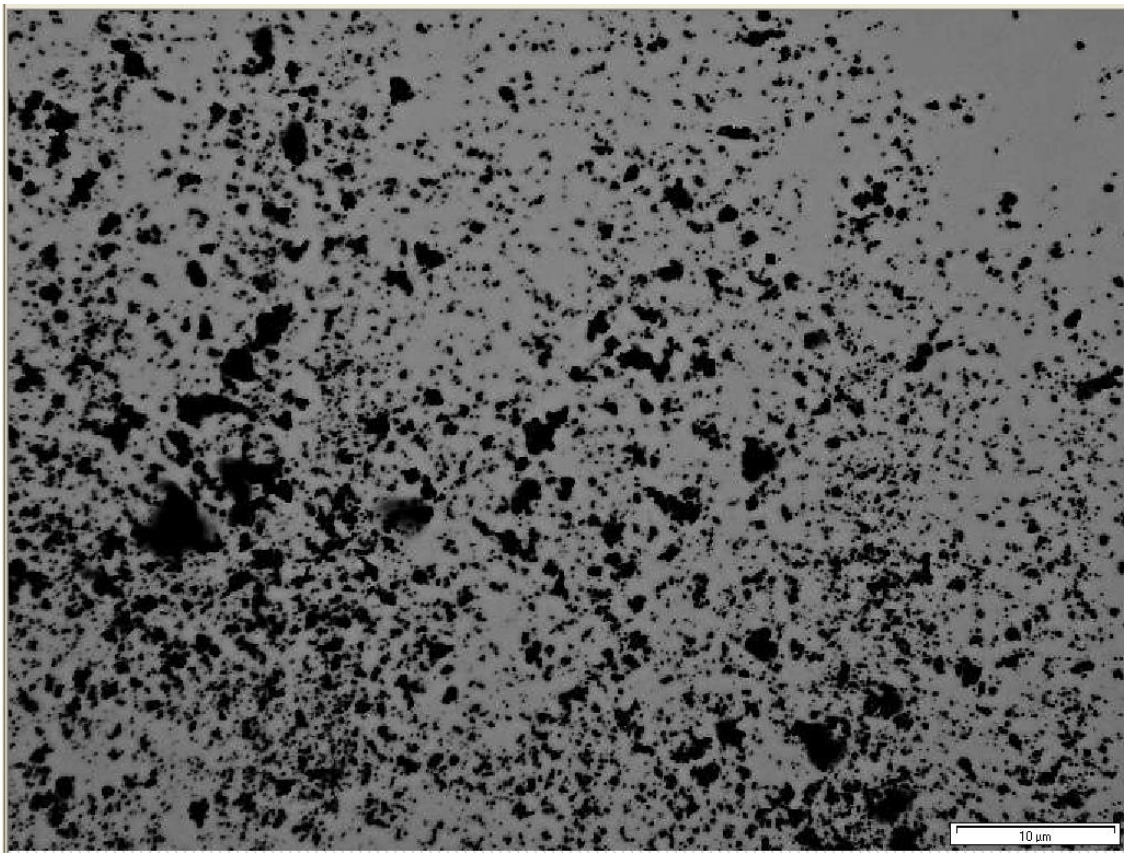

Figure 4.2 Light micrograph of ball milled Indulin AT kraft lignin

4.1.2 Mechanical Testing of Ball Milled Lignin Copolymers

It is expected that lignin particle size in the copolymers will influence mechanical properties. AA BD 0.8 based lignin-copolymers were prepared to evaluate the tensile properties of the ball milled lignin-copolymer samples as compared against non-ball milled controls. The Young's modulus, tensile strength and strain at break results are shown in Figure 4.3, Figure 4.4 and Figure 4.5, respectively. In the case of the Young's modulus the ball milled samples generally did not show much change as compared to original lignin based copolymers. The exception is at the 50 wt% lignin level where the ball milled samples (130 MPa) where over 4 times greater than the samples without ball milling (30 MPa). Table 4.1 shows the analysis of variance conducted on the young's modulus response analyzing the significance of the ball milling treatment. Because of the presence of an interaction between the lignin and ball milling factors it is not appropriate to analyze the significance of main effects.

Table 4.1 Analysis of variance for young's modulus of control and ball milled lignin-copolymers

	Sum Sq	Df	F value	Pr(>F)
(Intercept)	606.9914	1	1.075469	0.30502
lignin	12830.66	1	22.7334	1.84E-05
Ball.Mill	2295.027	1	4.066337	0.04948
lignin:Ball.Mill	5817.454	1	10.30738	0.002391
Residuals	26526.65	47		

In the case of the tensile strength the samples without ball milling at the 20 and 30 wt% lignin levels were about twice those of the samples that were ball milled. Table 4.2 shows the results from an analysis of variance conducted on the tensile strength in response to ball milling. The p-value of 0.139 indicates the lack of significance for the effect that ball milling has on the tensile strength.

Table 4.2 Analysis of variance for tensile strength of control and ball milled lignin-copolymers

	Sum Sq	Df	F value	Pr(>F)
(Intercept)	0.718429	1	6.01669	0.017937
lignin	1.201461	1	10.06198	0.002667
Ball.Mill	0.269296	1	2.255295	0.139847
lignin:Ball.Mill	0.079682	1	0.667322	0.418108
Residuals	5.612084	47		

For the strain at break the responses between the two were comparable except at the 30 wt% lignin level where the ball milled samples exhibited a strain at break of 130% while the un-ball milled samples were 30%. This is a 4-fold increase. Table 4.3 shows the results from an analysis of variance conducted on the strain at break response. The 0.178 p-value for the ball mill variable indicates that ball milling has no significant impact on the strain at break of the lignin copolymers.

Table 4.3 Analysis of variance for strain at break of control and ball milled lignin-copolymers

	Sum Sq	Df	F value	Pr(>F)
(Intercept)	6624.198	1	7.410397	0.009069
lignin	39.71147	1	0.044425	0.833977
Ball.Mill	1663.828	1	1.861301	0.178972
lignin:Ball.Mill	218.4391	1	0.244365	0.623374
Residuals	42013.58	47		

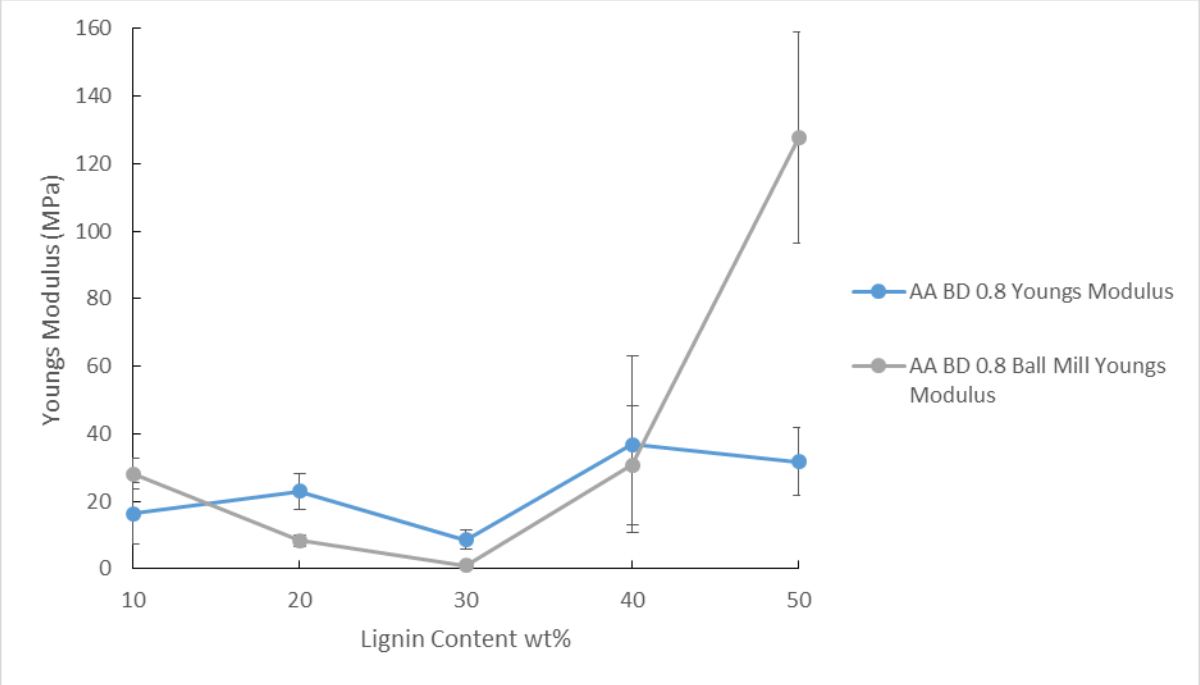

Figure 4.3 Young's modulus versus lignin content for AA BD 0.8 lignin-copolymers utilizing ball milled versus control Indulin AT lignin

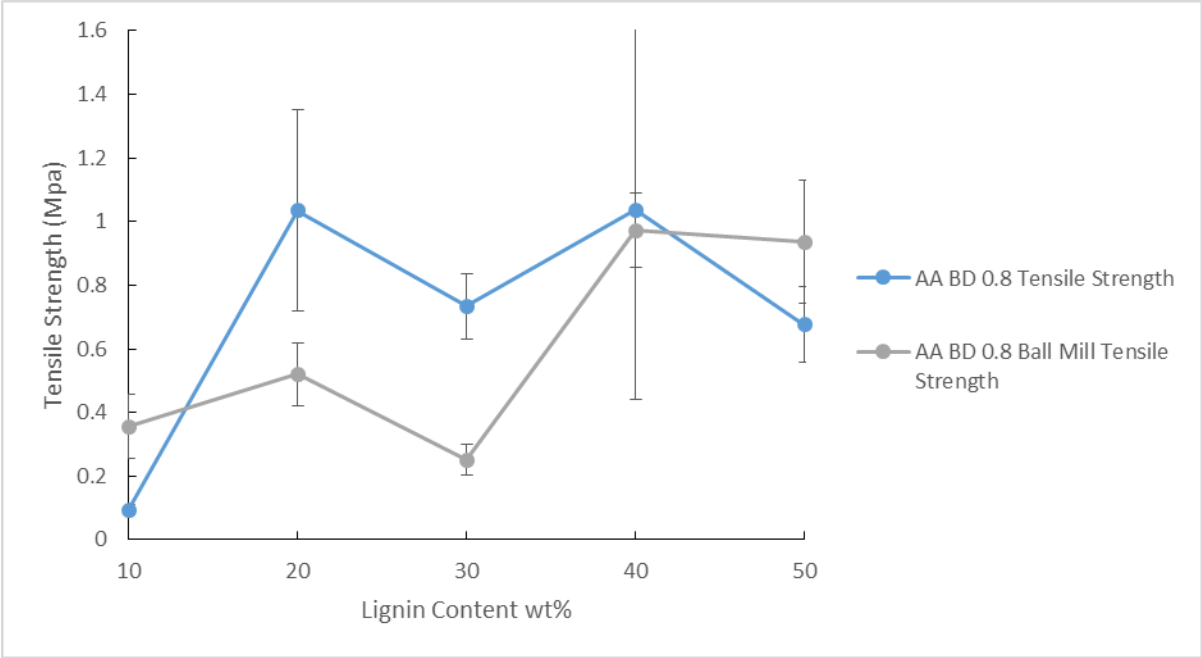

Figure 4.4 Tensile strength versus lignin content for AA BD 0.8 lignin copolymers utilizing ball milled versus control Indulin AT lignin

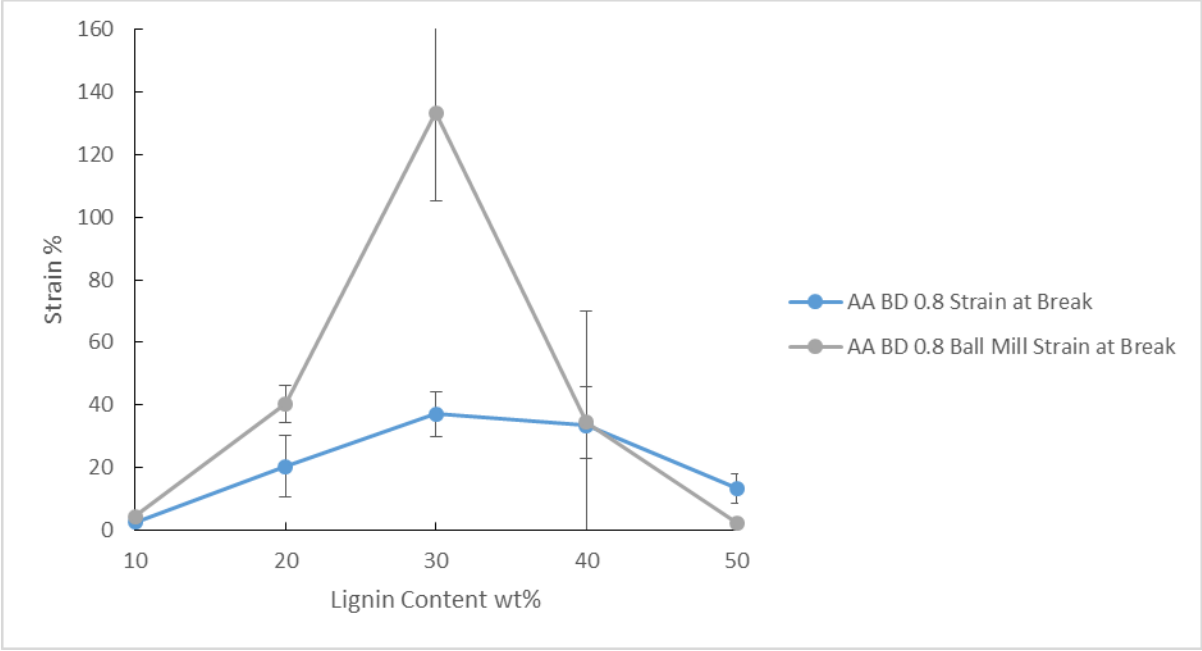

Figure 4.5 Strain at break versus lignin content for AA BD 0.8 lignin-copolymers utilizing ball milled versus control Indulin AT lignin

4.2 TSA Catalysis of Lignin Copolymers

To speed up the condensation reaction between lignin and prepolymer and fully polymerize the copolymer TSA catalyst was used. It was hypothesized that this will improve lignin copolymer properties. For this section of work only AA BD 1 based lignin-copolymers were prepared.

4.2.1 Prepolymer with TSA Catalyst

Prepolymers were made according to the previously outlined synthesis, however, TSA catalyst was added after 3 h into the melt condensation reaction (where the lignin would be added for the lignin copolymers). The prepolymer containing TSA catalyst was analyzed using FT-IR, DSC, DMA and ESI-MS.

4.2.1.1 FT-IR Analysis of Prepolymers with TSA Catalyst

The progression of polymerization for the TSA catalyzed AA BD 1 prepolymer was monitored using FT-IR spectroscopy for the ester band, after peak fitting and compared against the uncatalyzed prepolymer. The prepolymer ester content as a function of reaction time are shown in Figure 4.6. These results indicate that addition of TSA speeds the prepolymer polymerization reaction and extent of polymerization, as expected.

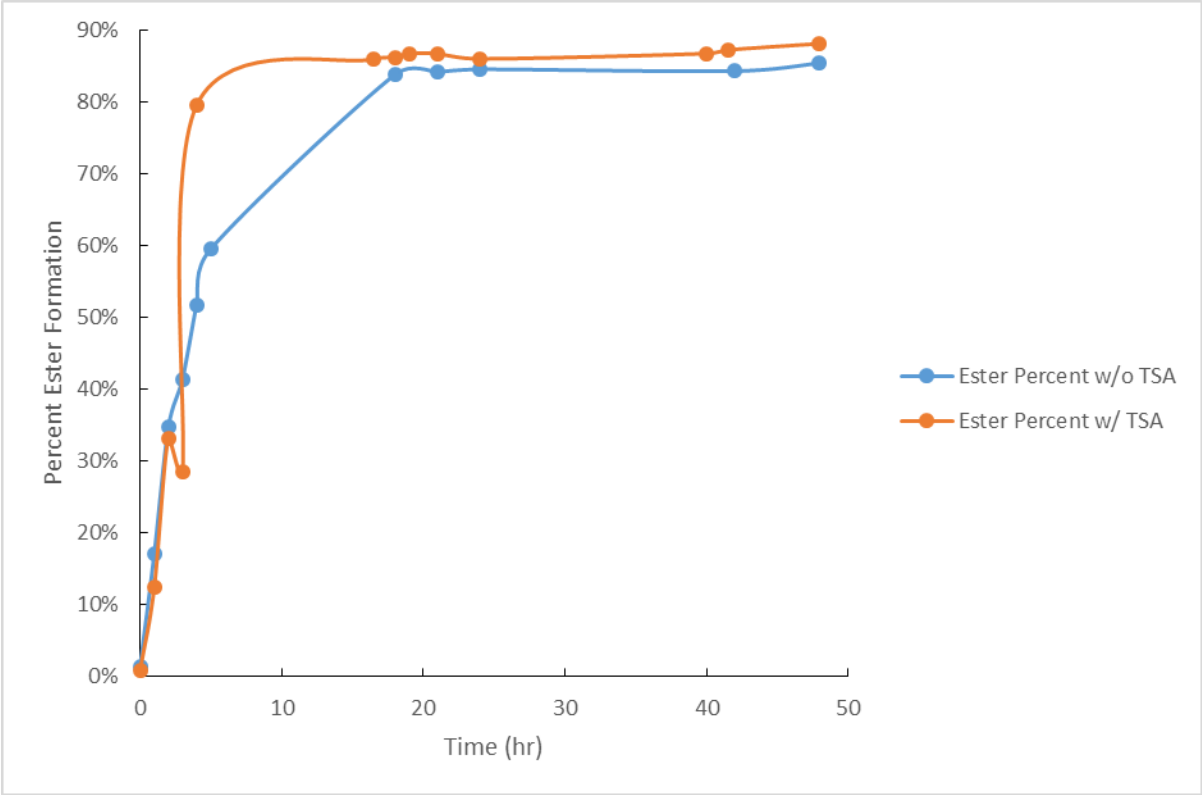

Figure 4.6 Prepolymer ester percentages resulting from FTIR spectral peak fitting of prepolymer with and without catalyst.

4.2.1.2 DSC Analysis of Prepolymer Containing TSA Catalyst

The AA BD 1 prepolymer with no catalyst gave a T_g and T_m of -54.6°C and 40.0°C, respectively. While the catalyzed prepolymer increased both prepolymer T_g and T_m at -20.8°C and 48.8°C, respectively. Both thermal transitions increase in response to presence of the catalyst. This is consistent with a more completely polymerized prepolymer having a greater chain length. Larger molecules result in greater intermolecular attractive forces and a higher melt temperature (Fatou & Mandelkern, 1984).

4.2.1.3 DMA of Prepolymer Containing TSA Catalyst

T_m values determined by DMA of the uncatalyzed and catalyzed AA BD 1 prepolymer are respectively at 44.4°C and 47.8°C. These results are in agreement with the observations from DSC analysis and further support the role that TSA catalyst plays in enhancing the polymerization reaction to generate molecules of greater chain length.

4.2.1.4 ESI-MS Analysis of Prepolymer Containing TSA Catalyst

To support the extent of polymerization of the prepolymer with and without TSA, ESI-MS analysis was performed on AA BD 1 PP samples with and without TSA catalyst. The results for number average molecular weights (M_n) calculated from the mass spectra are shown plotted against polymerization time in Figure 4.7. The M_n at 48 hours of polymerization were calculated at 1031 and 828 g/mol for the uncatalyzed and catalyzed prepolymers, respectively. Throughout the duration of the polymerization reaction the uncatalyzed prepolymer was observed to exhibit a higher M_n. These results conflict with what was expected, and FTIR results, in that the uncatalyzed prepolymer had a higher M_n and cannot be explained.

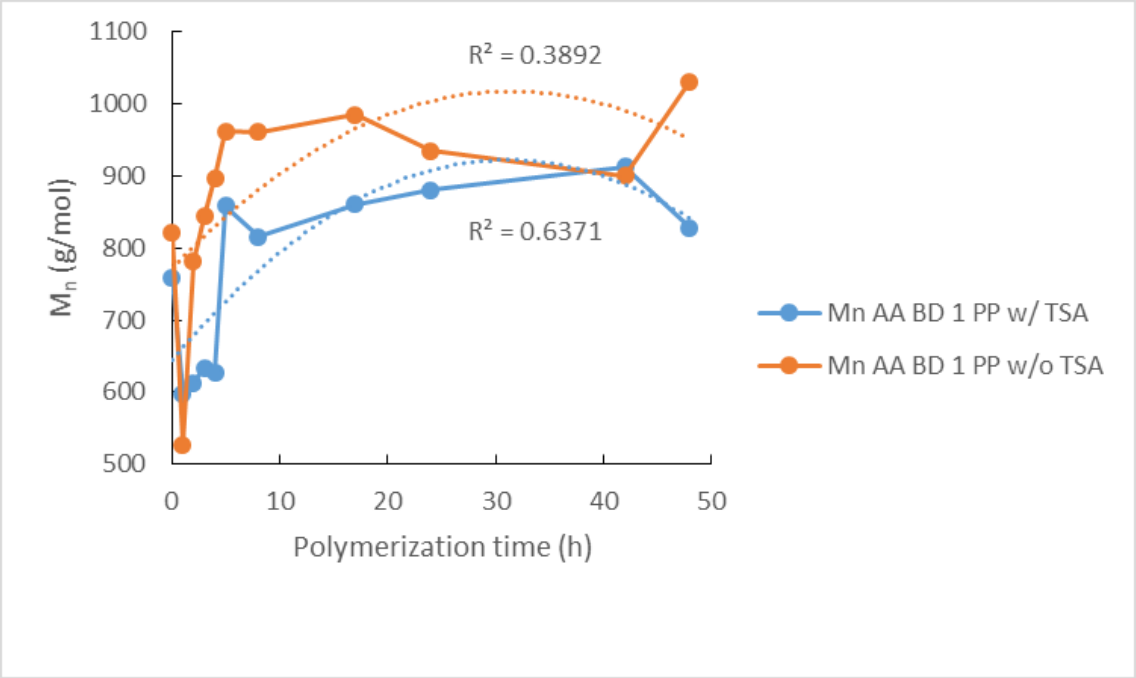

Figure 4.7 M_n calculated results from AA BD 1 PP with and without TSA catalyst plotted against length of polymerization time in h

4.2.2 Characterization of Lignin-Copolymers with TSA Catalyst

AA BD 1 based lignin-copolymers were synthesized using TSA catalyst which was added at the same time as lignin (3 h). The resulting copolymers where characterized by FT-IR, tensile stress strain testing, DSC, DMA and TGA.

4.2.2.1 FT-IR TSA Catalyst Comparison

Ester formation was monitored by FTIR spectroscopy, after peak fitting the carbonyl band. The progression of the ester band in sample lignin copolymer AA BD 1 30 wt% lignin is shown in Figure 4.8. The results show that there was no difference in ester formation by the addition of catalyst, which was unexpected, because differences were observed in prepolymer synthesis.

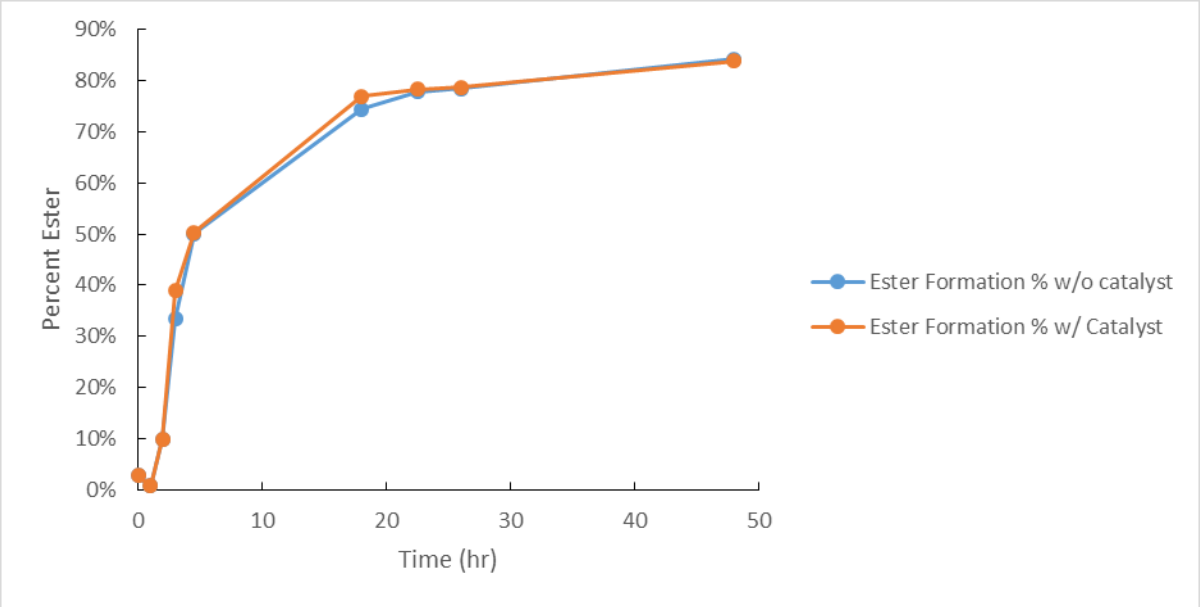

Figure 4.8 Ester formation in the catalyzed/uncatalyzed prepolymer by FT-IR peak fitting

4.2.2.2 Tensile Testing TSA Catalyst Comparison

The addition of TSA as a catalyst for polymerization of lignin and prepolymer was observed to impart enhanced mechanical properties. Plots of Young's modulus, tensile strength and strain at break with lignin content for the lignin-copolymer AA BD 1 are shown in Figure 4.9, Figure 4.10 and Figure 4.11, respectively.

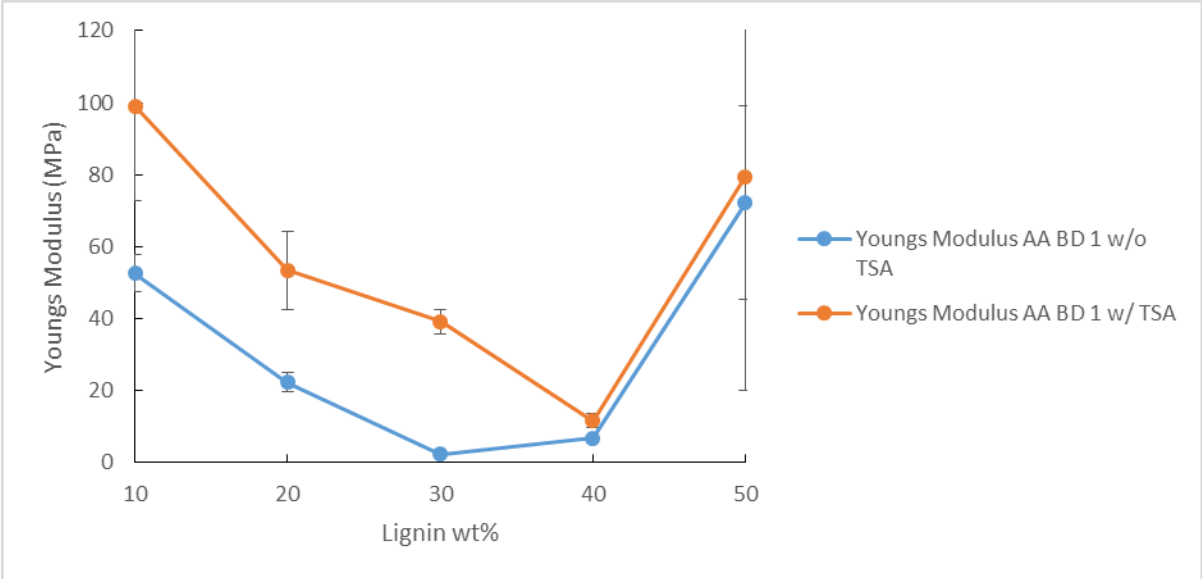

Figure 4.9 Plot of Young's modulus for the catalyzed and uncatalyzed AA BD 1 lignin copolymers with lignin content.

Young's modulus for the various AA BD 1 lignin-copolymers ranged between 5 and 100 MPa, with the 10% lignin copolymer polymerized with catalyst showed the highest stiffness (Figure 4.9). The TSA catalyzed lignin-copolymer series were about 40 MPa stiffer than the non-catalyzed series up to 30% lignin, and were only about 5 MPa stiffer at 40 and 50% lignin. The addition of lignin (up to 40%) decreased stiffness in a consistent manner from 50 to 10 MPa for the uncatalyzed series, while the TSA catalyzed series decreased from 100 to 15 MPa. At 50% lignin content, for catalyzed and uncatalyzed copolymers the modulus increased to about 70 MPa. It is likely that the presence of the catalyst served to increase the cross link density between the lignin and prepolymer. In a study concerned with tensile properties of PE it was found that samples containing higher cross-link density exhibited greater stiffness as well as tensile strength (Temenoff, Athanasiou, Lebaron, & Mikos, 2001). This behavior was likely observed in the current study.

An analysis of variance was performed to evaluate the significance of catalyst on young's modulus (Table 4.4). The p-value of 0.04 for the catalyst variable indicates that the catalyst did have a significant effect on the young's modulus response.

Table 4.4 Analysis of variance of Youngs modulus on lignin-copolymer properties by addition of TSA catalyst

	Sum Sq	Df	F value	Pr(>F)
(Intercept)	19658.73	1	13.04553	0.000714
Lignin	260.9729	1	0.173182	0.679117
Catalyst	6694.948	1	4.442766	0.040189
Lignin:Catalyst	2642.225	1	1.75338	0.191596
Residuals	73839.68	49		

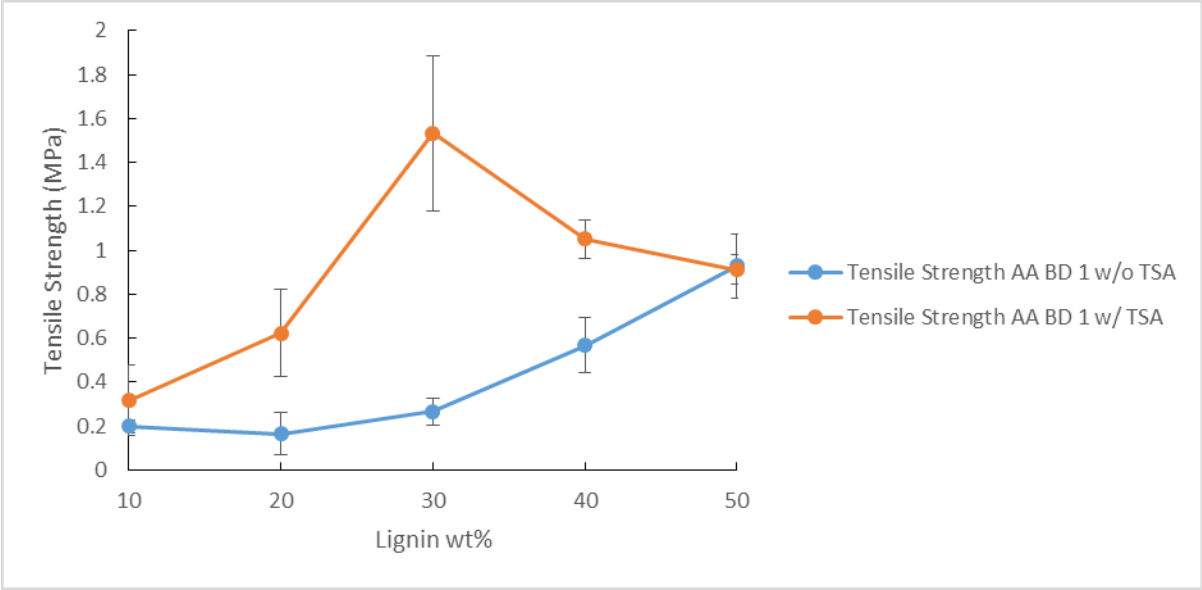

Figure 4.10 Plot of tensile strength for the catalyzed and uncatalyzed AA BD 1 lignin copolymers with lignin content.

The tensile strength values for the lignin-copolymers using no or with TSA ranged from 0.2 to 1.5 MPa with the highest value being attributed to the catalyzed copolymer at 30 wt% lignin. The catalyzed copolymers exhibit about higher tensile strength values at 10-40 lignin wt% levels while at the 50 wt% level the tensile strength is the same. The difference is the largest at the 30 wt% level where the tensile strength of the catalyzed copolymer is 1.3 MPa

higher than the uncatalyzed copolymer. The addition of lignin is observed to increase the tensile strength of copolymers in both the catalyzed and uncatalyzed samples. The uncatalyzed samples increase from 0.2 MPa at 10 wt% lignin to 0.9 MPa at 50 wt% lignin. The catalyzed samples increase from 0.3 MPa at 10 wt% lignin to 1.5 MPa at 30 wt% lignin before decreasing to 0.9 MPa at 50 wt% lignin. An analysis of variance was performed in order to evaluate the significance of the effect of catalyst on tensile strength. The results are shown in Table 4.5. The p-value of 0.02 for the catalyst variable indicates that the catalyst was significant on the tensile strength of the copolymer.

Table 4.5 Analysis of variance of tensile strength on lignin-copolymer properties by addition of TSA catalyst

	Sum Sq	Df	F value	Pr(>F)
(Intercept)	0.118857	1	1.123151	0.294437
Lignin	2.853257	1	26.96223	3.98E-06
Catalyst	0.580811	1	5.488453	0.023247
Lignin:Catalyst	0.031764	1	0.30016	0.58627
Residuals	5.185388	49		

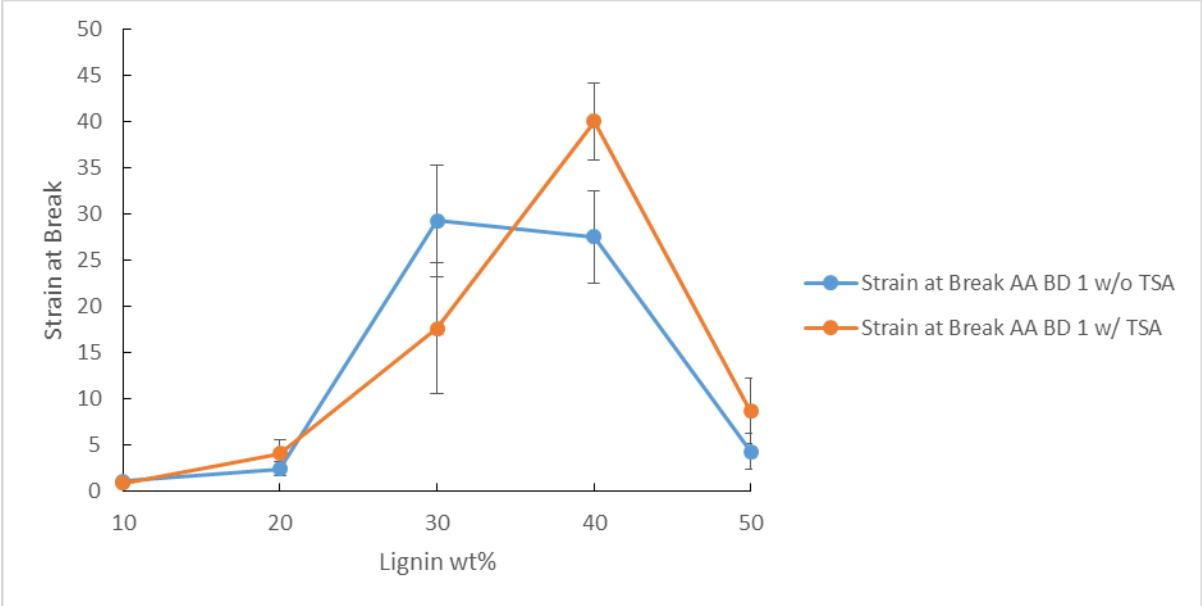

Figure 4.11 Plot of strain at break for the catalyzed and uncatalyzed AA BD 1 lignin copolymers with lignin content.

The strain at break values span a range from 1% to 39% with the maximum value attributed to the catalyzed 40 wt% lignin sample. Both the catalyzed and uncatalyzed samples at 10 wt% lignin have a value of 1% strain. Each show a modest increase in strain as lignin is increased to 20 wt%. At the 30 wt% level the uncatalyzed copolymer reaches a maximum value of 29% and surpasses the value of 16% for the catalyzed copolymer. At the 40 wt% lignin level the catalyzed copolymer reaches the maximum value of 39% while the uncatalyzed copolymer remains near 29%. Both the uncatalyzed and catalyzed copolymers drop around 25% as lignin content increase to 50 wt%. An analysis of variance was performed to determine the significance of the catalyst on strain at break results of copolymers. The results are shown in Table 4.6. The p-value of 0.5 for the catalyst variable indicates that the catalyst was not significant on the strain at break results from copolymers.

Table 4.6 Analysis of variance strain at break on lignin-copolymer properties by addition of TSA catalyst

	Sum Sq	Df	F value	Pr(>F)
(Intercept)	33.87893	1	0.197958	0.658334
Lignin	1309.715	1	7.652788	0.007973
Catalyst	65.46764	1	0.382534	0.539115
Lignin:Catalyst	111.5258	1	0.651656	0.423423
Residuals	8385.968	49		

4.2.2.3 DSC Analysis of the Catalyzed/Uncatalyzed Lignin Copolymers

To investigate the effect of catalysis on the T_g of lignin copolymers the samples were analyzed using DSC. The thermograms for the AA BD 1 copolymer ranging from 0-50 wt% lignin w/ TSA are shown in Figure 4.12. Figure 4.13 shows the DSC thermograms for the same series of copolymers without TSA catalyst.

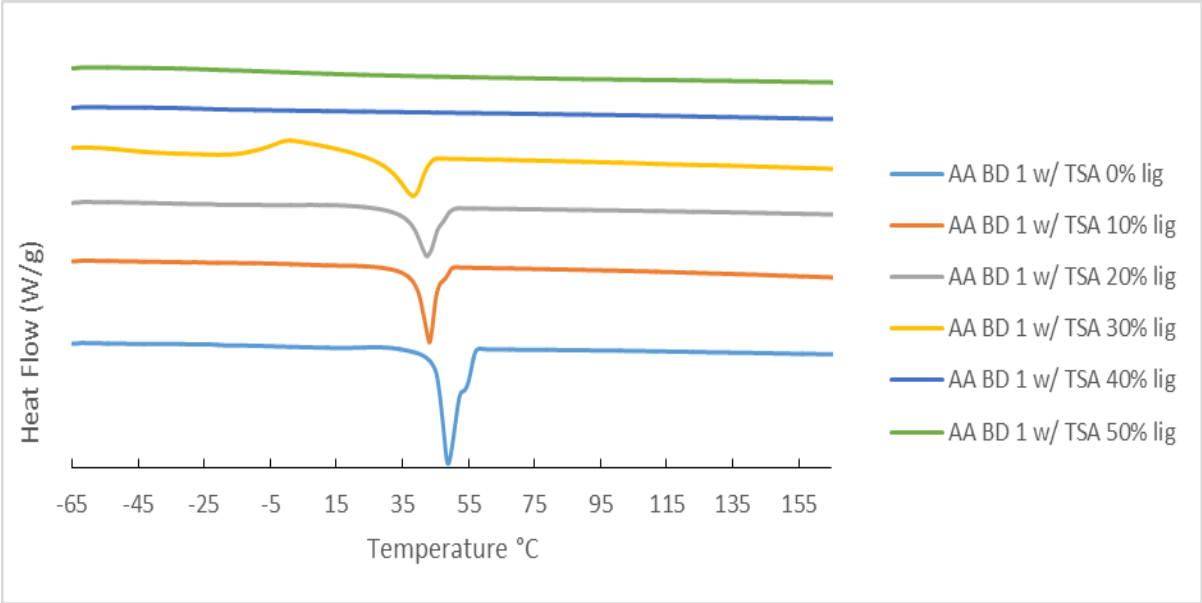

Figure 4.12 DSC thermograms of AA BD 1 0-50 wt% lignin copolymers with TSA catalyst

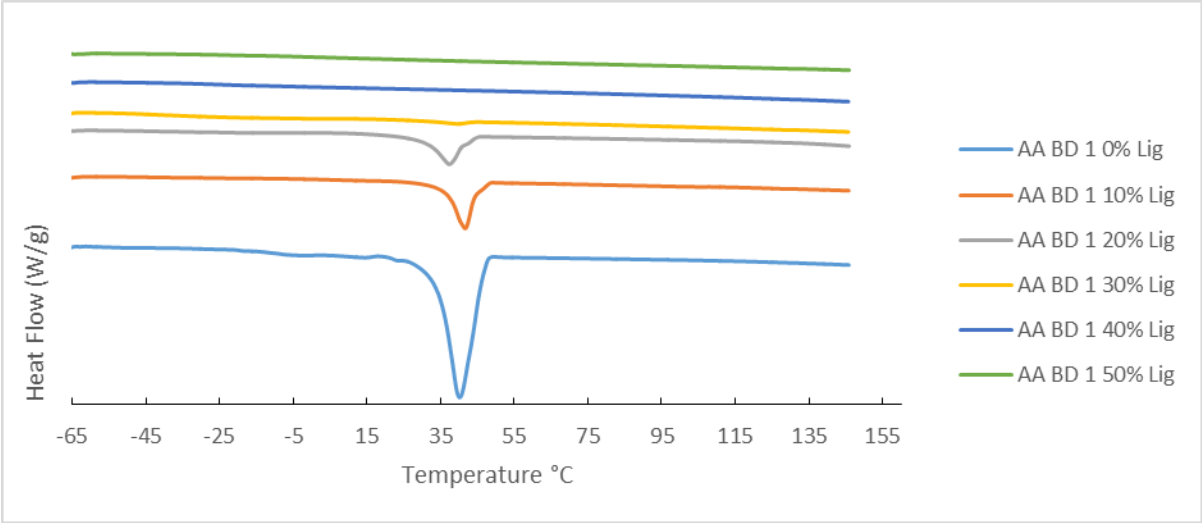

Figure 4.13 DSC thermograms of AA BD 1 0-50 wt% lignin copolymers without TSA catalyst

Figure 4.14 shows T_g values as determined by DSC analysis for an AA BD 1 series of copolymer produced both with and without TSA catalyst. As was mentioned before in section 3.3.2.1 the AA BD 1 T_g values for the 10 and 20 wt% lignin levels were not able to be determined. The T_g values for the catalyzed copolymers ranged from -49 °C to -5 °C compared to -43 °C to -4 °C for the uncatalyzed samples. The T_g values for the 0 and 30 wt%

samples show a decrease in T_g of about 10°C in the case of the catalyzed samples. At the 40 and 50 wt% lignin levels the T_g values for catalyzed vs uncatalyzed are unchanged.

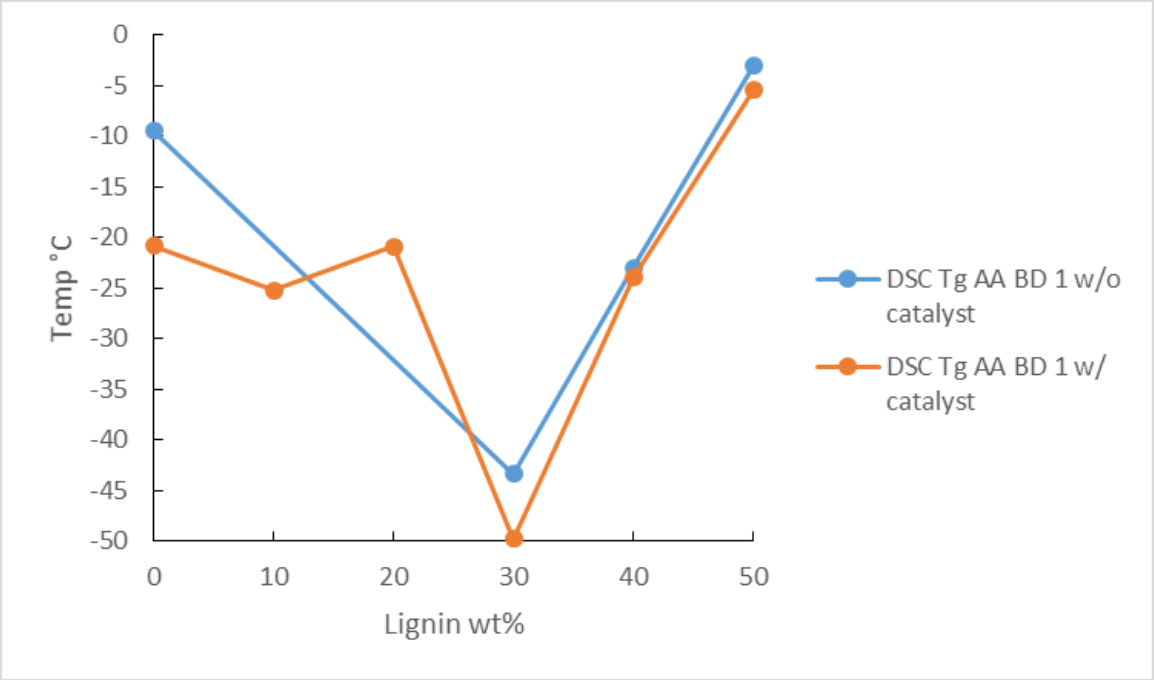

Figure 4.14 DSC AA BD 1 T_g catalyst comparison

The T_m for the catalyzed and uncatalyzed AA BD 1 copolymers was also determined by DSC. Figure 4.15 shows T_m for AA BD 1 samples with and without TSA catalyst as determined by DSC analysis. It can be seen that the presence of the TSA catalyst had an effect on the melt temperature of the copolymers. The presence of catalyst resulted in copolymers with higher T_m. The effect is most pronounced at 0 wt% lignin where the catalyzed prepolymer exhibits a T_m 9 °C higher than the uncatalyzed prepolymer. Also at 20 wt% lignin the T_m for the catalyzed copolymers was 8 °C higher. Another interesting observation here is that the catalyst did not change the ability of the sample to melt. The same samples that melted without catalyst also exhibited melt behavior in the presence of the catalyst.

Li et al. found that in the synthesis of a prepolymer the presence of triethanolamine acted as a catalyst for the esterification reaction between diacid and alcohol (Li, Sivasankarapillai, & McDonald, 2015). Upon replacing the triethanolamine triol with glycerol (inert in terms of catalysis, pH) the polymerization did not proceed under the same reaction conditions as

indicated by FT-IR. Therefore, the reaction temperature was increased from 100 to 150 °C. Because of the difference in reaction conditions as well as lignin contents in the resulting lignin copolymers it is not possible to ascertain the effect of catalysis on the thermal properties. However, the knowledge of the catalysis acting to encourage the polymerization reaction is congruous with the observation of an increased T_m in this study. More extensively polymerized copolymer with greater molecular weight would result in an increase in T_m (Fatou & Mandelkern, 1964).

The T_m response to catalyst is consistent with the results observed from DMA which will be discussed in the next section. In short, the transition observed through DMA exhibited an increase upon addition of catalyst to lignin copolymers which is what was observed in DSC analysis of T_m. Because of the correlation between the DMA transition and T_m this is not a surprising result. The increase in T_m also correlates well with the increase in young's modulus and tensile strength observed through mechanical tensile testing. As was explained earlier the change in tensile properties likely resulted from an increased cross link density in the copolymer which also helps to explain the increased T_m.

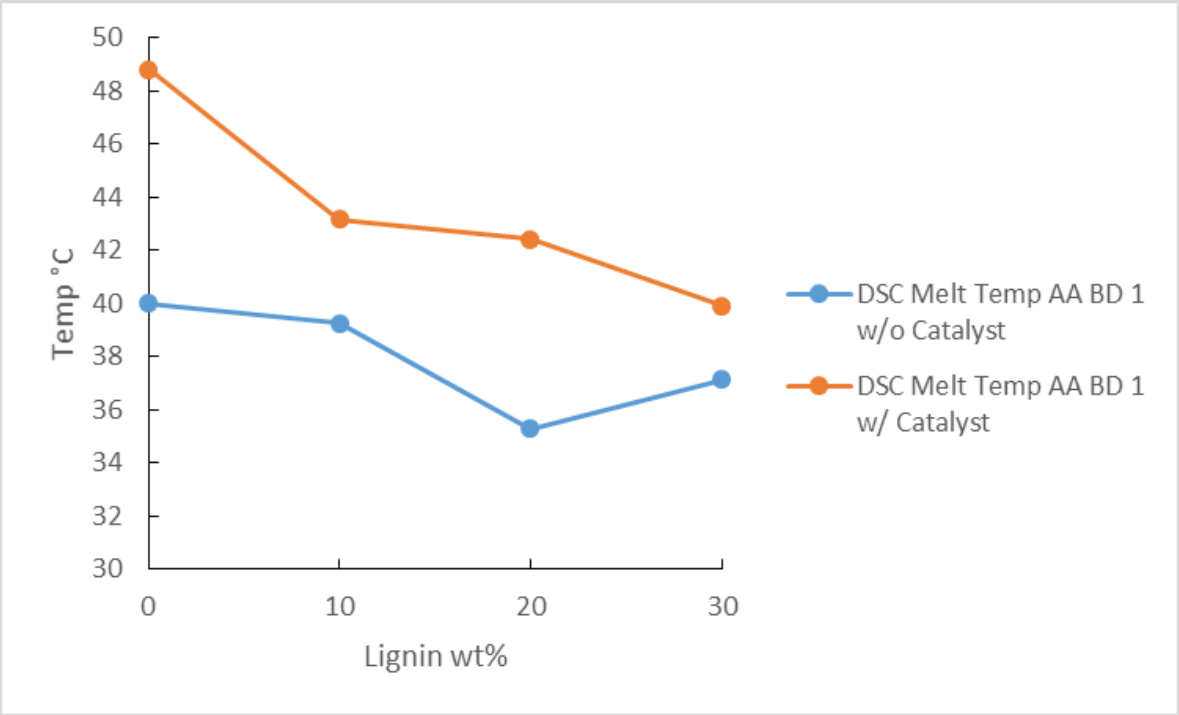

Figure 4.15 Plot of DSC T_m against lignin content for lignin copolymer AA BD 1 with and without catalyst addition

4.2.2.4 DMA of Copolymers Containing TSA Catalyst

The effect of catalysis on the thermal transitions of lignin copolymers was investigated using DMA. It was hypothesized that by furthering the extent of polymerization through incorporation of catalyst the resulting T_m as determined by DMA would be increased. Figure 4.16 shows the results from DMA compression analysis of samples utilizing TSA catalyst compared against the same samples without catalyst. It was found that the catalyzed lignin copolymerser exhibited a T_m about 5°C higher than the uncatalyzed copolymers. The catalyzed copolymers span a range from 44°C at the 30 wt% lignin level up to 85°C at the 50 wt% lignin level. The general trend of T_m values generated by DMA compression analysis mirrors the results for T_m obtained through DSC analysis. At the 0, 10 and 20 wt% lignin levels the copolymers containing TSA catalyst exhibit a T_m value greater than those without the catalyst present. At the 30 wt% lignin level the T_m value for the catalyst samples drops 3°C below the samples without catalyst. Both samples with and without the catalyst then increase dramatically at the 40 and 50 wt% lignin levels with the samples containing catalyst

again exhibiting higher T_m than without catalyst. The overall trend of T_m in response to increasing lignin content remains the same between catalyzed and uncatalyzed samples. In a similar study concerning polyurethane lignin networks catalyzed using di-n-butyltin dilaurate it was found that the increasing lignin from 0 to 15 wt% in the system increased the T_g by 26 °C from 80 to 106°C as determined by DMA (Pohjanlehto, Setala, Kiely, & McDonald, 2013). Over the same level of lignin wt% the lignin copolymers in this study are reported to decrease in T_m. However, after the 30 wt% lignin level the copolymers T_m increased as is reported in this study.

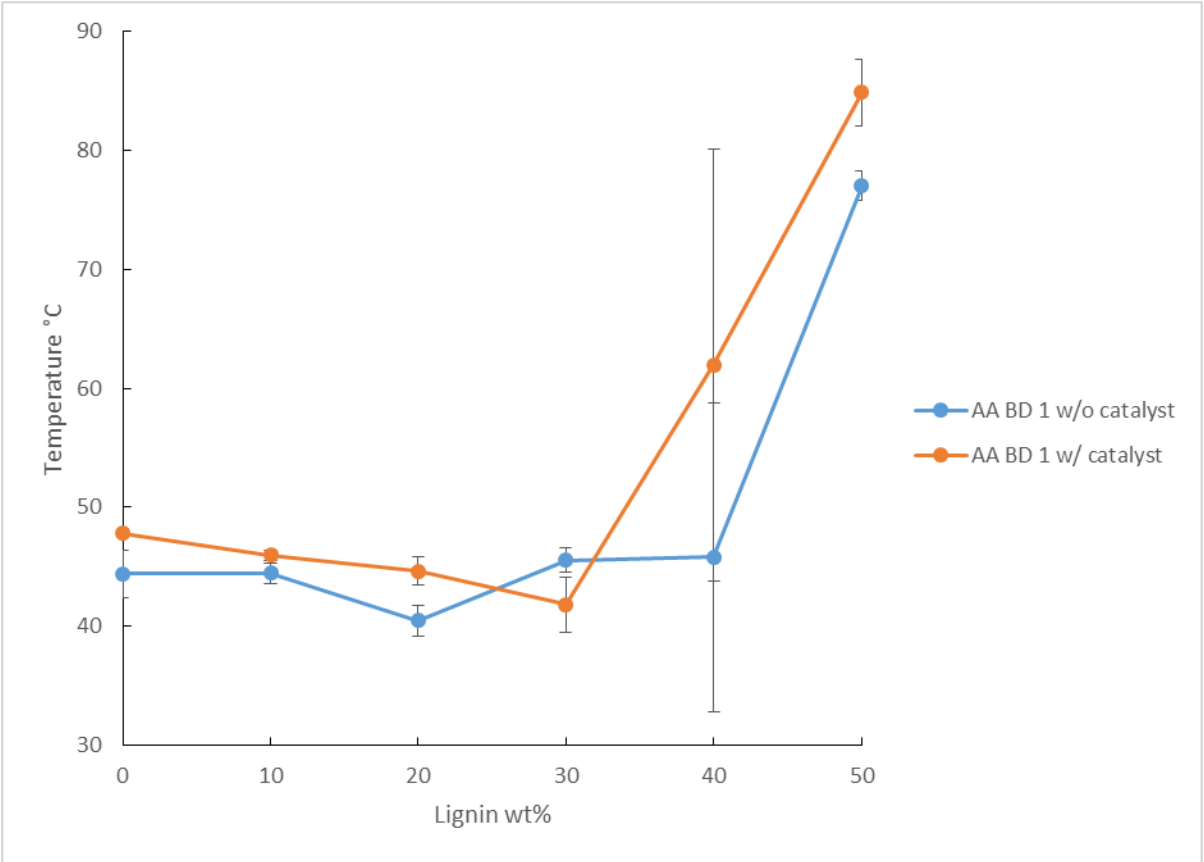

Figure 4.16 Plot of T_m by DMA against lignin content for lignin-copolymer AA BD 1 with and without TSA catalyst addition

4.2.2.5 TGA of Copolymers Containing TSA Catalyst

It was hypothesized that the addition of TSA catalyst to the lignin copolymers would result in a more thermally stable material through the development of a more extensively cross-linked

and fully polymerized product. The results from TGA analysis of catalyzed lignin copolymers as compared against the non-catalyzed samples are shown in Figure 4.17. The lowest degradation T_{onset} was the catalyzed sample at 0 wt% which gave a T_{onset} of 305°C. The highest T_{onset} was the uncatalyzed copolymer at 30 wt% lignin which gave a T_{onset} of 420°C. The T_{onset} for the AA BD 1 copolymers without catalyst yield higher onset values in all cases except at the 50 wt% lignin level. This is a surprising result as it was hypothesized that the catalyst would improve thermal stability in lignin copolymers. In a study by Arshanitsa et al it was found that a lignin polyurethane film catalyzed by dibutyltin dilaurate exhibited an increase in the temperature at which thermal degradation started (T_d5) from 274 to 281°C upon increasing lignin content from 0 to 5 wt% (Arshanitsa, Krumina, Telysheva, & Dizhbite, 2016). However, as the lignin content was increased from 5 to 30 wt% the start of thermal degradation temperature decreased to 238°C. This behavior is also evident in the catalyzed lignin copolymers from this study which show an increase in T_{onset} from 305 to 400°C upon increasing lignin from 0 to 10 wt%. Furthermore, the T_{onset} shows a decrease to 375°C upon increasing lignin content to 30 wt%.

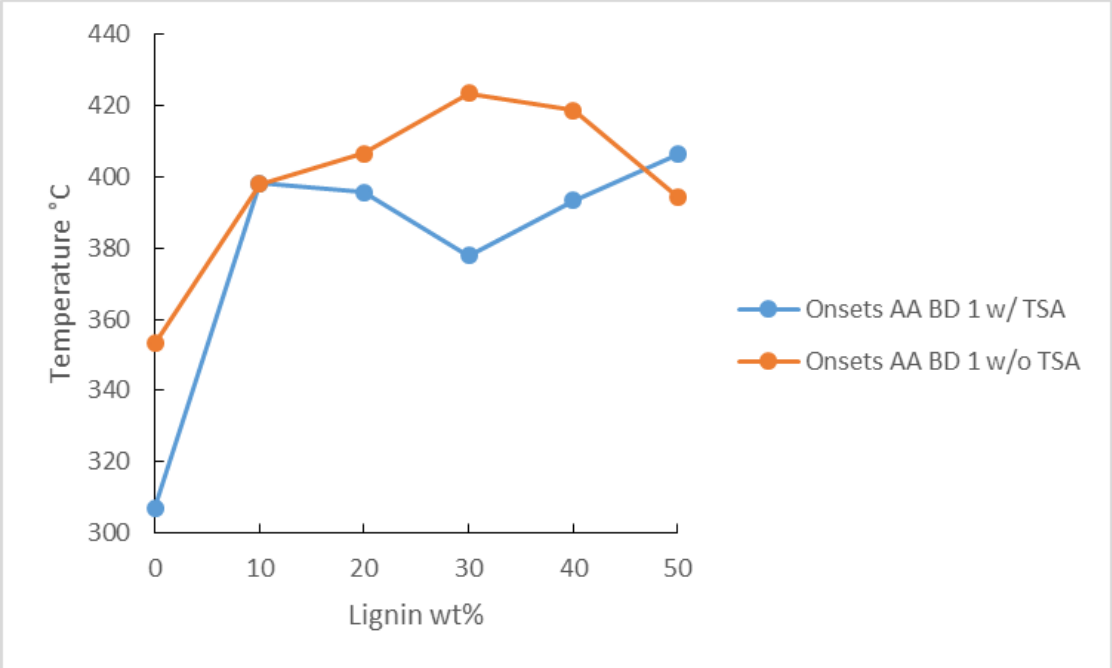

Figure 4.17 Plot of TGA degradation onset temperatures against lignin content for lignin-copolymer AA BD 1 with and without TSA catalyst addition

5 Conclusion

Lignin copolymers were generated through a green synthesis method that avoided the use of solvent. The melt condensation synthesis route was observed to be relatively simple. Additionally, the resulting copolymer utilized kraft lignin, an abundantly available, renewable polymer as well as other monomers with potential renewable sourcing. Evidence of successful polymerization were supported by FT-IR and ESI-MS analyses. FT-IR showed an increase in the area of the carbonyl stretch band attributed to ester + amide from 0 to 90% over the course of the 48 h polymerization reaction. ESI-MS showed an increase from 600 to 1100 g/mol for the prepolymers after 48 hours of polymerization.

The copolymers exhibited a range of mechanical and thermal properties that demonstrated the ability to be tuned based on the lignin content, DAB content and type of diacid. For instance, the T_m values from DSC analysis could be adjusted from 30-106°C based on DAB and lignin content. The SA copolymers were observed to be relatively stiff, brittle materials while the AA copolymers were more capable of flexing and stretching. The SuA copolymers fell somewhere between the other two. The observed Young's modulus values ranged from 5 MPa to 340 MPa and were comparable to natural rubber and other elastomers at 100 MPa. The observed tensile strength values ranged from 0.1 MPa to 1.8 MPa compared with 10 MPa for natural rubber. The strain at break values ranged from <1 to 70% where natural rubber is capable of exceeding 500% elongation before failure. These comparisons reveal that despite a successful polymerization reaction the copolymers resulting from this synthesis exhibit characteristics of an elastomeric thermoplastic material.

A regression analysis was applied to the results from mechanical tensile testing in order to generate a 3D surface plot of response plotted against lignin and DAB content. This allowed for the optimization of the various tensile properties by modifying the lignin and DAB variables.

DSC was used to compare glass transitions and melt temperatures. The samples were shown to exhibit melt behavior up to 30 wt% lignin. The T_g ranged from -50 to 21°C while the T_m

ranged from 29-106°C. The mechanical properties were observed to diminish as a result of melt processing with an 83% loss in Young's modulus, 70% loss in tensile strength while the strain at break remained the same.

DMA revealed the presence of thermal transitions (T_{11}) at lignin levels exceeding 30 wt%. These were likened unto a quasi-melt transition occurring within the amorphous regions where the association of lignin aggregates broke down and allowed for greater mobility. In addition, the molecular mobility and dampening effects of copolymers generated from the various diacids were explored through the intensity of the tan δ peak. The AA copolymers were found to exhibit the best dampening ability as evidenced by the superior height of the peak in the tan δ signal. The T_m values for lignin copolymers as determined by DMA ranged from 38-103°C. Evidence of melt behavior was reaffirmed by TMA analysis. At higher lignin concentrations where melt behavior was not observed the TMA exhibited a response to the T_s at temperatures similar to the T_g temperatures observed through DSC.

XRD analysis was used to gain information about the crystallinity of the sample and substantiate theories about the effect that crystallinity had on mechanical properties. It was found that the crystallinity decreased as lignin content increased from a maximum of 45.9% at 0 wt% lignin to 3.2% at 50 wt% lignin.

The standard deviations from mechanical testing were large due to material defects. In an effort to reduce this variation lignin was subjected to ball milling and used to generate copolymers. It was hypothesized that by reducing lignin particle size the nucleation efficiency of the lignin would be reduced, thereby reducing the amount of material defects in the material that resulted from vaporization of water evolved through condensation reactions occurring during polymerization. It was found that the defects persisted although the mechanical properties were altered.

To improve mechanical properties in pursuit of a material more closely resembling a traditional thermoplastic a TSA catalyst was employed to encourage the formation of covalent linkages between the prepolymer matrix and lignin molecules. The result was a

material demonstrating improved mechanical properties over the non-catalyzed counterparts. The Youngs modulus was increased by 100% in many cases. The tensile strength was increased by 100-200% depending on lignin level. The strain at break however did not change much as a result of TSA catalysis. The T_g of the TSA catalyzed copolymers as determined by DSC did not exhibit much change. The T_m temperatures did exhibit an increase of about 5°C upon catalysis.

6 Future Work

It was noted that many of the samples at lower lignin content of 10 and 20 wt% were brittle samples. It would be interesting to explore the effect of a free radical cross linking agent such as a peroxide in the presence of a small amount of diacid containing a C=C double bond. This would likely induce a change in the thermal behavior and mechanical properties. Also, several other diacids were explored but were not reported on due to their highly viscous nature, particularly pimelic acid and glutaric acid. The cross linking approach could also be used to generate a material using these diacids that could further be used to generate lignin copolymers with an even greater range of properties. In addition, due to the promise of a greatly expanded bio-ethanol and bio-butanol industry it would be prudent to investigate the lignins resulting from these processes.

Further research should also be focused on reducing the presence of material defects in copolymers, this would likely result in a material with more consistent, reproducible properties. In addition the improvement of mechanical properties would go a long way toward creating a copolymer material that could feasibly replace commodity type thermoplastics.

7 References

Aracri, E., Blanco, C. D., & Tzanov, T. (2014). An Enzymatic Approach to Develop a Lignin-Based Adhesive for Wool Floor Coverings. *Green Chemistry*, 2597-2603.

Arshanitsa, A., Krumina, L., Telysheva, G., & Dizhbite, T. (2016). Exploring the Application of Incompletely Soluble Organosolv Lignin as a Macromonomer for Polyurethane Synthesis. *Industrial Crops and Products*, 1-12.

Banu, D., El-Aghoury, A., & Feldman, D. (2006). Contributions to Characterization of Poly(Vinyl Chloride)-Lignin Blends. *Journal of Applied Polymer Science*, 2732-2748.

Bouajila, J., Dole, P., Joly, C., & Limare, A. (2006). Some Laws of a Lignin Plasticization. *Journal of Applied Polymer Science*, 1445-1451.

Bova, T., Tran, C. D., Balakshin, M. Y., Chen, J., Capanema, E. A., & Naskar, A. K. (2016). An Approach Towards Tailoring Interfacial Structures and Properties of Multiphase Renewable Thermoplastics From Lignin-Nitrile Rubber. *Royal Society of Chemistry*, 5423-5437.

Campbell, M. M., & Sederoff, R. R. (1996). Variation in Lignin Content and Composition. *Plant Physiology*, 3-13.

Chakar, F. S., & Ragauskas, A. J. (2004). Review of Current and Future Softwood Kraft Lignin Process Chemistry. *Industrial Crops and Products*, 131-141.

Chung, Y.-L., Olsson, J. V., Li, R. J., Frank, C. W., Waymouth, R. M., Billington, S. L., & Sattely, E. S. (2013). A Renewable Lignin-Lactide Copolymer and Application in Biobased Composites. *Sustainable Chemistry & Engineering*, 1231-1238.

Chung, Y.-L., Olsson, J. V., Li, R. j., Franke, C. W., Waymouth, R. M., Billington, S. L., & Sattely, E. S. (2013). A Renewable Lignin-Lactide Copolymer and Application in Biobased Composites. *Sustainable Chemistry & Engineering*, 1231-1238.

Cowie, J. M., & Arrighi, V. (2008). Graft Copolymer Synthesis. In J. M. Cowie, & V. Arrighi, *Polymers: Chemistry and Physics of Modern Materials* (pp. 145-146). Boca Raton: CRC Press.

Cowie, J. M., & Arrighi, V. (2008). Polymers: Chemistry and Physics of Modern Materials. In J. M. Cowie, *Polymers: Chemistry and Physics of Modern Materials* (p. 20). Boca Raton: CRC Press.

David, D. J., & Sincock, T. F. (1992). Estimation of Miscibility of Polymer Blends Using the Solubility Parameter Concept. *Polymer*, 4505-4514.

Dehne, L., Vila, C., Saake, B., & Schwarz, K. U. (2017). Esterification of Kraft Lignin as a Method to Improve Structural and Mechanical Properties of Lignin-Polyethylene Blends. *Journal of Applied Polymer Science*, 1-8.

Dence, C. W., & Lin, S. Y. (1992). Methods in Lignin Chemistry. In C. W. Dence, *Methods in Lignin Chemistry* (pp. 3-6). Heidelberg: Springer.

Deng, Y., Ma, L., & Mao, Y. (2016). Biological Production of Adipic Acid from Renewable Substrates: Current and Future Methods. *Biochemical Engineering Journal*, 16-26.

Dodd, A. P., Kadla, J. F., & Straus, S. K. (2015). Characterization of Fractions Obtained from Two Industrial Softwood Kraft Lignins. *Sustainable Chemistry & Engineering*, 103-110.

Durand, D., Delsanti, M., Adam, M., & Luck, J. M. (1987). Frequency Dependence of Viscoelastic Properties of Branched Polymers near Gelation Threshold. *Europhysics Letters*, 297-301.

Fatou, J. G., & Mandelkern, L. (1964). The Effect of Molecular Weight on the Melting Temperature and Fusion of Polyethylene. *The Journal of Physical Chemistry*, 417-428.

Feldman, D., Banu, D., Manley, R. S., & Zhu, H. (2003). Highly Filled Blends of a Vinylic Copolymer with Plasticized Lignin: Thermal and Mechanical Properties. *Journal of Applied Polymer Science*, 2000-2010.

Gao, G., Karaaslan, M. A., & Kadla, J. F. (2014). Hydrogen-Bonding Based Reversible Polymer Networks Based on Kraft Lignin and POly92-Dimethylamino)Ethyl Methacrylate Series Polymers. *Macromolecular Materials and Engineering*, 990-1002.

Gao, Q., Yanshai, W., Yingying, R., & Yang, L. (2013). Novel Dual-Grafted Copolymer Bearing Glassy Polystyrene and Crystalline Poly(Ethylene Oxide) as Side Chains. *Journal of Macromolecular Science Part A-Pure and Applied Chemistry*, 1157-1165.

Ge, Y. P., Yuan, D., Luo, Z. L., & Wang, B. B. (2014). Synthesis and Characterization of Poly(Ester Amide) From Renewable Resources Through Melt Polycondensation. *eXPRESS Polymer Letters*, 50-54.

Gkartzou, E., Koumoulos, E. P., & Charitidis, C. A. (2016). Production and 3D Printing Processing of Bio-Based Thermoplastic Filament. *Manufacturing Review*, 1-14.

Graham, P. R. (1973). Phthalate Ester Plasticizers-Why and How They Are Used. *Environmental Health Perspectives*, 3-12.

Hasegawa, D., Teramoto, Y., & Nishio, Y. (2008). Molecular Complex of LIgnosulfonic Acid/Poly(Vinyl Pyridine) via Ionic Interaction. *Journal of Wood Science*, 143-152.

Janata, M., Masar, B., Toman, L., Vlcek, P., Latalova, P., Brus, J., & Holler, P. (2003). Synthesis of Novel Types of Graft Copolymers by a "Grafting-From" Method using Ring-Opening Polymerization of Lactones and Lactides. *Reactive and Functional Polymers*, 137-146.

Kadla, J. F., & Kubo, S. (2003). Miscibility and Hydrogen Bonding in Blends of Poly(ethylene oxide) and Kraft Lignin. *Macromolecules*, 7803-7811.

Kadla, J. F., & Kubo, S. (2004). Lignin-Based Polymer Blends: Analysis of Intermolecular Interactions in Lignin-Synthetric Polymer Blends. *Composites part A: Applied Science and Manufacturing*, 395-400.

Kelley, S. S. (1990). Multiphase Materials with Lignin. *Journal of Applied Polymer Science*, 2813-2828.

Kim, S. J. (2016). Synthesis and Characterization of Kraft Lignin-graft-Polylactide Copolymers. *Wood Science and Technology*, 1293-1304.

Kim, S. J., Kim, Y. S., Lee, O.-K., & Ahn, B.-J. (2016). Synthesis and Characterization of Kraft Lignin-graft-Polylactide Copolymers. *Wood Science and Technology*, 1293-1304.

Koivu, K. A., Sadeghifar, H., Paula, N. A., Argyropoulos, D. S., & Sipila, J. (2016). Effect of Fatty Acid Esterification on the Thermal Properties of Softwood Kraft Lignin. *Sustainable Chemistry & Engineering*, 5238-5247.

Kubo, S., & Kadla, J. F. (2005). Hydrogen Bonding in Lignin: A Fourier Transform Infrared Model Compound Study. *Biomacromolecules*, 2815-2821.

Lee, A., & Deng, Y. (2015). Green Polyurethane from Lignin and Soybean Oil through Non-Isocyanate Reactions. *European Polymer Journal*, 67-73.

Lewis, H. F. (1947). *US Patent No. 2429102.*

Li, H., & McDonald, A. G. (2014). Fractionation and Characterization of Industrial Lignins. *Industrial Crops and Products*, 67-76.

Li, H., Sivasankarapillai, G., & McDonald, A. G. (2014). Lignin Valorization by Forming Thermally Stimulated Shape Memory Copolymeric Elastomers-Partially Crystalline Hyperbranched Polymer as Crosslinks. *Journal of Applied Polymer Science*.

Li, H., Sivasankarapillai, G., & McDonald, A. G. (2014). Lignin Valorization by Forming Toughened Thermally Stimulated Shape Memory Copolymeric Elastomers: Evaluation of Different Fractionated Industrial Lignins. *Journal of Applied Polymer Science*, 1-12.

Li, H., Sivasankarapillai, G., & McDonald, A. G. (2015). Highly Biobased Thermally-Stimulated Shape Memory Copolymeric Elastomers Derivated from Lignin and glycerol-Adipic Acid Based Hyperbranched Prepolymer. *Industrial Crops and Products*, 143-154.

Li, H., Sivasankarapillai, G., & McDonald, A. G. (2016). Highly Biobased Thermally-Stimulated Shape Memory Copolymeric Elastomers Derived from Lignin and Glycerol-Adipic Acid Based Hyperbranched Prepolymer. *Industrial Crops and Productrs*, 143-154.

Li, P. G., Lee-Sullivan, P., & Thring, R. W. (2000). Determination of Activation Energy for Glass Transition of an Epoxy Adhesive Using Dynamic Mechanical Analysis. *Journal of Thermal Analysis and Calorimetry*, 377-390.

Lora, J. H., & Glasser, W. G. (2002). Recent Industrial Applications of Lignin: A Sustainable Alternative to Nonrenewable Materials. *Journal of Polymers and the Environment*, 39-48.

Luo, S., Cao, J., & McDonald, A. G. (2016). Interfacial Improvements in a Green Biopolymer Alloy of Poly(3-hydroxybutyrate-cl-3-hydroxyvalerate) and Lignin via in Situ Reactive Extrusion. *Sustainable Chemistry & Engineering*, 3465-3476.

Luo, S., Cao, J., & McDonald, A. G. (2017). Esterification of Industrial Lignin and its Effect on the Resulting Poly(3-hydroxybutyrate-co-3-hydroxyvalerate) or Polypropylene Blends. *Industrial Crops and Products*, 281-291.

Menard, K. P. (1999). Time-Temperature Scans: Transitions in Polymers. In K. P. Menard, *Dynamic Mechanical Analysis: A Practical Introduction* (pp. 102-109). Boca Raton, Florida: CRC Press LLC.

Miao, C., & Hamad, W. Y. (2016). Controlling Lignin Particle Size for Polymer Blends Applications. *Journal of Applied Polymer Science*, 5136-5151.

Migliaresi, C., Cohn, D., Lollis, A. D., & Fambri, L. (1991). Dynamic Mechanical and Calorimetric Analysis of Compression-Molded PLLA of Different Molecular Weights: Effect of Thermal Treatments. *Journal of Applied Polymer Science*, 83-95.

Mousavioun, P., Doherty, W. O., & George, G. (2010). Thermal Stability and Miscibility of Poly(hydroxybutyrate) and Soda Lignin Blends. *Industrial Crops and Products*, 656-661.

Pan, M., Gan, X., Mei, C., & Liang, Y. (2017). Structural Analysis and Transformation of Biosilica During Lignocellulose Fractionation of Rice Straw. *Journal of Molecular Structure*, 575-582.

Perego, G., Cella, G. D., & Bastioli, C. (1996). Effect of Molecular Weight and Crystallinity on Poly(lactic acid) Mechanical Properties. *Journal of Applied Polymer Science*, 37-43.

Pohjanlehto, H., Setala, H. M., Kiely, D. E., & McDonald, A. G. (2013). Lignin-Xylaric Acid-Polyurethane Based Polymer Network Systems: Preparation and Characterization. *Journal of Applied Polymer Science*, 1-7.

Renewable Fuel Standard. (2017, May 21). Retrieved from Alternative Fuels Data Center: http://www.afdc.energy.gov/laws/RFS.html

Rizzuto, M., Marinetti, L., Caretti, D., Mugica, A., Zubitur, m., & Muller, A. J. (2017). Can Poly(e-caprolactone) Crystals Nucleate Glassy Polylactide? *CrystEngComm*, 3178-3191.

Sallem-Idrissi, N., Sclavons, M., & Debecker, D. P. (2015). Miscible Raw Lignin/Nylon 6 Blends: Thermal and Mechanical Performances. *Journal of Applied Polymer Science*, 1-10.

Schorr, D., Diouf, P. N., & Stevanovic, T. (2014). Evaluation of Industrial Lignins for Biocomposites Production. *Industrial Crops and Products*, 65-73.

Shmulsky, R. (2011). Pulp and Paper. In R. Shmulsky, & P. D. Jones, *Forest Products and Wood Science* (pp. 401-403). West Sussex: Wiley-Blackwell.

Sivasankarapillai, G., & McDonald, A. G. (2010). Synthesis and Properties of Lignin-Highly Branched Poly(ester-amine) Polymeric Systems. *Biomass and Bioenergy*, 919-931.

Sperry, J. S. (2002). Evolution of Water Transport and Xylem Structure. *International Journal of Plant Sciences*, 115-127.

Temenoff, J. S., Athanasiou, K. A., Lebaron, R. G., & Mikos, A. G. (2001). Effect of Poly(ethylene glycol) Molecular Weight on Tensile and Swelling Properties of Oligo(poly(ethylene glycol) fumarate) Hydrogels for Cartilage Tissue Engineering. *Journal of Biomedical Materials Research*, 429-437.

Teramoto, Y., Lee, S.-H., & Endo, T. (2012). Molecular Composite of Lignin: Miscibility and Complex Formulation of Organosolv Lignin and its Acetates with Synthetic Polymers Containing Vinyl Pyrrolidone and/or Vinyl Acetate Units. *Journal of Applied Polymer Science*, 2063-2070.

Terinte, N., Ibbett, R., & Schuster, K. C. (2011). Overview on Native Cellulose and Micxrocrystalline Cellulose I Structures Studied by X-Ray Diffraction (WAXD): Comparison Between Measurement Techniques. *Lenzinger Berichte*, 118-131.

Thibaud, D., Eric, P., & Luc, A. (2017). Synthesis and Characterization of Biobased Poly(Butylene Succinate-ran-Butylene Adipate). Analysis of the Composition-Dependent Physicochemical Properties. *European Polymer Journal*, 84-98.

Vance, C. P., Kirk, T. K., & Sherwood, R. T. (1980). Lignification as a Mechanism of Disease Resistance. *Annual Review of Phytopathology*, 259-288.

Vieira, A. C., Vieira, J. C., Ferra, J. M., Magalhaes, F. D., Guedes, R. M., & Marques, A. T. (2011). Mechanical Study of PLA-PCL Fibers During in Vitro Degradation. *Journal of the Mechanical Behavior of Biomedical Materials*, 451-460.

Vyazovkin, S., Shirrazzuoli, N., & Dranca, I. (2006). Variation in Activation Energy of the Glass Transition for Polymers of Different Dynamic Fragility. *Macromolecular Chemistry and Physics*, 1126-1130.

Wang, C., Kelley, S. S., & Venditti, R. A. (2016). Lignin-Based Thermoplastic Materials. *Chemistry & Sustainability Energy & Materials*, 770-783.

Wang, J., Manley, J. R., & Feldman, D. (1992). Synthetic- Polymer Lignin Copolymers and Blends. *Progress in Polymer Science*, 611-646.

Wang, R., Ren, T., Bai, Y., Wang, Y., Chen, J., Zhang, L., & Zhao, X. (2016). One-Pot Synthesis of Biodegradable and Linear Poly(Ester Amide)s Based on Renewable Resources. *Journal of Applied Polymer Science*.

Watkins, D., Nuruddin, M., Hosur, M., Narteh, A. T., & Jeelani, S. (2015). Extraction and Characterization of Lignin from Different Biomass Resources. *Journal of Materials Research and Technology*, 26-32.

Werpy, T., Frye, J., & Holladay, J. (2006). Succinic Acid - A Model Building Block for Chemical Production from Renewable Resources. *Biorefineries*, 367-379.

Wool, R., & Sun, X. S. (2005). Preface. In R. Wool, *Bio-Based Polymers and Composites* (p. XIII). London: Elsevier Academic Press.

Wunderlich, B. (2005). Single Component Materials. In B. Wunderlich, *Thermal Analysis of Polymeric Materials* (pp. 609-610). Berlin: Springer.

Zakzeski, J., Bruijnincx, P. C., Jongerius, A. L., & Weckhuysen, B. M. (2010). The Catalytic Valorization of LIgnin for the Production of Renewable Chemicals. *Chemical Review*, 3552-3599.

Zhao, X., Huang, Z., Zhang, Y., Yang, M., Chen, D., Huang, K., . . . Feng, Z. (2017). Efficient Solid-Phase Synthesis of Acetylated Lignin and a Comparison of the Properties of Different Modified Lignins. *Applied Polymer Science*.

Zhou, Q.-H., Li, M., Yang, P., & Gu, Y. (2013). Effects of Hydrogen Bonds on Structures and Glass Transition Temperatures of Maleimide-Isobutene Alternating Copolymers: Molecular Dynamics Simulation Study. *Macromolecular Theory and Simulations*, 107-114.

Zhu, C., Zhao, F., Diao, H., & You, Y. (n.d.). Study on the Synthesis and Biodegradation of Starch-Graft_(VAc-co_MMA) Copolymer.**}**

8 Appendix of Data

Table 8.1 Youngs modulus results for AA copolymers

	AA BD 0.8 Youngs Modulus (MPa)					AA BD 0.9 Youngs Modulus (MPa)					AA BD 1 Youngs Modulus (MPa)				
	10%	20%	30%	40%	50%	10%	20%	30%	40%	50%	10%	20%	30%	40%	50%
1	27.81	18.79	9.90	83.86	29.77	37.13	14.45	2.46	16.88	35.45	50.31	24.46	2.65	7.75	109.70
2	11.58	22.57	8.77	40.85	46.05	42.69	11.70	2.15	14.49	92.74	48.84	23.19	2.02	6.10	70.64
3	19.46	28.22	7.18	13.33	28.97	31.94	12.19	2.89	20.97	101.50	58.67	19.26	2.30	6.09	61.62
4	7.04	22.99	8.76	41.60	22.32			9.31						7.18	46.56
5		26.81	10.16	27.21				10.79							
6		12.42	7.65												
7		18.57	5.17												
8		29.21	13.50												
9		19.85	11.20												
10		27.74	2.02												
11		24.91	9.08												
12			10.56												
avg	16.47	22.92	8.66	41.37	31.78	37.25	12.78	5.52	17.45	76.56	52.61	22.30	2.32	6.78	72.13
stdev	9.14	5.16	2.97	26.42	10.08	5.38	1.47	4.18	3.28	35.87	5.30	2.71	0.32	0.83	26.94

Table 8.2 Tensile strength results for AA copolymers

	AA BD 0.8 Tensile Strength (MPa)					AA BD 0.9 Tensile Strength (MPa)					AA BD 1 Tensile Strength (MPa)				
	10%	20%	30%	40%	50%	10%	20%	30%	40%	50%	10%	20%	30%	40%	50%
1	0.11	1.72	0.83	1.53	0.76	0.25	0.29	0.50	0.72	0.66	0.22	0.27	0.30	0.73	0.89
2	0.09	0.92	0.83	1.72	0.75	0.46	0.29	0.33	0.73	1.47	0.17	0.09	0.30	0.56	0.97
3	0.10	0.88	0.73	0.21	0.69	0.45	0.25	0.38	0.67	0.65	0.21	0.14	0.19	0.54	1.10
4	0.07	0.92	0.79	0.87	0.50			0.80						0.43	0.76
5		1.13	0.74	1.36				0.81							
6		0.87	0.70												
7		0.81	0.53												
8		0.85	0.92												
9		0.73	0.65												
10		0.80	0.54												
11		0.95	0.75												
12			0.85												
avg	0.09	0.96	0.74	1.14	0.68	0.39	0.28	0.56	0.71	0.93	0.20	0.16	0.26	0.57	0.93
stdev	0.02	0.27	0.12	0.61	0.12	0.12	0.02	0.23	0.03	0.47	0.03	0.09	0.06	0.12	0.15

Table 8.3 Strain at break results for AA copolymers

	AA BD 0.8 Strain at Break %					AA BD 0.9 Strain at Break %					AA BD 1 Strain at Break %				
	10%	20%	30%	40%	50%	10%	20%	30%	40%	50%	10%	20%	30%	40%	50%
1	2.01	40.93	32.27	12.81	20.07	1.83	16.41	83.85	25.54	11.90	1.21	3.05	32.35	32.37	2.51
2	2.61	18.72	30.88	14.54	12.72	2.64	15.68	79.41	18.33	6.23	1.26	1.57	33.21	29.64	2.83
3	2.70	10.59	40.65	15.86	8.92	6.76	9.11	104.20	14.78	2.27	0.92	2.68	22.33	27.47	5.54
4	2.53	12.57	33.91	23.24	12.04			54.27						20.78	6.44
5		20.87	31.18	27.11				41.33							
6		20.31	40.83												
7		18.55	50.10												
8		11.12	28.80												
9		14.01	33.41												
10		12.36	40.22												
11		19.03	45.41												
12			36.80												
avg	2.46	18.10	37.04	17.93	13.44	3.74	13.73	72.61	19.55	6.80	1.13	2.43	29.30	27.57	4.33
stdev	0.31	8.49	6.50	21.12	4.72	2.65	4.02	24.93	5.48	4.84	0.19	0.77	6.05	4.95	1.95

Table 8.4 Youngs modulus results for SA copolymers

	SA BD 0.8 Youngs Modulus (MPa)					SA BD 0.9 Youngs Modulus (MPa)					SA BD 1 Youngs Modulus (MPa)				
	10%	20%	30%	40%	50%	10%	20%	30%	40%	50%	10%	20%	30%	40%	50%
1	77.53	61.93	17.70	44.51	85.23	384.50	158.80	198.00	38.94	207.70	209.10	149.90	111.80	98.88	116.50
2	67.81	93.86	22.23	71.67	142.00	228.70	274.90	89.15	17.02	64.43	271.80	237.40	169.00	87.74	109.40
3	134.50	184.80	30.91	27.40	239.70	400.50	210.70	70.54	161.30	80.19	148.00	317.80	133.50	14.78	126.80
4			18.47					65.68	55.38		192.10				
5								126.10							
6								90.58							
avg	93.28	113.53	22.33	47.86	155.64	337.90	214.80	106.68	68.16	117.44	205.25	235.03	138.10	67.13	117.57
stdev	36.03	63.75	6.05	22.32	78.13	94.91	58.16	49.54	64.05	78.56	51.30	83.98	28.88	45.68	8.75

Table 8.5 Tensile strength results for SA copolymers

	SA BD 0.8 Tensile Strength (MPa)					SA BD 0.9 Tensile Strength (MPa)					SA BD 1 Tensile Strength (MPa)				
	10%	20%	30%	40%	50%	10%	20%	30%	40%	50%	10%	20%	30%	40%	50%
1	0.23	0.05	0.38	1.02	1.59	0.19	0.33	0.64	1.78	1.15	0.37	2.01	1.79	1.50	1.11
2	0.23	0.32	0.78	0.67	1.74	0.48	0.39	2.04	0.56	0.52	0.42	1.28	1.97	1.34	1.21
3	0.31	1.02	0.41	0.47	0.54	0.77	0.56	1.75	1.80	0.96	0.29	2.21	1.85	1.22	1.39
4			0.55					1.82	0.68		0.29				
5								2.31							
6								1.90							
avg	0.26	0.46	0.53	0.72	1.29	0.48	0.43	1.74	1.20	0.88	0.34	1.83	1.87	1.35	1.24
stdev	0.04	0.50	0.18	0.28	0.65	0.29	0.12	0.57	0.68	0.32	0.07	0.49	0.09	0.14	0.14

Table 8.6 Strain at break results for SA copolymers

	SA BD 0.8 Strain at Break %					SA BD 0.9 Strain at Break %					SA BD 1 Strain at Break %				
	10%	20%	30%	40%	50%	10%	20%	30%	40%	50%	10%	20%	30%	40%	50%
1	0.73	0.52	15.46	19.17	5.72	0.14	0.49	0.60	57.72	1.76	0.33	1.46	2.52	2.60	3.20
2	0.97	0.87	37.66	6.09	4.14	0.41	0.29	6.45	16.00	2.81	0.25	0.86	3.17	3.32	2.84
3	0.42	0.87	10.80	12.18	0.62	0.31	0.94	12.02	2.73	2.80	0.30	1.31	2.95	5.28	1.77
4			16.77					14.40	8.63		0.30				
5								6.42							
6								8.95							
avg	0.71	0.76	20.17	12.48	3.49	0.29	0.58	8.14	21.27	2.46	0.30	1.21	2.88	3.74	2.60
stdev	0.27	0.20	11.94	6.55	2.61	0.14	0.33	4.85	24.90	0.60	0.03	0.31	0.33	1.39	0.74

Table 8.7 Youngs modulus results for SuA copolymers

	SuA BD 0.8 Youngs Modulus (MPa)					SuA BD 0.9 Youngs Modulus (MPa)					SuA BD 1 Youngs Modulus (MPa)				
	10%	20%	30%	40%	50%	10%	20%	30%	40%	50%	10%	20%	30%	40%	50%
1	34.01	43.80	22.25	20.14	110.10	58.13	137.50	59.19	14.60	24.97	315.40	154.50	27.28	17.40	91.37
2	81.67	85.50	13.26	14.08	117.80	85.52	100.60	58.28	16.78	67.98	216.50	194.10	33.25	19.57	77.64
3	37.57	64.73	26.61	45.02	110.30	137.00	96.52	91.57	17.96	56.89	238.50	121.00	59.89	17.27	133.40
4	36.11					78.33						124.40			
5	46.23														
avg	47.12	64.68	20.71	26.41	112.73	89.75	111.54	69.68	16.45	49.95	256.80	148.50	40.14	18.08	100.80
stdev	19.87	20.85	6.81	16.40	4.39	33.57	22.57	18.96	1.70	22.33	51.93	33.92	17.36	1.29	29.05

Table 8.8 Tensile strength results for SuA copolymers

	SuA BD 0.8 Tensile Strength (MPa)					SuA BD 0.9 Tensile Strength (MPa)					SuA BD 1 Tensile Strength (MPa)				
	10%	20%	30%	40%	50%	10%	20%	30%	40%	50%	10%	20%	30%	40%	50%
1	0.09	0.48	0.72	1.28	1.06	0.10	1.05	1.38	1.22	0.94	0.54	1.07	1.43	0.85	0.77
2	0.21	1.03	0.53	0.42	0.96	0.53	1.03	1.24	1.38	0.91	0.46	0.78	1.73	0.80	0.78
3	0.19	0.44	0.68	1.91	0.75	0.30	0.88	0.77	0.69	1.05	0.41	0.57	1.62	0.63	1.07
4	0.40					0.20						1.02			
5	0.45														
avg	0.27	0.65	0.64	1.20	0.92	0.28	0.99	1.13	1.10	0.97	0.47	0.86	1.59	0.76	0.87
stdev	0.15	0.33	0.10	0.75	0.16	0.18	0.09	0.32	0.36	0.07	0.07	0.23	0.15	0.12	0.17

Table 8.9 Strain at break results for SuA copolymers

	SuA BD 0.8 Strain at Break %					SuA BD 0.9 Strain at Break %					SuA BD 1 Strain at Break %				
	10%	20%	30%	40%	50%	10%	20%	30%	40%	50%	10%	20%	30%	40%	50%
1	1.01	3.29	11.20	28.67	2.05	0.78	2.07	9.88	45.80	8.09	0.39	2.40	17.63	18.24	3.90
2	0.77	3.97	17.83	14.16	1.75	1.36	2.94	6.05	47.71	7.73	0.41	0.70	19.60	29.71	2.48
3	1.77	3.01	9.05	24.13	1.34	0.85	3.70	2.67	13.98	6.54	0.36	1.11	10.32	14.18	2.81
4	4.24					1.31						1.56			
5	2.59														
6															
7															
avg	2.08	3.42	12.69	22.32	1.71	1.07	2.91	6.20	35.83	7.45	0.39	1.44	15.85	20.71	3.06
stdev	1.41	0.49	4.58	7.42	0.36	0.30	0.81	3.61	18.95	0.81	0.03	0.73	4.89	8.05	0.75

Table 8.10 Tensile stress strain results for AA BD 0.8 copolymers using ball milled lignin

	AA BD 0.8 Ball Mill Youngs Modulus (MPa)					AA BD 0.8 Ball Mill Tensile Strength (MPa)					AA BD 0.8 Ball Mill Strain at Break %				
	10%	20%	30%	40%	50%	10%	20%	30%	40%	50%	10%	20%	30%	40%	50%
1	23.53	9.47	0.93	23.28	98.06	0.35	0.62	0.26	1.03	1.11	6.23	45.72	101.20	38.76	3.60
2	28.25	9.01	0.88	50.89	160.40	0.26	0.52	0.29	0.84	0.73	3.36	33.83	154.60	21.35	1.32
3	32.62	6.54	1.09	18.13	124.50	0.46	0.42	0.20	1.05	0.96	3.32	41.49	144.40	43.16	2.02
avg	28.13	8.34	0.97	30.77	127.65	0.36	0.52	0.25	0.97	0.94	4.30	40.35	133.40	34.42	2.31
stdev	4.55	1.58	0.11	17.62	31.29	0.10	0.10	0.05	0.12	0.19	1.67	6.03	28.35	11.53	1.17

Table 8.11 Tensile stress strain results for AA BD 1 copolymers using TSA catalyst

	AA BD 1 TSA Catalyst Youngs Modulus (MPa)					AA BD 1 TSA Catalyst Tensile Strength (MPa)					AA BD 1 TSA Catalyst Strain at Break %				
	10%	20%	30%	40%	50%	10%	20%	30%	40%	50%	10%	20%	30%	40%	50%
1	147.40	40.77	38.47	10.73	223.90	0.48	0.37	1.59	1.07	0.88	0.67	2.99	15.56	42.41	3.44
2	76.98	52.78	34.54	10.25	61.95	0.45	0.44	0.83	1.03	1.00	1.16	2.35	8.88	39.02	7.73
3	96.49	56.76	40.04	14.65	60.71	0.46	0.52	1.67	1.06	0.92	1.22	5.47	16.55	34.33	6.55
4	104.00	54.44	43.52	8.56	58.05	0.20	0.91	1.61	0.88	0.86	0.38	5.02	15.88	36.10	14.24
5	65.69	51.22	36.53	12.33	67.41	0.36	0.71	1.76	1.16	0.99	1.45	5.45	30.55	43.43	12.36
6	111.70	41.96	42.27	13.00	71.55	0.17	0.86	1.74	1.07	0.80	0.75	6.00	18.55	39.23	5.65
7	91.26	53.34		11.98	37.74	0.09	0.50		1.10	0.91	0.55	2.97		45.90	10.51
8		76.36			53.49		0.68			0.94		2.86			9.25
avg	99.07	53.45	39.23	11.64	79.35	0.32	0.62	1.53	1.05	0.91	0.88	4.14	17.66	40.06	8.72
stdev	26.42	10.92	3.41	1.99	59.28	0.16	0.20	0.35	0.09	0.07	0.39	1.48	7.11	4.11	3.59

Table 8.12 AA Tg by DMA compression

	AA BD 0.8 Tg by DMA compression						AA BD 0.9 Tg by DMA compression						AA BD 1 Tg by DMA compression					
	0%	10%	20%	30%	40%	50%	0%	10%	20%	30%	40%	50%	0%	10%	20%	30%	40%	50%
1	48.36	49.00	57.66	55.69	78.46	80.57	41.94	36.75	40.98	38.38	54.09	77.62	43.56	45.36	38.97	46.51	36.46	78.48
2	42.26	45.90	59.63	47.84	64.57	88.21	42.40	39.16	42.44	40.70	43.41	74.50	42.99	44.21	41.32	44.46	39.24	76.13
3	46.90	49.78	43.06	47.70	61.15	83.67	42.60	38.77	40.91	44.63	51.60	73.51	46.68	43.71	41.08	45.67	42.56	76.46
4	51.64	42.09		55.86	65.97						48.21	79.93					64.92	
5				50.70							49.22	74.78						
6				46.72														
7				40.26														
avg	47.29	46.69	53.45	49.25	67.54	84.15	0.34	1.30	0.87	3.16	4.01	2.65	44.41	44.43	40.45	45.55	45.80	77.03
stdev	3.90	3.50	9.05	5.46	7.56	3.84	42.31	38.23	41.44	41.24	49.31	76.07	1.99	0.84	1.29	1.03	12.99	1.27

Table 8.13 SA Tg by DMA compression

	SA BD 0.8 Tg by DMA compression						SA BD 0.9 Tg by DMA compression						SA BD 1 Tg by DMA compression					
	0%	10%	20%	30%	40%	50%	0%	10%	20%	30%	40%	50%	0%	10%	20%	30%	40%	50%
1	100.09	84.28	88.31	55.10	63.23	68.88	103.70	96.61	101.00	89.19	71.12	73.73	98.82	99.99	51.09	98.95	106.76	75.29
2	101.97	89.67	91.77	51.36	63.18	70.22	101.60	96.18	94.76	89.90	65.79	77.64	100.53	99.17	51.20	80.80	72.65	82.30
3	103.98	89.49	90.81	45.89	58.11	69.48	102.13	95.99	93.90	93.80	70.19	74.29	100.24	99.27	101.04	77.20	77.73	84.78
4				68.61		67.77								100.59		87.22		
5				48.78														
6				56.77														
avg	102.01	87.81	90.30	54.42	61.51	69.09	1.09	0.32	3.87	2.48	2.85	2.37	0.92	0.67	28.80	9.55	18.40	4.92
stdev	1.94	3.06	1.79	8.01	2.94	1.03	102.48	96.26	96.55	90.96	69.03	75.97	99.86	99.75	67.78	86.04	85.71	80.79

Table 8.14 SuA Tg by DMA compression

	SuA BD 0.8 Tg by DMA compression						SuA BD 0.9 Tg by DMA compression						SuA BD 1 Tg by DMA compression					
	0%	10%	20%	30%	40%	50%	0%	10%	20%	30%	40%	50%	0%	10%	20%	30%	40%	50%
1	74.76	41.59	47.03	57.10	53.37	85.16	51.36	48.50	58.79	49.44	54.69	76.09	44.59	46.97	45.57	44.06	54.35	95.22
2	73.09	40.73	43.44	46.26	71.91	86.53	52.04	49.43	53.15	44.47	54.43	73.67	44.62	48.64	46.75	45.28	53.37	88.23
3	54.32	37.51	43.90	46.83	59.35	89.05	51.04	49.66	52.71	41.82	51.77	74.59	44.37	47.40	45.20	46.05	55.60	85.53
4																42.69		
5																41.85		
6																39.36		
7																45.65		
Avg	67.39	39.94	44.79	50.06	61.54	86.91	51.48	49.19	54.88	45.24	53.63	74.78	0.13	0.86	0.81	2.42	1.12	1.91
stdev	11.35	2.15	1.95	6.10	9.46	1.97	0.51	0.62	3.39	3.86	1.61	1.22	44.53	47.67	45.84	43.56	54.44	86.88

Table 8.15 AA BD 0.8 w/ ball mill lignin, AA BD 1 w/ TSA catalyst Tg by DMA compression

	AA BD 0.8 Ball Mill Tg by DMA compression					AA BD 1 TSA Catalyst Tg by DMA Compression					
	10%	20%	30%	40%	50%	0%	10%	20%	30%	40%	50%
1	46.64	39.33	48.01	65.84	88.26	47.81	46.34	44.16	39.15	93.43	85.08
2	48.08	48.54	54.28	60.15	87.39	48.23	45.99	43.69	43.31	43.39	87.53
3	51.06	48.48	47.11	60.60	102.16	47.42	45.51	45.97	43.01	67.77	82.02
4		52.25	46.70	67.24						47.06	
5										55.05	
6										65.19	
avg	2.25	5.50	3.55	3.61	8.29	0.41	0.42	1.20	2.32	18.16	2.76
stdev	48.60	47.15	49.02	63.46	92.60	47.82	45.95	44.61	41.82	61.98	84.88

Table 8.16 AA copolymers Tg, Tm and lignin Tg by DSC at various heating rates

	AA BD 0.8 Tg			AA BD 0.8 Tm			AA BD 0.8 lignin Tg		
	5C/min	10C/min	15C/min	5C/min	10C/min	15C/min	5C/min	10C/min	15C/min
0%	-50.63	-49.02	-47.56	29.51	30.29	30.06			
10%	-46.29	-44.22	-44.27	29.47	30.55	30.04	125.98	125.95	125.29
20%	-23.77	-24.32	-22.26	32.13	32.39	31.56	122.92	122.28	122.02
30%	-23.48	-24.08	-23.51				123.63	122.82	123.06
40%	-5.14	-4.99	-3.78				121.99	121.91	120.97
50%	18.23	16.74	10.88				116.09	123.15	123.5

	AA BD 0.9 Tg			AA BD 0.9 Tm			AA BD 0.9 lignin Tg		
	5C/min	10C/min	15C/min	5C/min	10C/min	15C/min	5C/min	10C/min	15C/min
0%				35.97	36.17	35.83			
10%	-42.5	-44.2	-40.45	31.9	32.27	31.8	124.97	126.16	127.07
20%	-49.47	-47.79	-46.81	36.51	36.73	37.37	119.74	121.49	121.33
30%	-33.74	-42.9	-42.15	31.91	33.61	34.58	121.36	121.5	120.96
40%	-21.89	-22.24	-22.15				120.58	121.87	121.01
50%	-4.12	-4.65	-4.09				123.68	122.95	121.63

	AA BD 1 Tg			AA BD 1 Tm			AA BD 1 lignin Tg		
	5C/min	10C/min	15C/min	5C/min	10C/min	15C/min	5C/min	10C/min	15C/min
0%	-9.47	-8.18	-7.27	40.1	40.54	40.56			
10%				41.67	41.61	42.01			
20%				37.34	36.98	37.02	127.21	125.24	125.47
30%	-33.23	-39.95	-42.78				121.43	122.32	121.56
40%	-23.02	-23.62	-24.56						
50%	-3.06	-4.01	-4.11						

Table 8.17 SA copolymers Tg, Tm and lignin Tg by DSC at various heating rates

	SA BD 0.8 Tg			SA BD 0.8 Tm			SA BD 0.8 lignin Tg		
	5C/min	10C/min	15C/min	5C/min	10C/min	15C/min	5C/min	10C/min	15C/min
0%	-24.3	-24.51	-24.82	103.76	100.98	101.38			
10%	-31.11	-30.09	-29.65	90.06	88.97	86.97	122.88	122.6	122.29
20%	-23.96	-22.83	-22.67	91.08	90.34	90.03	125.21	124.59	124.43
30%	-5.88	-5.13	-4.11				122.7	124.27	124.41
40%	-0.05	4.42	6.63				125.85	125.09	125.03
50%	14.73	16.4	16.6				124.86	125.25	124.77

	SA BD 0.9 Tg			SA BD 0.9 Tm			SA BD 0.9 lignin Tg		
	5C/min	10C/min	15C/min	5C/min	10C/min	15C/min	5C/min	10C/min	15C/min
0%	-23.91	-22.86	-22.69	106.16	104.95	104.3	122.39	122.74	121.77
10%				100.32	99.09	97.63			
20%	-28.9	-25.34	-25.28	95.79	94.58	94.13			
30%	-25.6	-23.94	-23.52	89.31	89.81	88.73	130.98	126.34	124.28
40%	-7.56	-6.53	-5.62				123.32	123.07	123.62
50%	22.65	18.26	17.72				123.02	122.63	121.89

	SA BD 1 Tg			SA BD 1 Tm			SA BD 1 lignin Tg		
	5C/min	10C/min	15C/min	5C/min	10C/min	15C/min	5C/min	10C/min	15C/min
0%	-26.46	22.99	-22.45	103.26	103.12	102			
10%	-23.74	-23.37	-24.03	104.67	102.86	100.63	128.46	123.31	123.03
20%	-23.83	-23.7	-23.49	101.42	100.69	99.84			
30%	-25.62	-24.6	-24.4	94.89	95.95	95.07	124.59	122.98	123.74
40%	-23.46	-22.28	-22.2				126.43	125.53	123.7
50%	10.2	12.95	11.9				123.44	123.83	123.32

Table 8.18 SuA copolymers Tg, Tm and lignin Tg by DSC at various heating rates

	SuA BD 0.8 Tg			SuA BD 0.8 Tm			SuA BD 0.8 lignin Tg		
	5C/min	10C/min	15C/min	5C/min	10C/min	15C/min	5C/min	10C/min	15C/min
0%	-4.86	4.35	-2.63	31.52	31.83	31.77			
10%				40.04	39.48	39.09	121.25	121.39	121.79
20%				40.59	40.4	40.72	124.39	128.09	128
30%	-27.46	-36.24	-36.63				122.02	122.99	122.67
40%	-24.15	-29.54	-27.43				123.77	124.09	123.57
50%	8.26	-4.52	4.5				126.63	126.79	126.42

	SuA BD 0.9 Tg			SuA BD 0.9 Tm			SuA BD 0.9 lignin Tg		
	5C/min	10C/min	15C/min	5C/min	10C/min	15C/min	5C/min	10C/min	15C/min
0%				44.26	44.32	44.79	124.32	127.38	127.4
10%				42.66	42.52	42.5	125.32	125.31	125.31
20%				39.59	39.89	40.62	120.26	124.54	123.61
30%				38.49	35.96	39.8	126.42	127.41	126.16
40%	-31.74	-31.33	-30.84				125.75	125.38	125.28
50%	-0.79	-1.13	-3.83				121.86	122.23	121.35

	SuA BD 1 Tg			SuA BD 1 Tm			SuA BD 1 lignin Tg		
	5C/min	10C/min	15C/min	5C/min	10C/min	15C/min	5C/min	10C/min	15C/min
0%	-24.32	-23.56	-24.15	44.66	44.52	44.66	126.24	126.19	125.63
10%	-23.21	-23.47	-24.07	45.59	45.86	46.11	120.69	121.42	120.61
20%	-24.07	-23.82	-25.03	44.23	43.9	43.78	118.44	117.71	119.46
30%				41.61	41.76	41.74	119.18	120.12	120.21
40%	-23.83	-24.15	-23.19				123.64	123.85	122.62
50%	-23.91	-5.4	-4.96				124.43	126.01	125.76

Table 8.19 AA copolymers ball milled lignin, TSA catalyst Tg, Tm and lignin Tg by DSC at various heating rates

	AA BD 0.8 ball mill Tg			AA BD 0.8 ball mill Tm			AA BD 0.8 ball mill lignin Tg		
	5C/min	10C/min	15C/min	5C/min	10C/min	15C/min	5C/min	10C/min	15C/min
0%									
10%	-45.81	-44.14	-42.06	33.22	32.57	32.78	124.82	123.99	122.13
20%	-38.12	-37.84	-39.56				123.05	122.23	121.61
30%	-25.37	-21.65	-23.52				126.17	125.79	125.8
40%	-4.81	-4.32	-4.38				112.44	117.44	118.06
50%	16.28	23.01	20.36				126.16	126.16	124.79

	AA BD 1 w/ TSA catalyst Tg	AA BD 1 w/ TSA catalyst Tm	AA BD 1 w/ TSA catalyst lignin Tg
	5C/min	5C/min	5C/min
0%	-20.82	48.82	
10%	-25.24	43.17	
20%	-20.92	42.43	
30%	-49.83	39.92	110.09
40%	-23.95		
50%	-5.41		

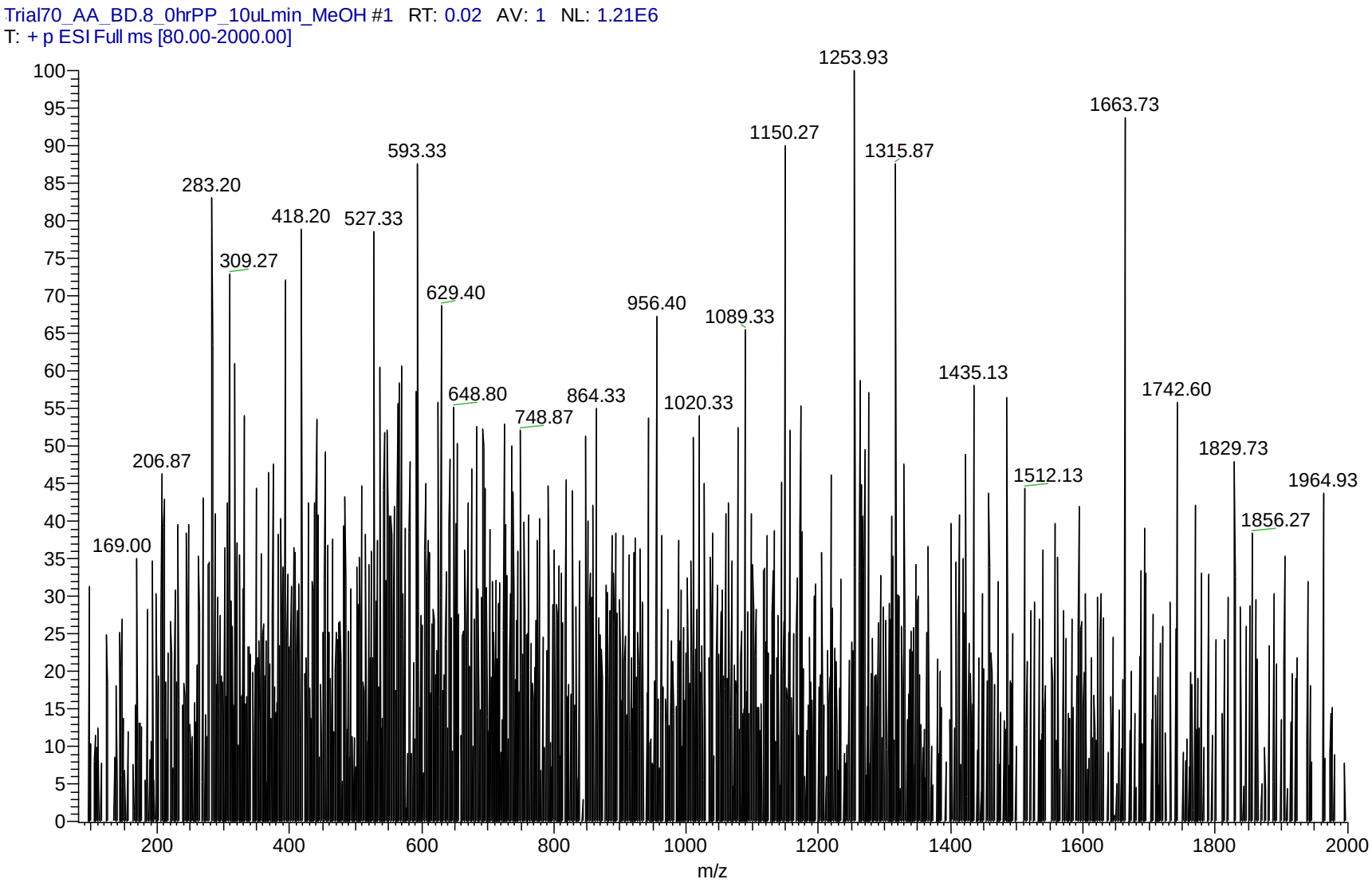

Figure 8.1 AA BD 0.8 0 hr PP ESI-MS positive ion mass spectrum

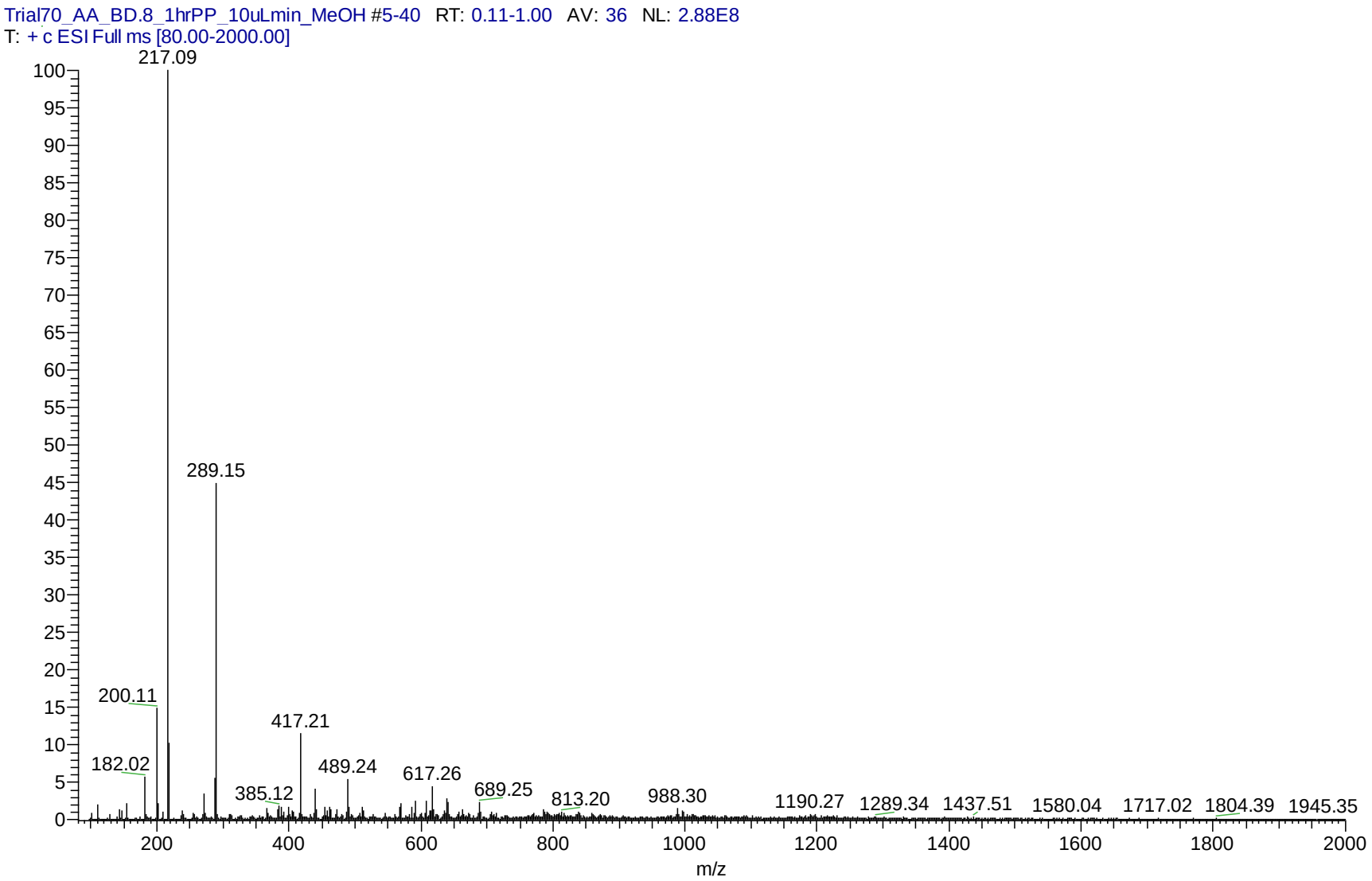

Figure 8.2 AA BD 0.8 1 hr PP ESI-MS positive ion mass spectrum

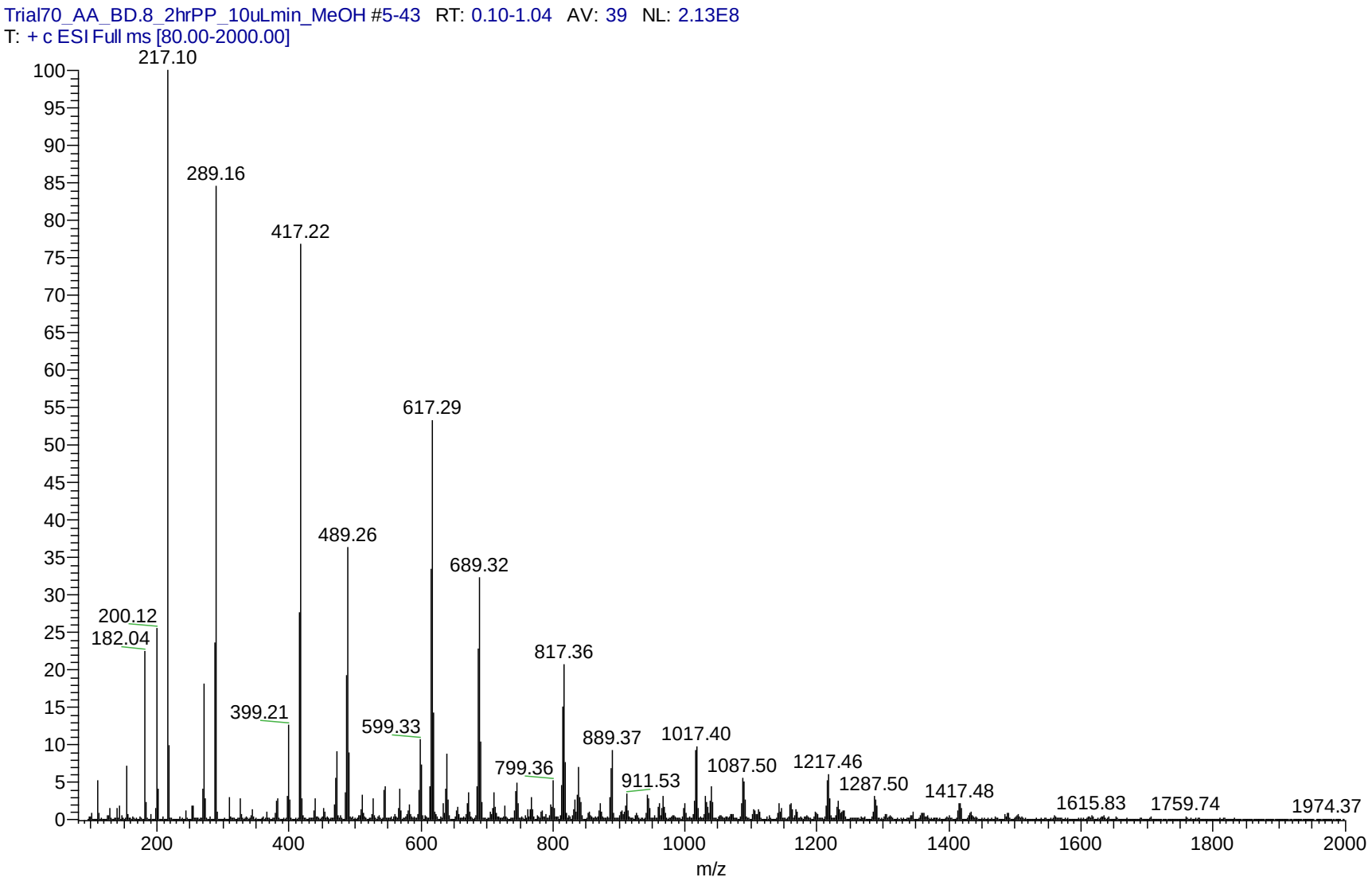

Figure 8.3 AA BD 0.8 2 hr PP ESI-MS positive ion mass spectrum

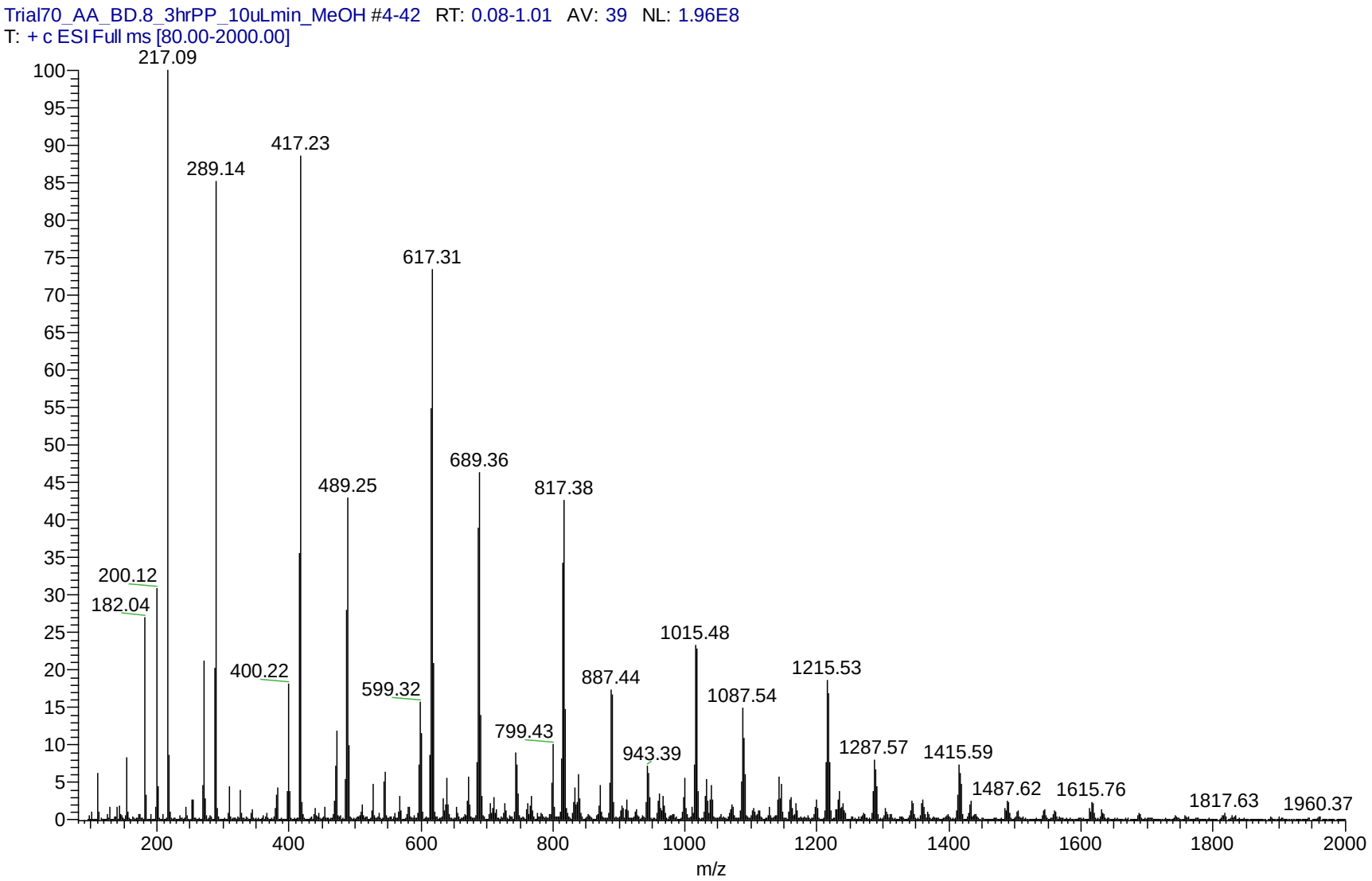

Figure 8.4 AA BD 0.8 3 hr PP ESI-MS positive ion mass spectrum

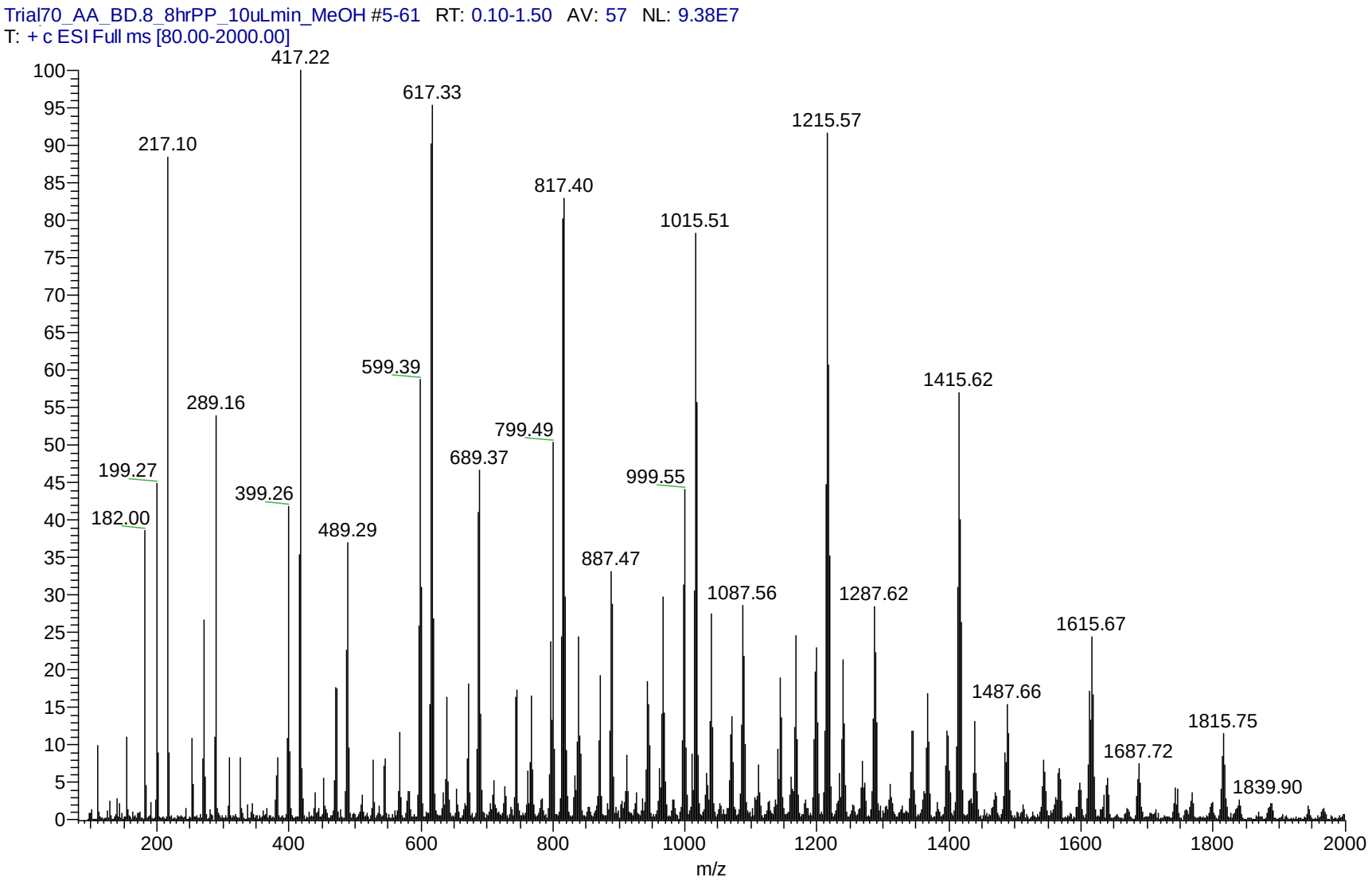

Figure 8.5 AA BD 0.8 8 hr PP ESI-MS positive ion mass spectrum

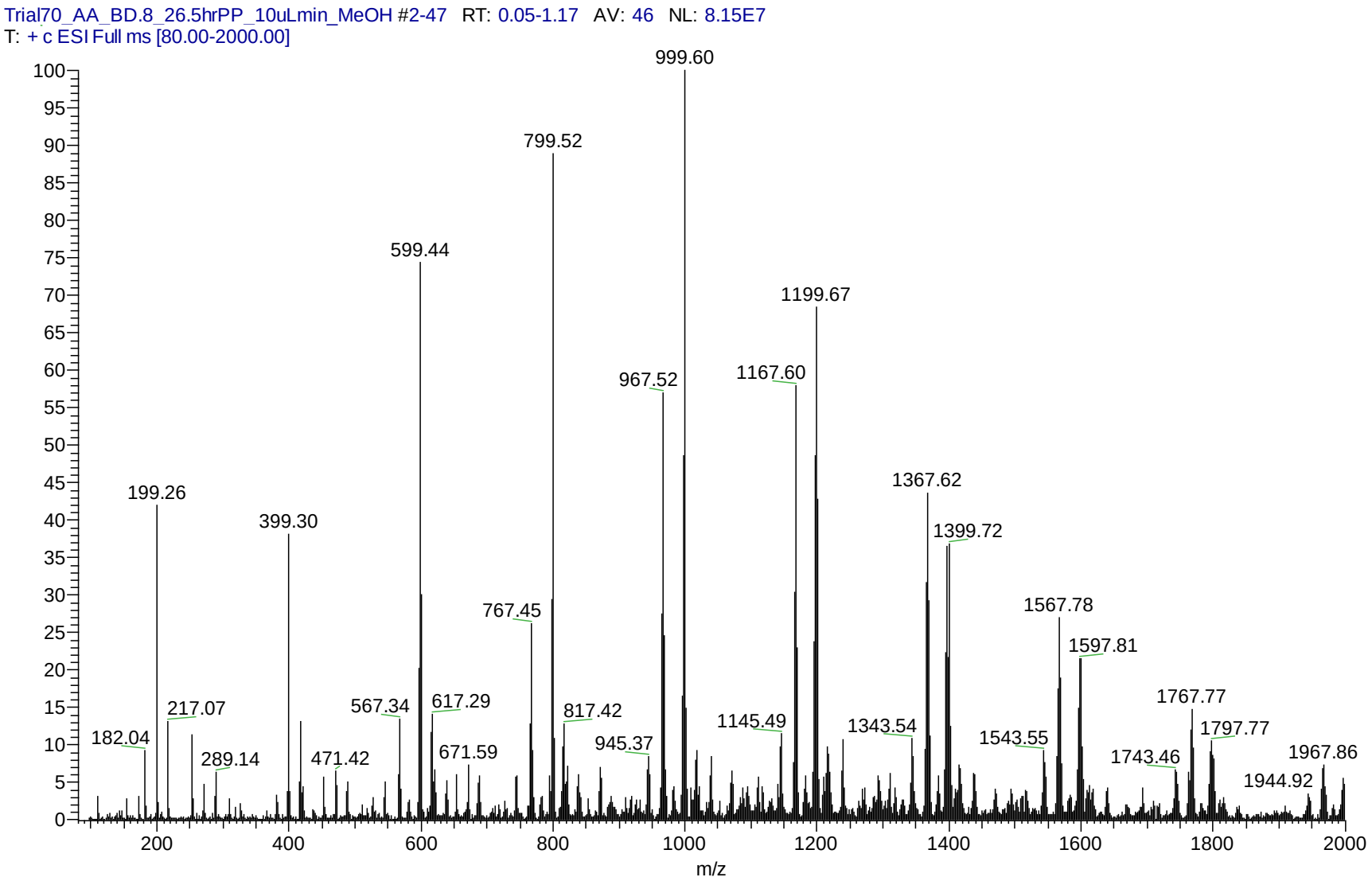

Figure 8.6 AA BD 0.8 26.5 hr PP ESI-MS positive ion mass spectrum

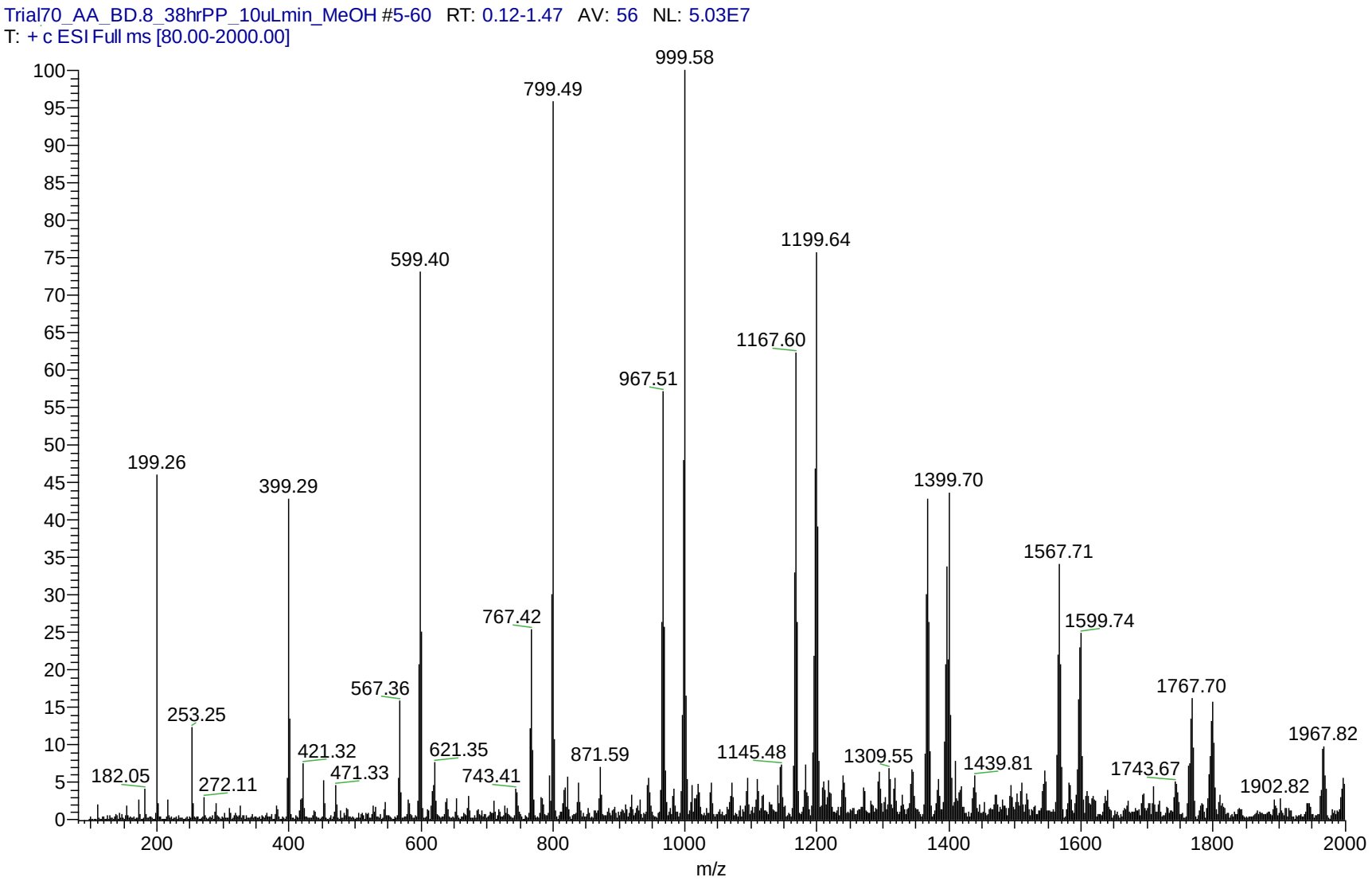

Figure 8.7 AA BD 0.8 38 hr PP ESI-MS positive ion mass spectrum

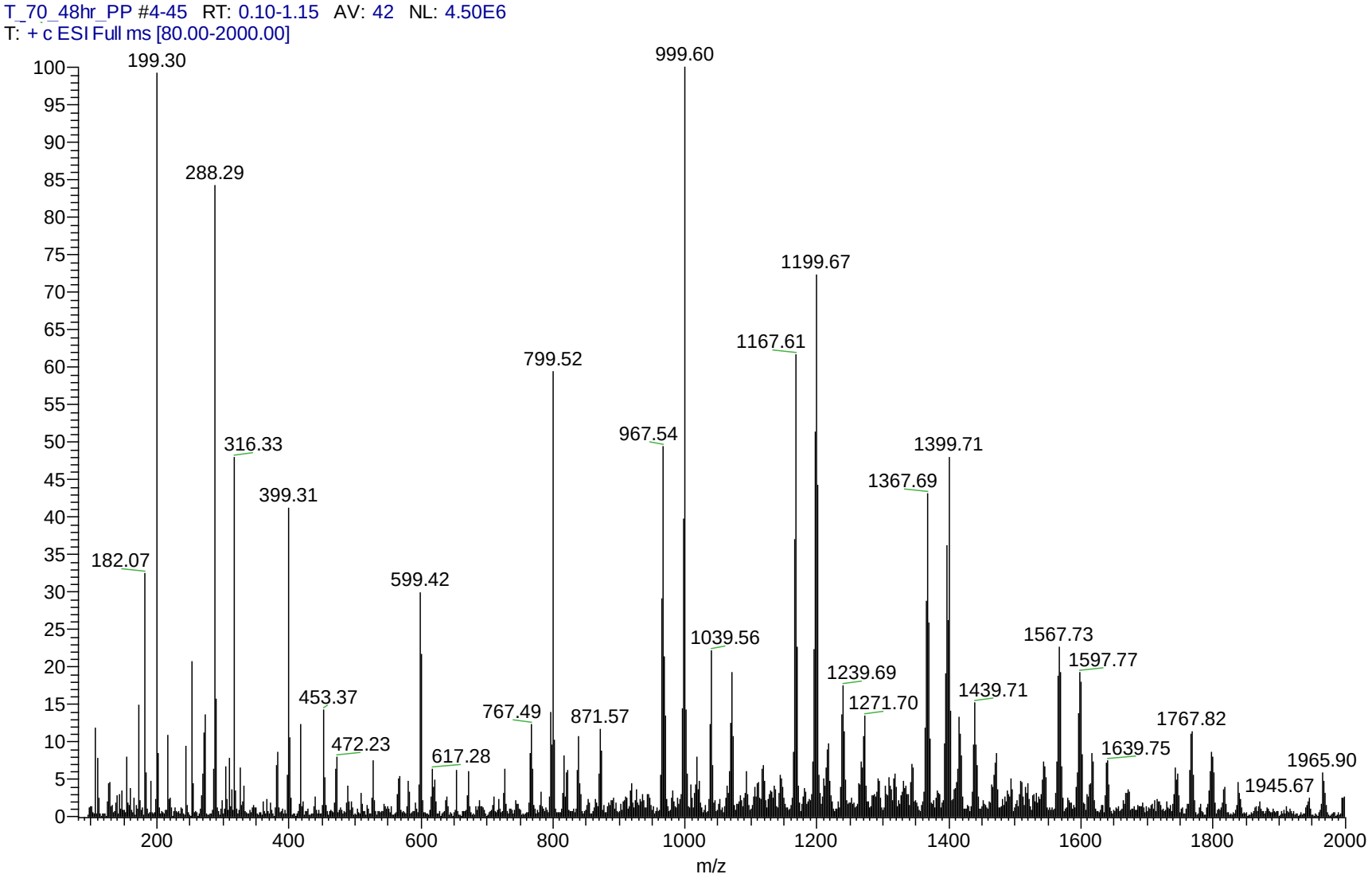

Figure 8.8 AA BD 0.8 48 hr PP ESI-MS positive ion mass spectrum

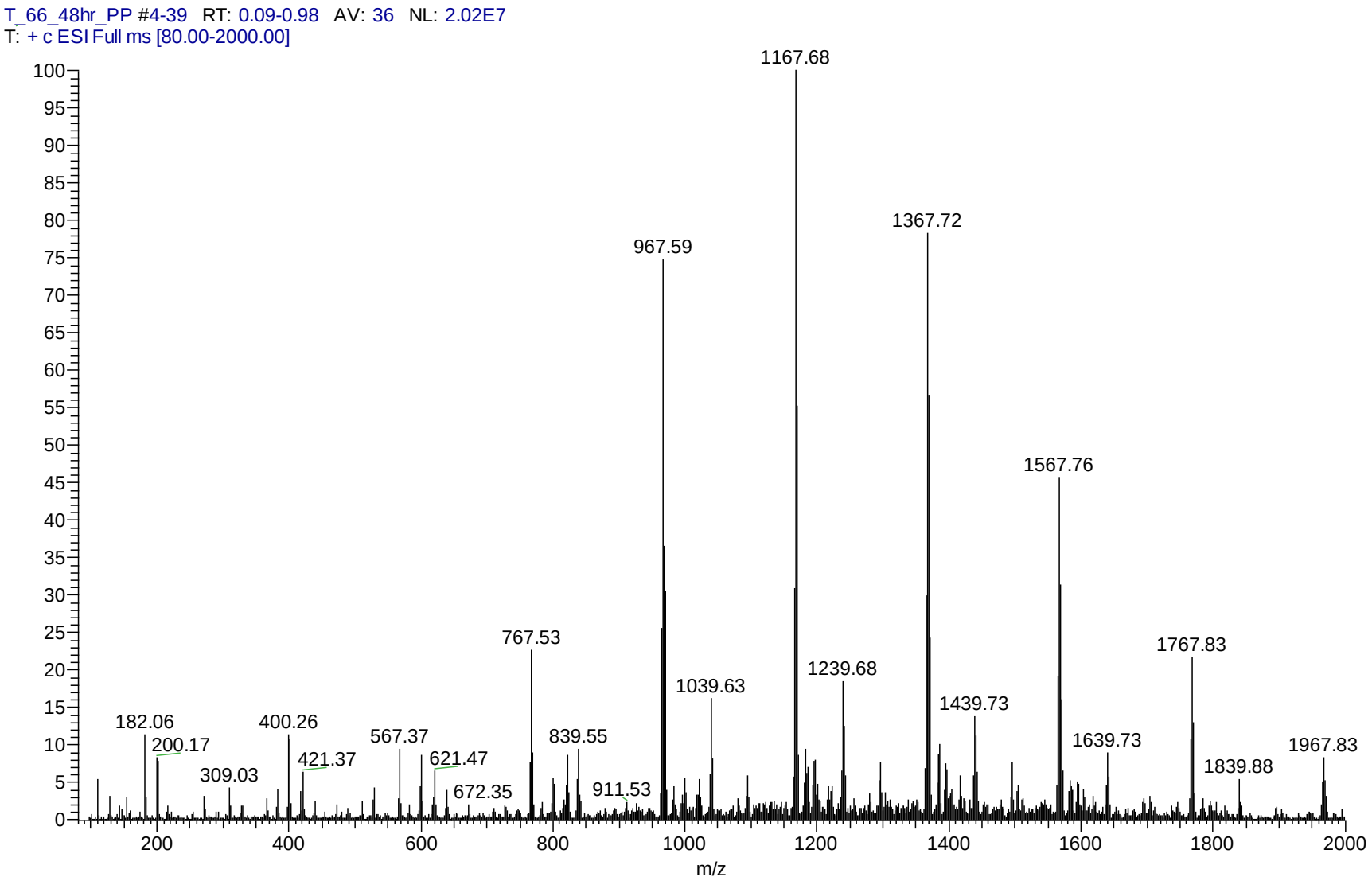

Figure 8.9 AA BD 0.9 48 hr PP ESI-MS positive ion mass spectrum

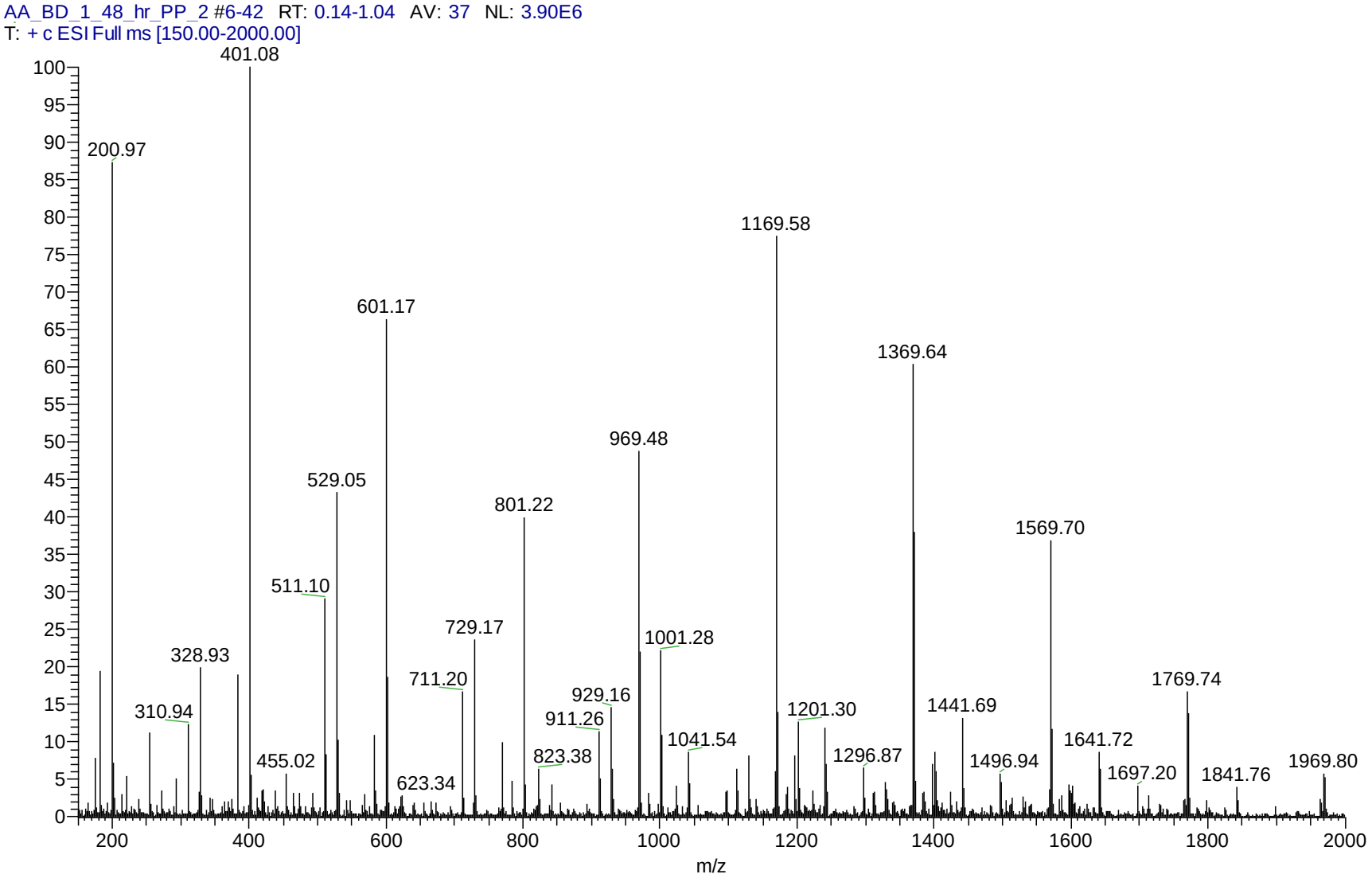

Figure 8.10 AA BD 1 48 hr PP ESI-MS positive ion mass spectrum

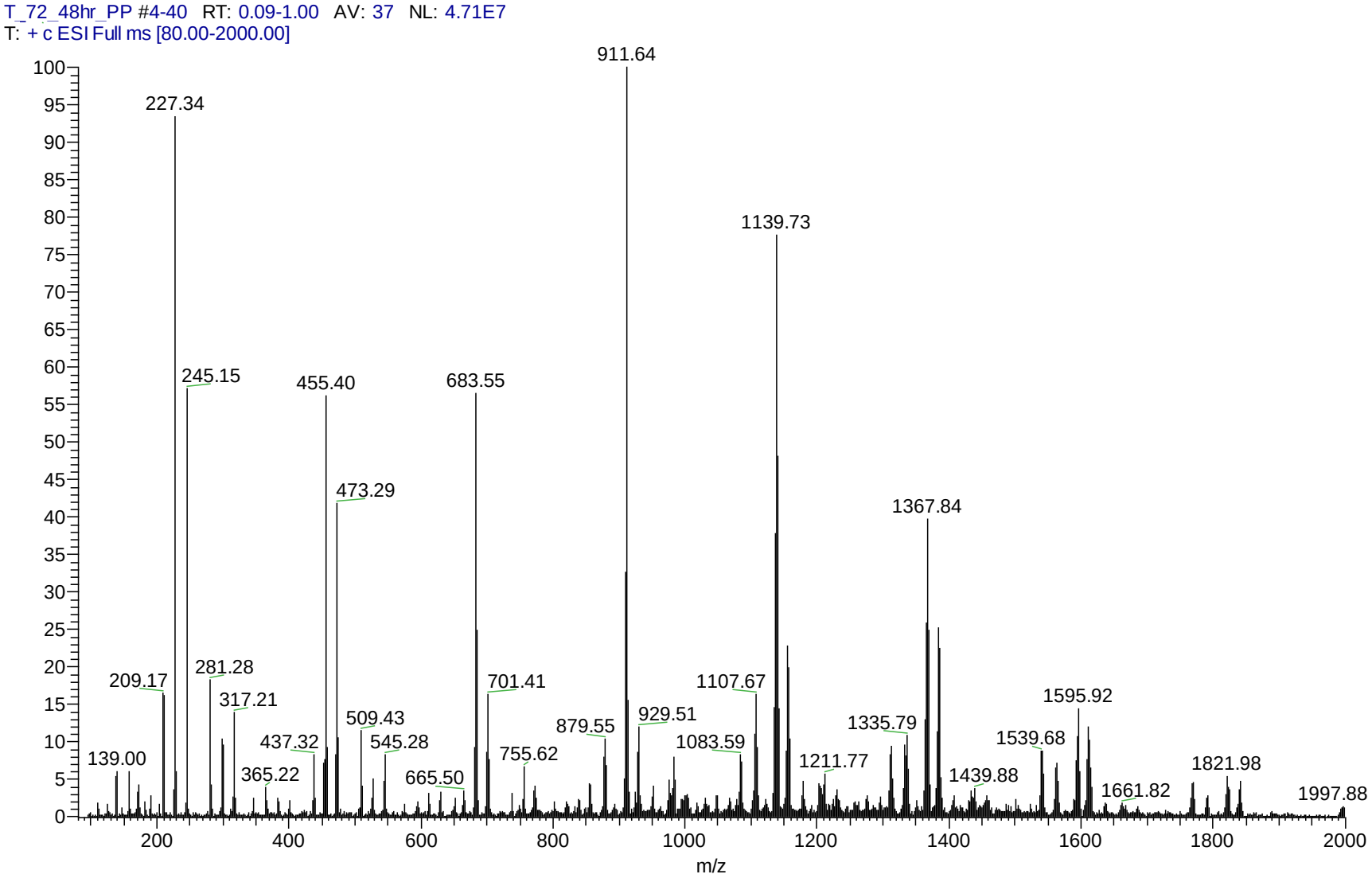

Figure 8.11 SuA BD 0.8 48 hr PP ESI-MS positive ion mass spectrum

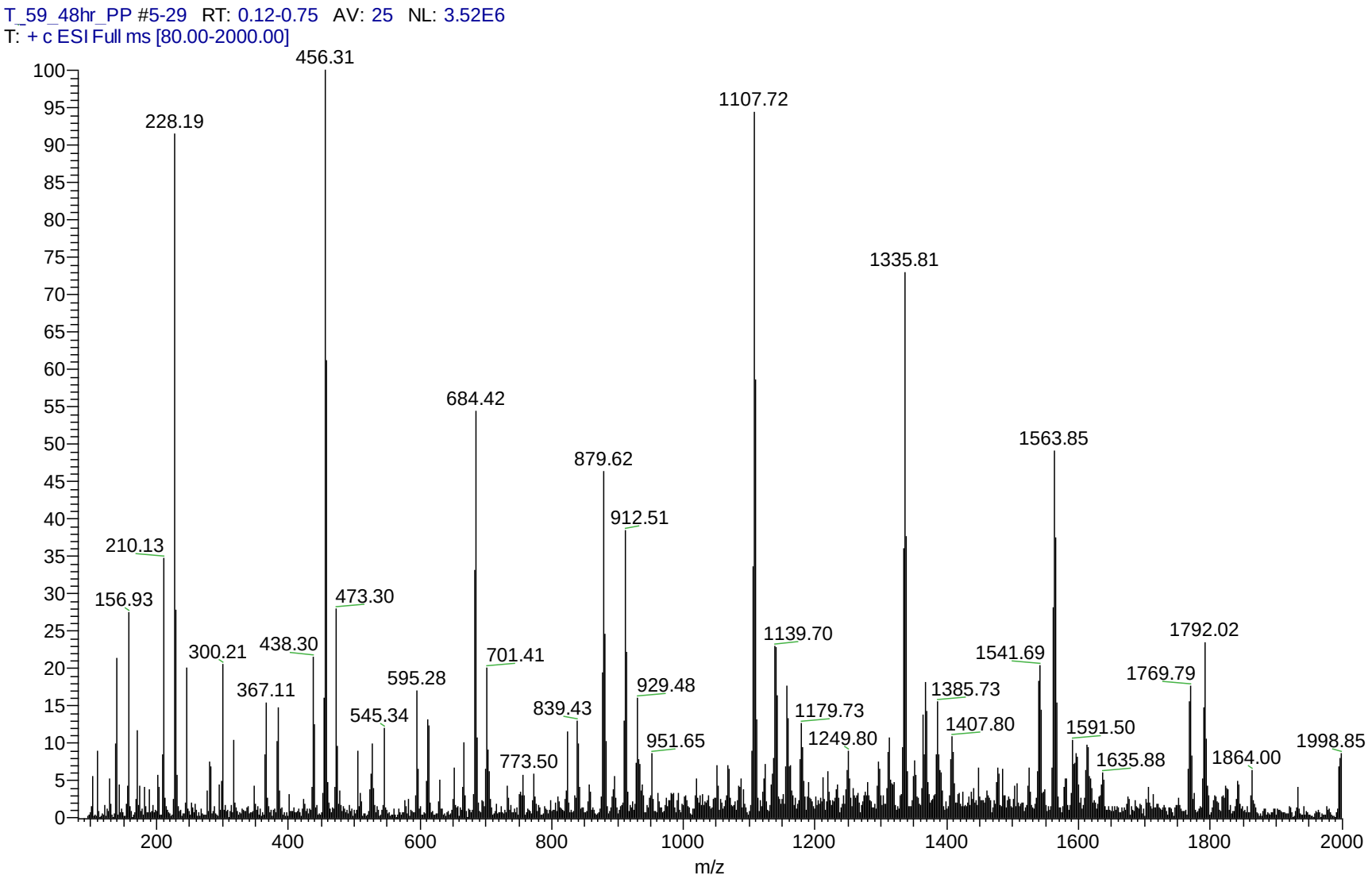

Figure 8.12 SuA BD 0.9 48 hr PP ESI-MS positive ion mass spectrum

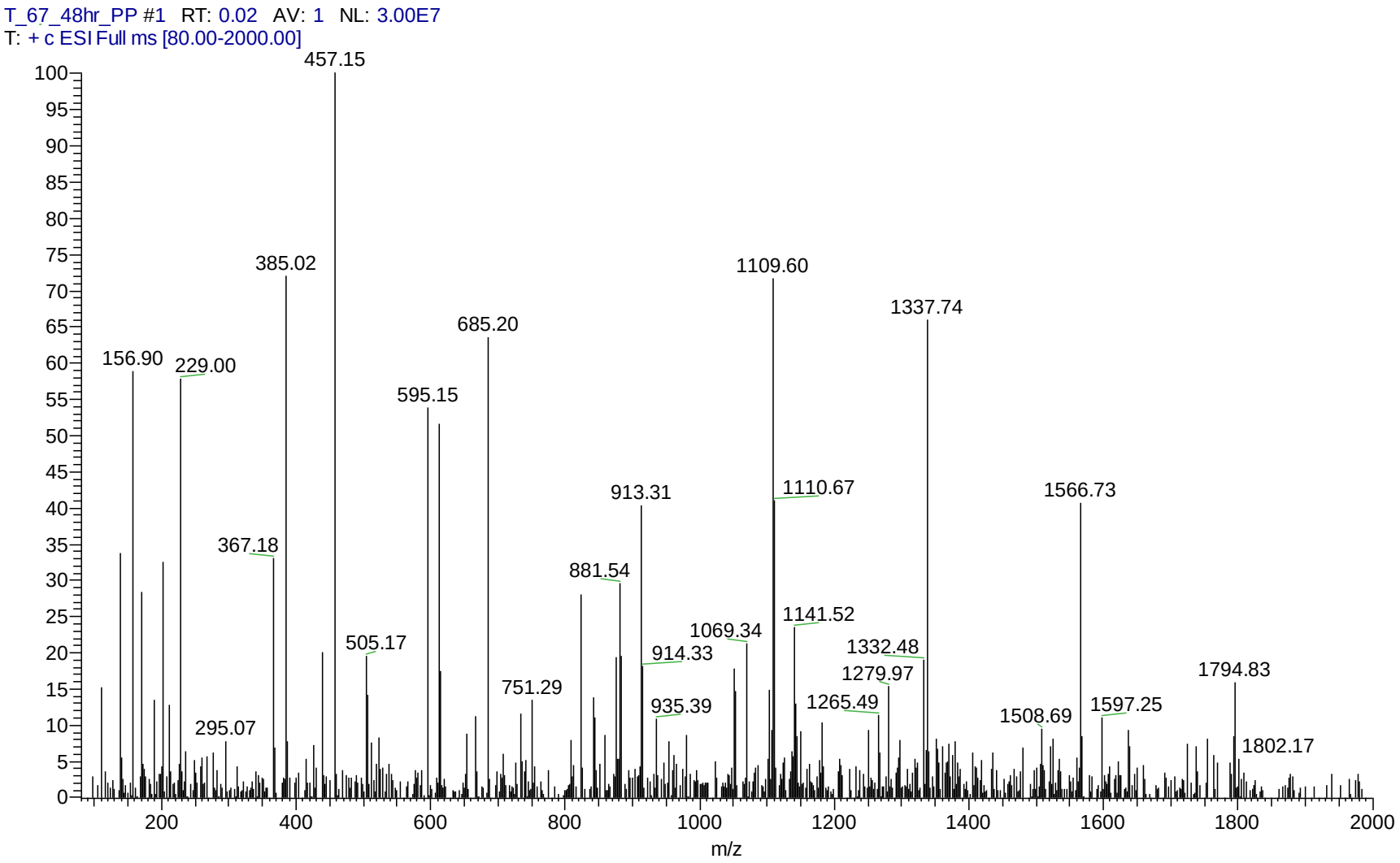

Figure 8.13 SuA BD 1 48 hr PP ESI-MS positive ion mass spectrum

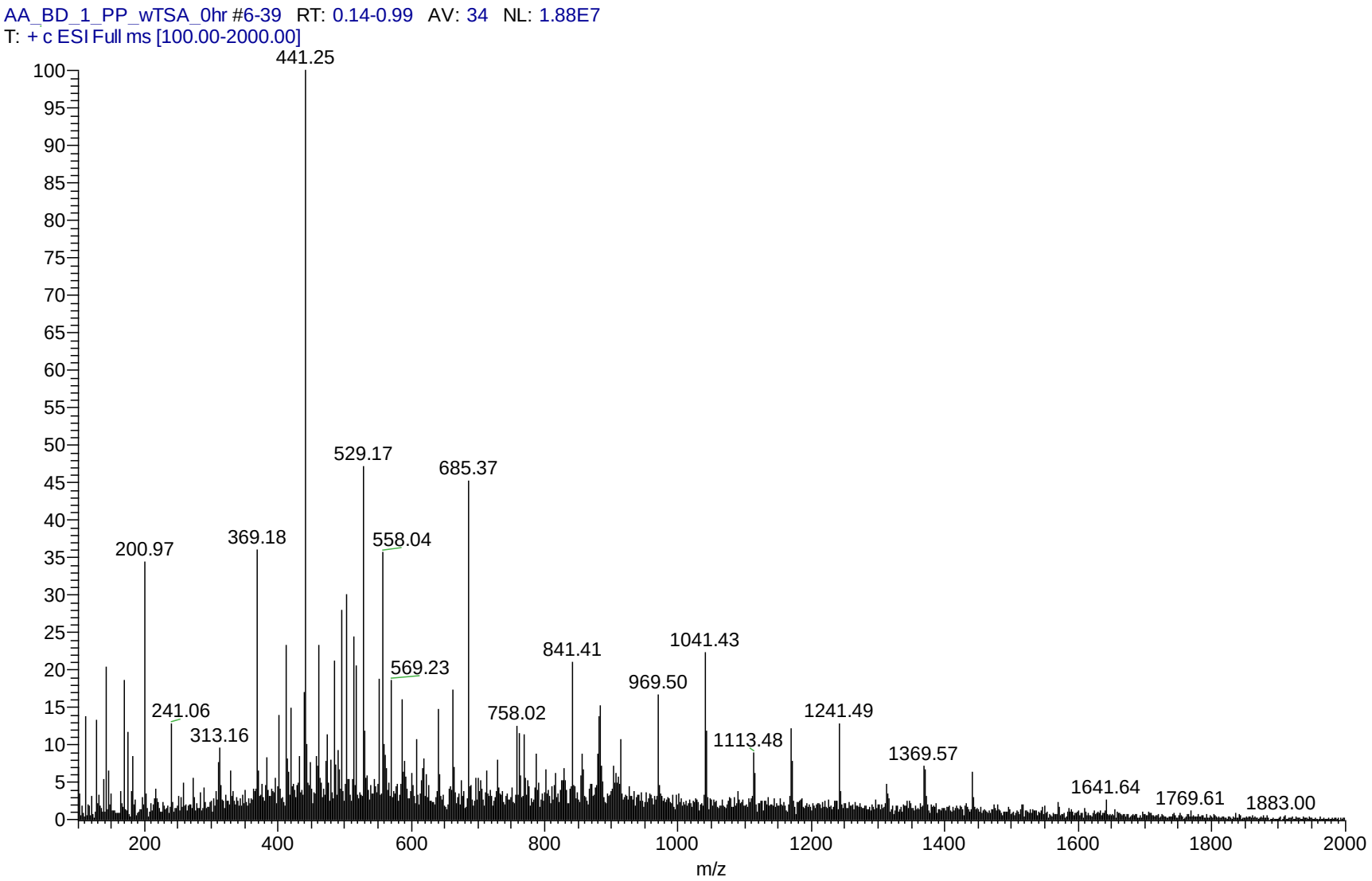

Figure 8.14 AA BD 1 0 hr PP w/ TSA ESI-MS positive ion mass spectrum

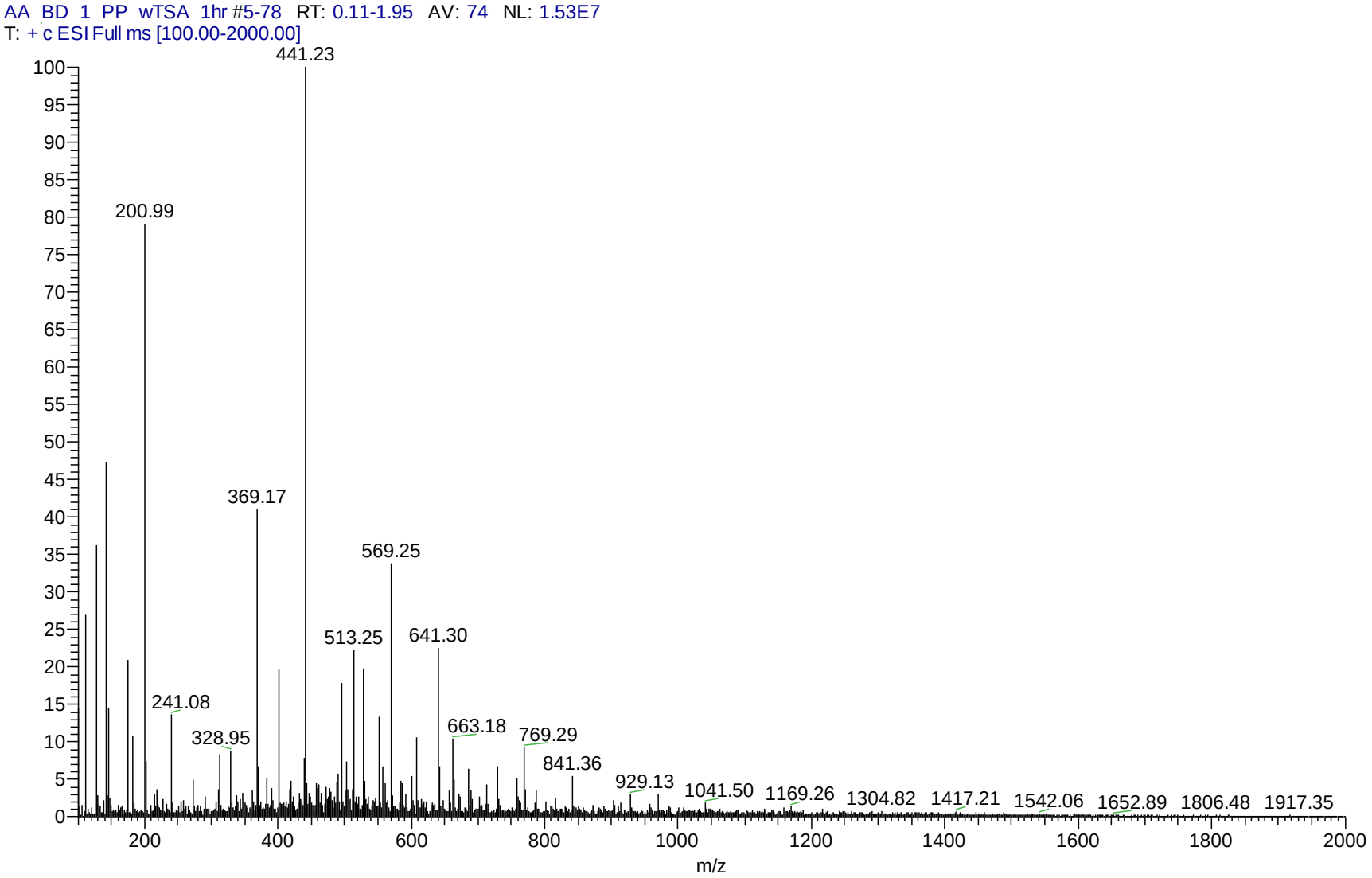

Figure 8.15 AA BD 1 1 hr PP w/ TSA ESI-MS positive ion mass spectrum

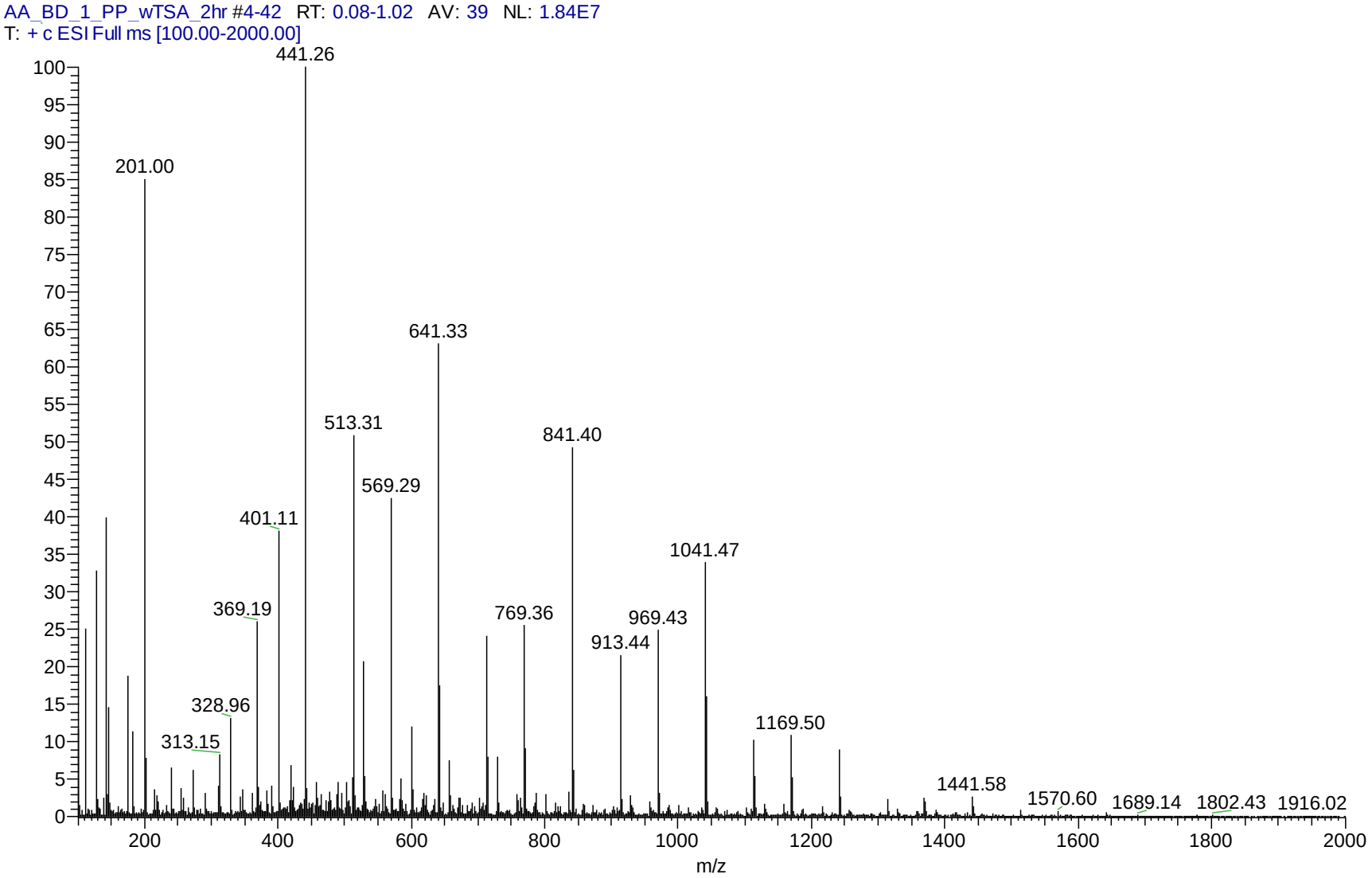

Figure 8.16 AA BD 1 2 hr PP w/ TSA ESI-MS positive ion mass spectrum

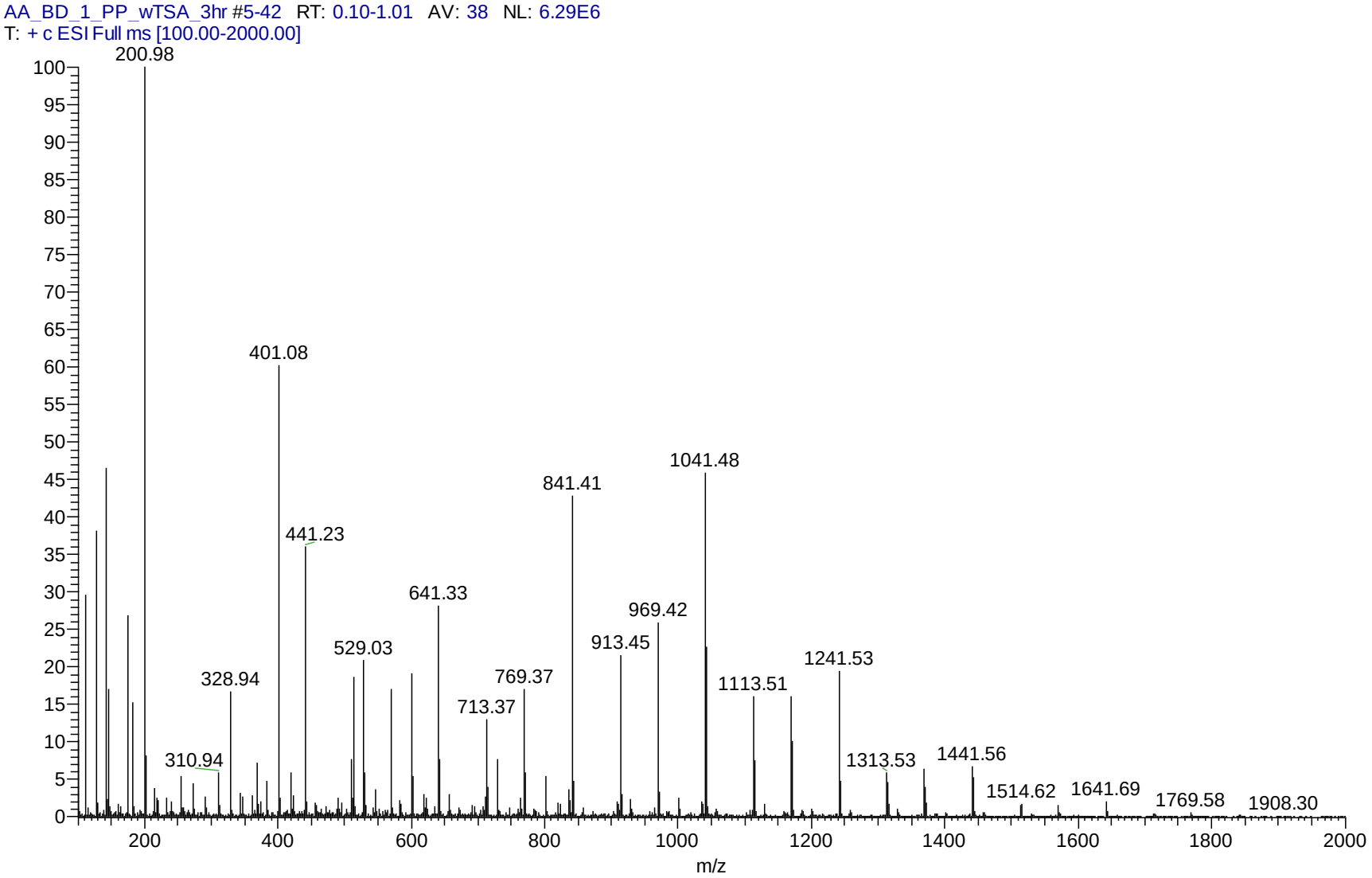

Figure 8.17 AA BD 1 3 hr PP w/ TSA ESI-MS positive ion mass spectrum

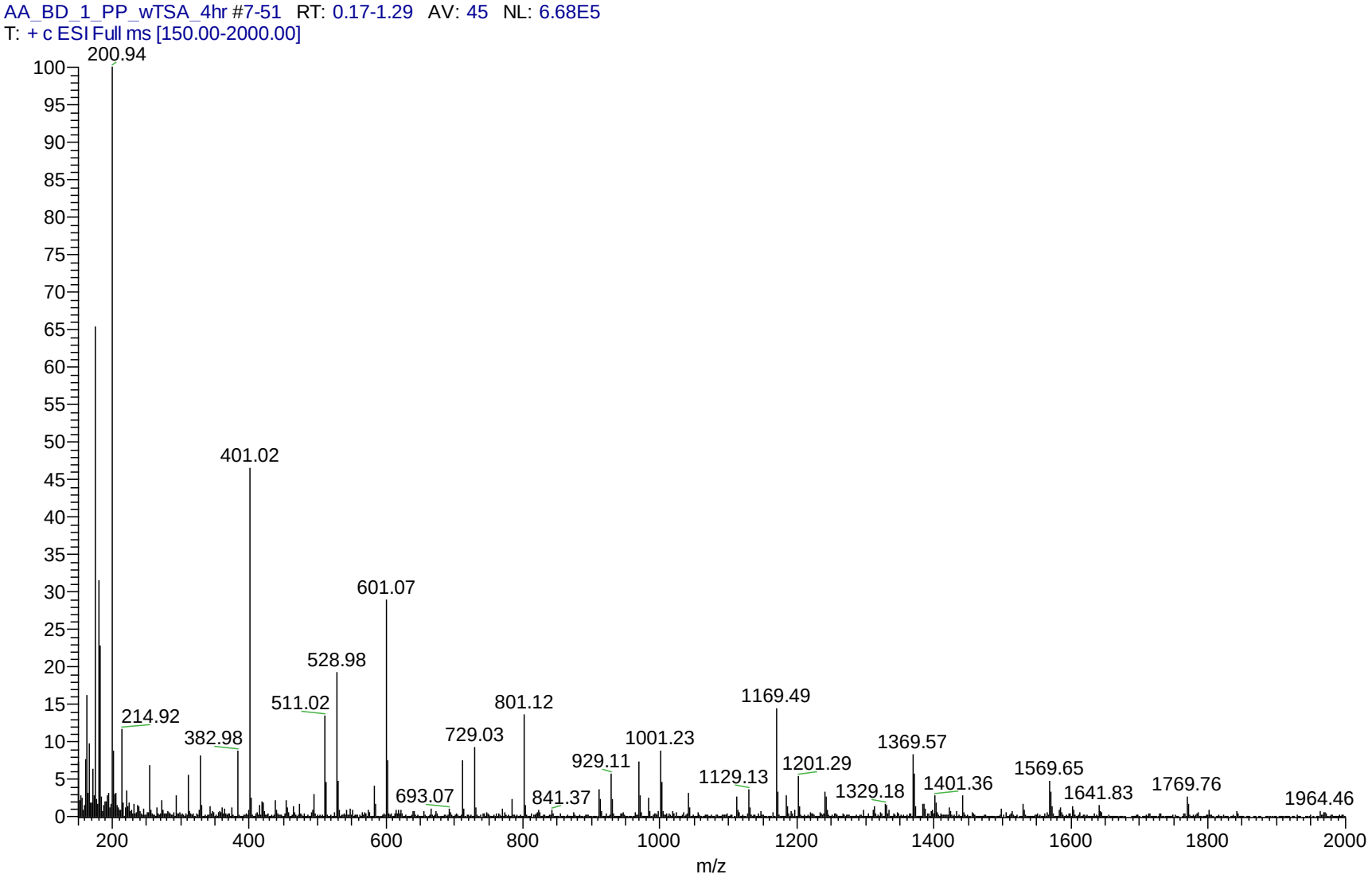

Figure 8.18 AA BD 1 4 hr PP w/ TSA ESI-MS positive ion mass spectrum

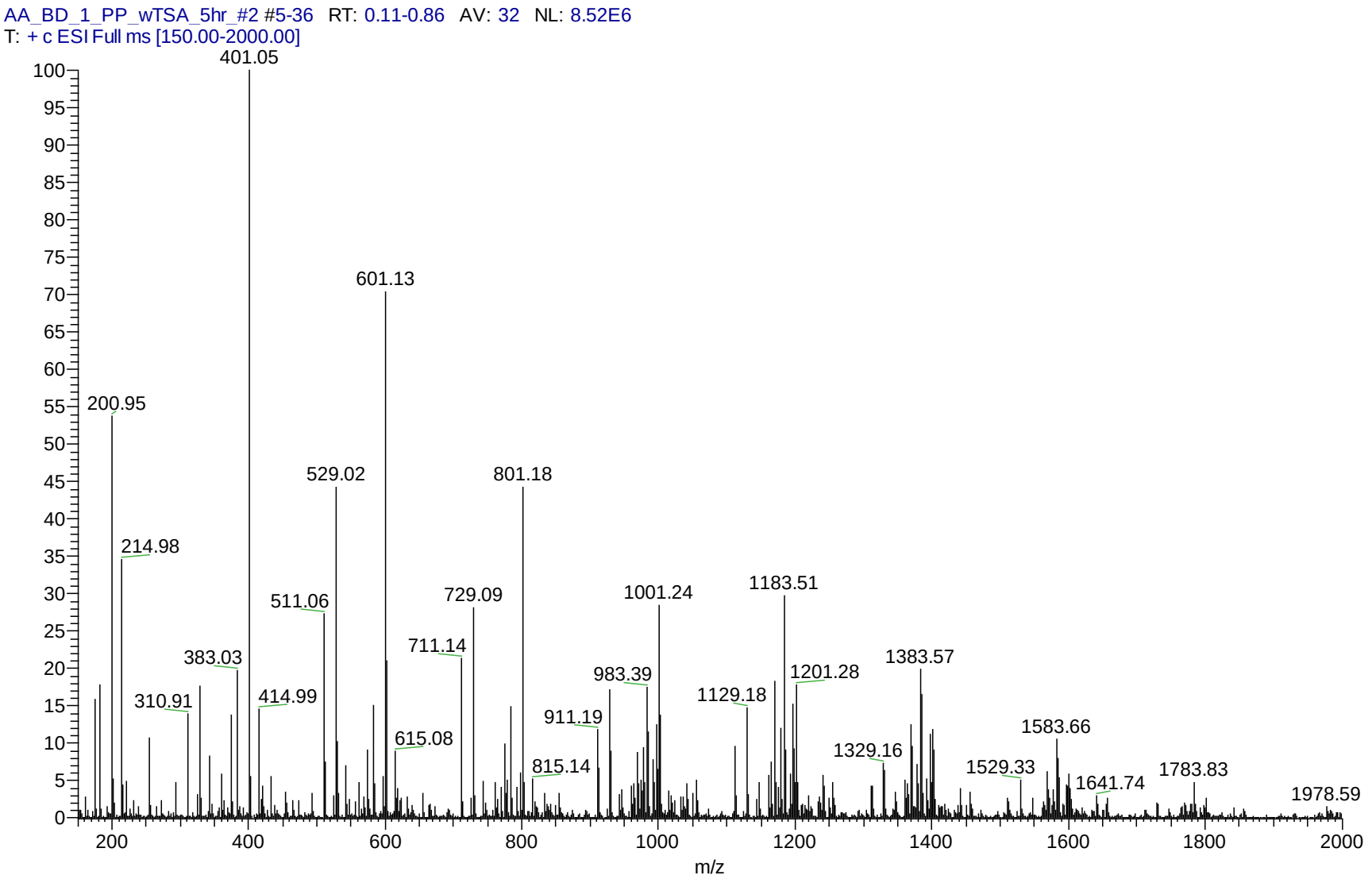

Figure 8.19 AA BD 1 5 hr PP w/ TSA ESI-MS positive ion mass spectrum

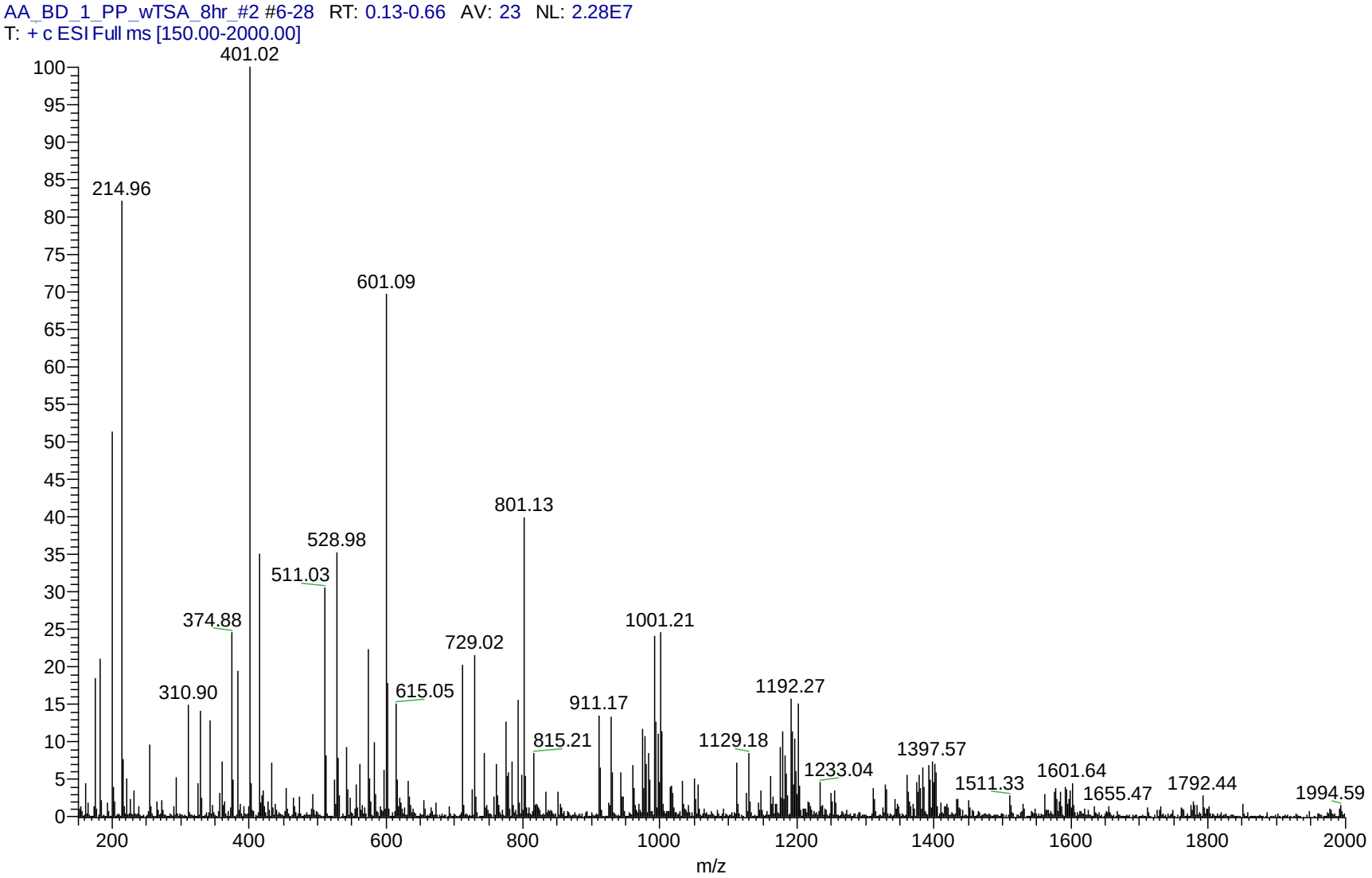

Figure 8.20 AA BD 1 8 hr PP w/ TSA ESI-MS positive ion mass spectrum

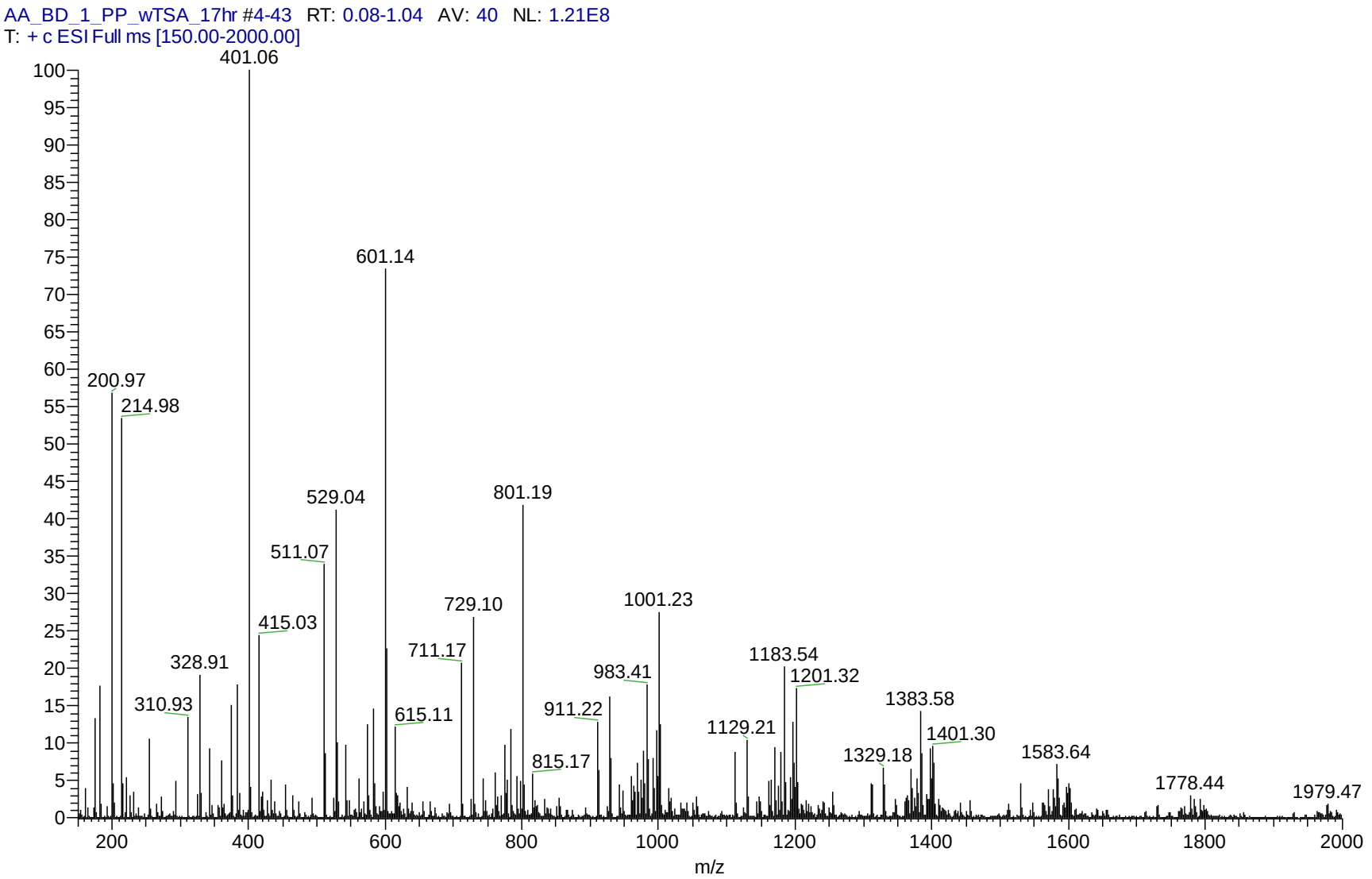

Figure 8.21 AA BD 1 17 hr PP w/ TSA ESI-MS positive ion mass spectrum

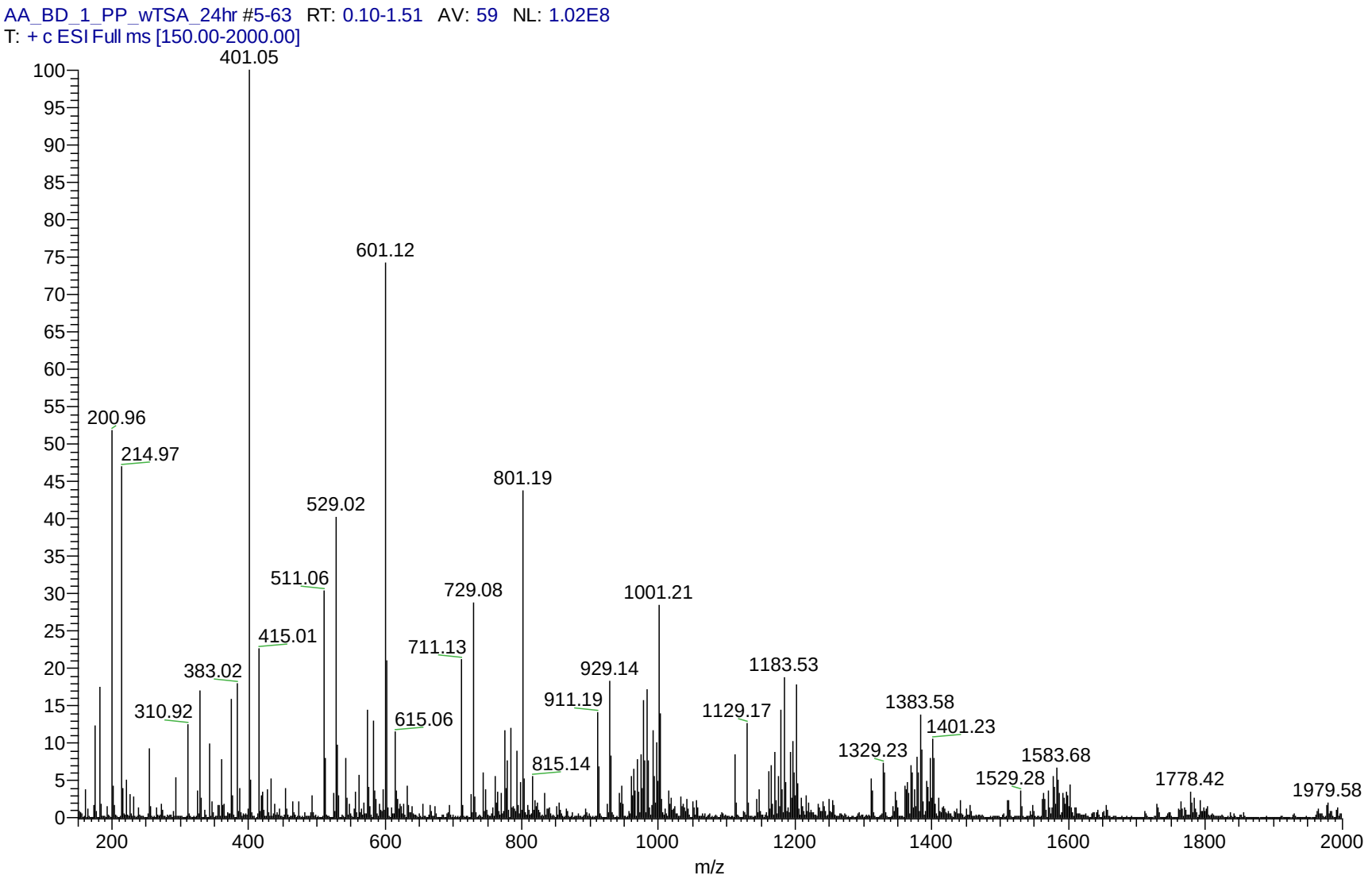

Figure 8.22 AA BD 1 24 hr PP w/ TSA ESI-MS positive ion mass spectrum

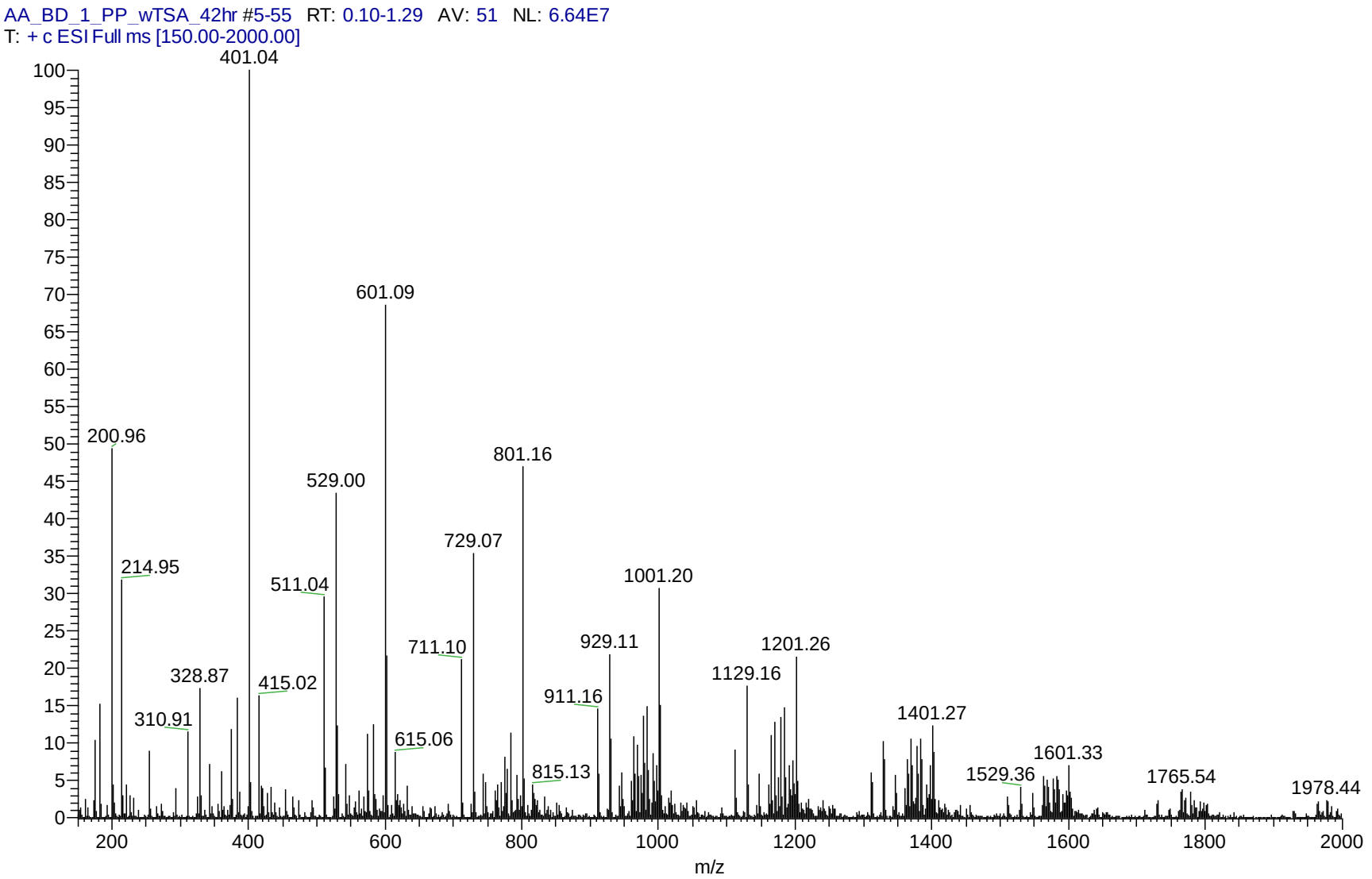

Figure 8.23 AA BD 1 42 hr PP w/ TSA ESI-MS positive ion mass spectrum

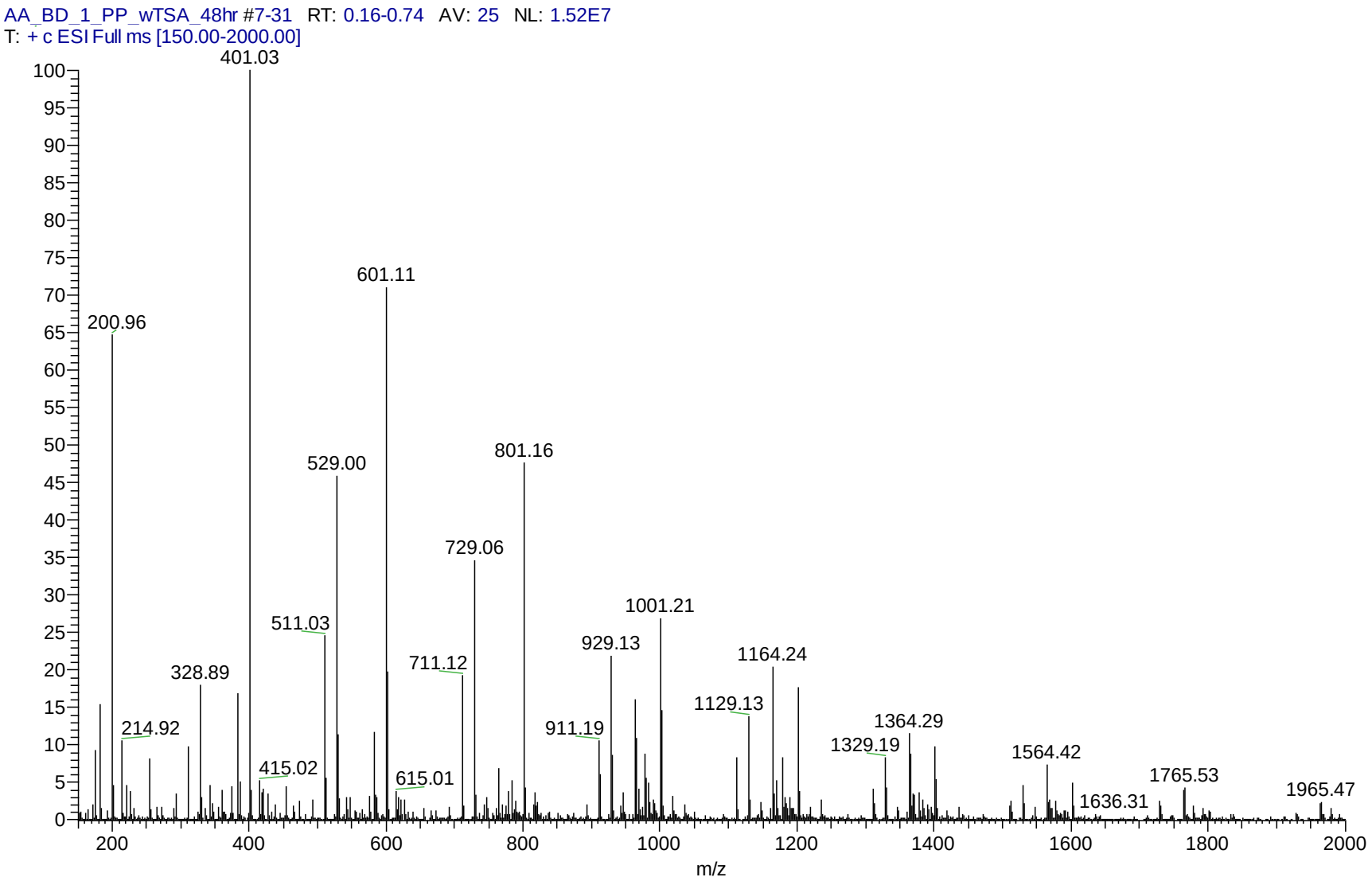

Figure 8.24 AA BD 1 48 hr PP w/ TSA ESI-MS positive ion mass spectrum

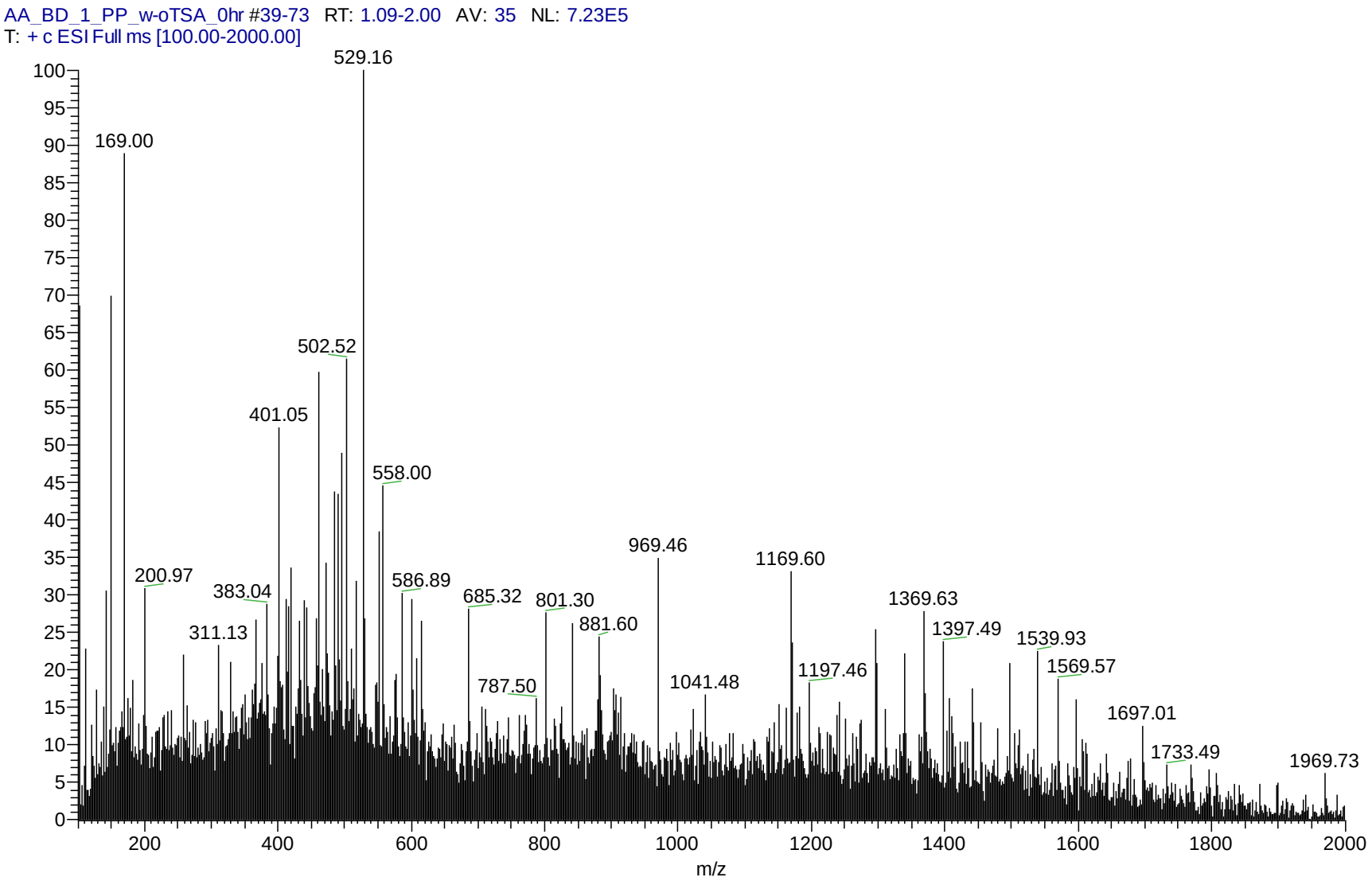

Figure 8.25 AA BD 1 0 hr PP w/o TSA ESI-MS positive ion mass spectrum

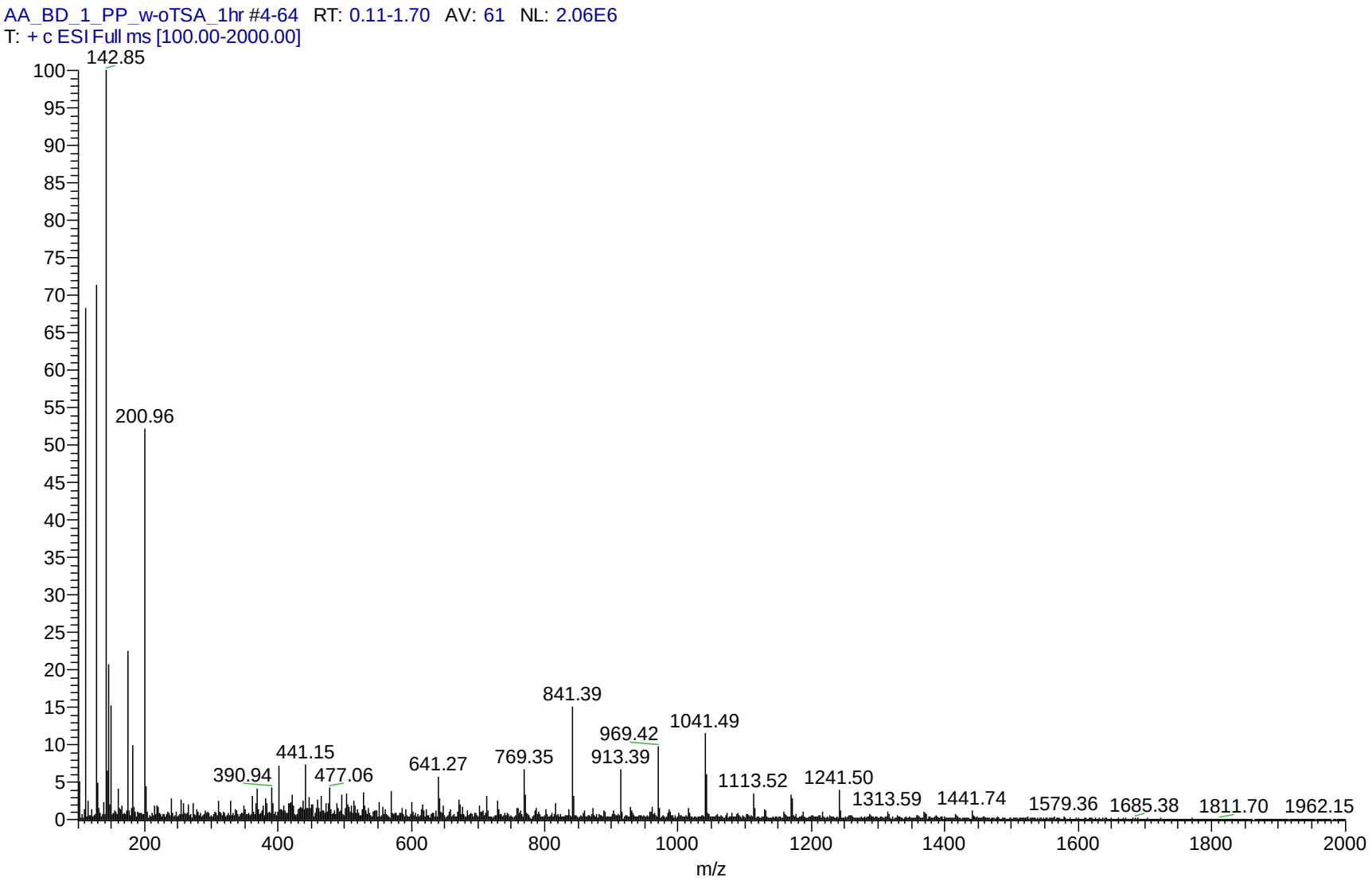

Figure 8.26 AA BD 1 1 hr PP w/o TSA ESI-MS positive ion mass spectrum

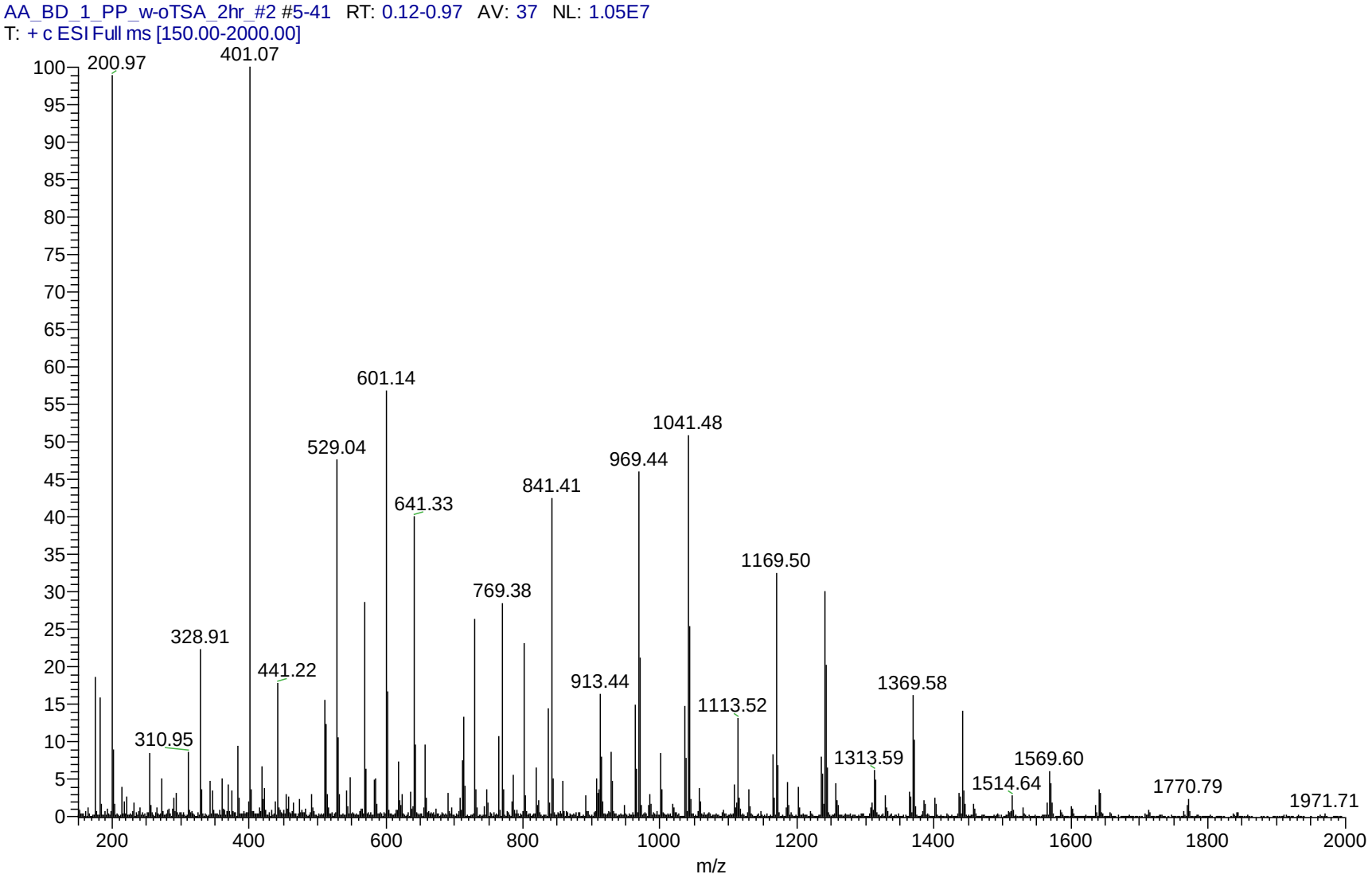

Figure 8.27 AA BD 1 2 hr PP w/o TSA ESI-MS positive ion mass spectrum

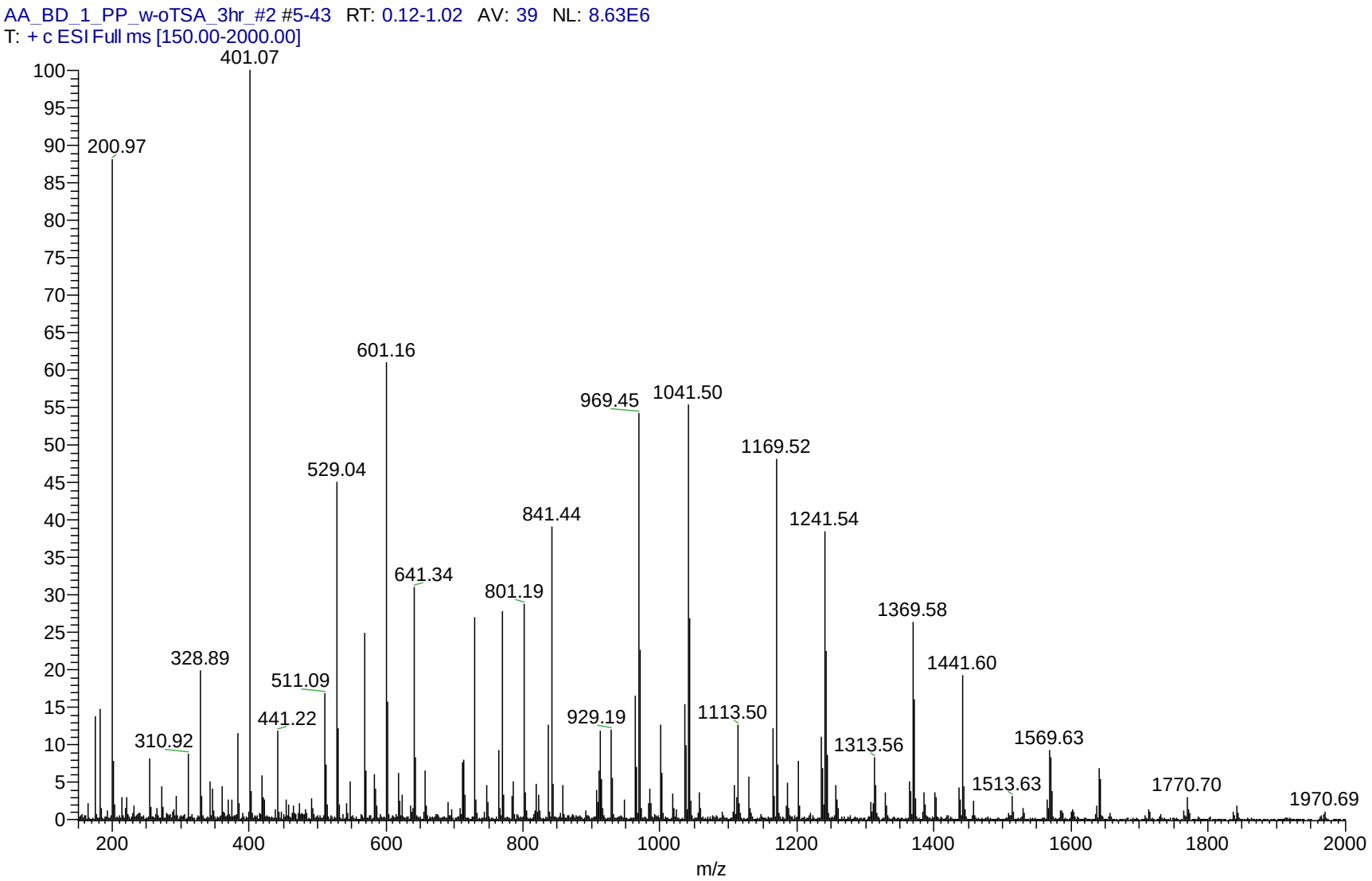

Figure 8.28 AA BD 1 3 hr PP w/o TSA ESI-MS positive ion mass spectrum

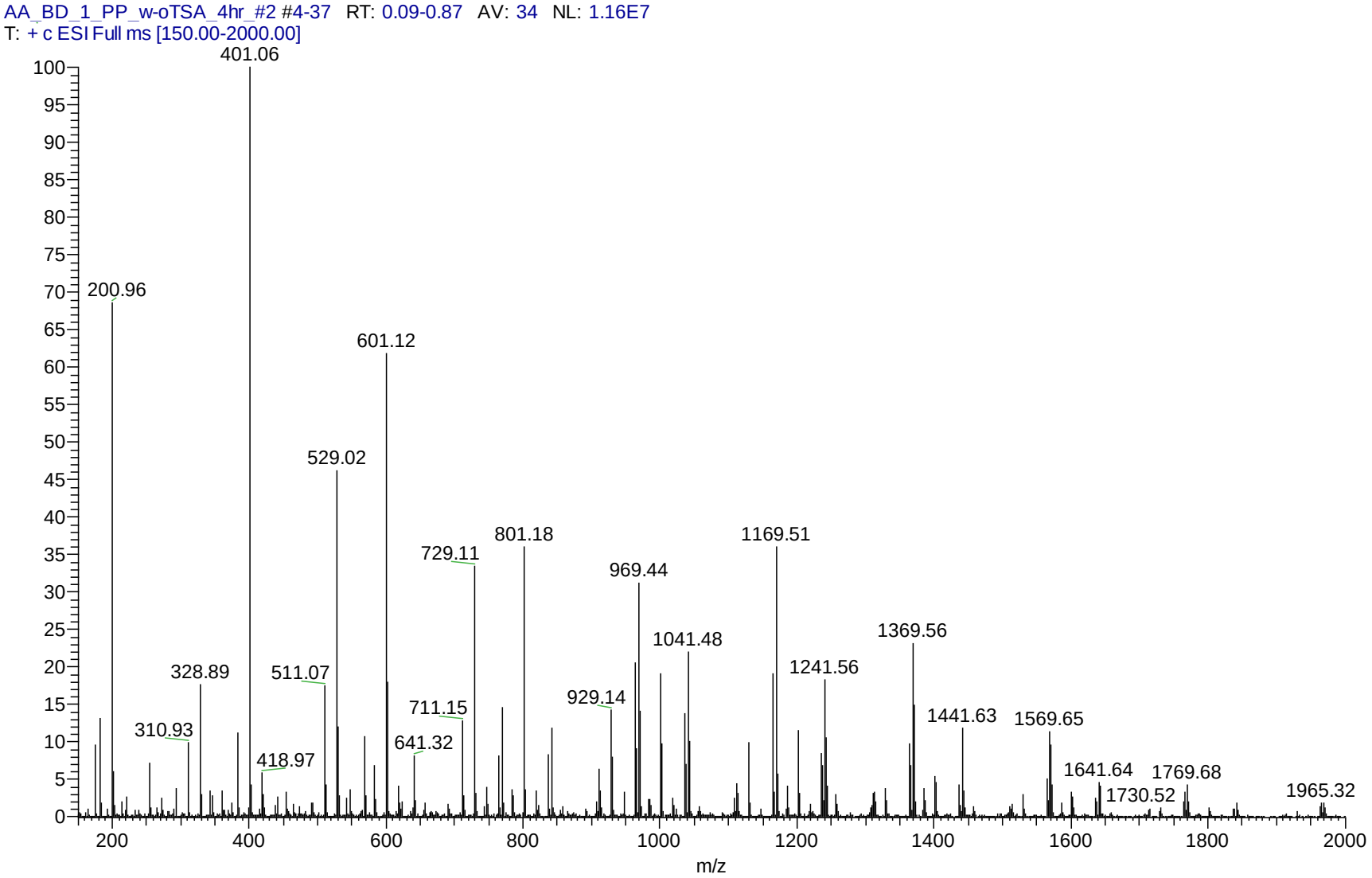

Figure 8.29 AA BD 1 4 hr PP w/o TSA ESI-MS positive ion mass spectrum

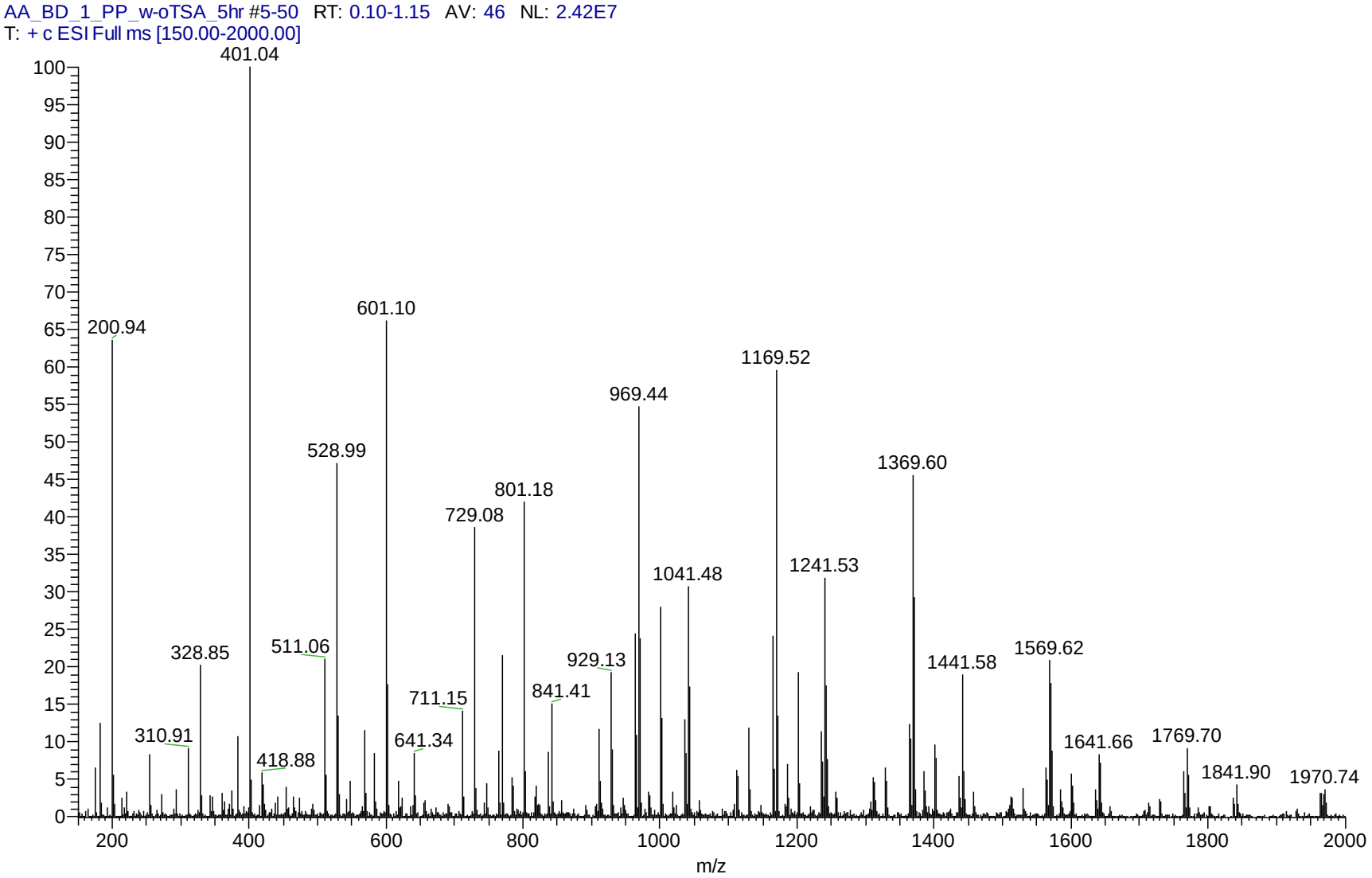

Figure 8.30 AA BD 1 5 hr PP w/o TSA ESI-MS positive ion mass spectrum

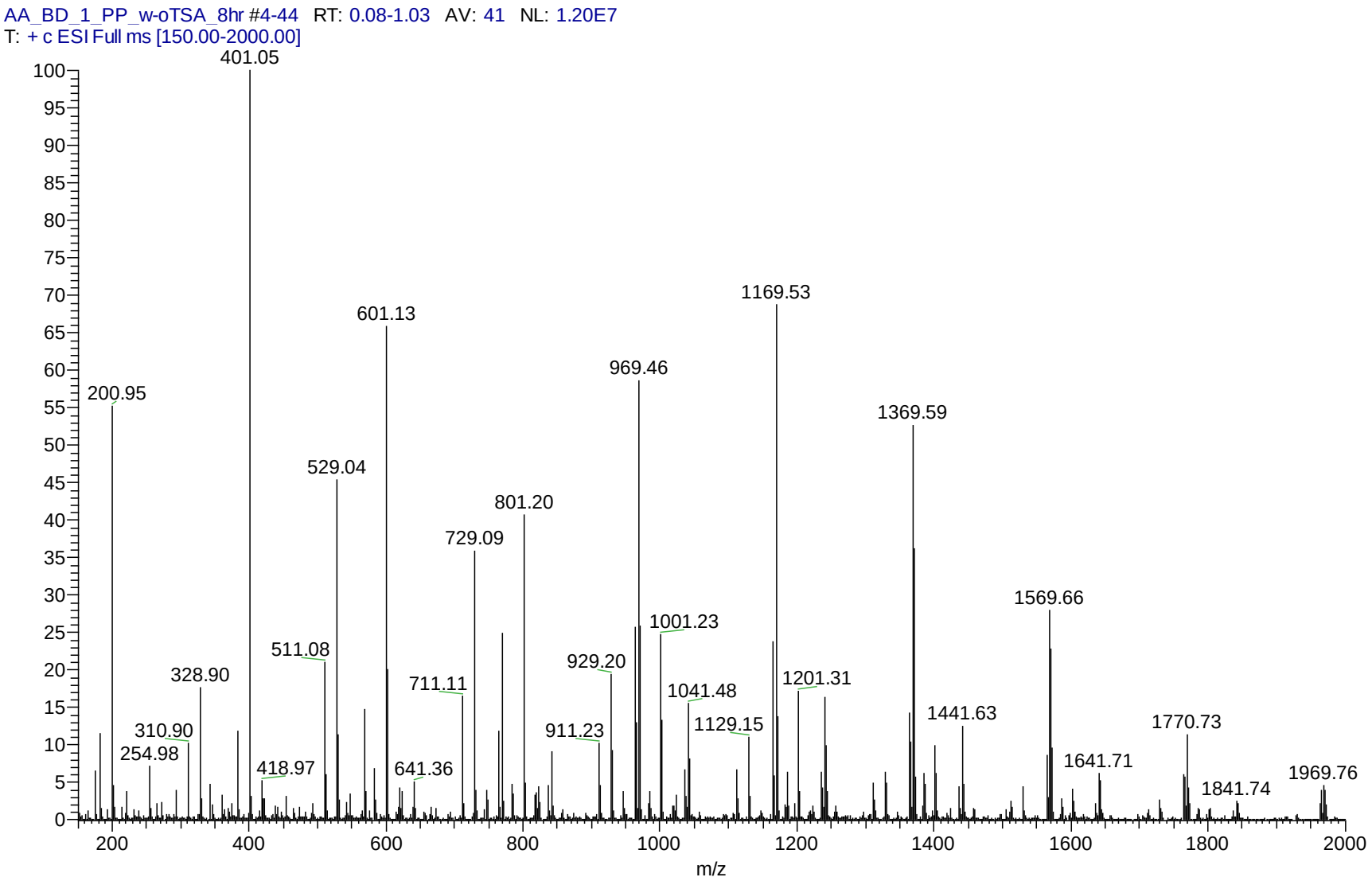

Figure 8.31 AA BD 1 8 hr PP w/o TSA ESI-MS positive ion mass spectrum

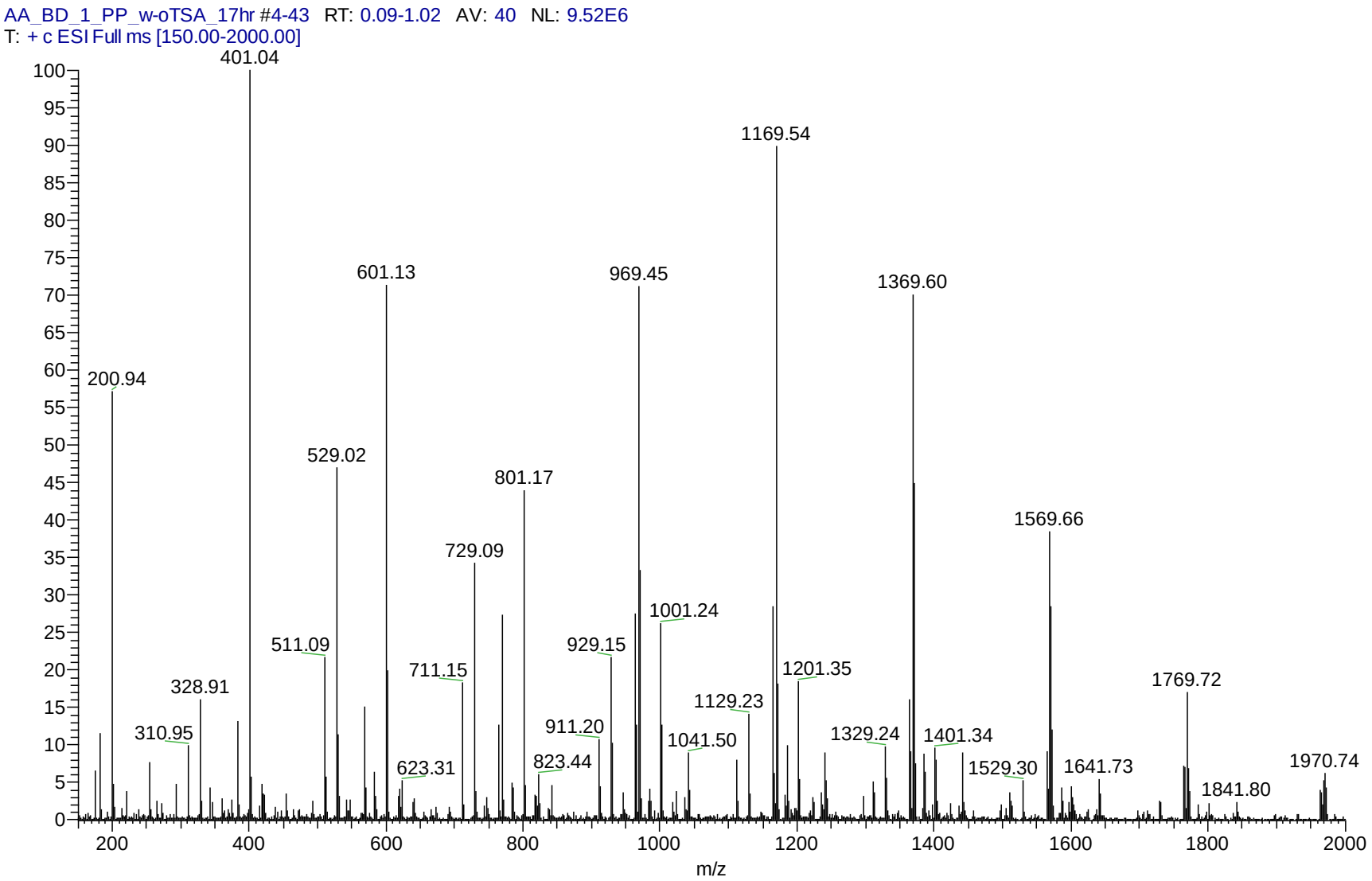

Figure 8.32 AA BD 1 17 hr PP w/o TSA ESI-MS positive ion mass spectrum

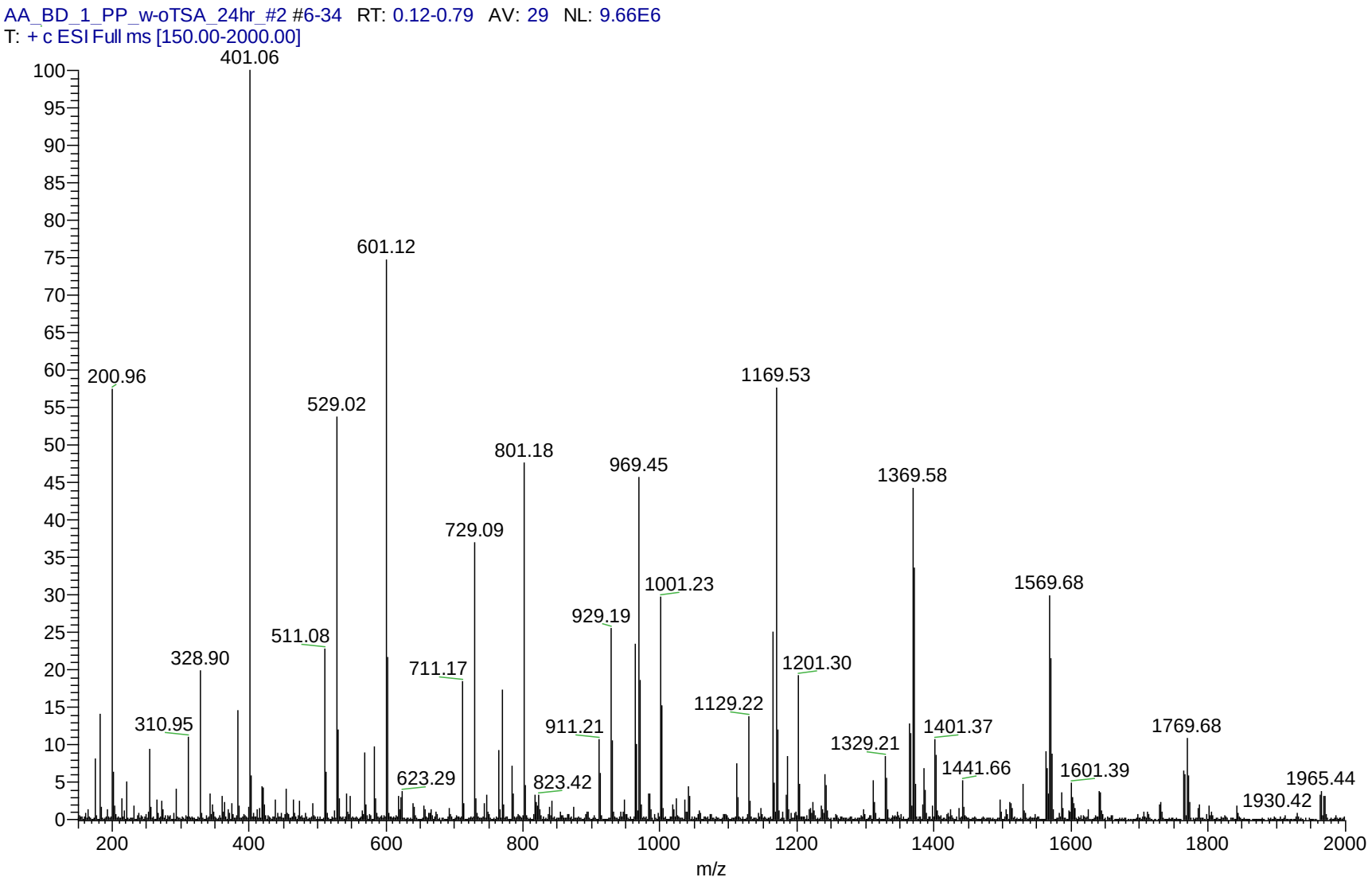

Figure 8.33 AA BD 1 24 hr PP w/o TSA ESI-MS positive ion mass spectrum

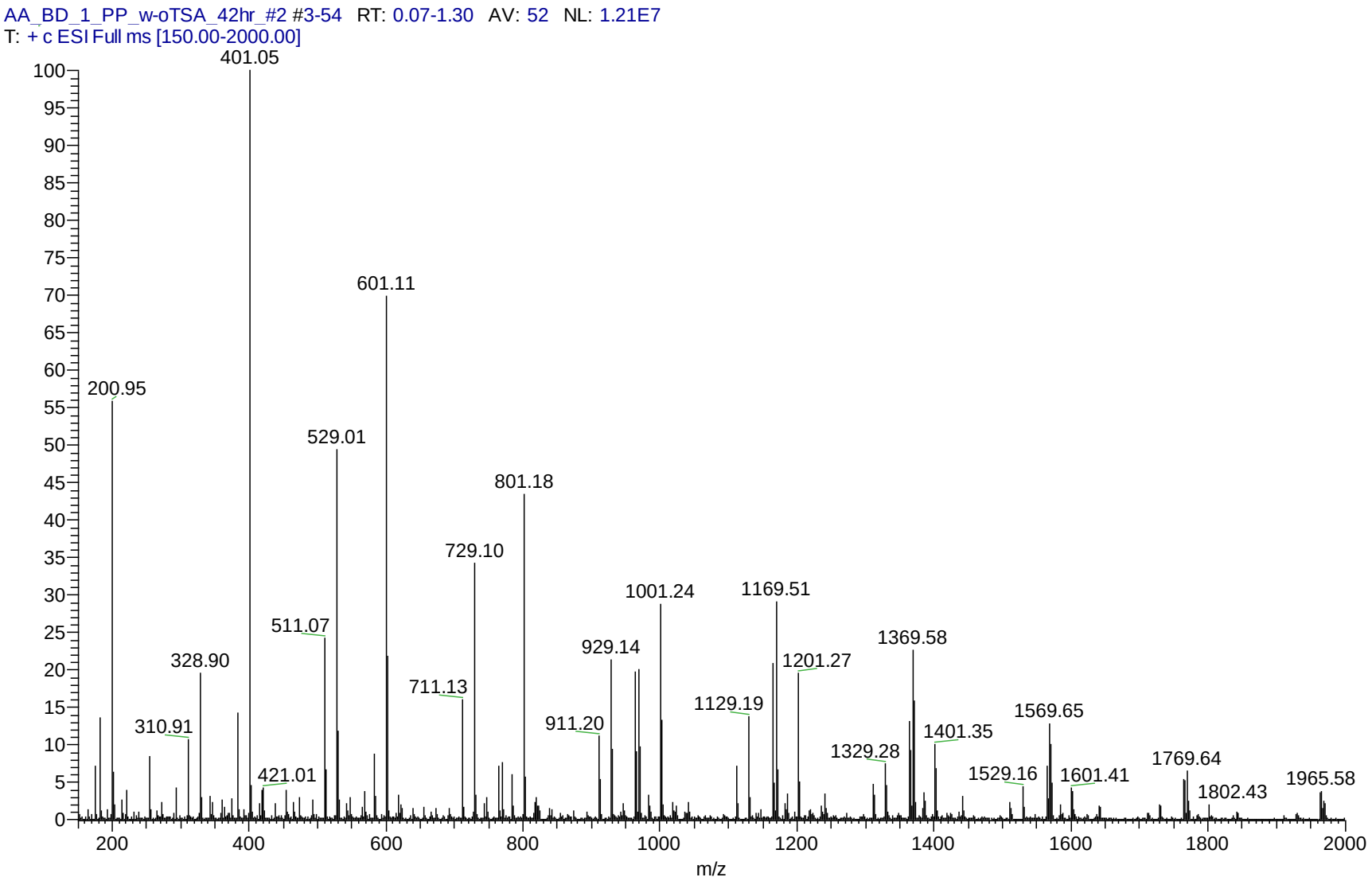

Figure 8.34 AA BD 1 42 hr PP w/o TSA ESI-MS positive ion mass spectrum

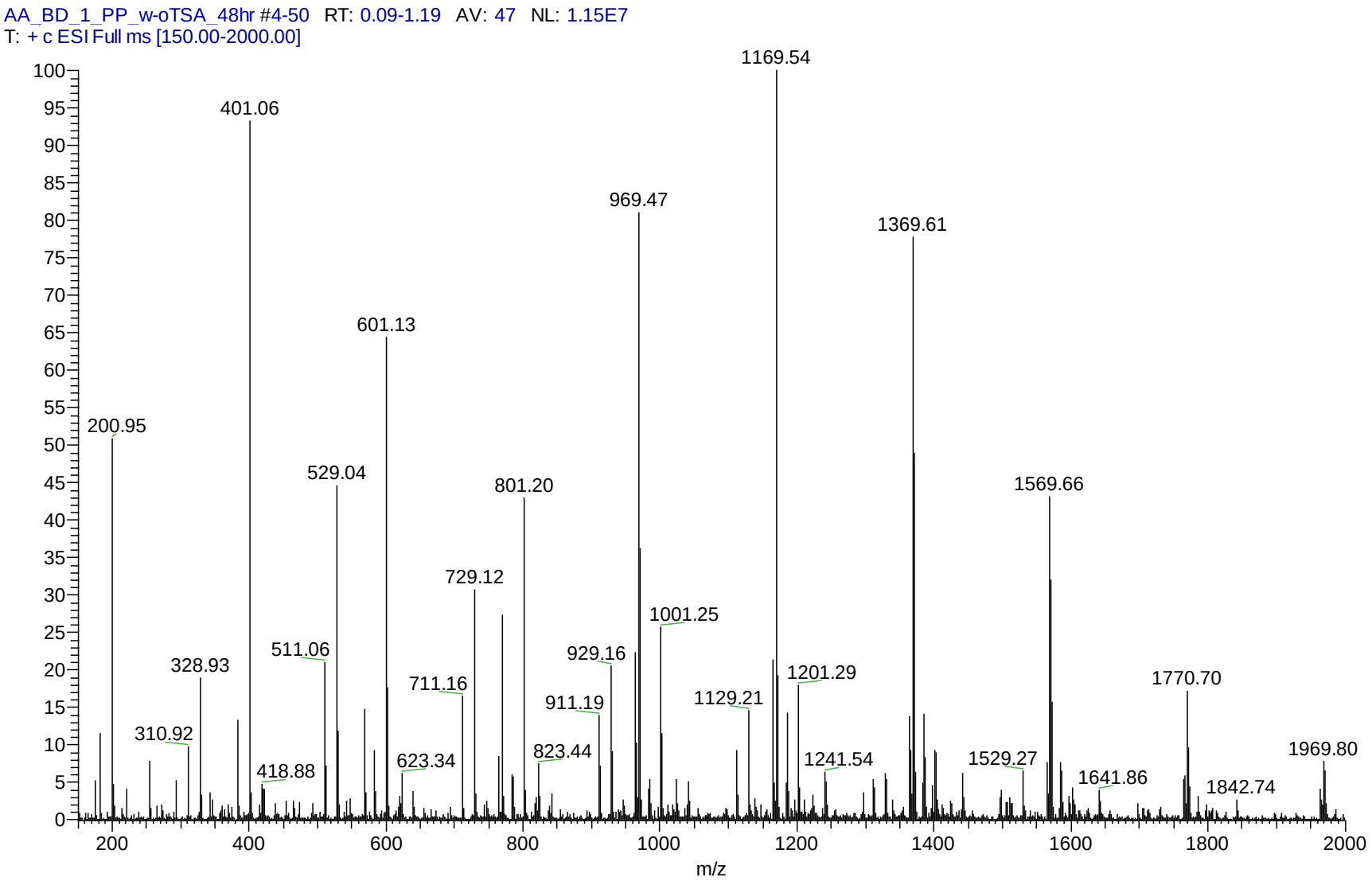

Figure 8.35 AA BD 1 48 hr PP w/o TSA ESI-MS positive ion mass spectrum

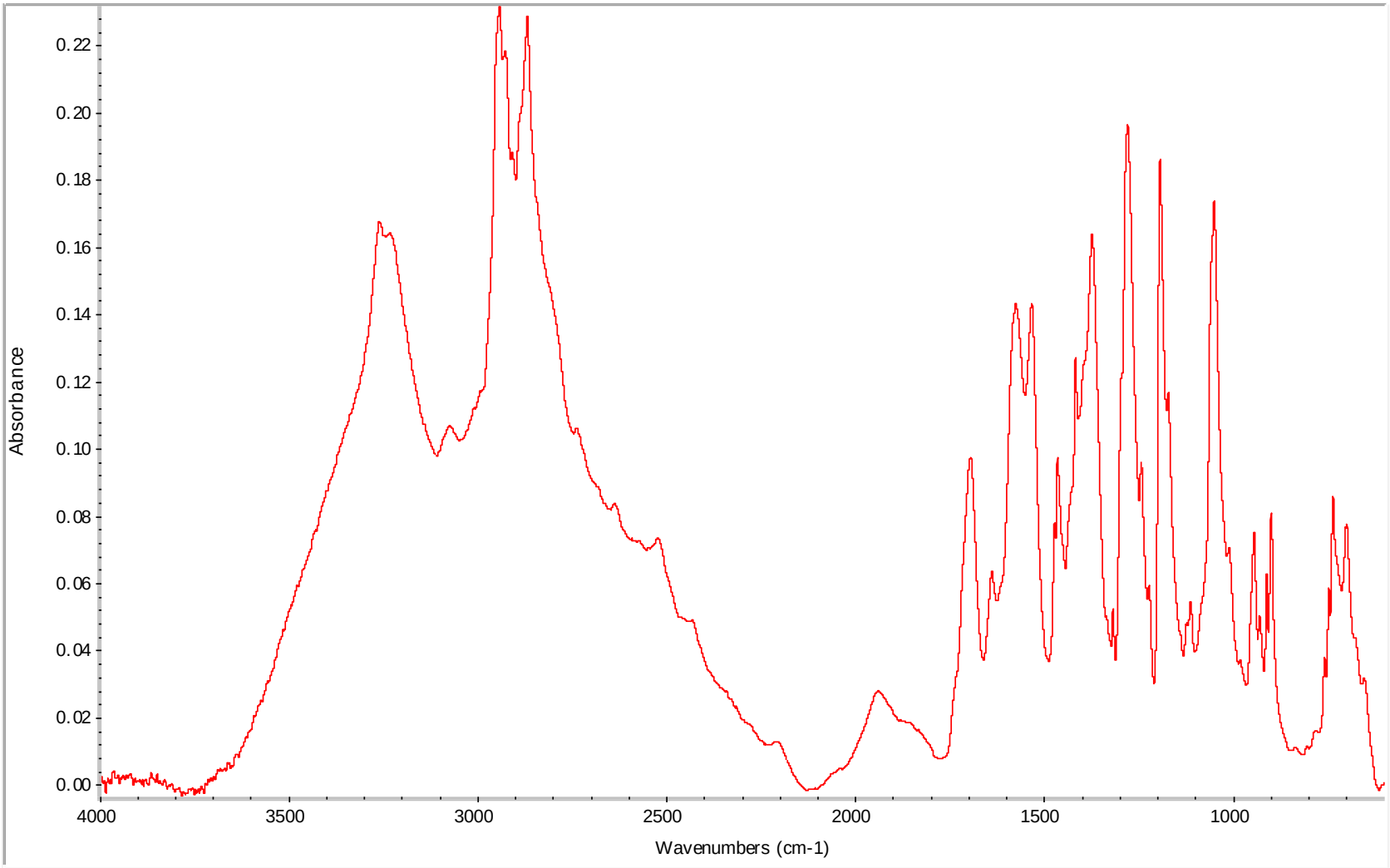

Figure 8.36 AA BD 0.8 0 hr PP FT-IR spectrum

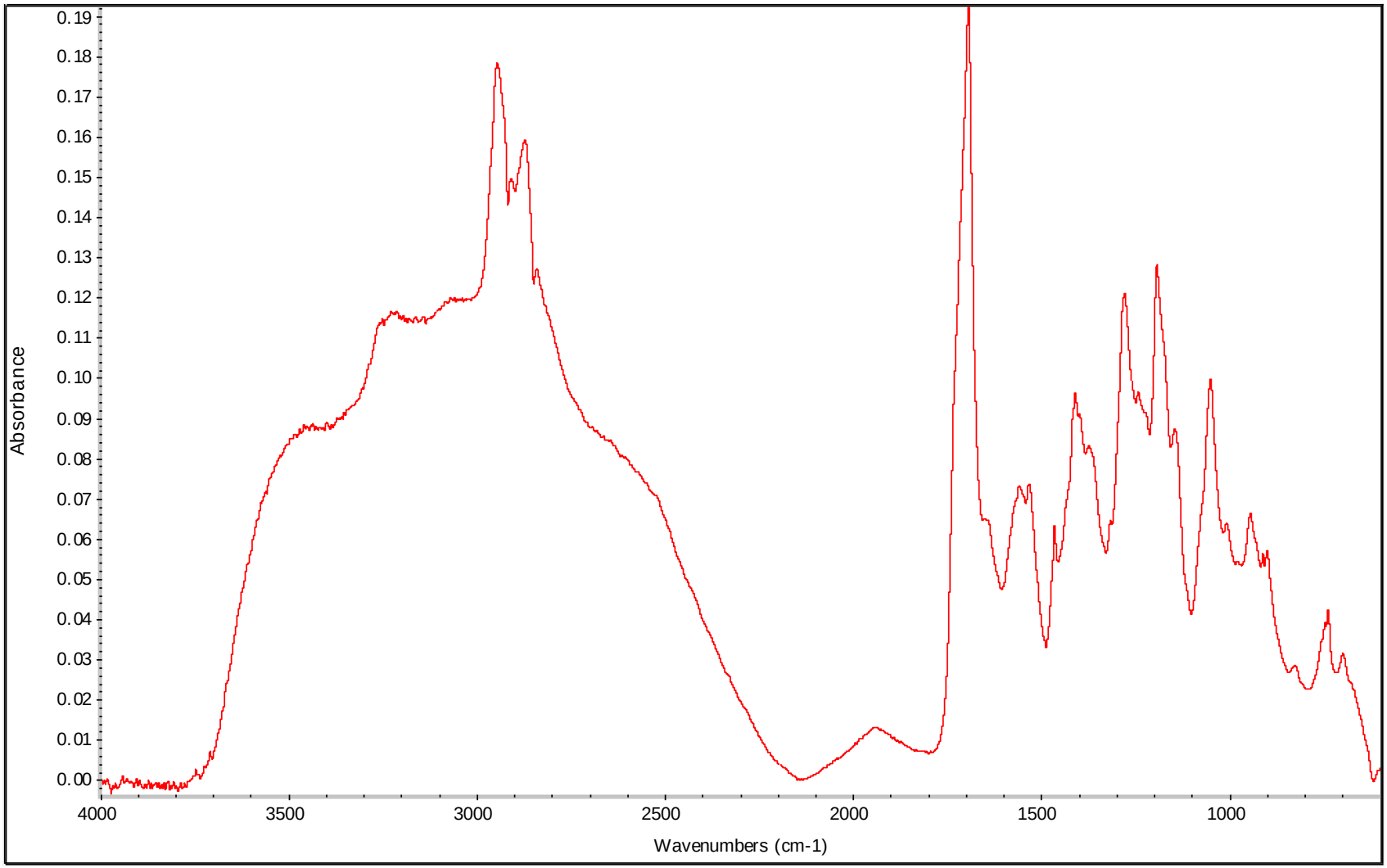

Figure 8.37 AA BD 0.8 1 hr PP FT-IR spectrum

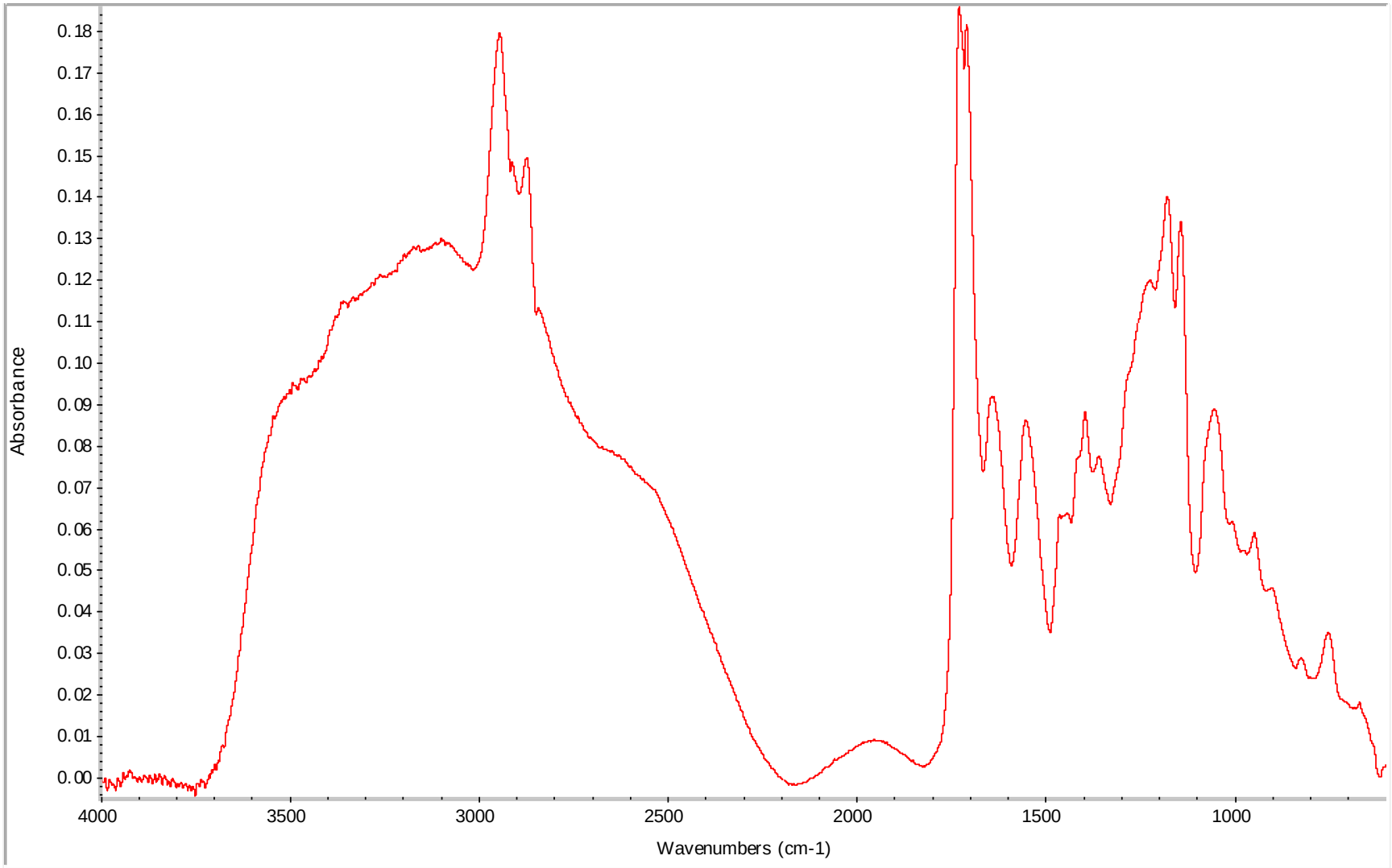

Figure 8.38 AA BD 0.8 2 hr PP FT-IR spectrum

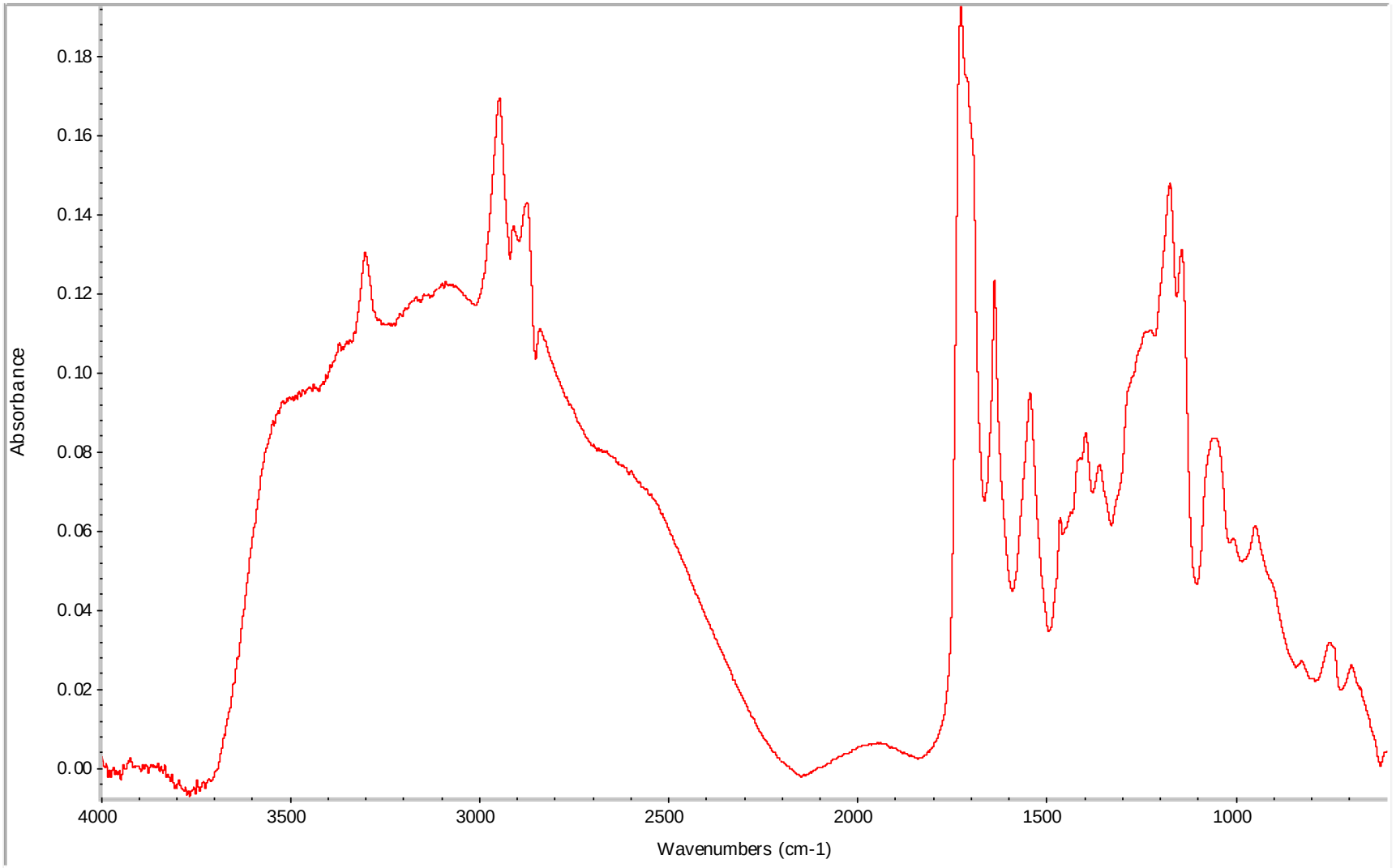

Figure 8.39 AA BD 0.8 3 hr PP FT-IR spectrum

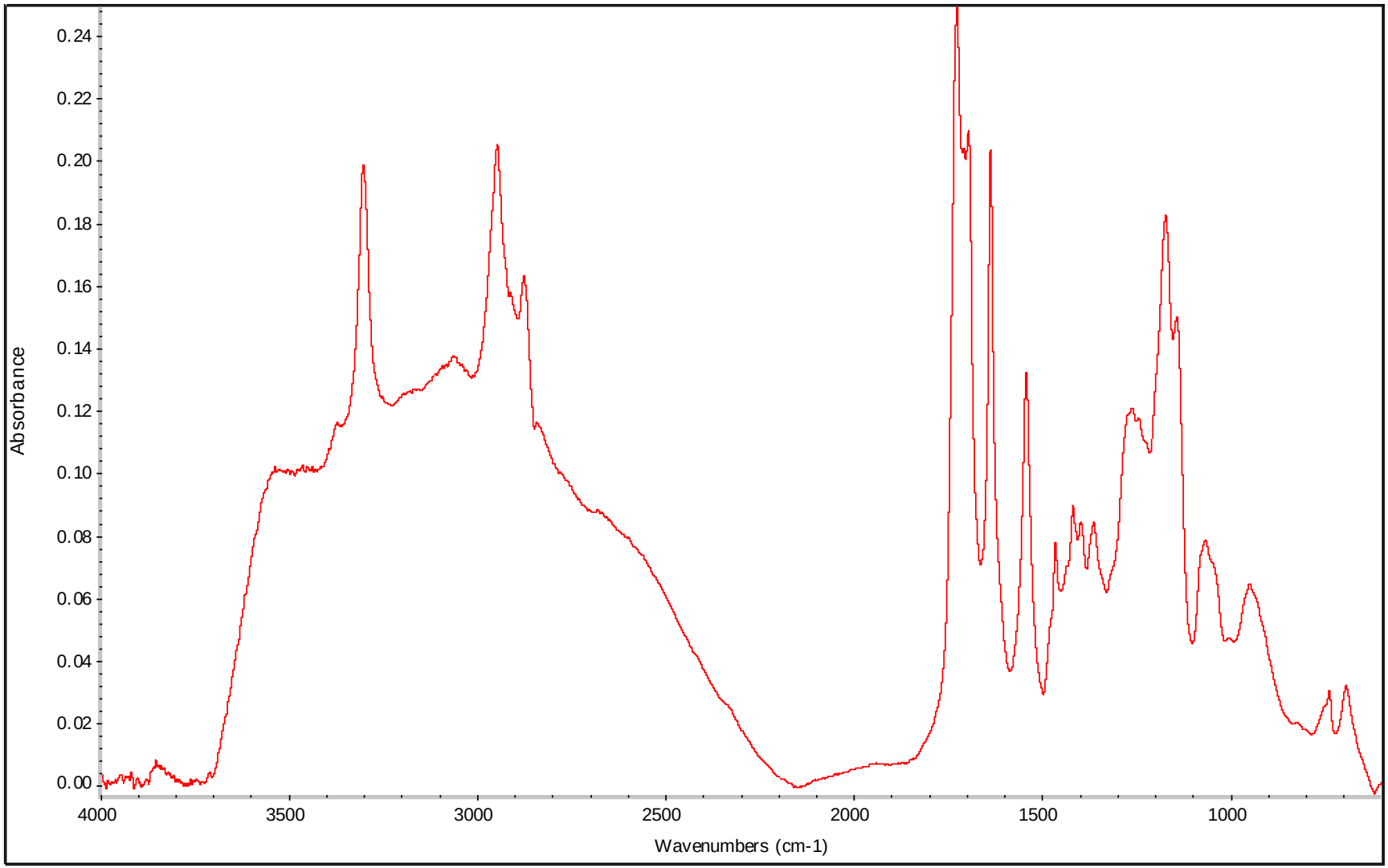

Figure 8.40 AA BD 0.8 8 hr PP FT-IR spectrum

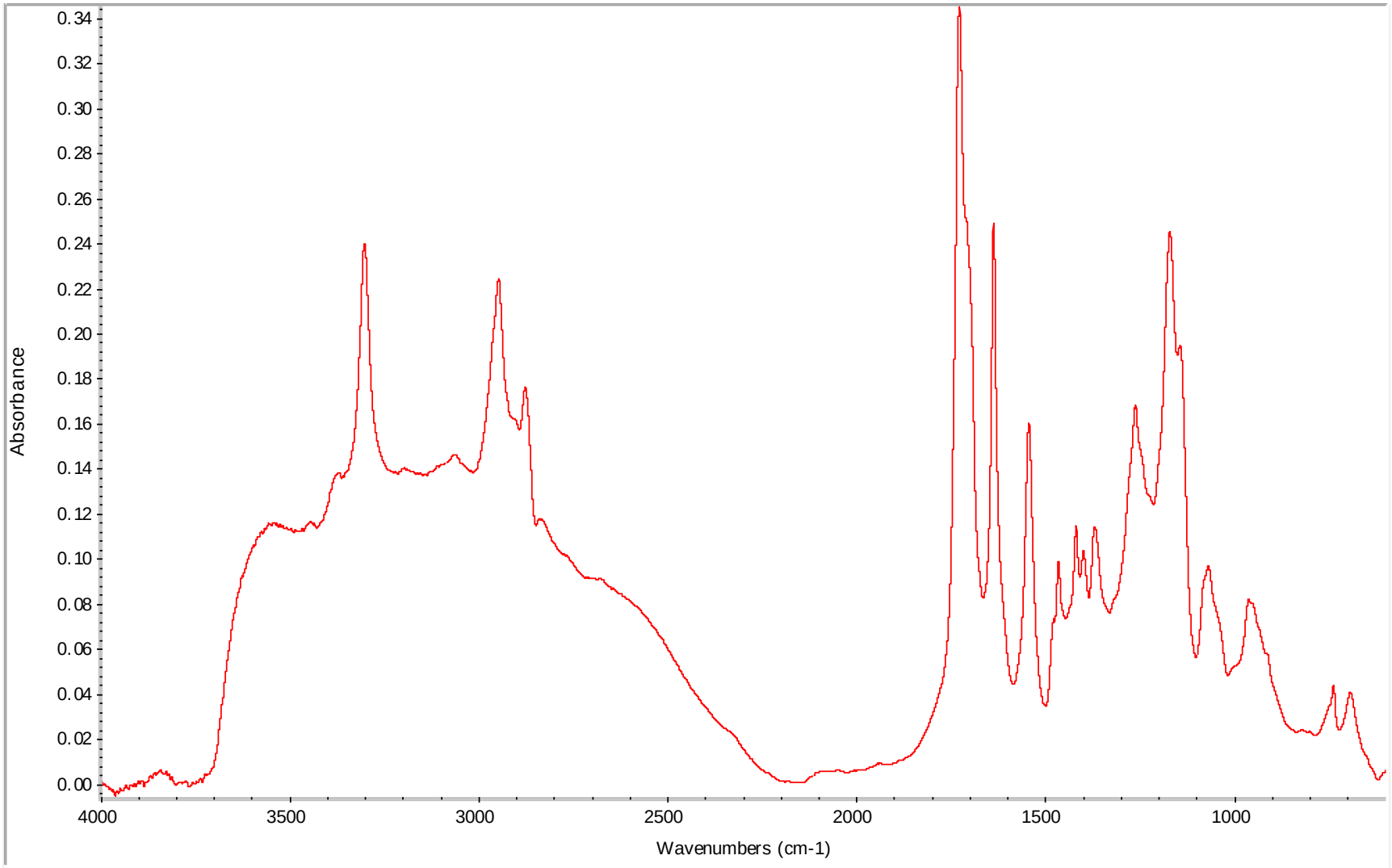

Figure 8.41 AA BD 0.8 26.5 hr PP FT-IR spectrum

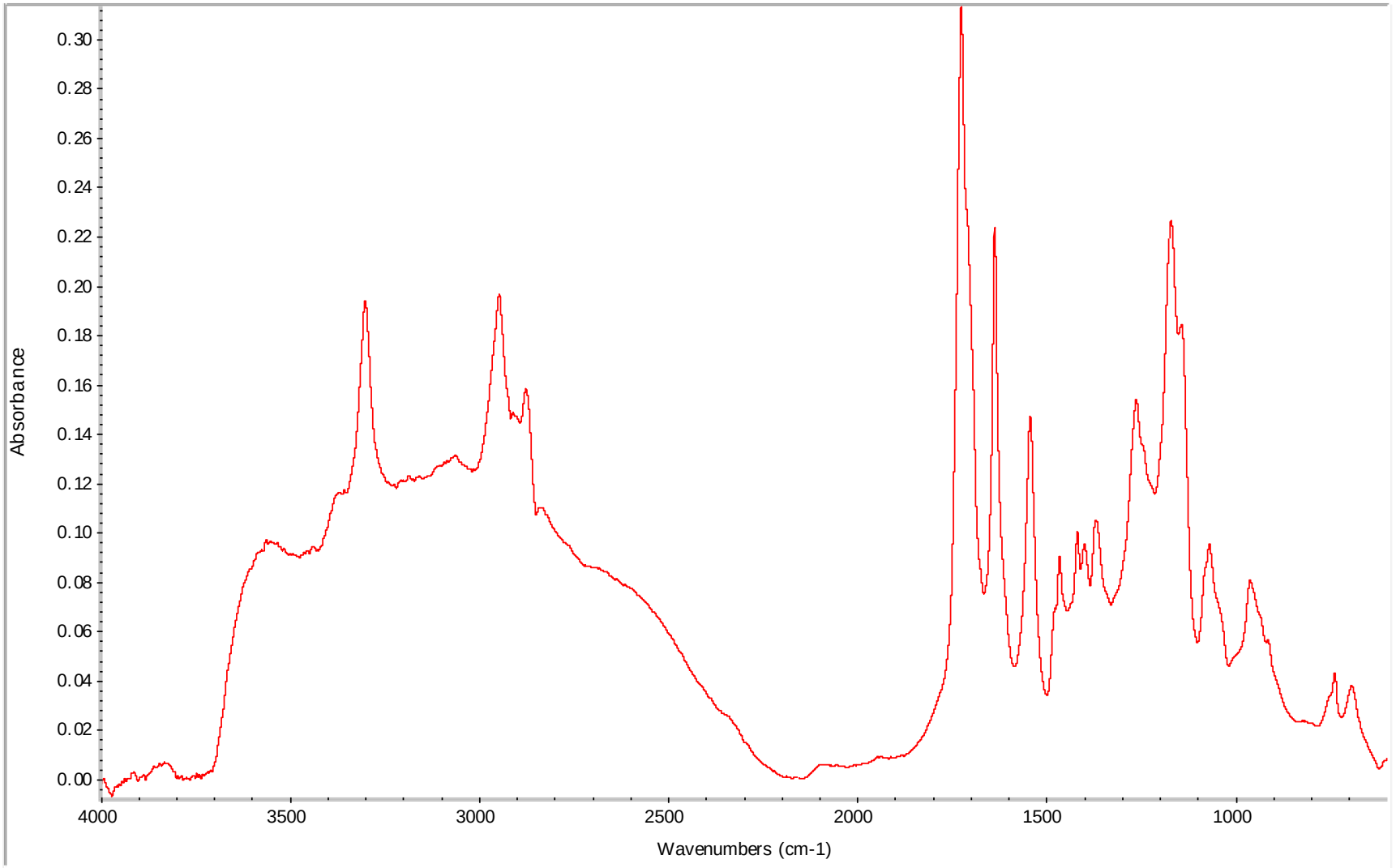

Figure 8.42 AA BD 0.8 38 hr PP FT-IR spectrum

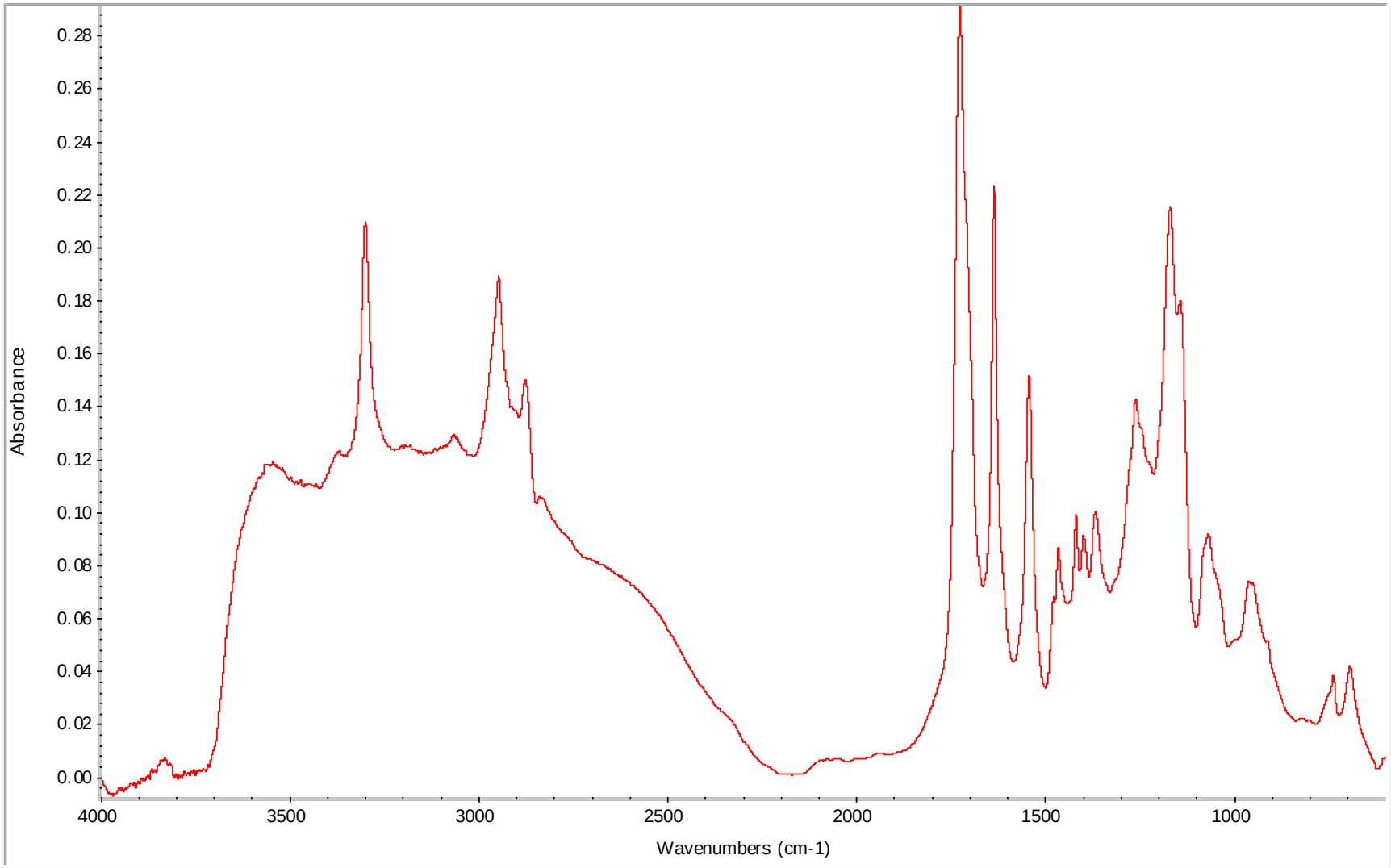

Figure 8.43 AA BD 0.8 48 hr PP FT-IR spectrum

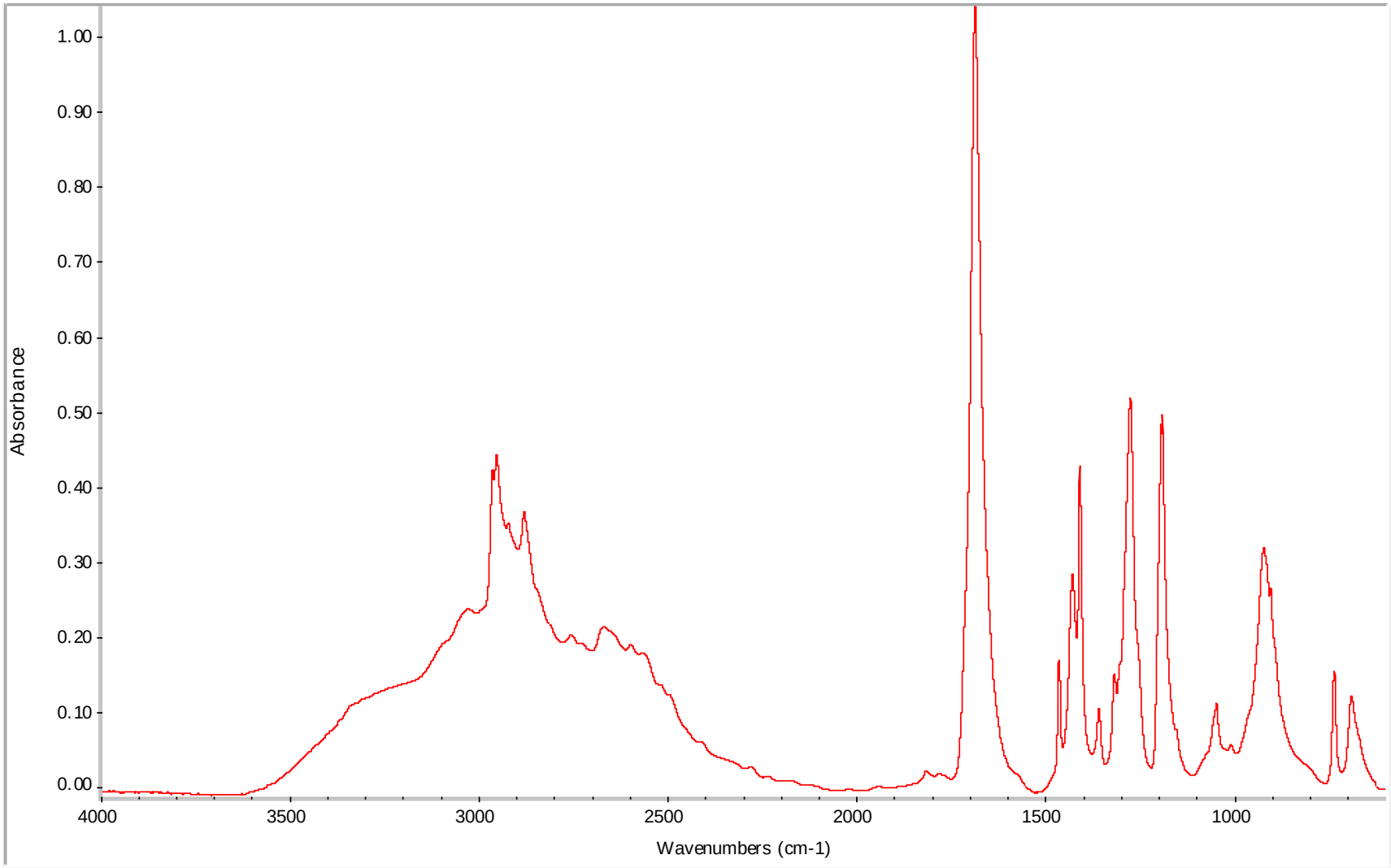

Figure 8.44 AA BD 1 0 hr PP w/o TSA catalyst FT-IR spectrum

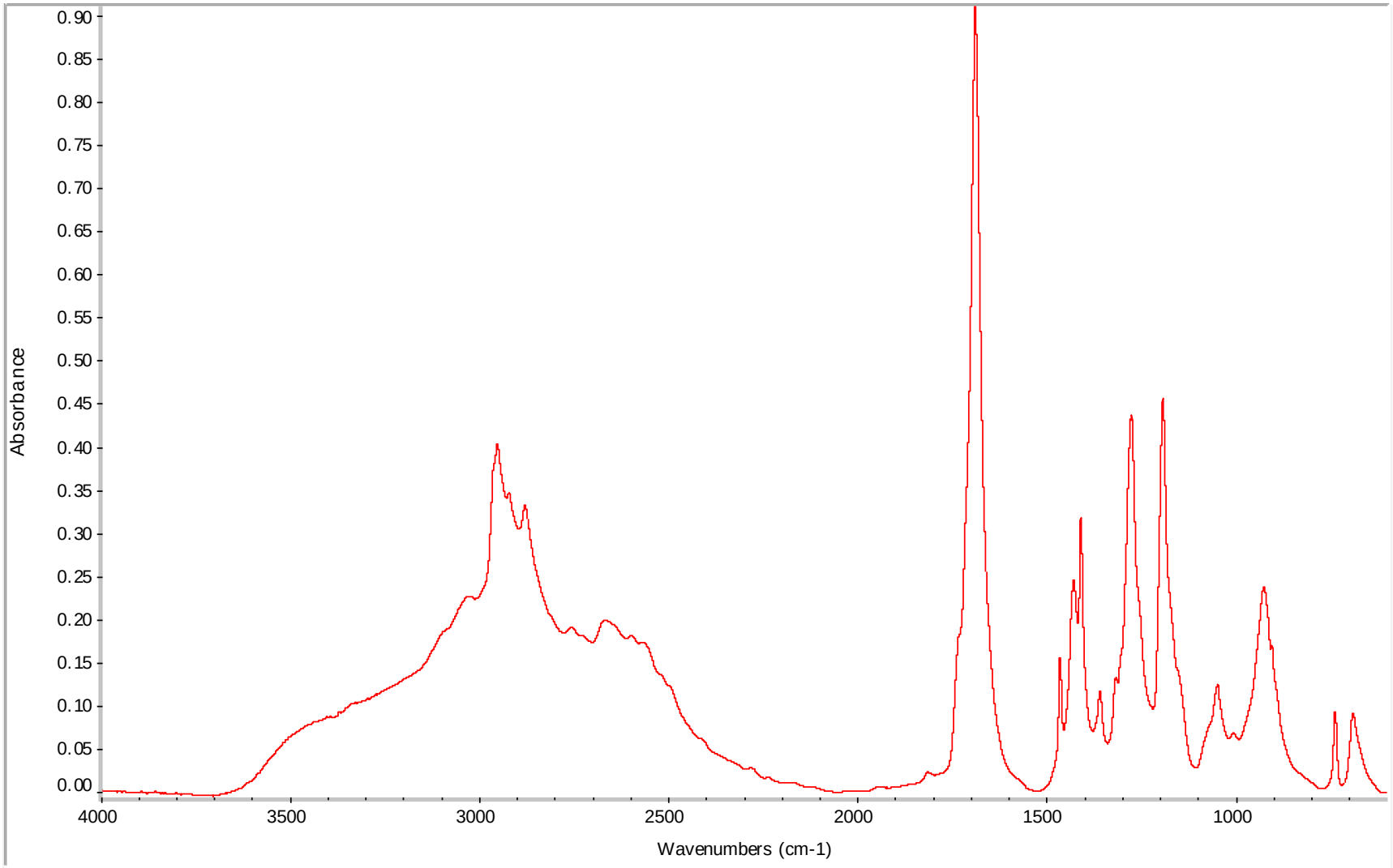

Figure 8.45 AA BD 1 1 hr PP w/o TSA catalyst FT-IR spectrum

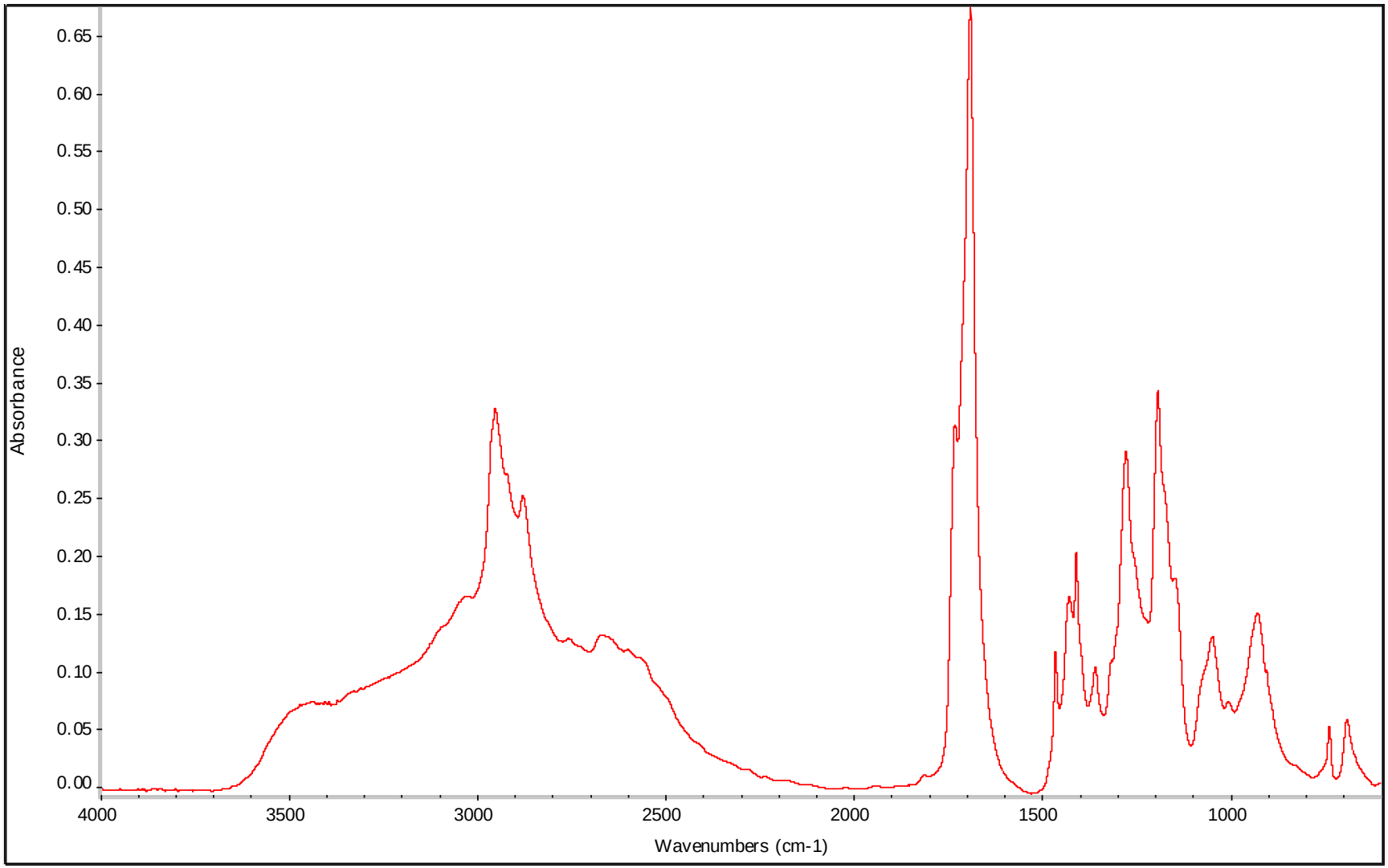

Figure 8.46 AA BD 1 2 hr PP w/o TSA catalyst FT-IR spectrum

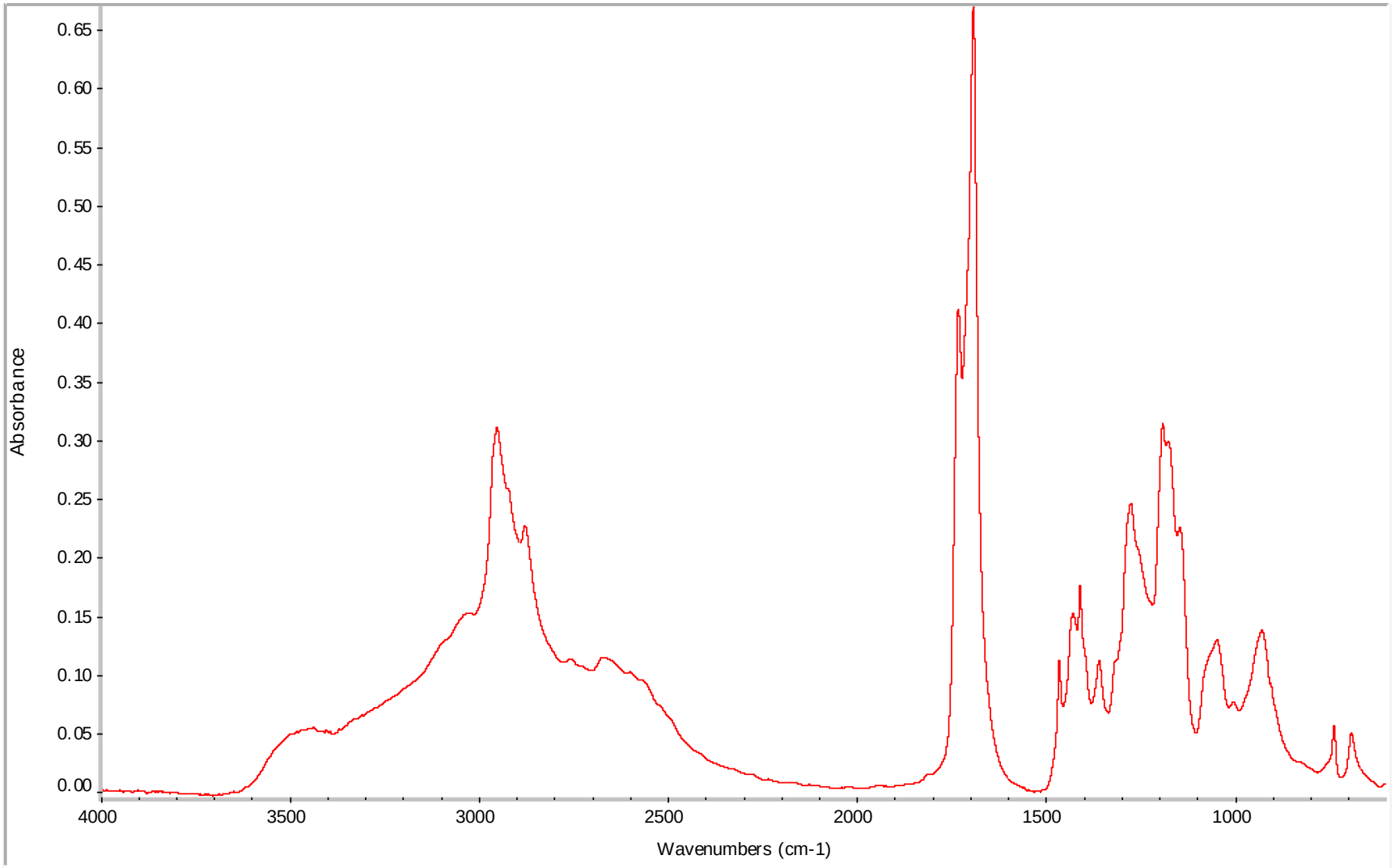

Figure 8.47 AA BD 1 3 hr PP w/o TSA catalyst FT-IR spectrum

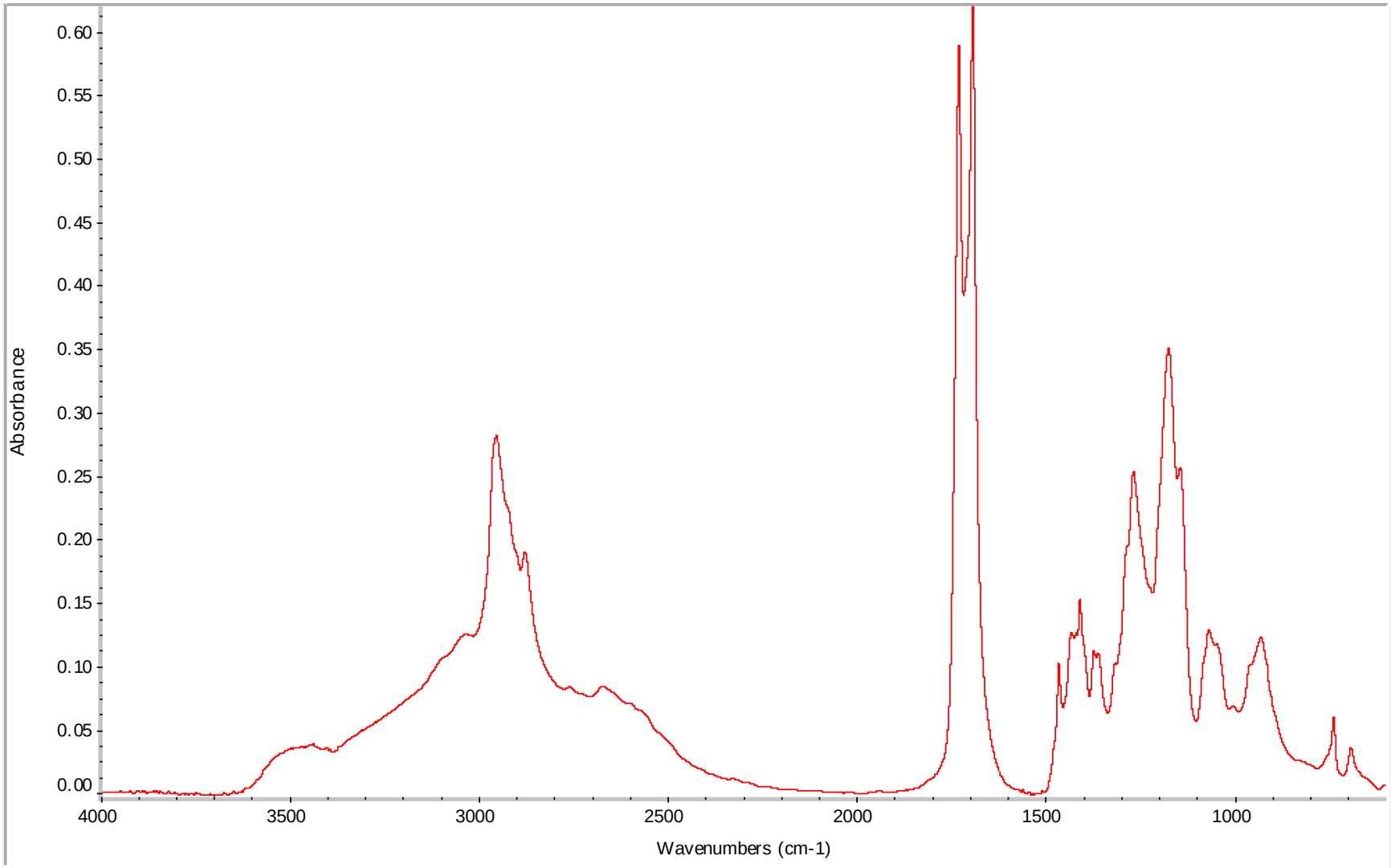

Figure 8.48 AA BD 1 4 hr PP w/o TSA catalyst FT-IR spectrum

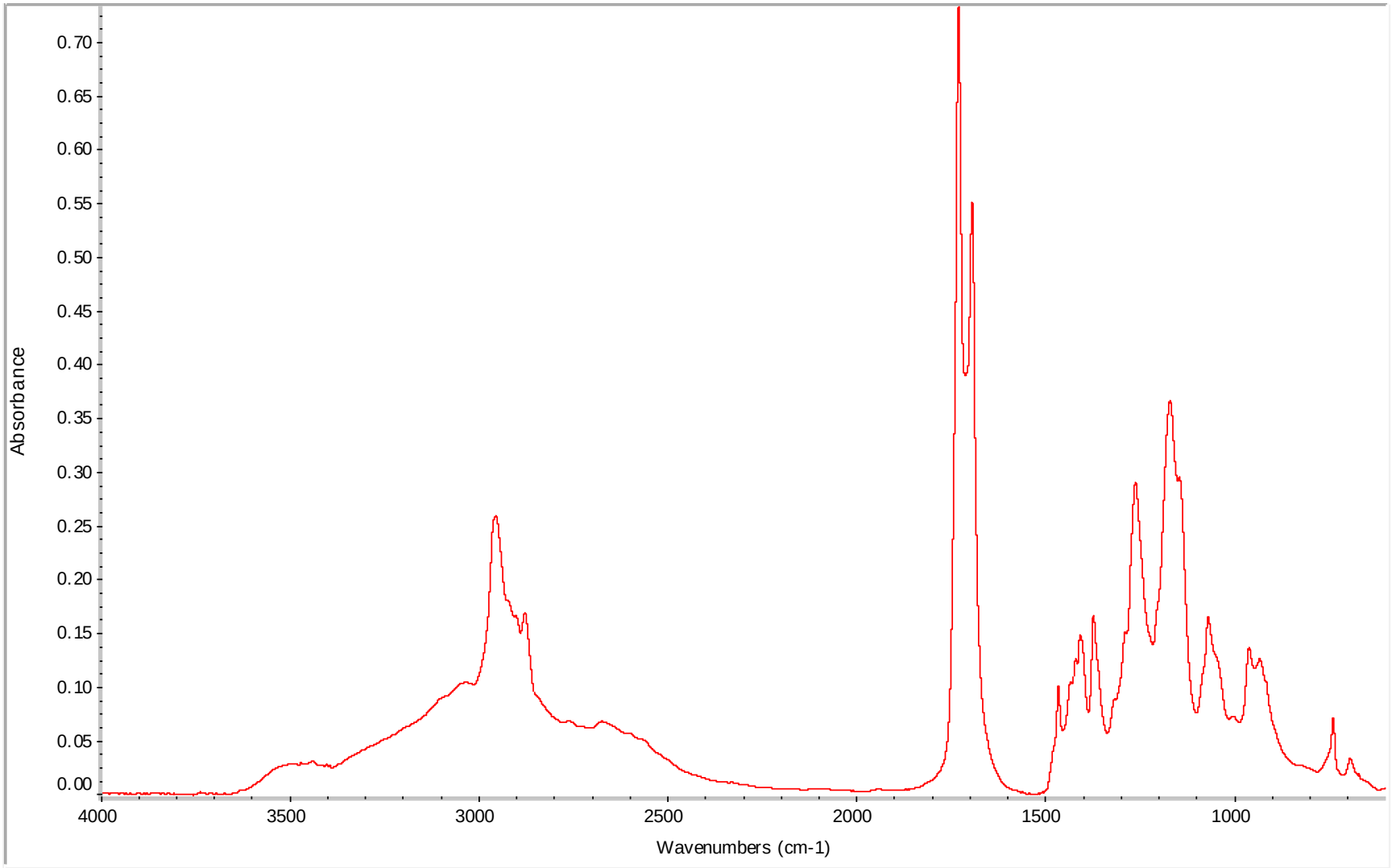

Figure 8.49 AA BD 1 5 hr PP w/o TSA catalyst FT-IR spectrum

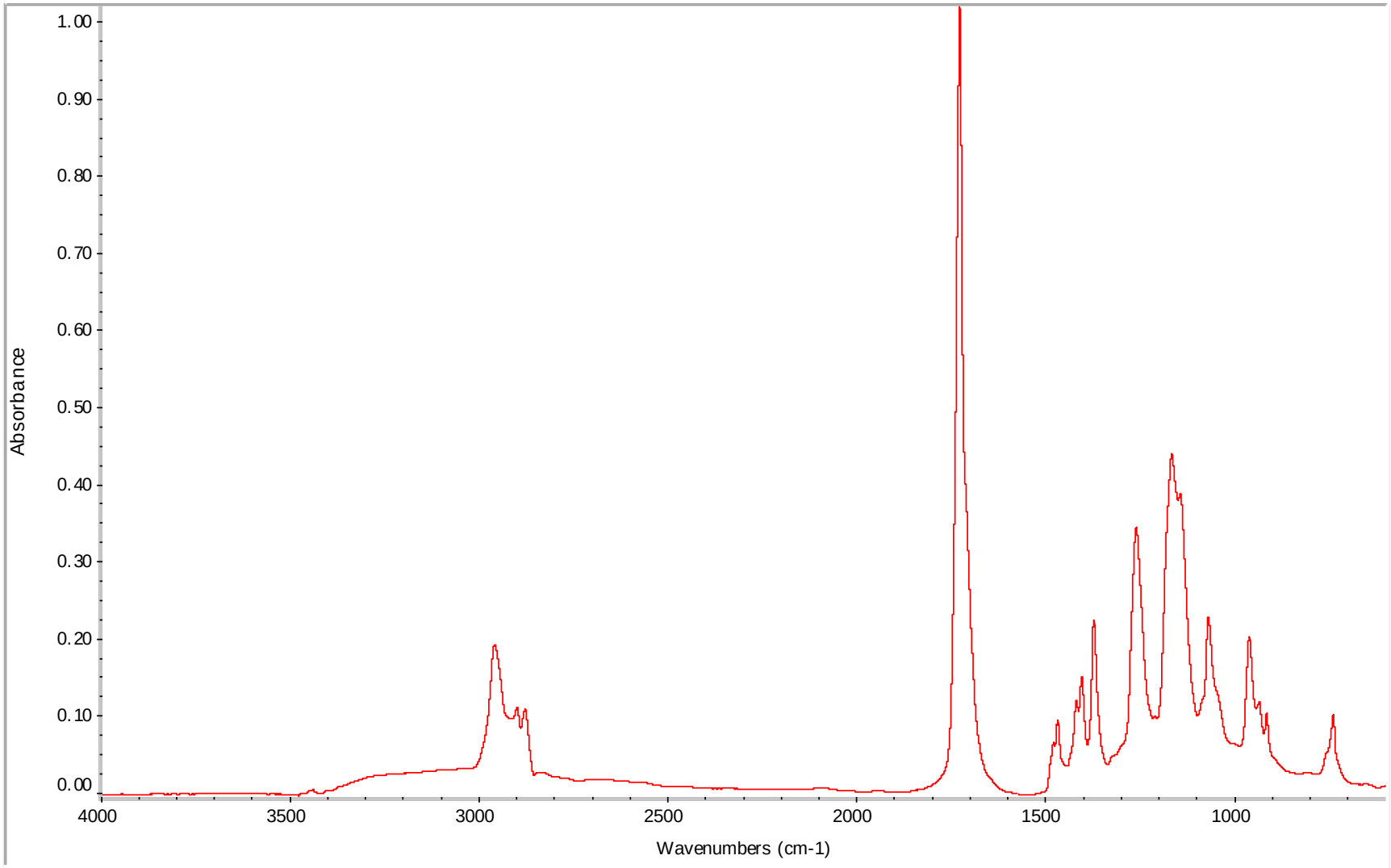

Figure 8.50 AA BD 1 18 hr PP w/o TSA catalyst FT-IR spectrum

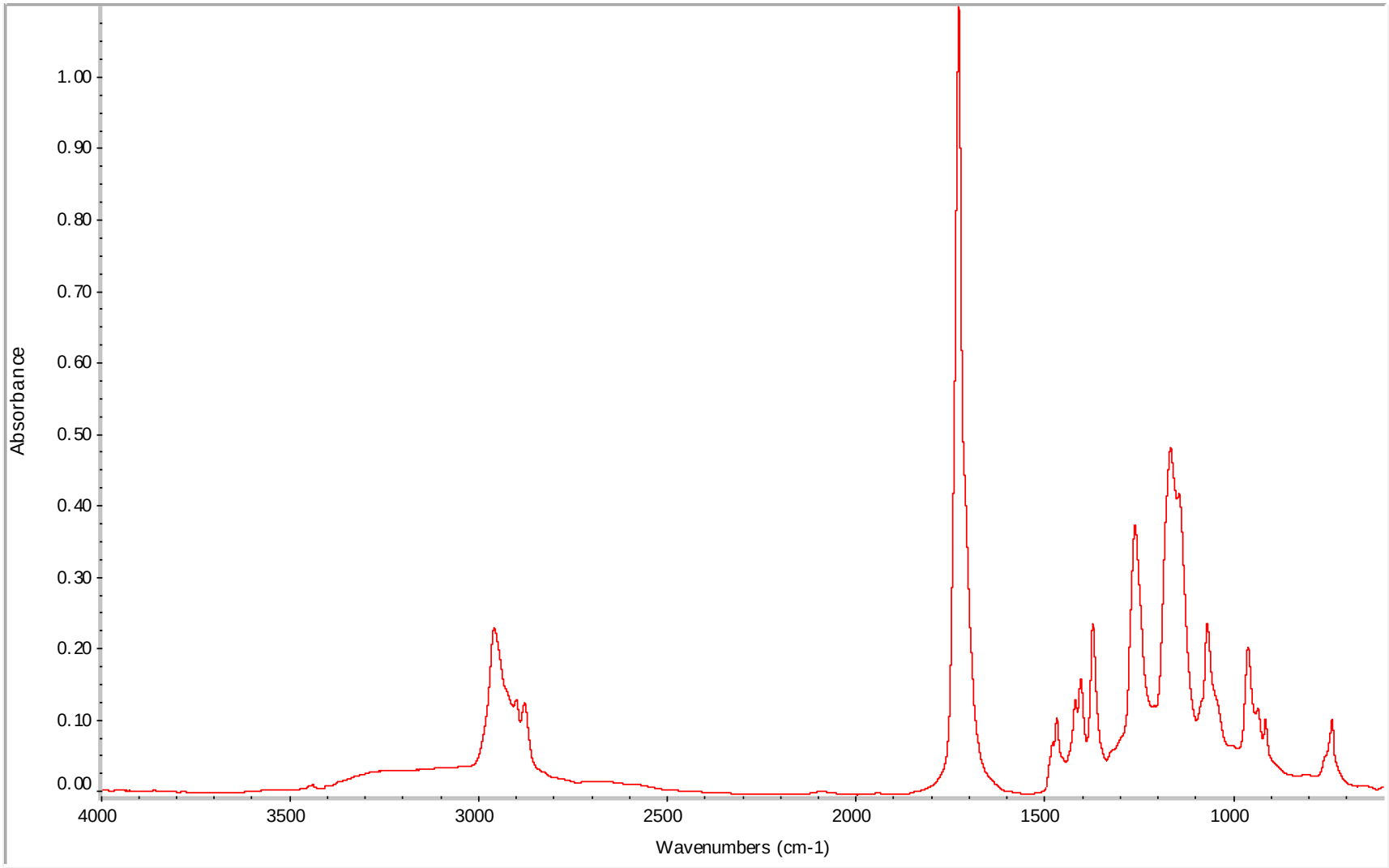

Figure 8.51 AA BD 1 21 hr PP w/o TSA catalyst FT-IR spectrum

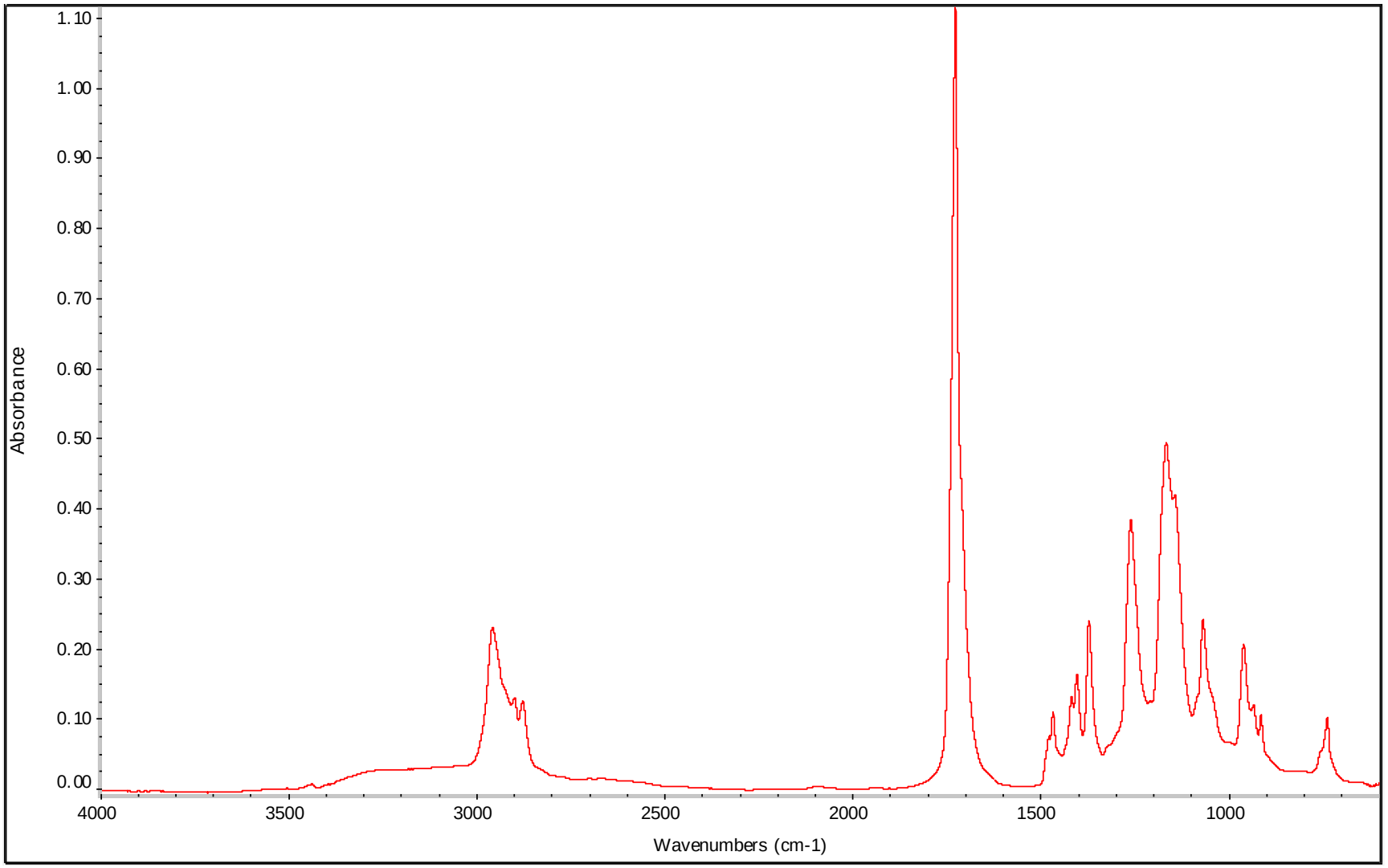

Figure 8.52 AA BD 1 24 hr PP w/o TSA catalyst FT-IR spectrum

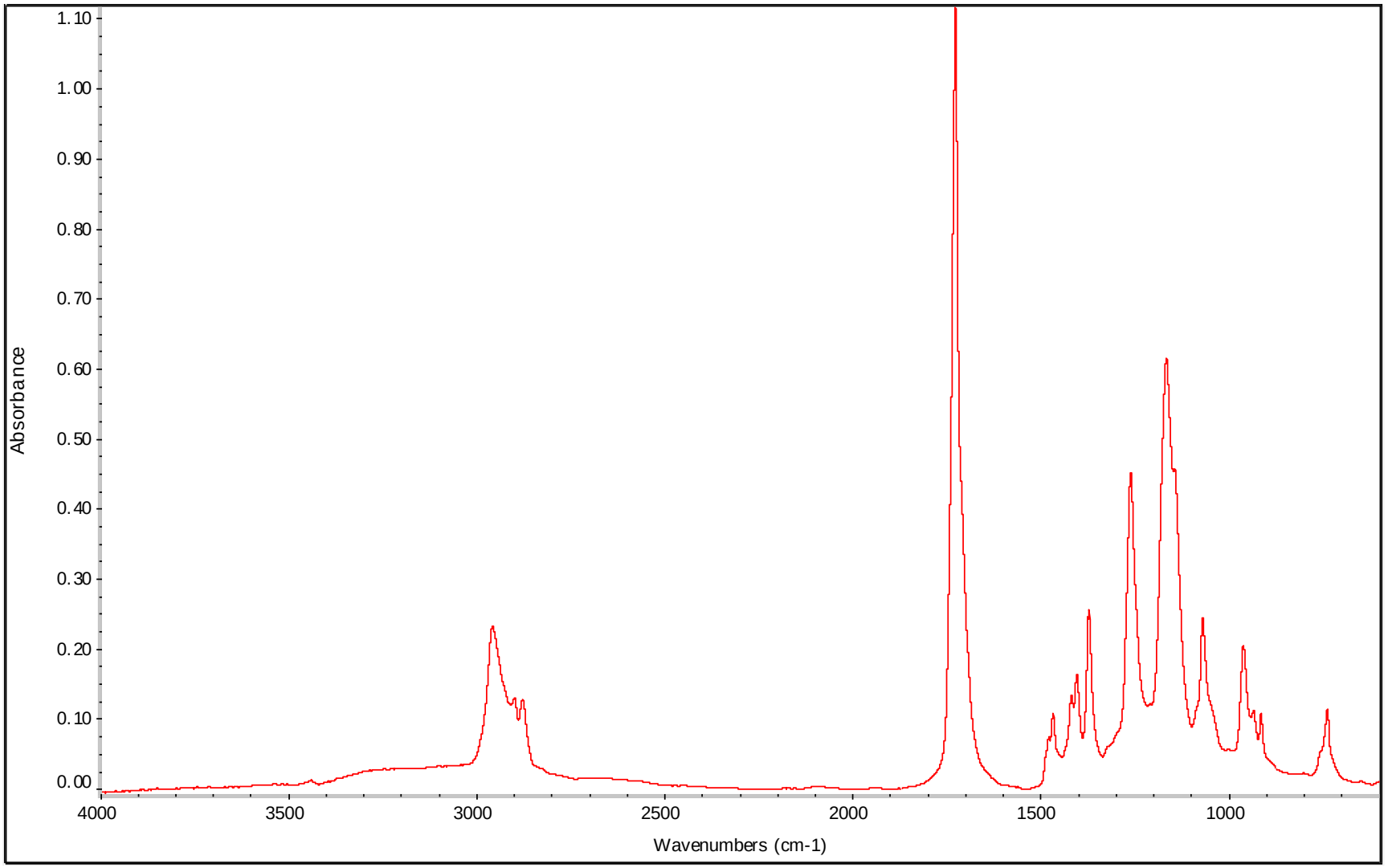

Figure 8.53 AA BD 1 42 hr PP w/o TSA catalyst FT-IR spectrum

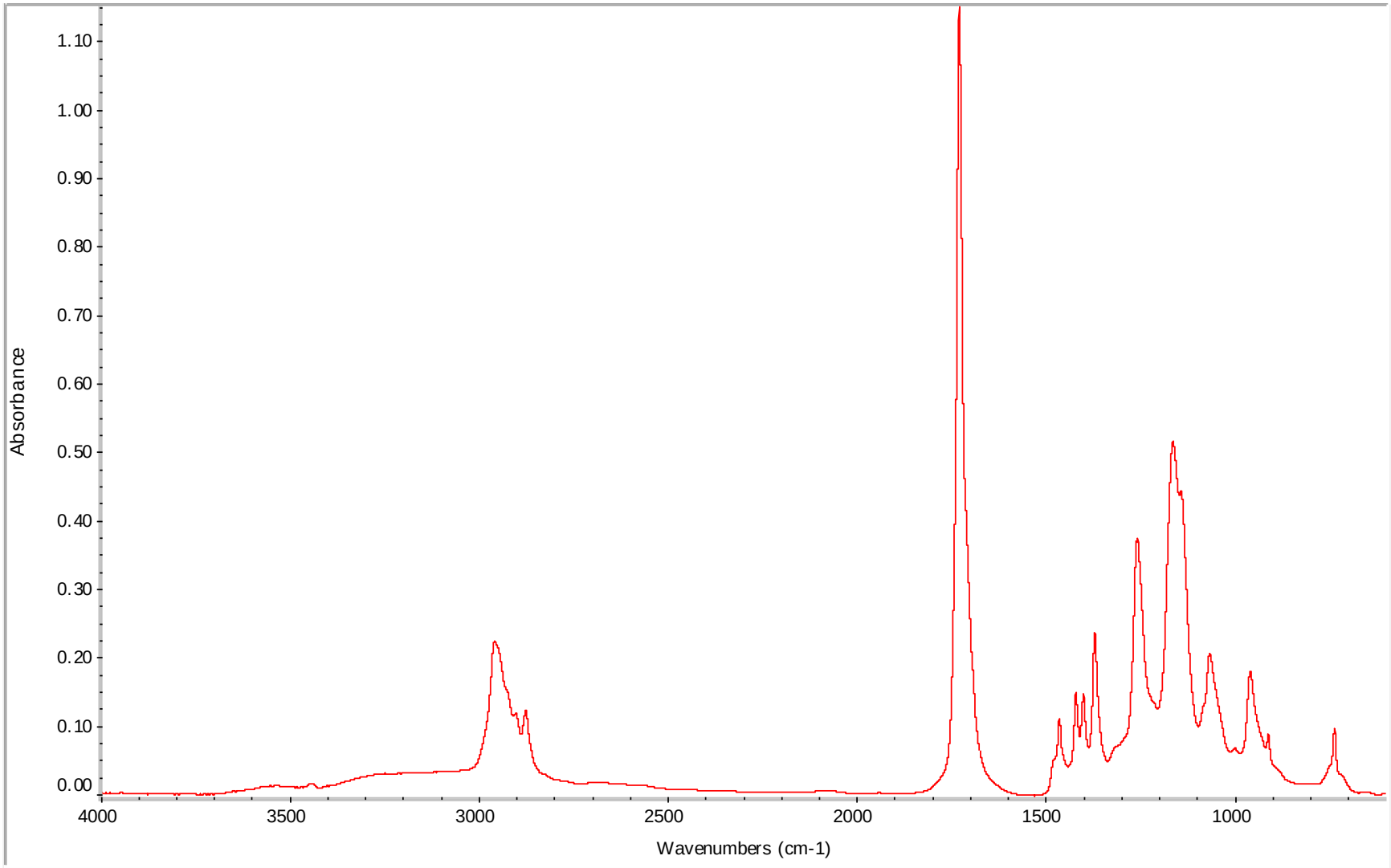

Figure 8.54 AA BD 1 48 hr PP w/o TSA catalyst FT-IR spectrum

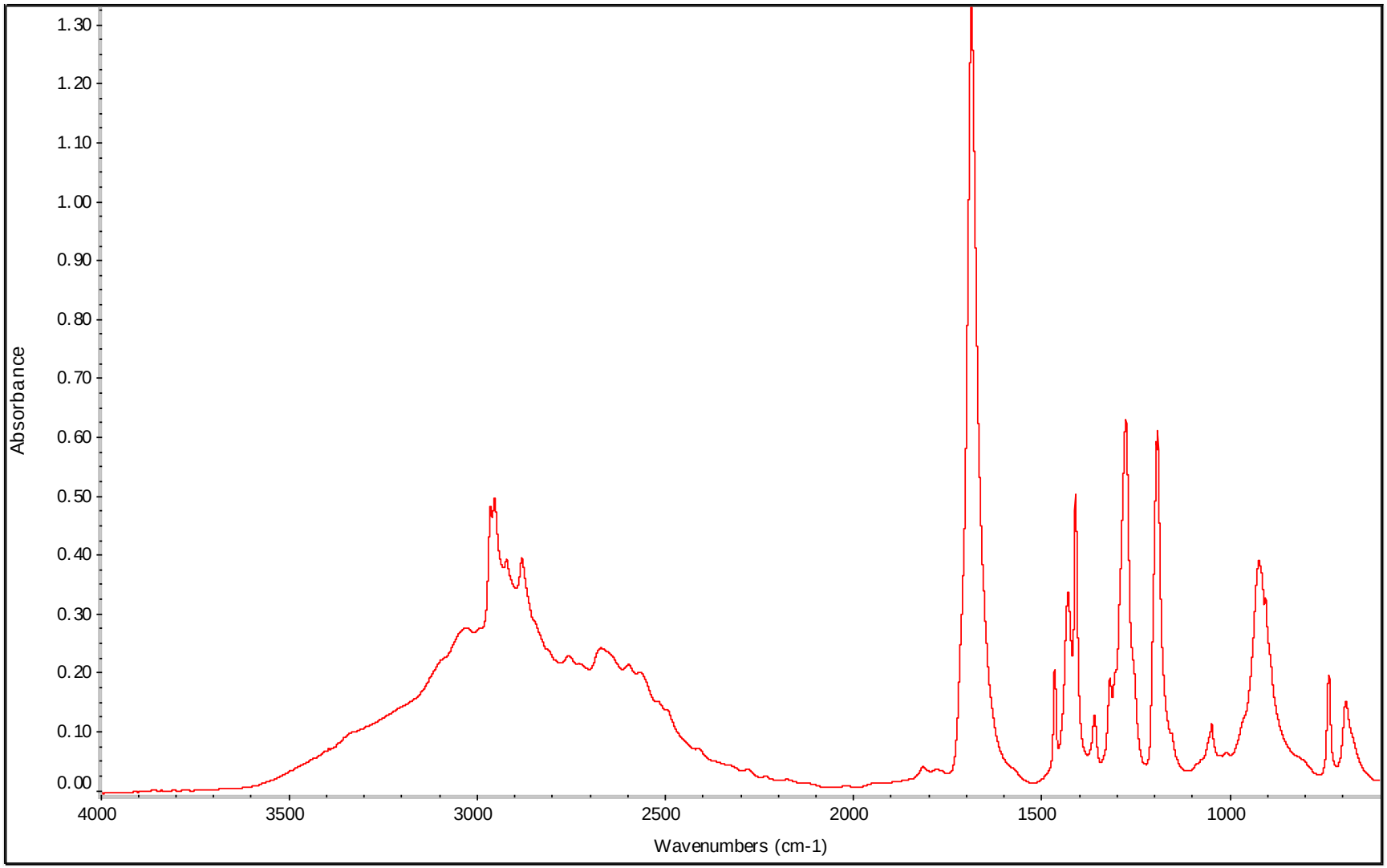

Figure 8.55 AA BD 1 0 hr PP w/ TSA catalyst FT-IR spectrum

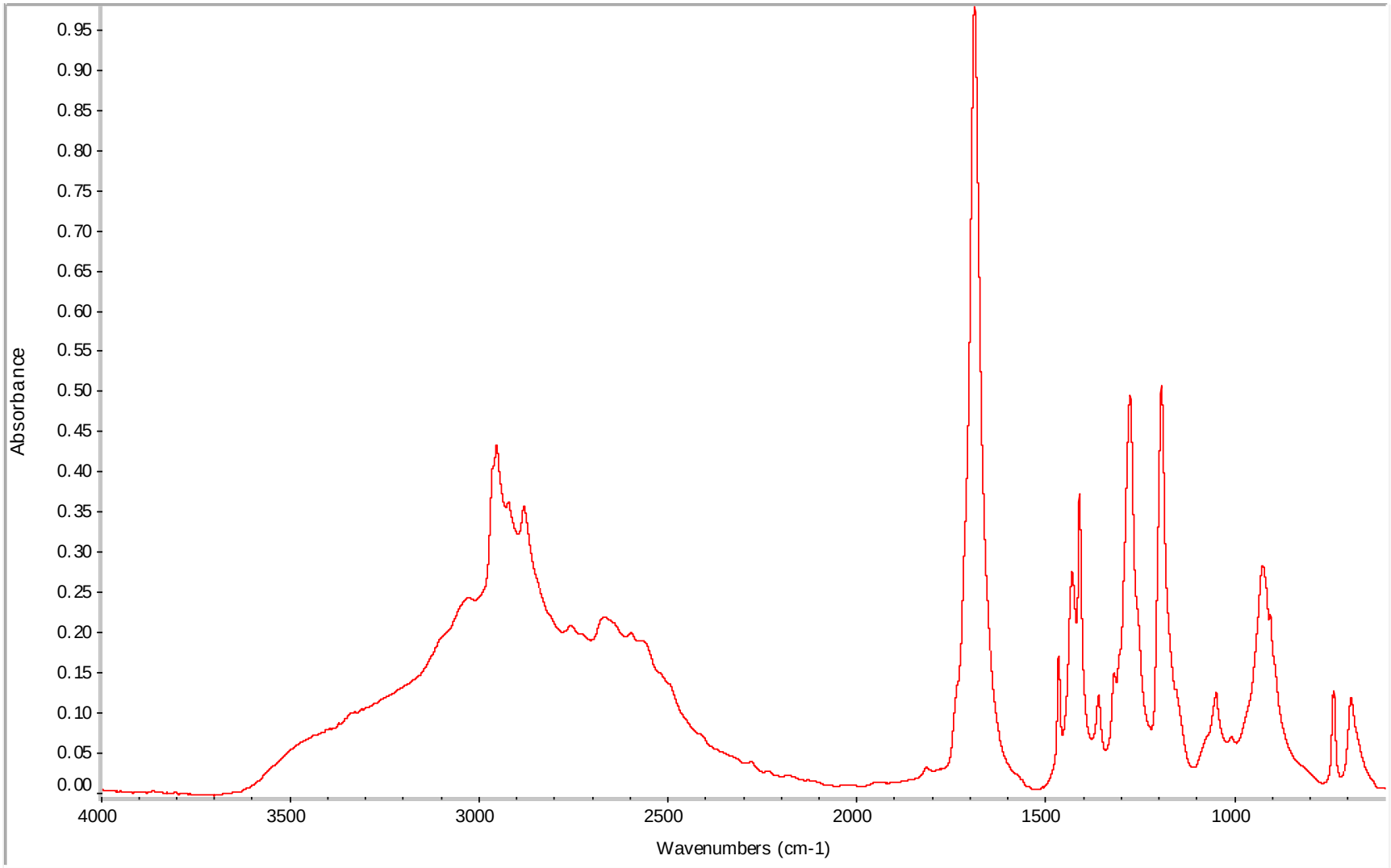

Figure 8.56 AA BD 1 1 hr PP w/ TSA catalyst FT-IR spectrum

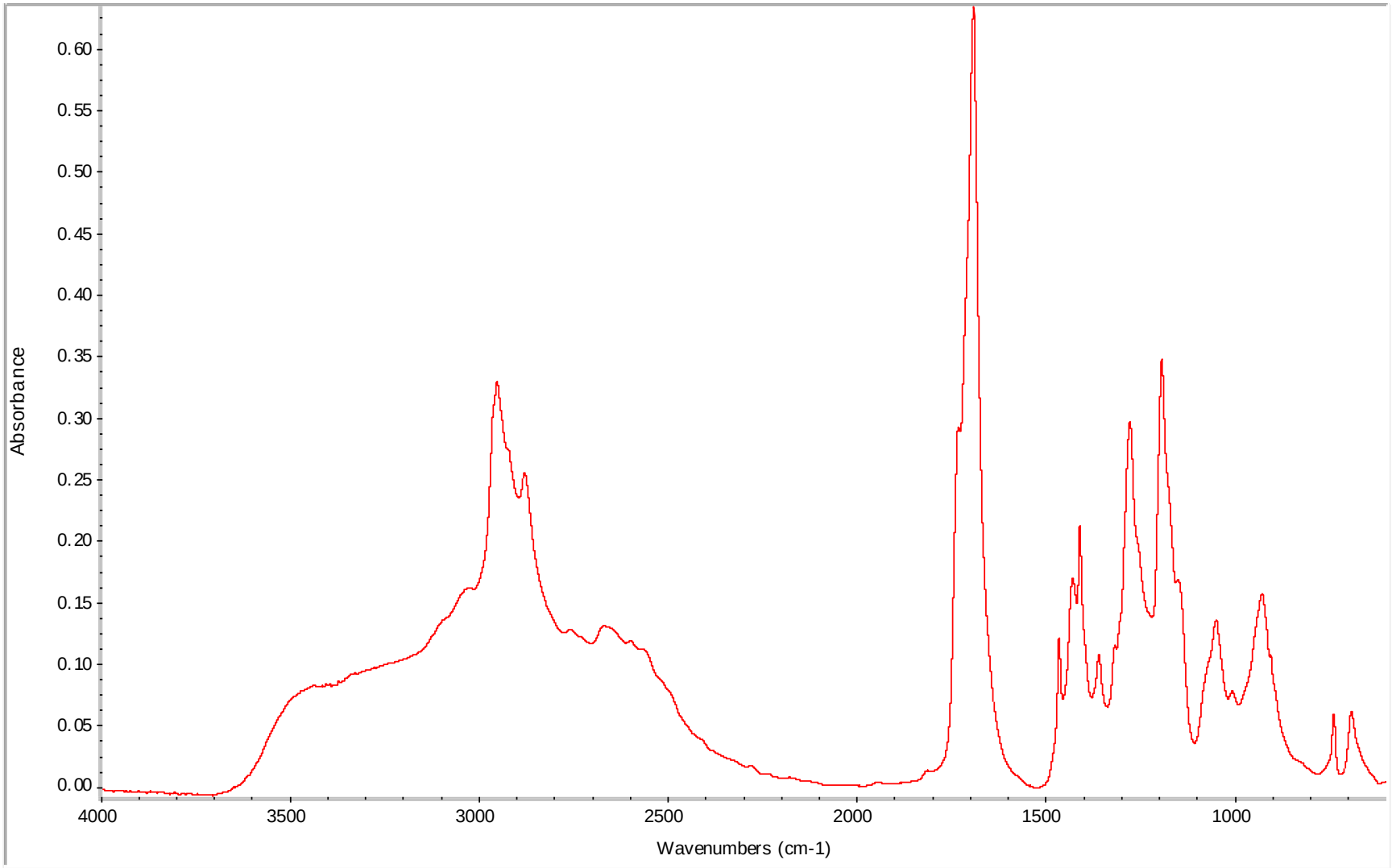

Figure 8.57 AA BD 1 2 hr PP w/ TSA catalyst FT-IR spectrum

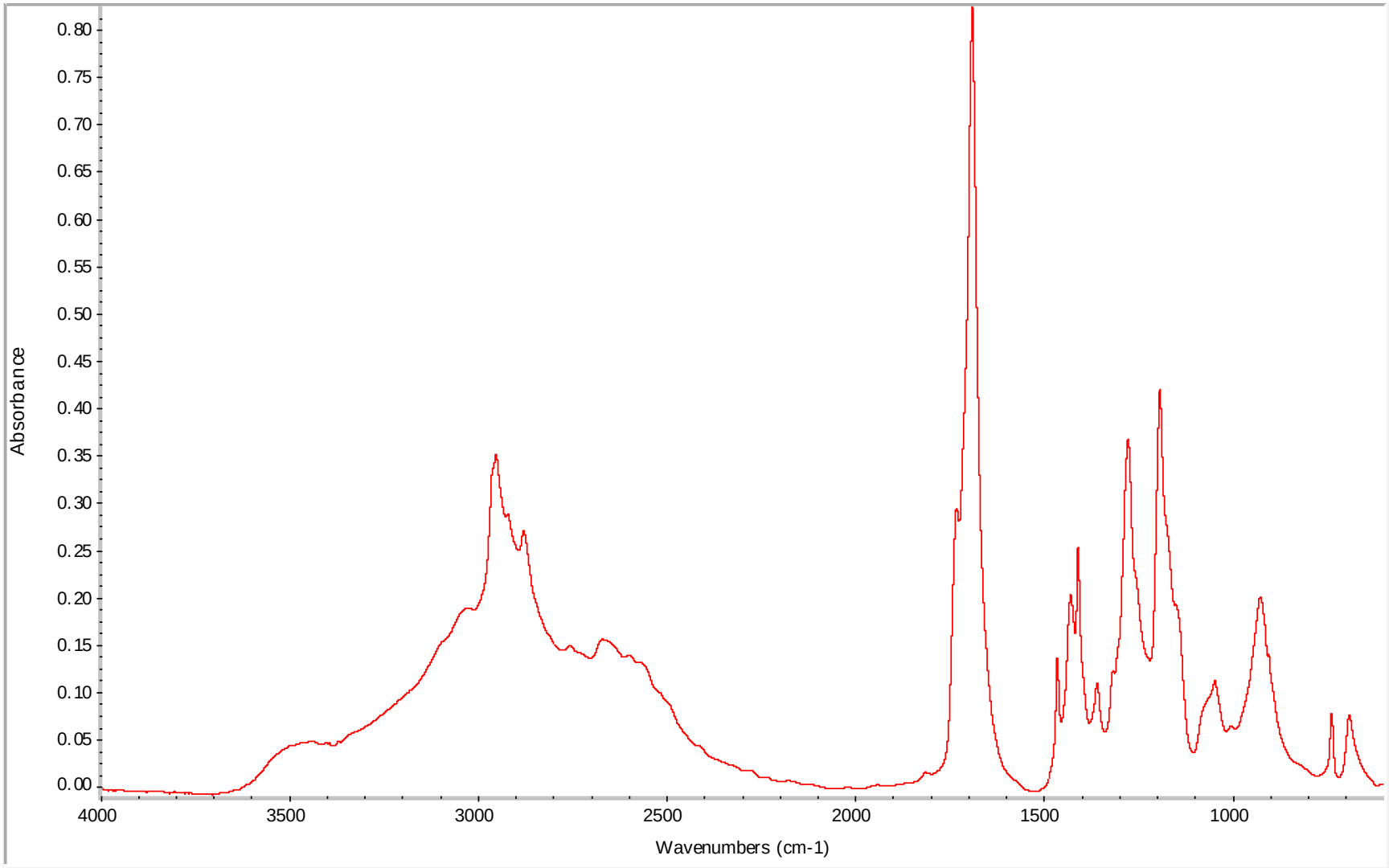

Figure 8.58 AA BD 1 3 hr PP w/ TSA catalyst FT-IR spectrum

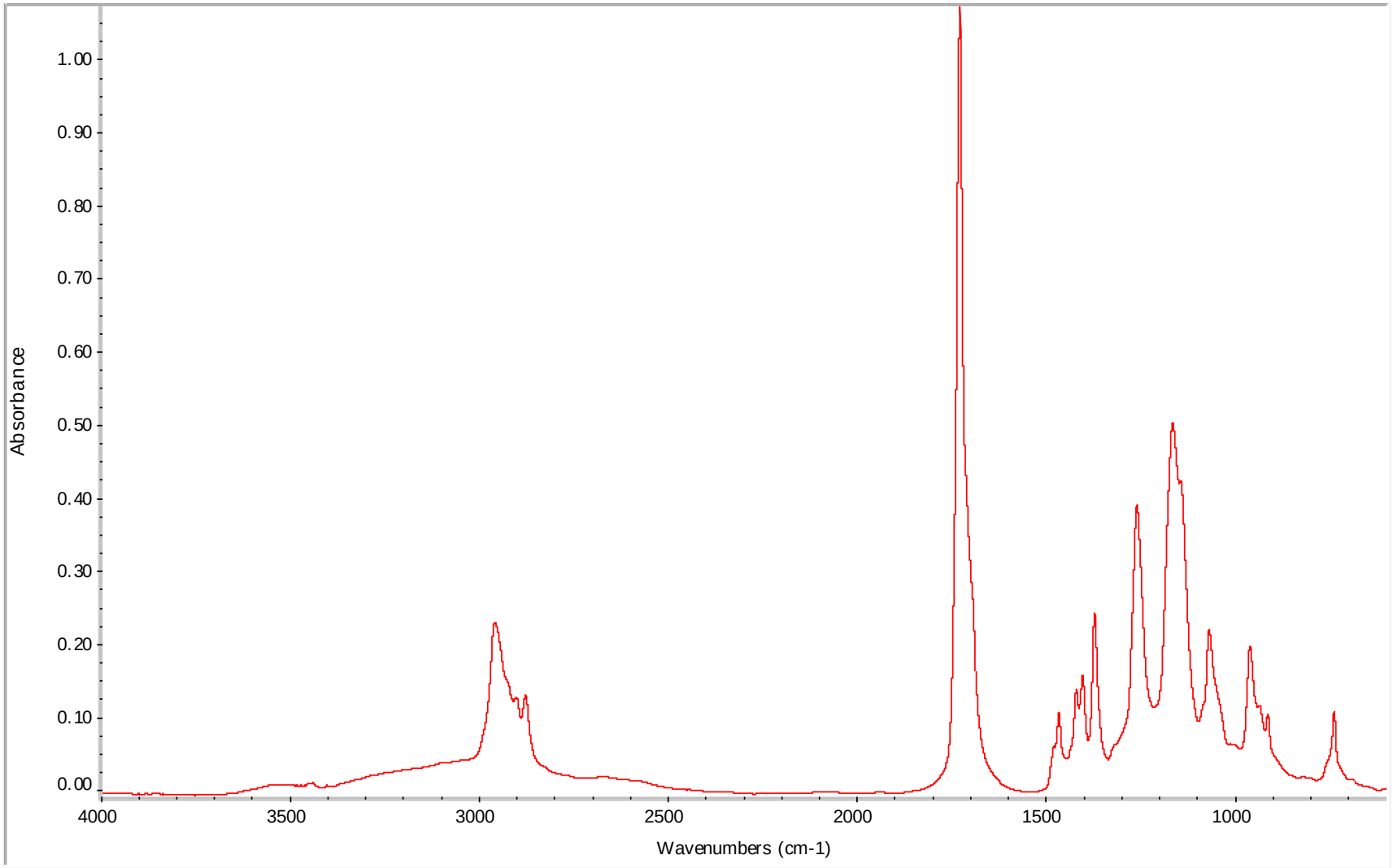

Figure 8.59 AA BD 1 4 hr PP w/ TSA catalyst FT-IR spectrum

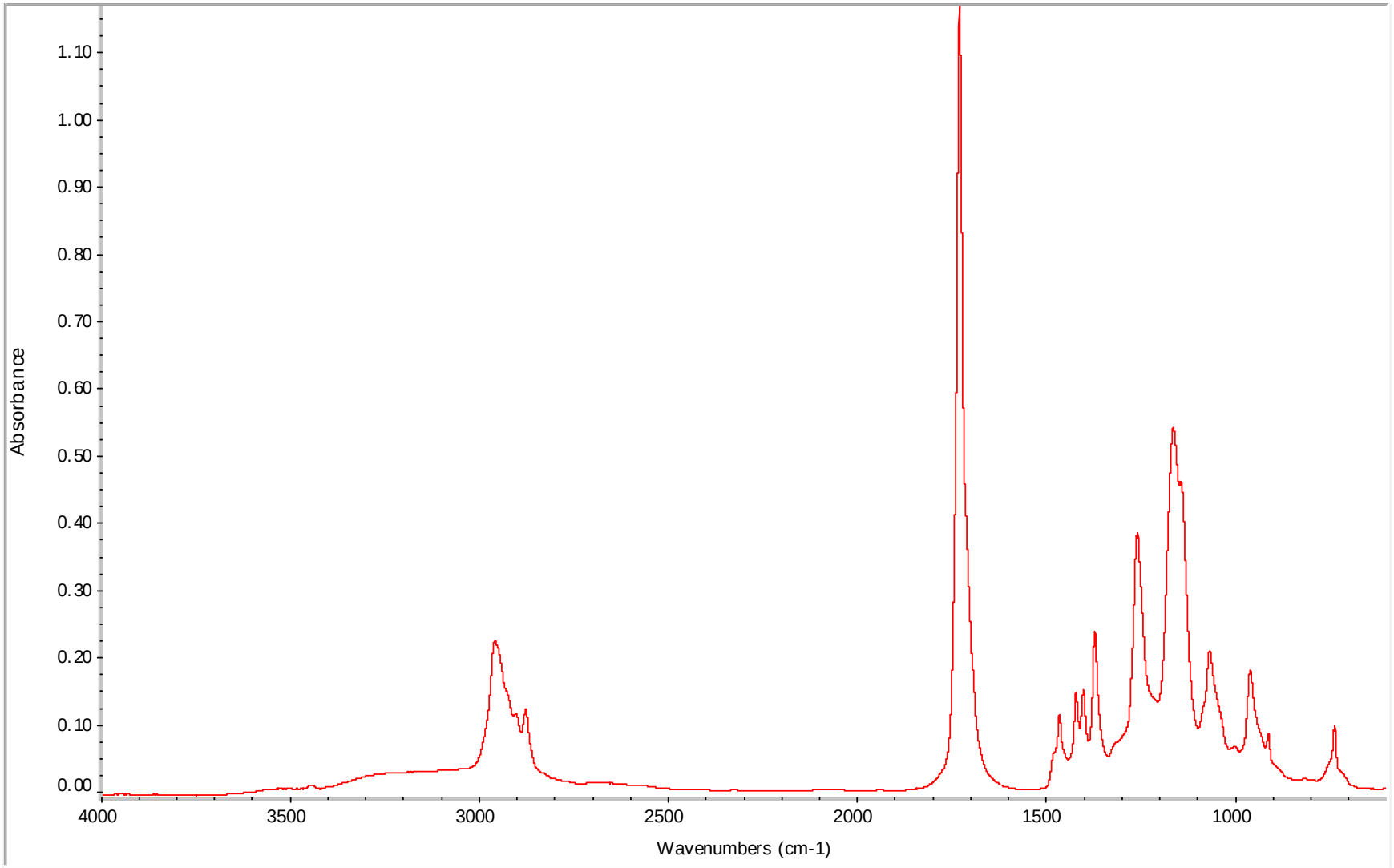

Figure 8.60 AA BD 1 16.5 hr PP w/ TSA catalyst FT-IR spectrum

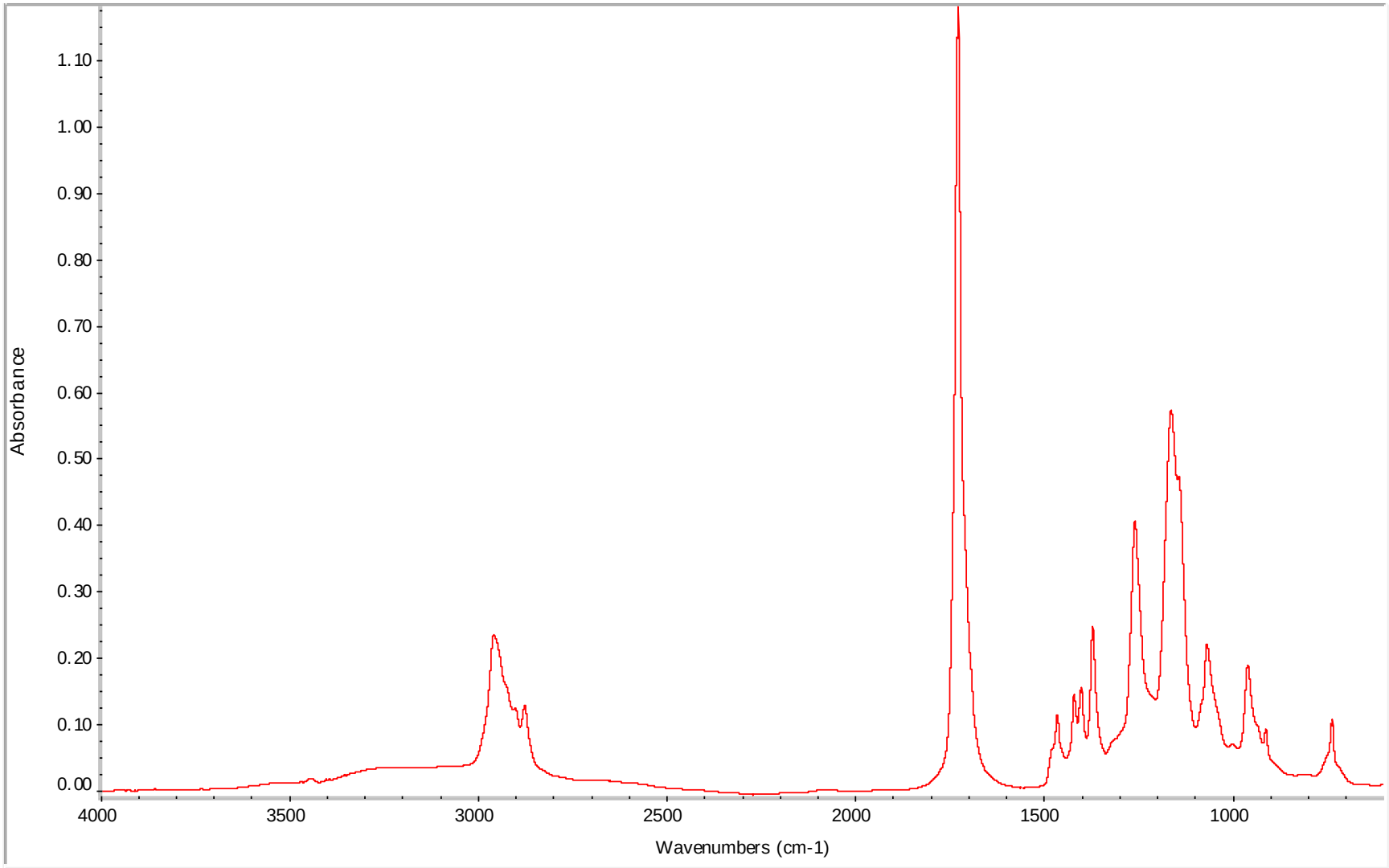

Figure 8.61 AA BD 1 18 hr PP w/ TSA catalyst FT-IR spectrum

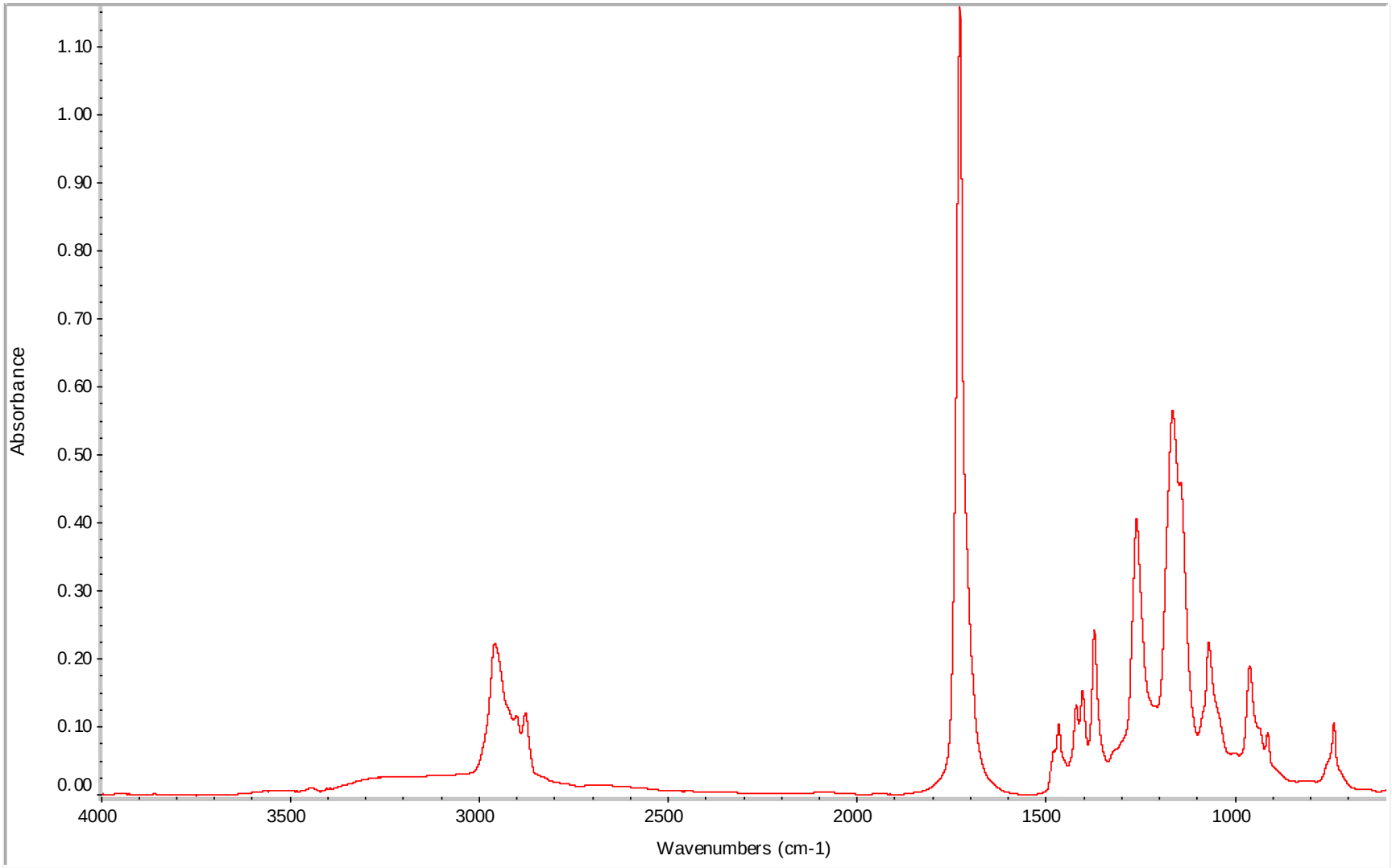

Figure 8.62 AA BD 1 19 hr PP w/ TSA catalyst FT-IR spectrum

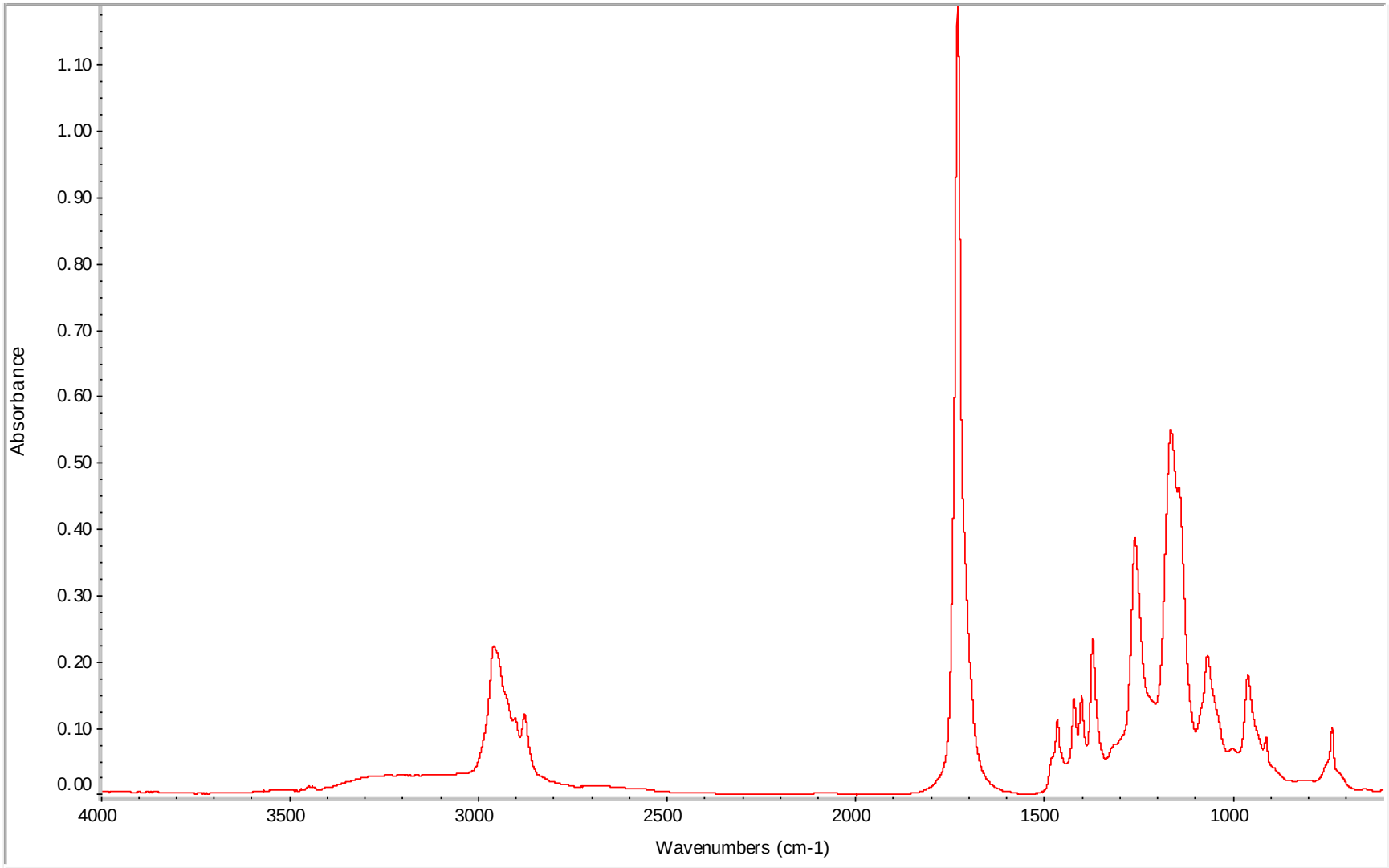

Figure 8.63 AA BD 1 21 hr PP w/ TSA catalyst FT-IR spectrum

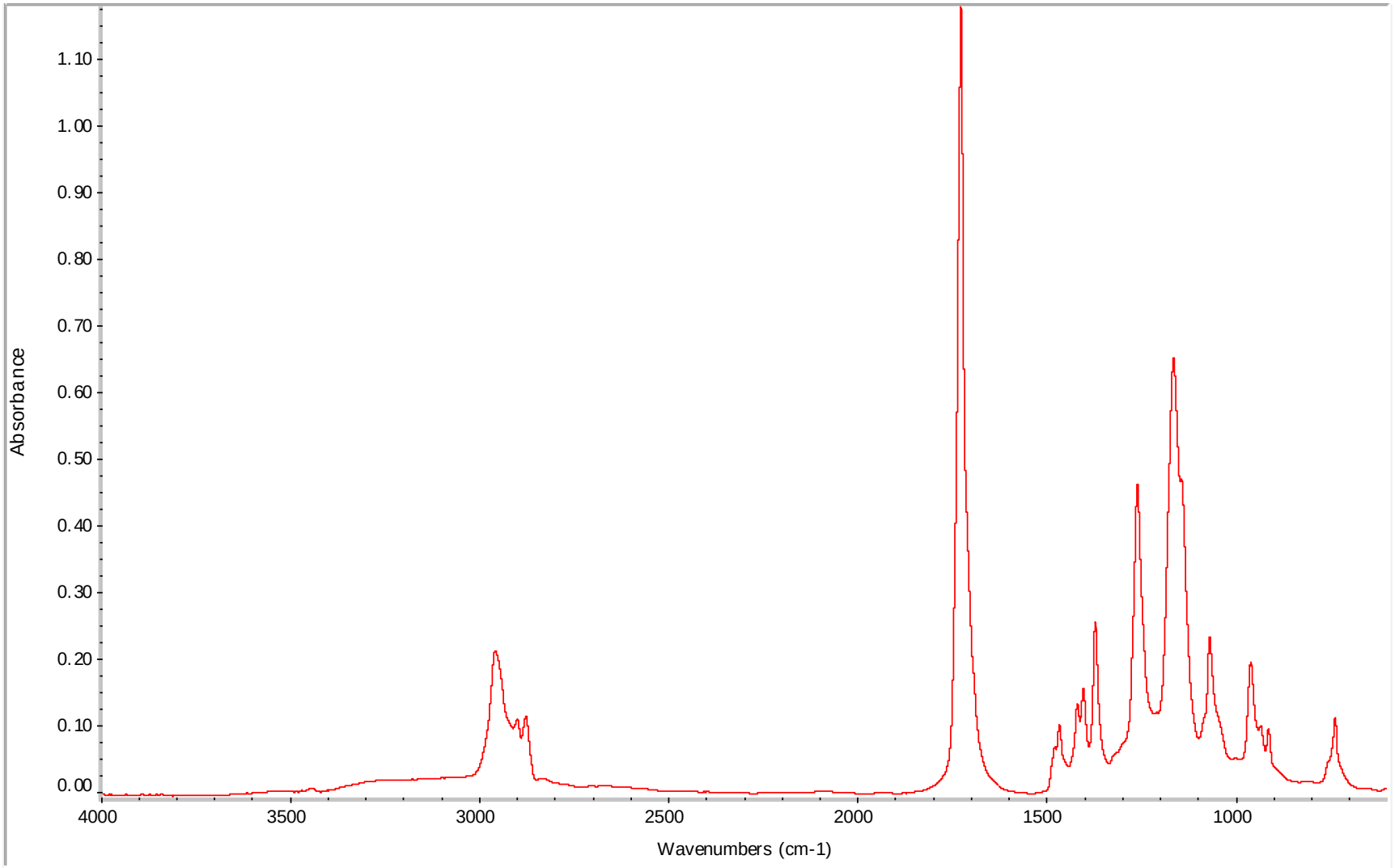

Figure 8.64 AA BD 1 24 hr PP w/ TSA catalyst FT-IR spectrum

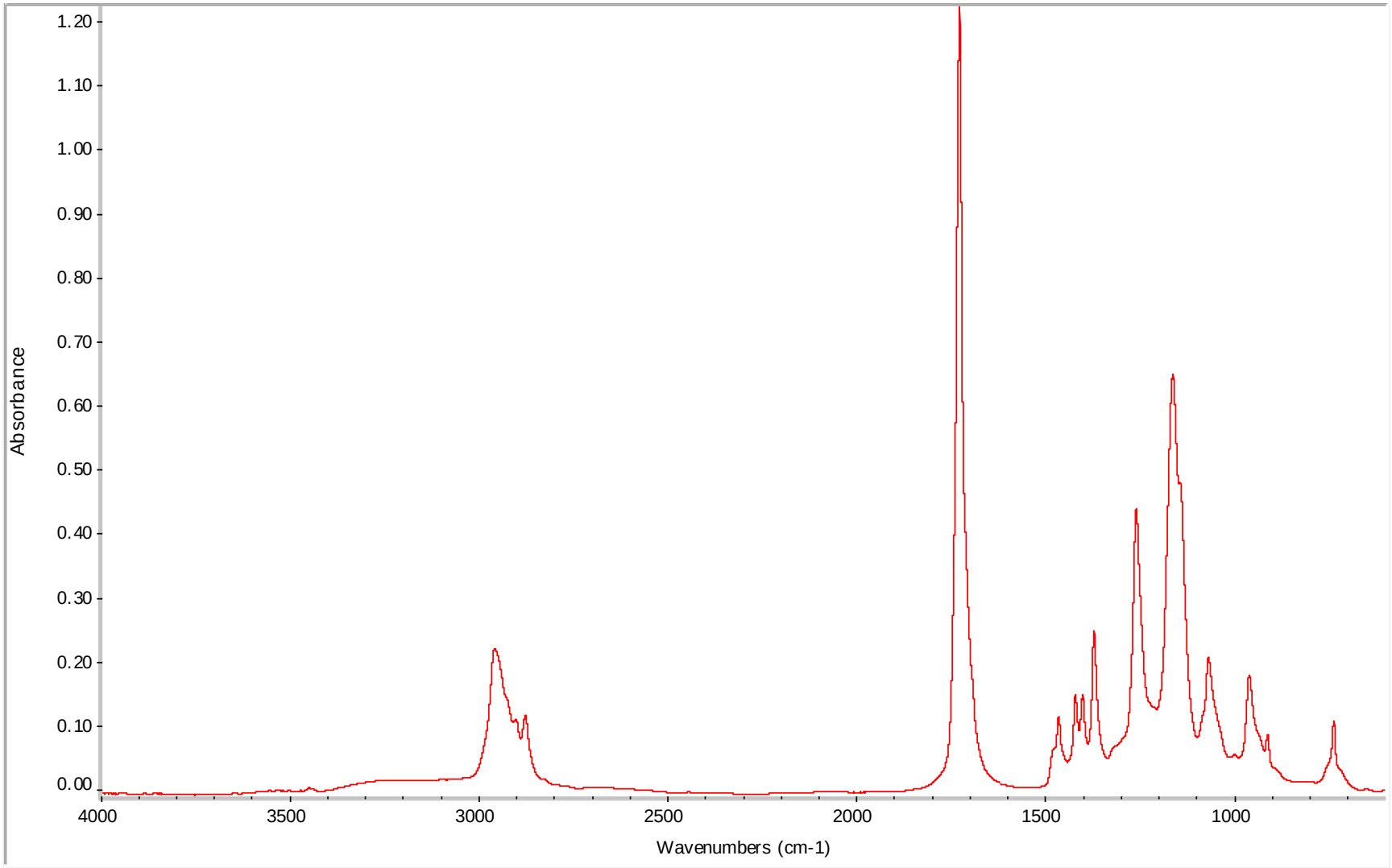

Figure 8.65 AA BD 1 40 hr PP w/ TSA catalyst FT-IR spectrum

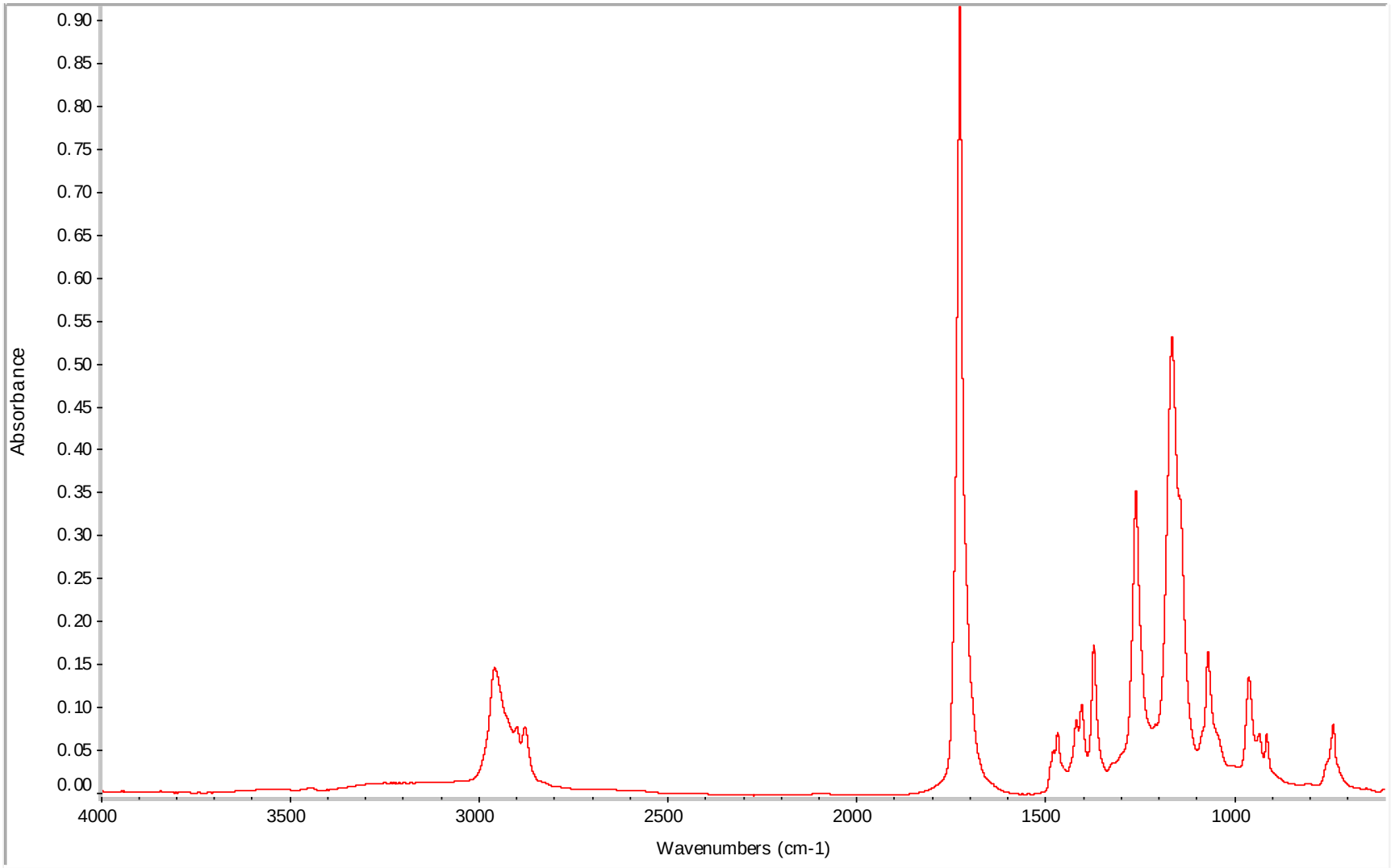

Figure 8.66 AA BD 1 41.5 hr PP w/ TSA catalyst FT-IR spectrum

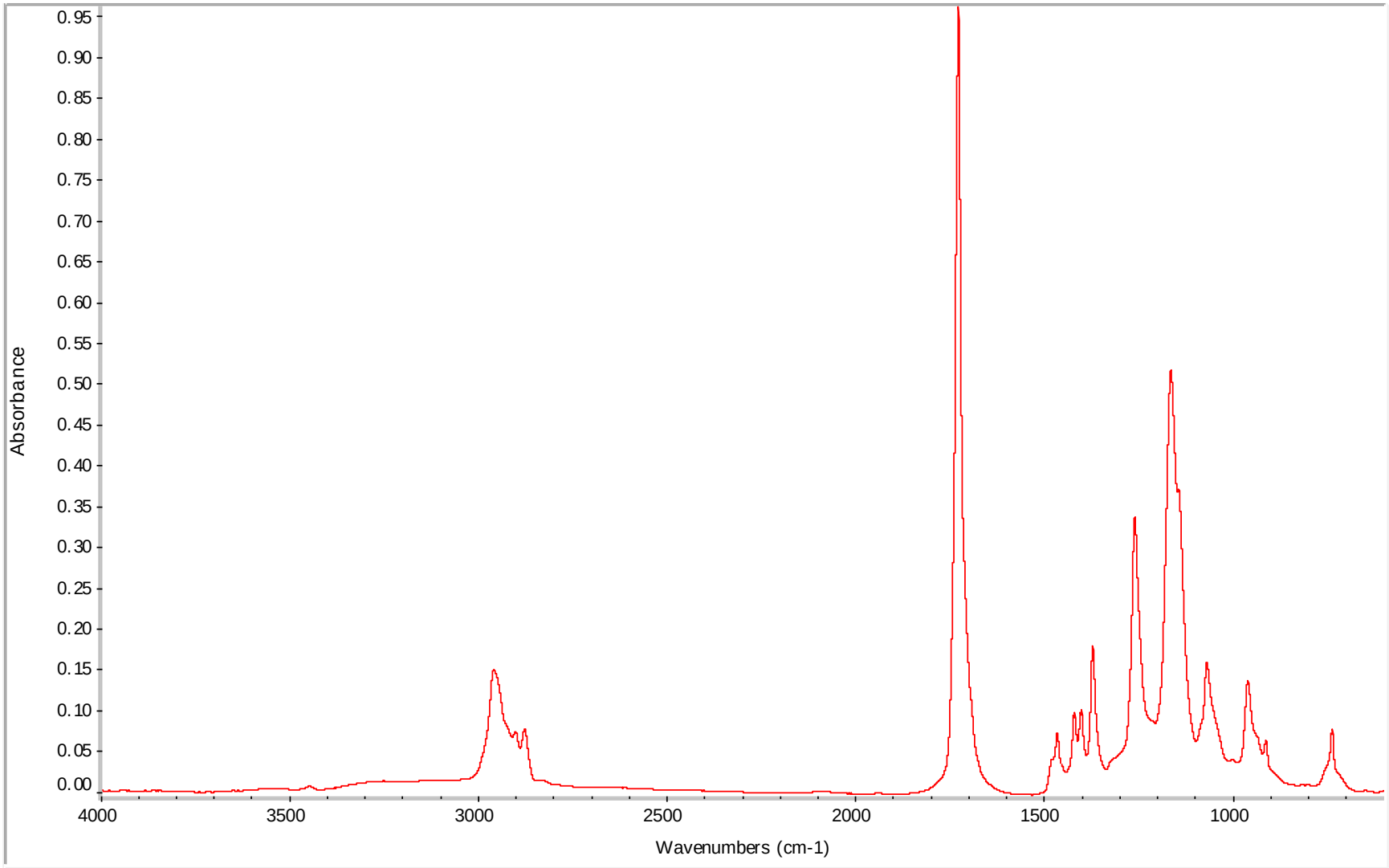

Figure 8.67 AA BD 1 48 hr PP w/ TSA catalyst FT-IR spectrum

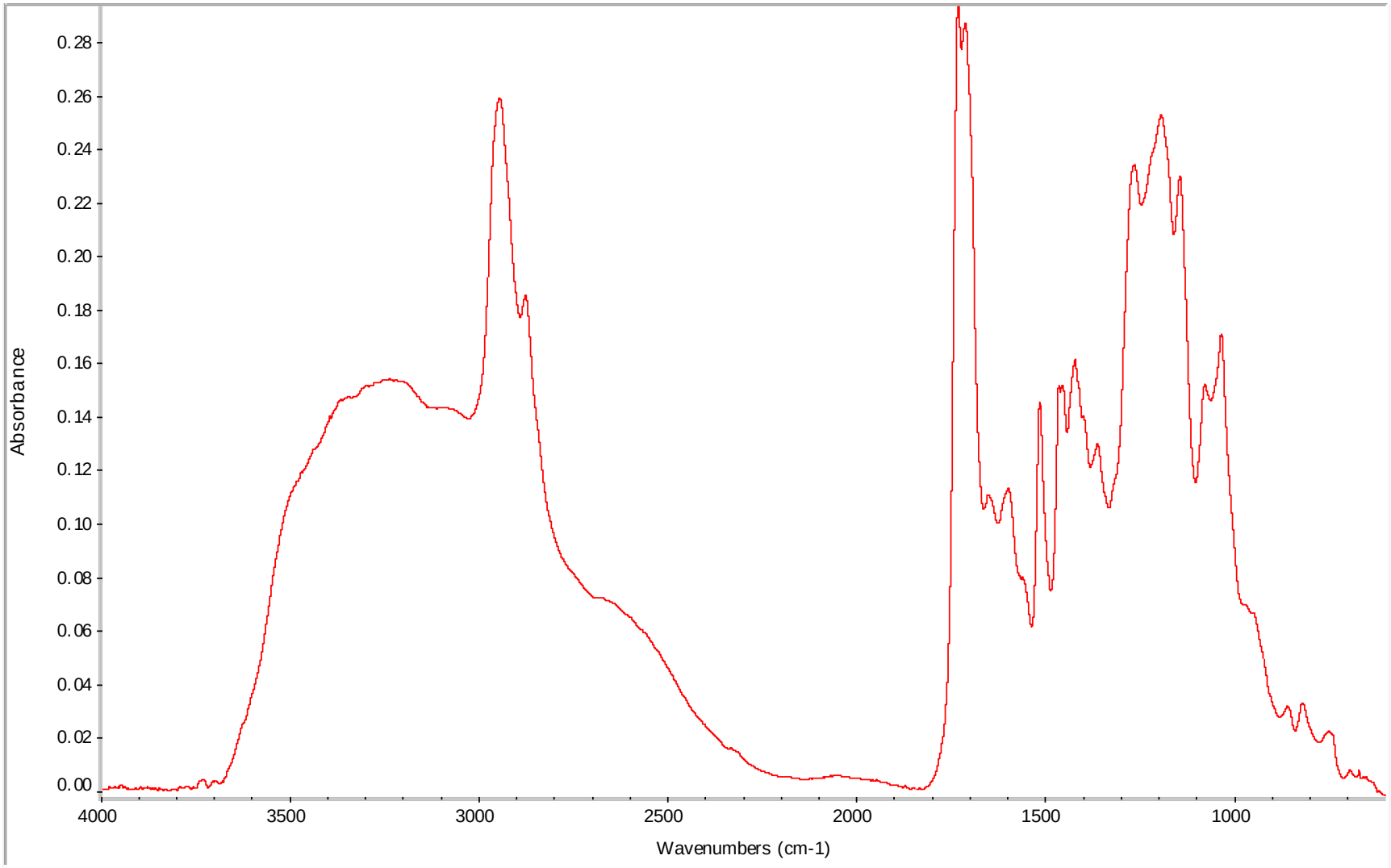

Figure 8.68 AA BD 0.8 3 hr copolymer FT-IR spectrum

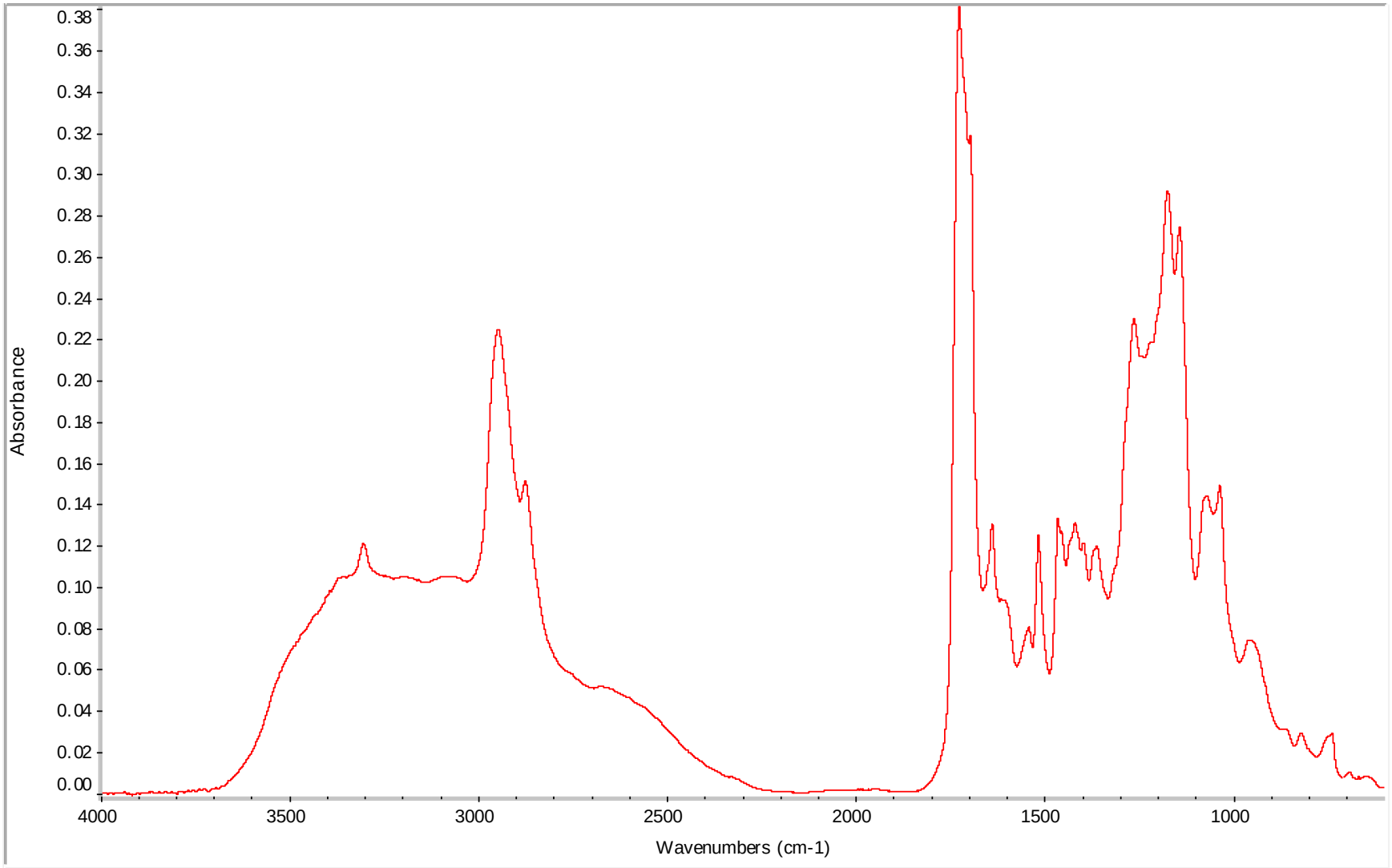

Figure 8.69 AA BD 0.8 4 hr copolymer FT-IR spectrum

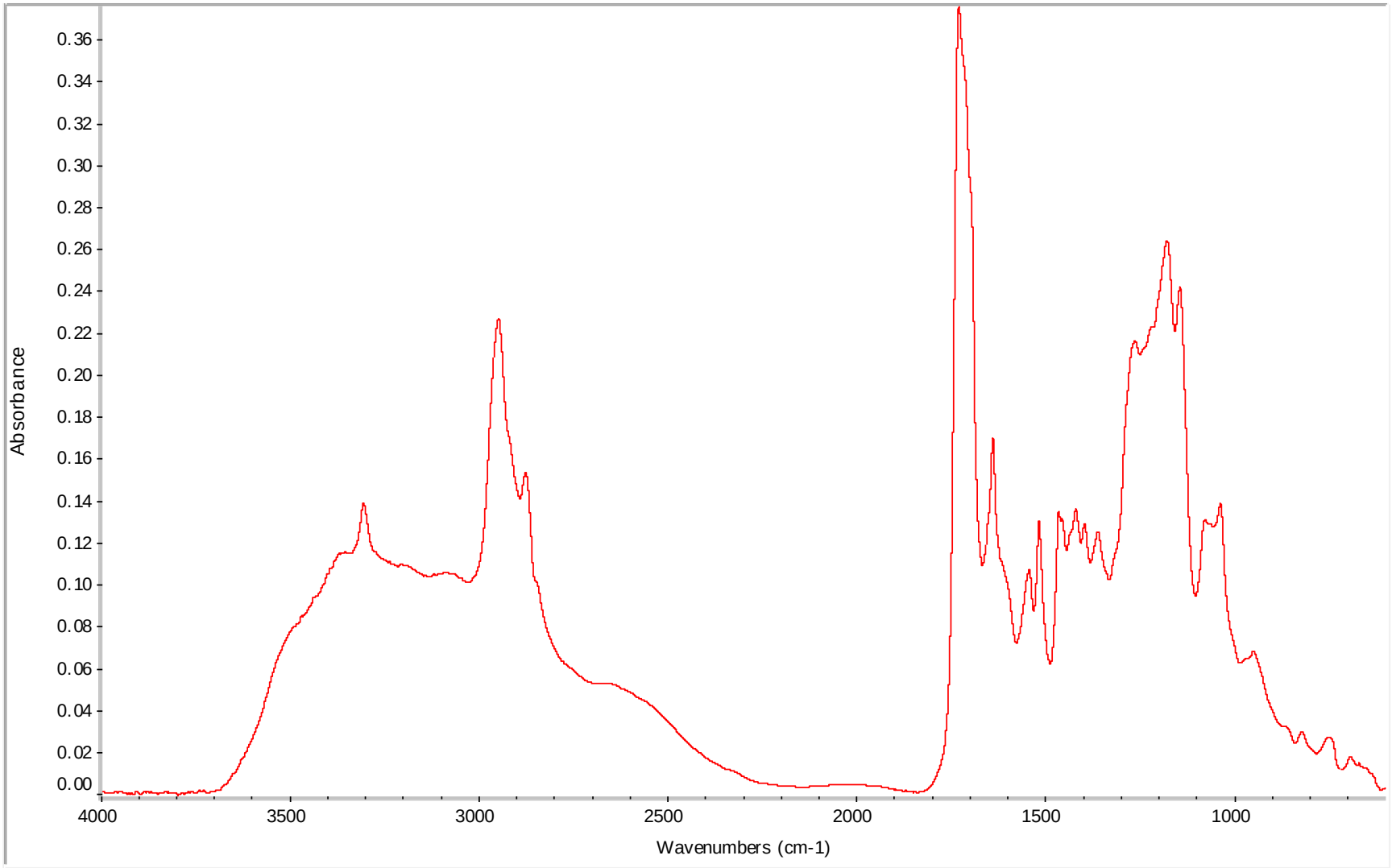

Figure 8.70 AA BD 0.8 5 hr copolymer FT-IR spectrum

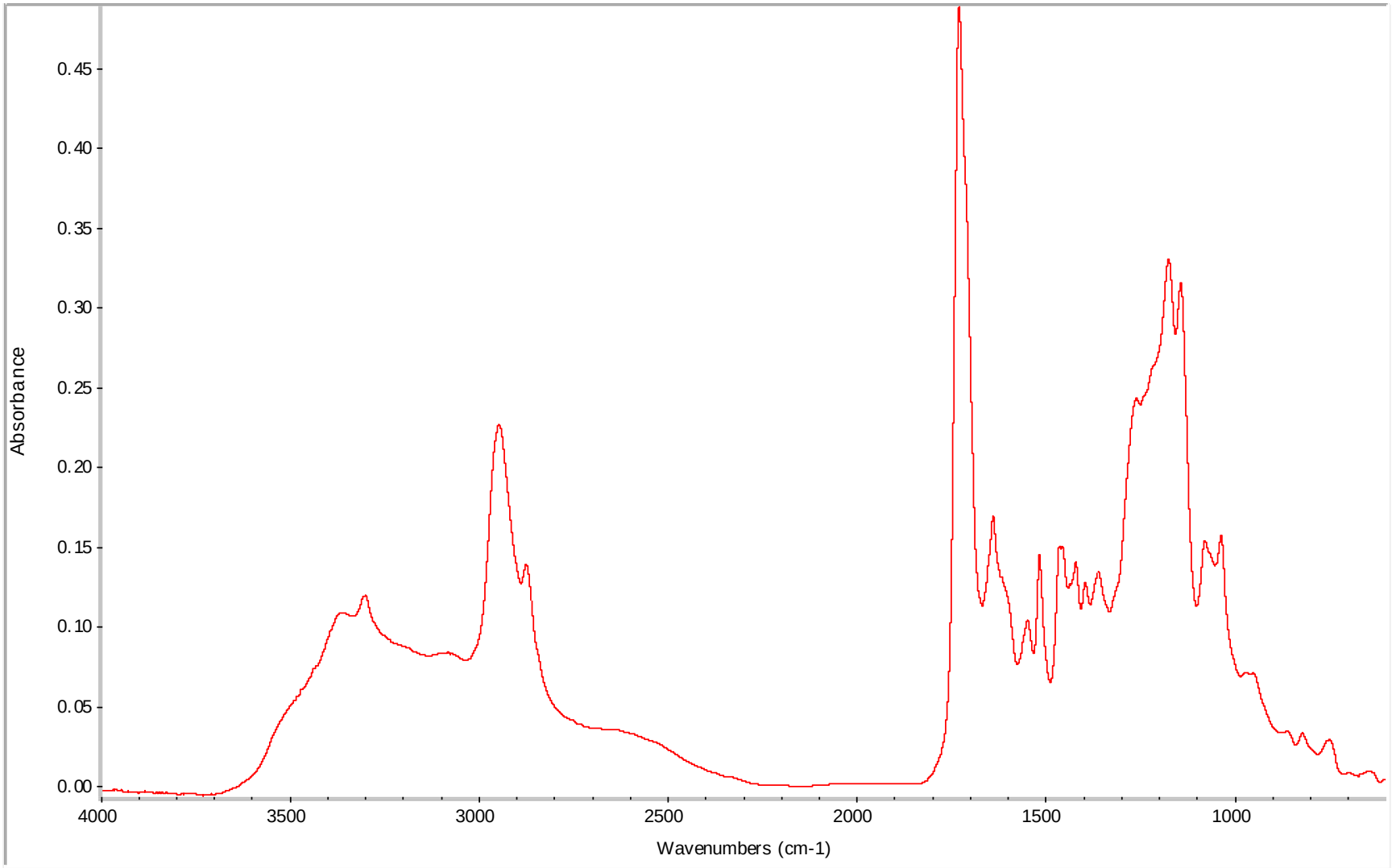

Figure 8.71 AA BD 0.8 8 hr copolymer FT-IR spectrum

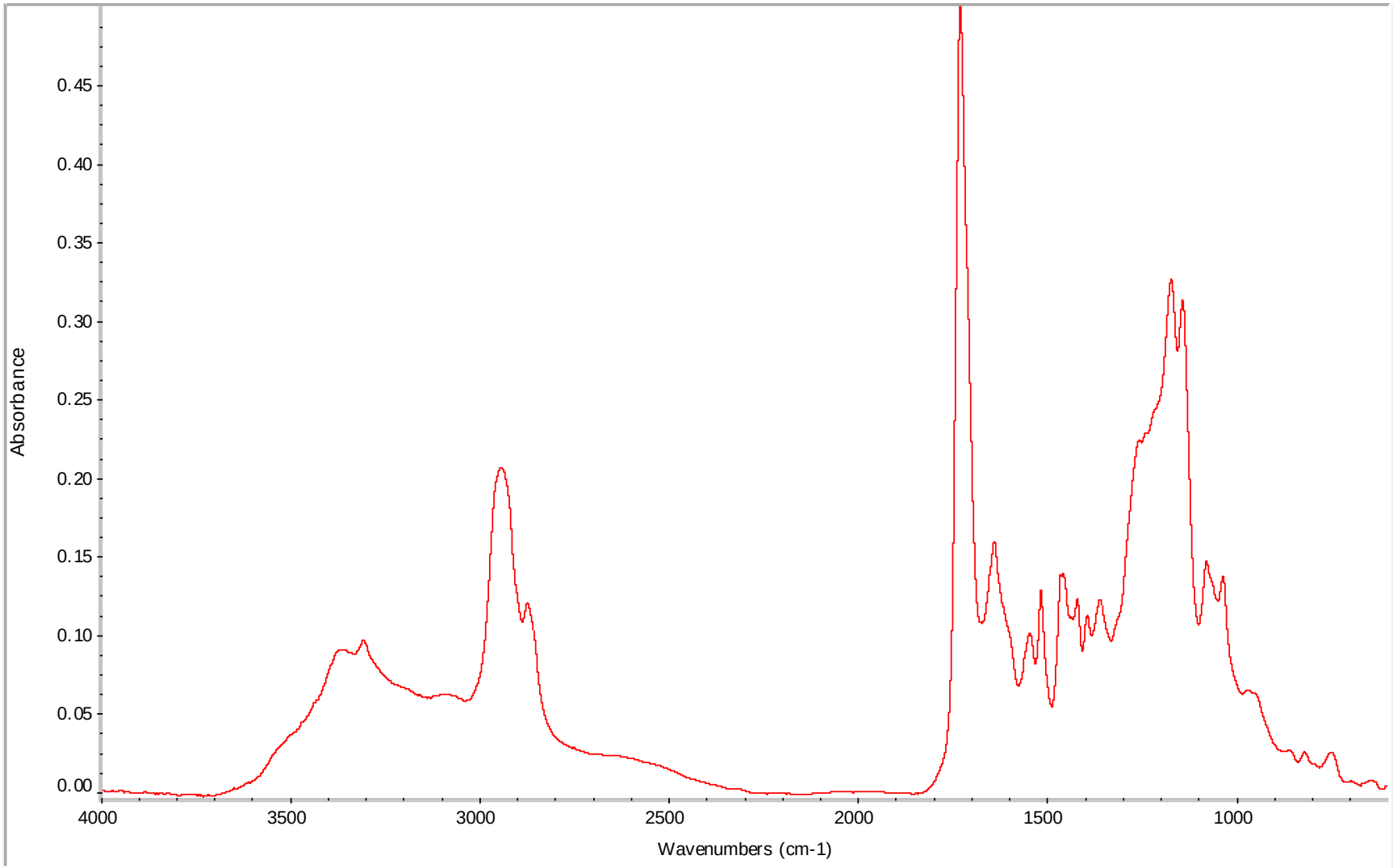

Figure 8.72 AA BD 0.8 17 hr copolymer FT-IR spectrum

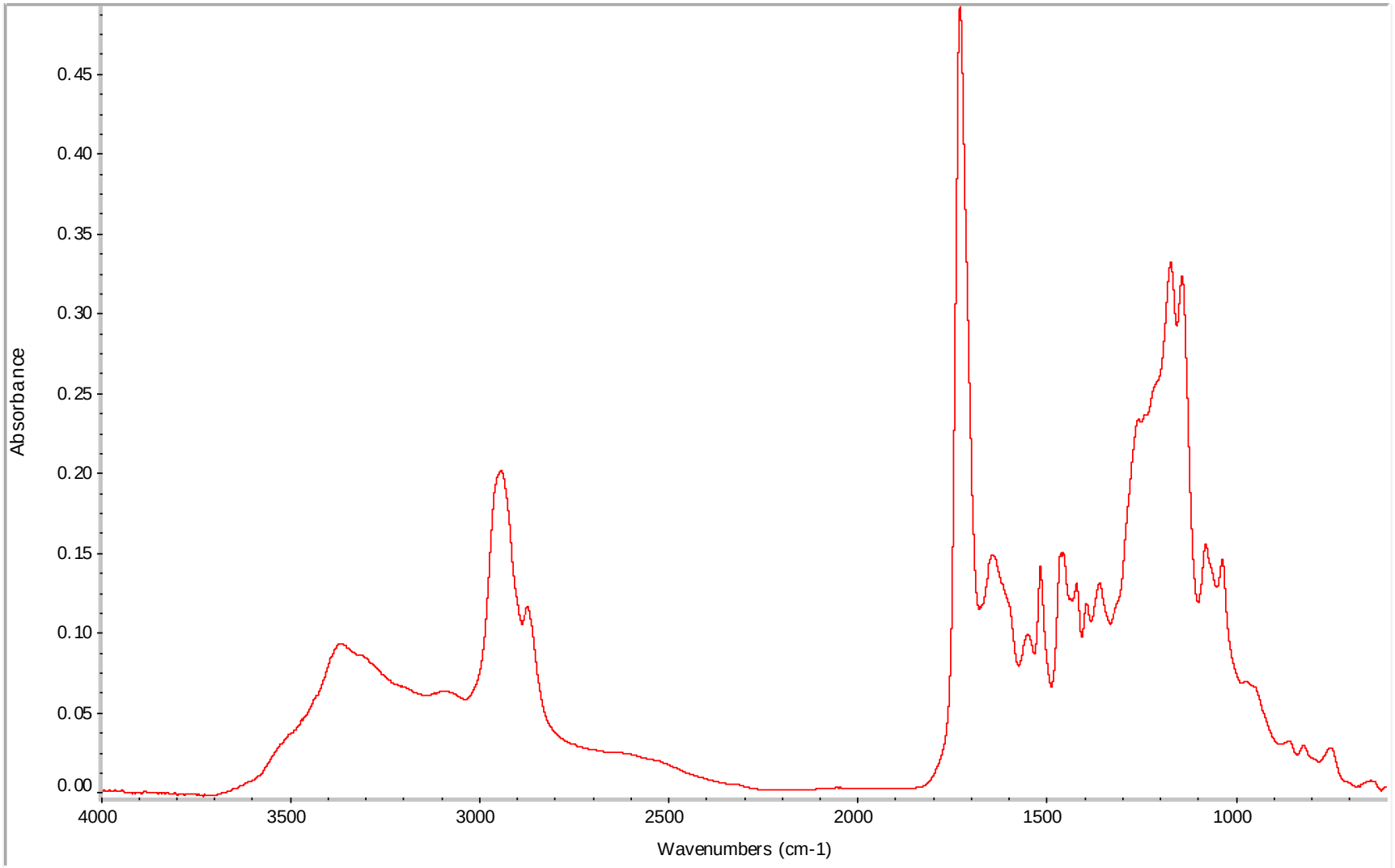

Figure 8.73 AA BD 0.8 24 hr copolymer FT-IR spectrum

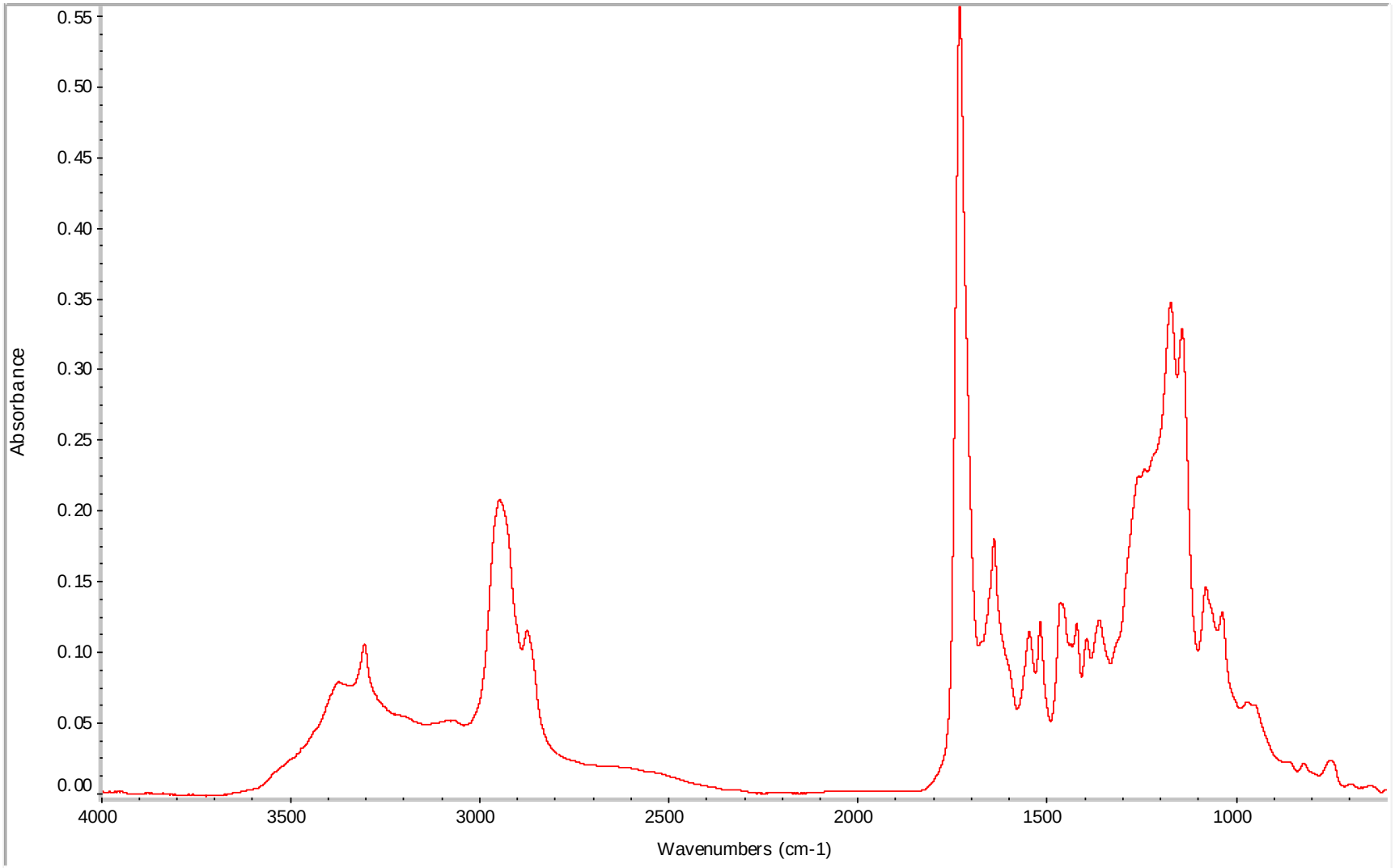

Figure 8.74 AA BD 0.8 42 hr copolymer FT-IR spectrum

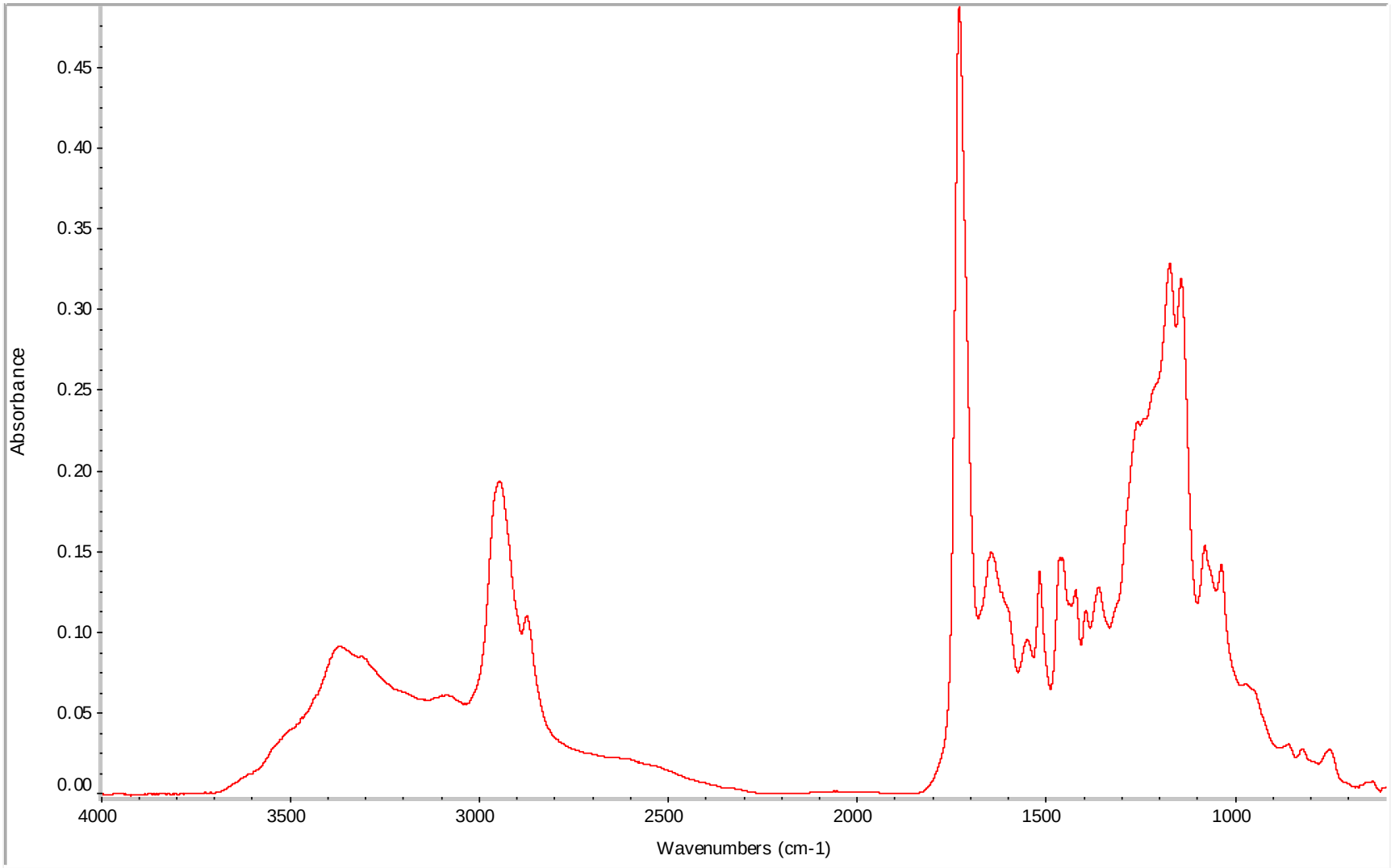

Figure 8.75 AA BD 0.8 48 hr copolymer FT-IR spectrum

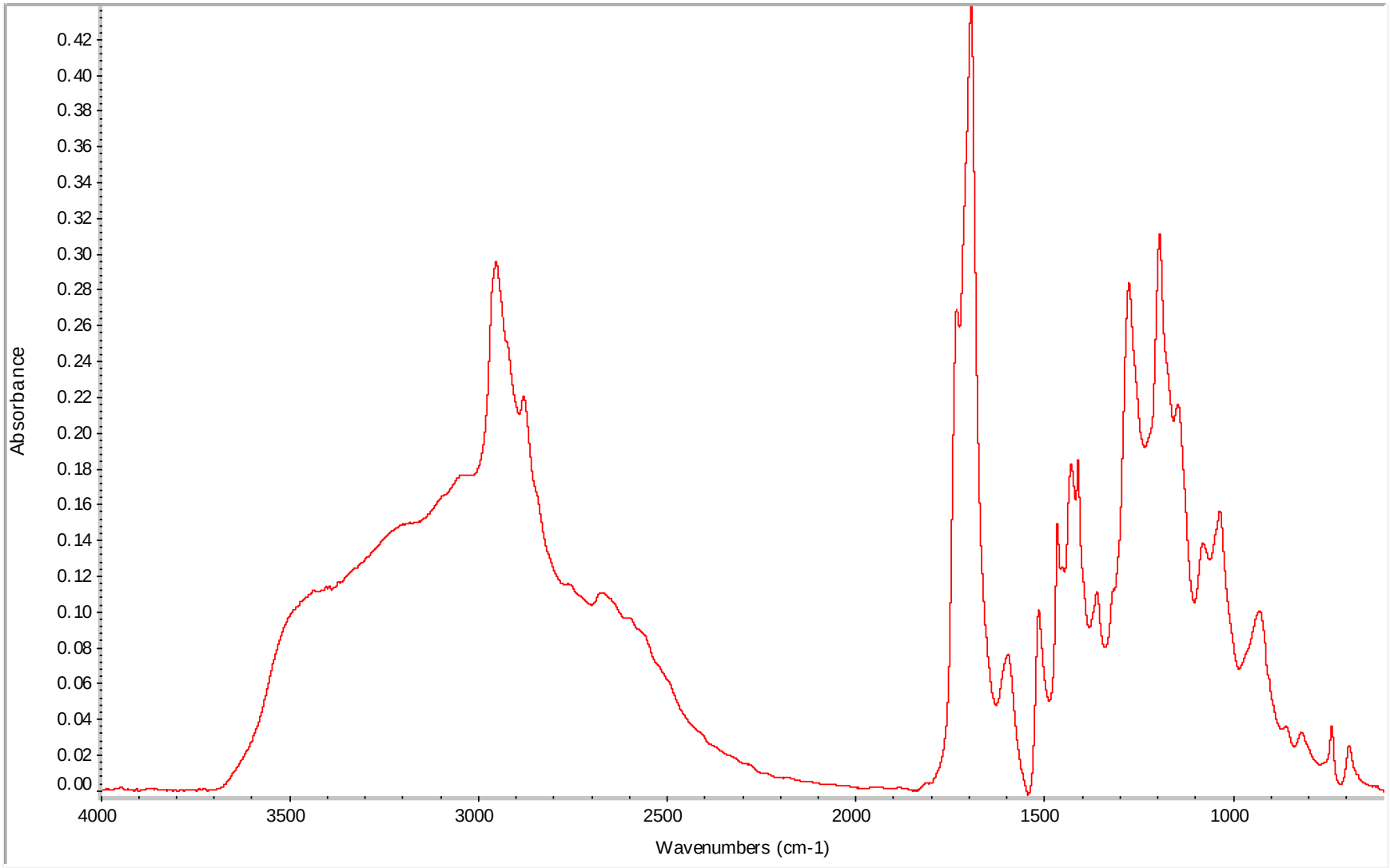

Figure 8.76 AA BD 1 3 hr copolymer FT-IR spectrum

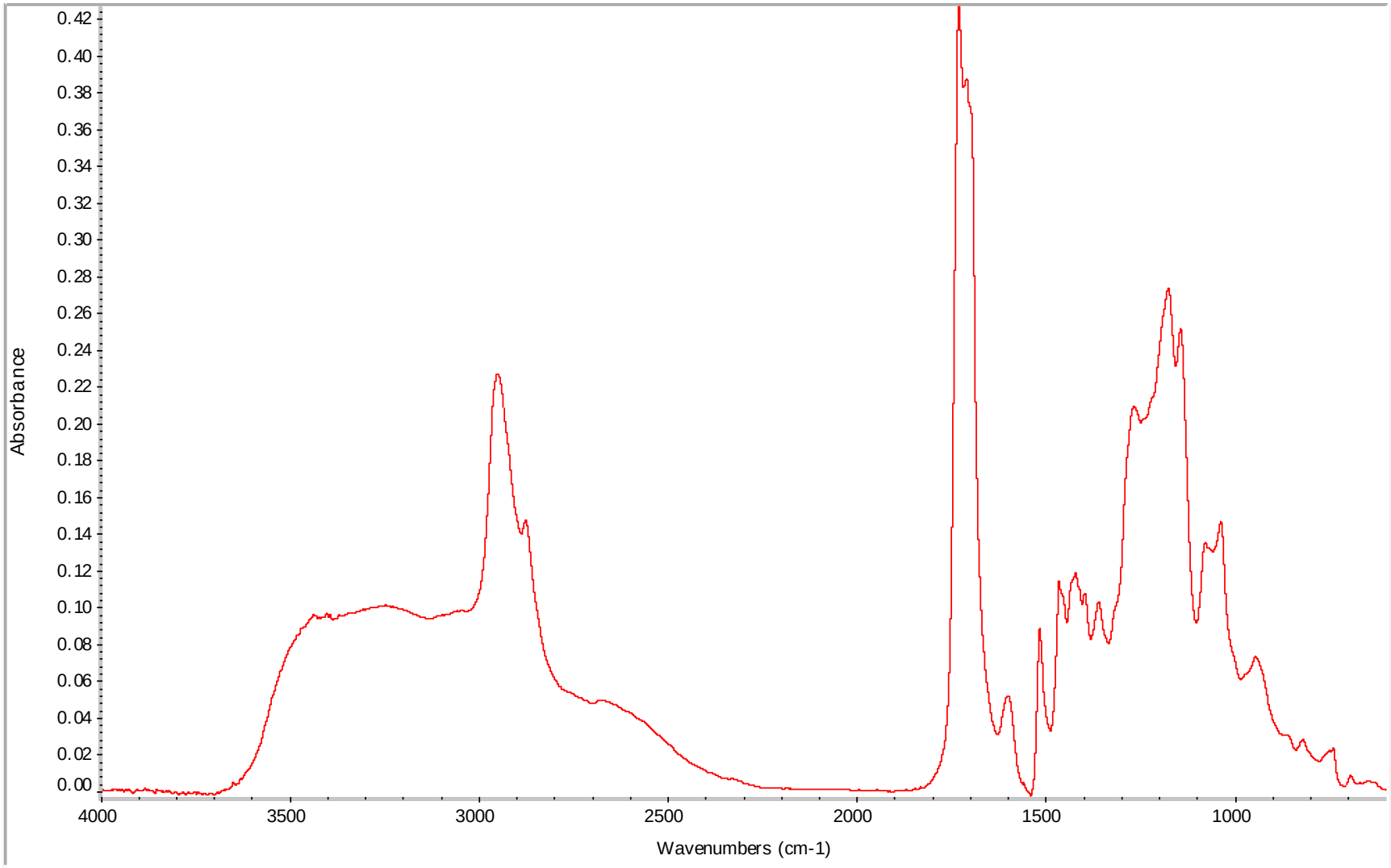

Figure 8.77 AA BD 1 4 hr copolymer FT-IR spectrum

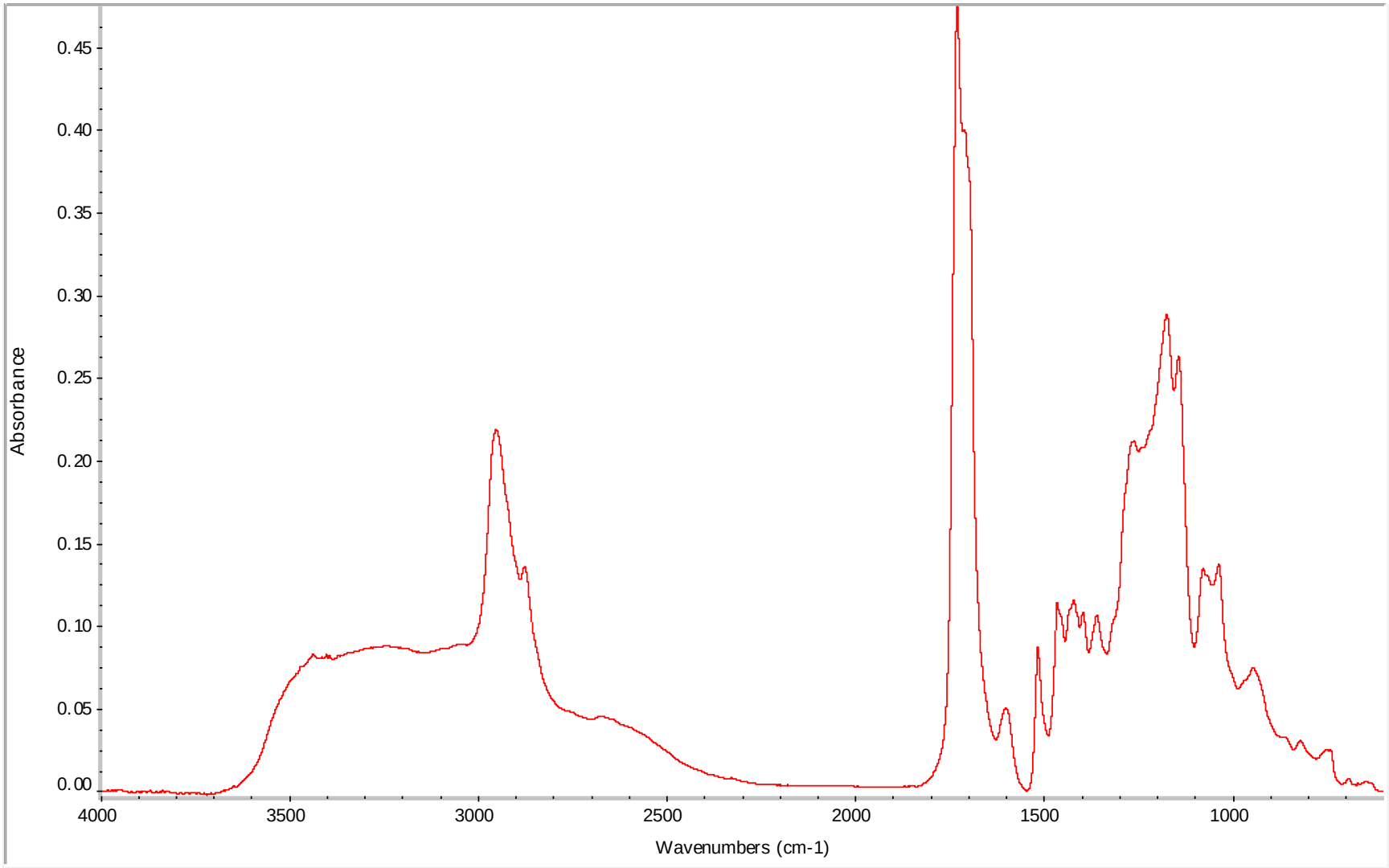

Figure 8.78 AA BD 1 5 hr copolymer FT-IR spectrum

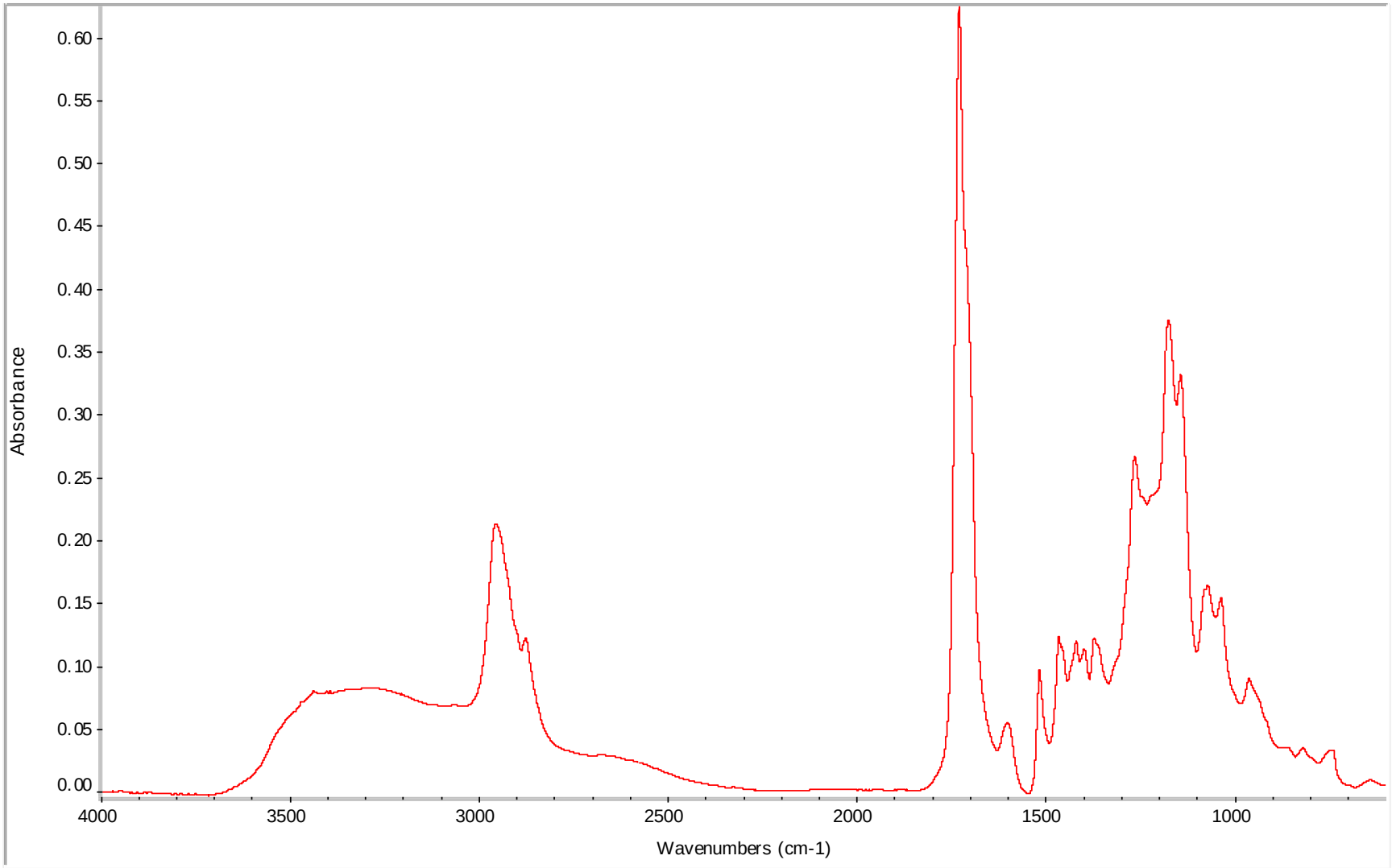

Figure 8.79 AA BD 1 8 hr copolymer FT-IR spectrum

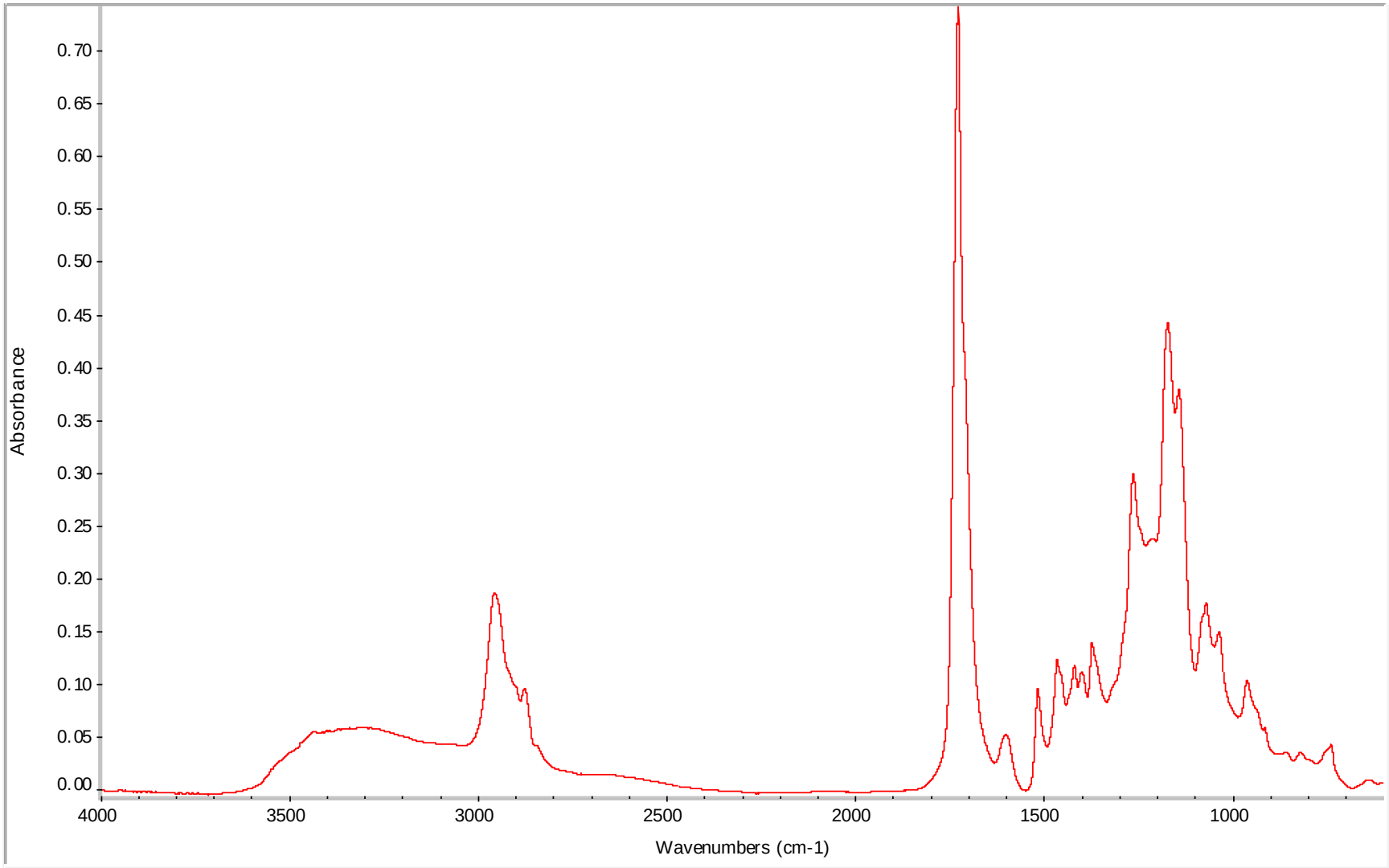

Figure 8.80 AA BD 1 17 hr copolymer FT-IR spectrum

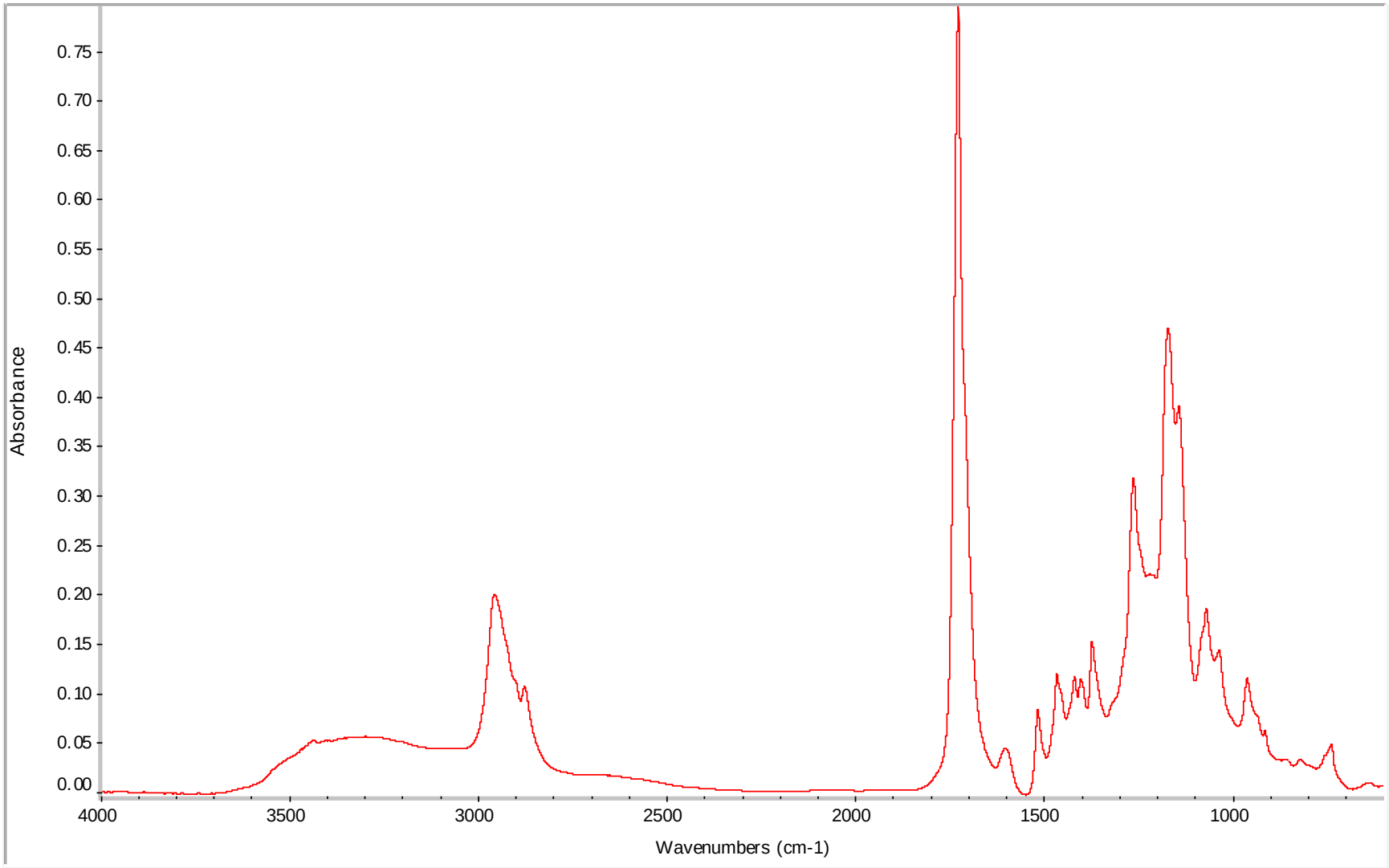

Figure 8.81 AA BD 1 24 hr copolymer FT-IR spectrum

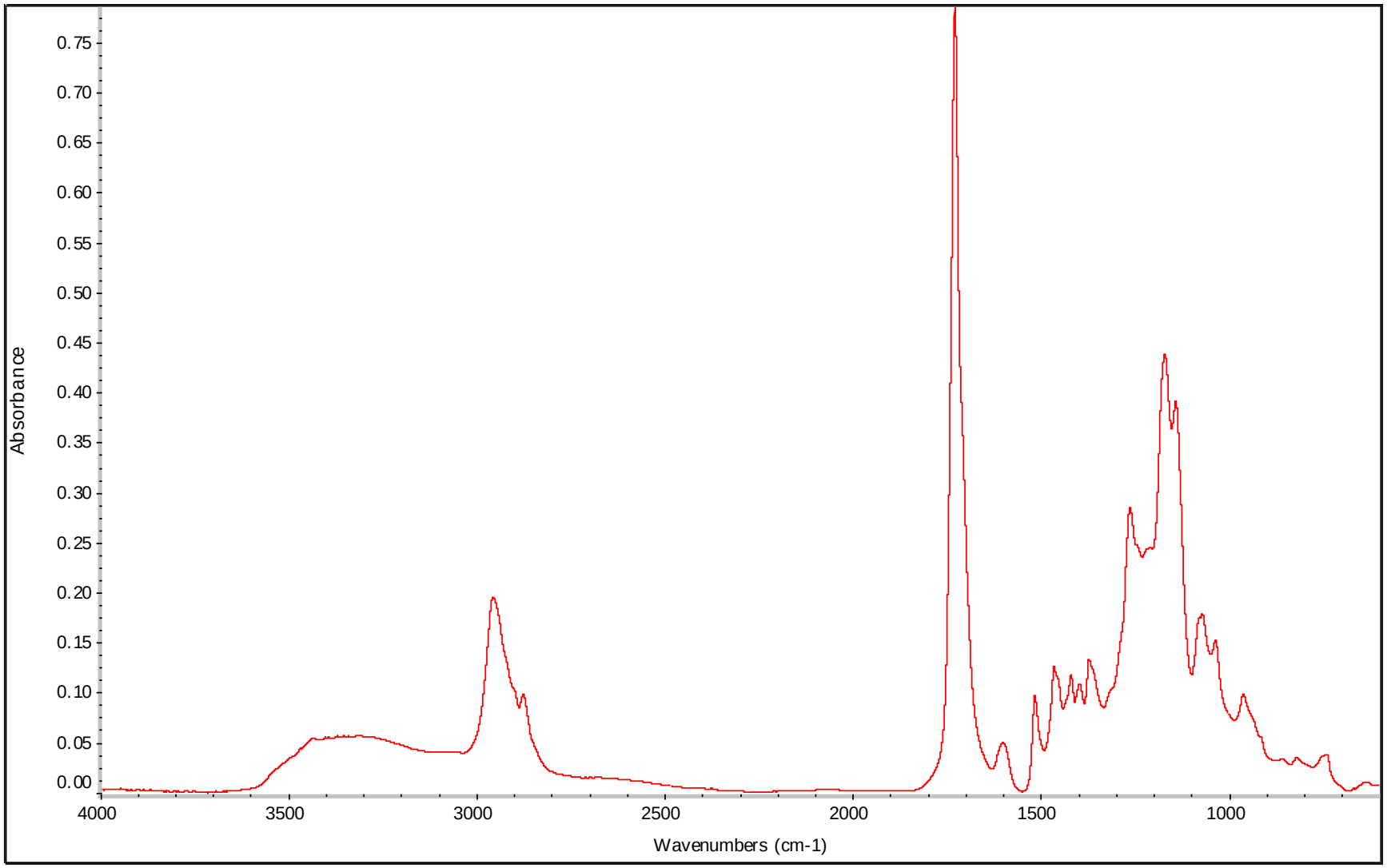

Figure 8.82 AA BD 1 42 hr copolymer FT-IR spectrum

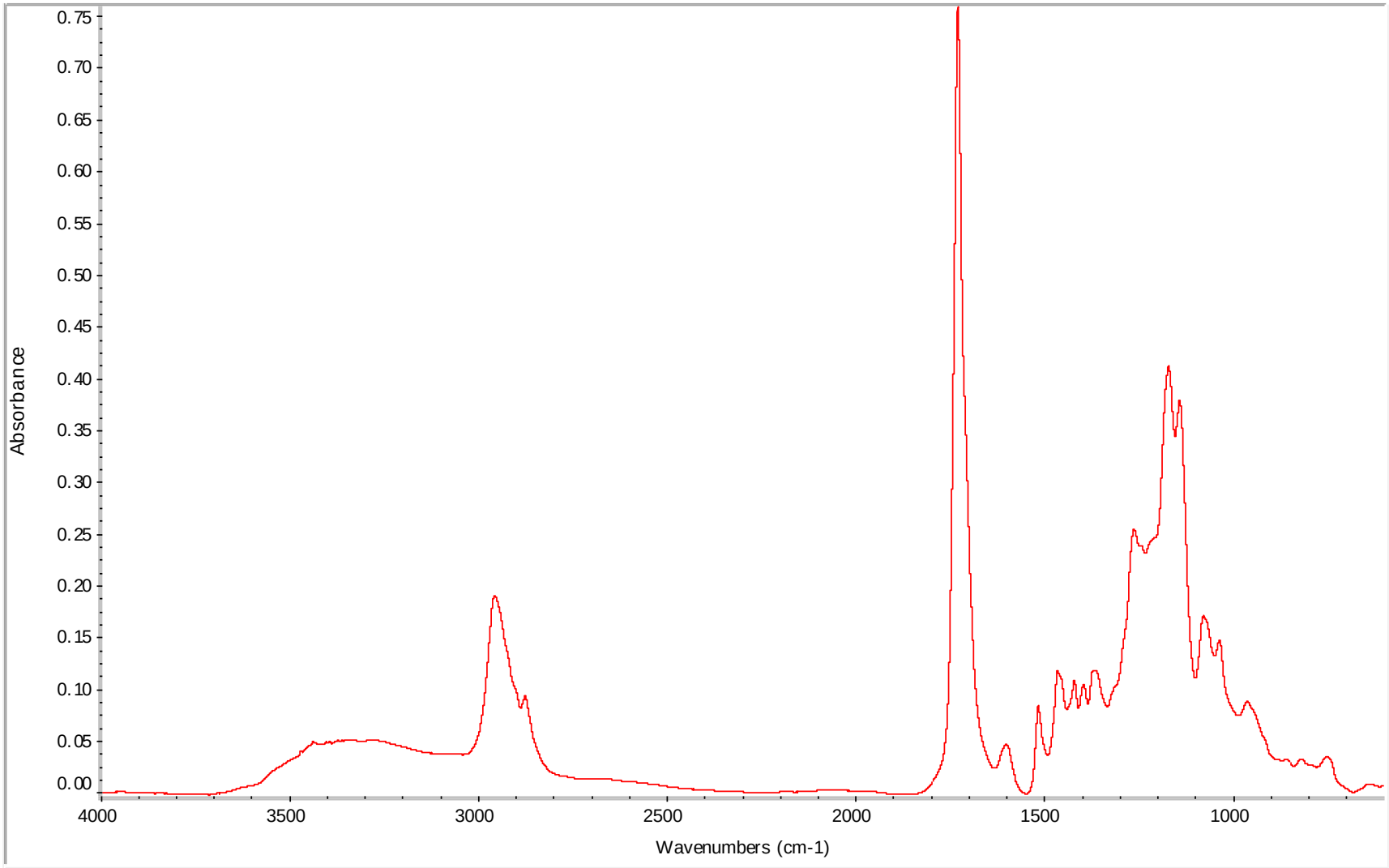

Figure 8.83 AA BD 1 48 hr copolymer FT-IR spectrum

Table 8.20 TGA T_{onset} of lignin copolymers

	AA			SA			SuA		
lignin wt%	BD 0.8	BD 0.9	BD 1	BD 0.8	BD 0.9	BD 1	BD 0.8	BD 0.9	BD 1
0%	323.07	355.15	274.33	278.71	287.89	290.19	305.36	330.35	248.5
10%	346.61	351.67	356.98	286.51	282.31	307.51	338.81	372.49	383.56
20%	336.55	350.69	361.3	306.36	316.33	316.61	340.06	355	377.75
30%	356.9	292.54	345.97	301.76	298.29	311.01	299.23	325.37	362.38
40%	340.84	345.66	366.26	282.98	298.48	312.23	316.46	341.33	354.71
50%	268.8	294.11	288.09	280.44	299.69	306.06	328.19	328.25	342.15

Table 8.21 TGA T_{d5} of lignin copolymers

	AA			SA			SuA		
lignin wt%	BD 0.8	BD 0.9	BD 1	BD 0.8	BD 0.9	BD 1	BD 0.8	BD 0.9	BD 1
0%	299.85	332.867	280.648	291.762	280.1	290.56	275.939	297.711	257.224
10%	323.813	310.848	330.345	282.734	303.191	324.018	314.174	328.199	334.491
20%	323.692	341.048	325.945	307.045	308.417	323.803	310.049	324.064	333.814
30%	321.959	295.86	348.4	291.735	302.798	320.596	276.901	300.706	355.002
40%	321.274	344.917	338.652	295.317	312.106	312.383	297.13	329.107	310.322
50%	272.663	313.208	326.725	292.291	310.517	292.951	322.125	316.311	343.046

Table 8.22 TGA T_{onset} of AA BD 1 copolymers w/ TSA catalyst

	AA BD 1 w/ TSA Catalyst		
	replicate 1	replicate 2	replicate 3
0%	306.97	270.37	315.33
10%	398.29	390.85	407.23
20%	395.62	414.8	407.96
30%	378.03	420.43	414.91
40%	393.35	403.89	414.49
50%	406.31	399.58	394.85

	TMA T_s AA BD 0.8				
	10%	20%	30%	40%	50%
1	35.47	33.60	-3.68	-4.39	44.05
2	35.74	28.99	12.26	3.18	44.22
3	36.15	36.06	-16.35	13.67	
4			-15.20		
5			-5.14		
average	35.79	32.88	-5.62	4.15	44.14
stdev	0.34	3.59	11.52	9.07	0.12

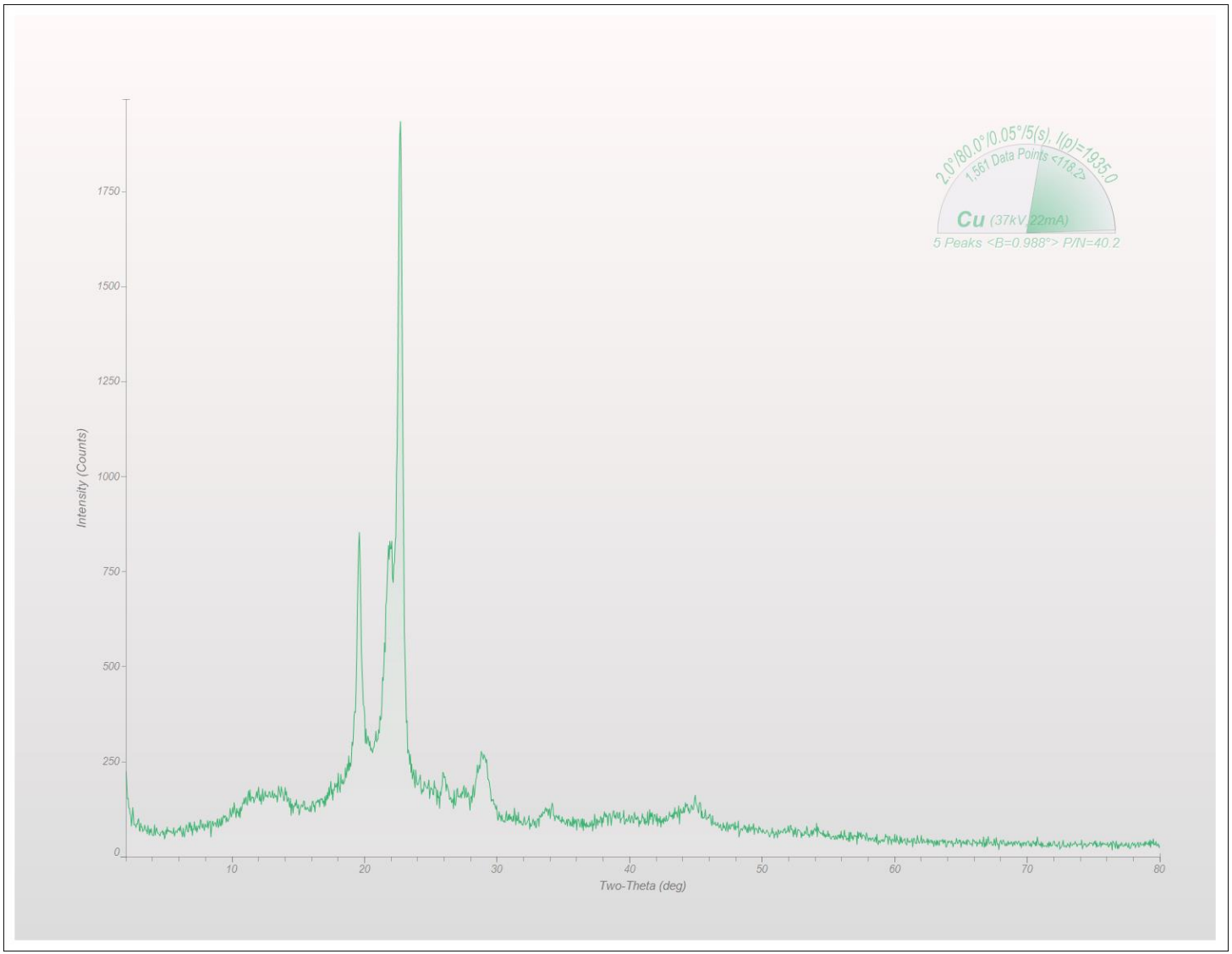

Figure 8.84 SA BD 1 0% lignin XRD diffractogram

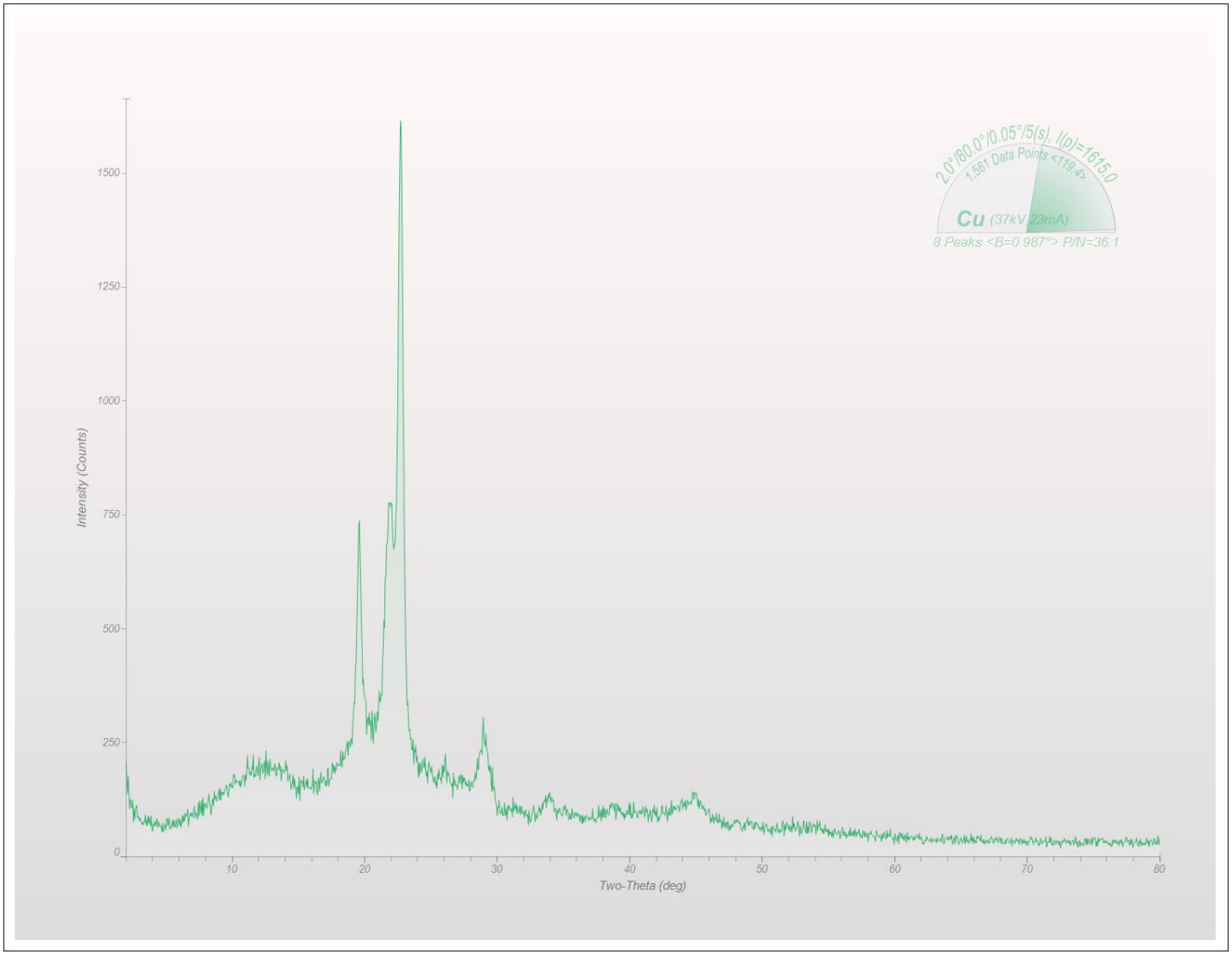

Figure 8.85 SA BD 1 10% lignin XRD diffractogram

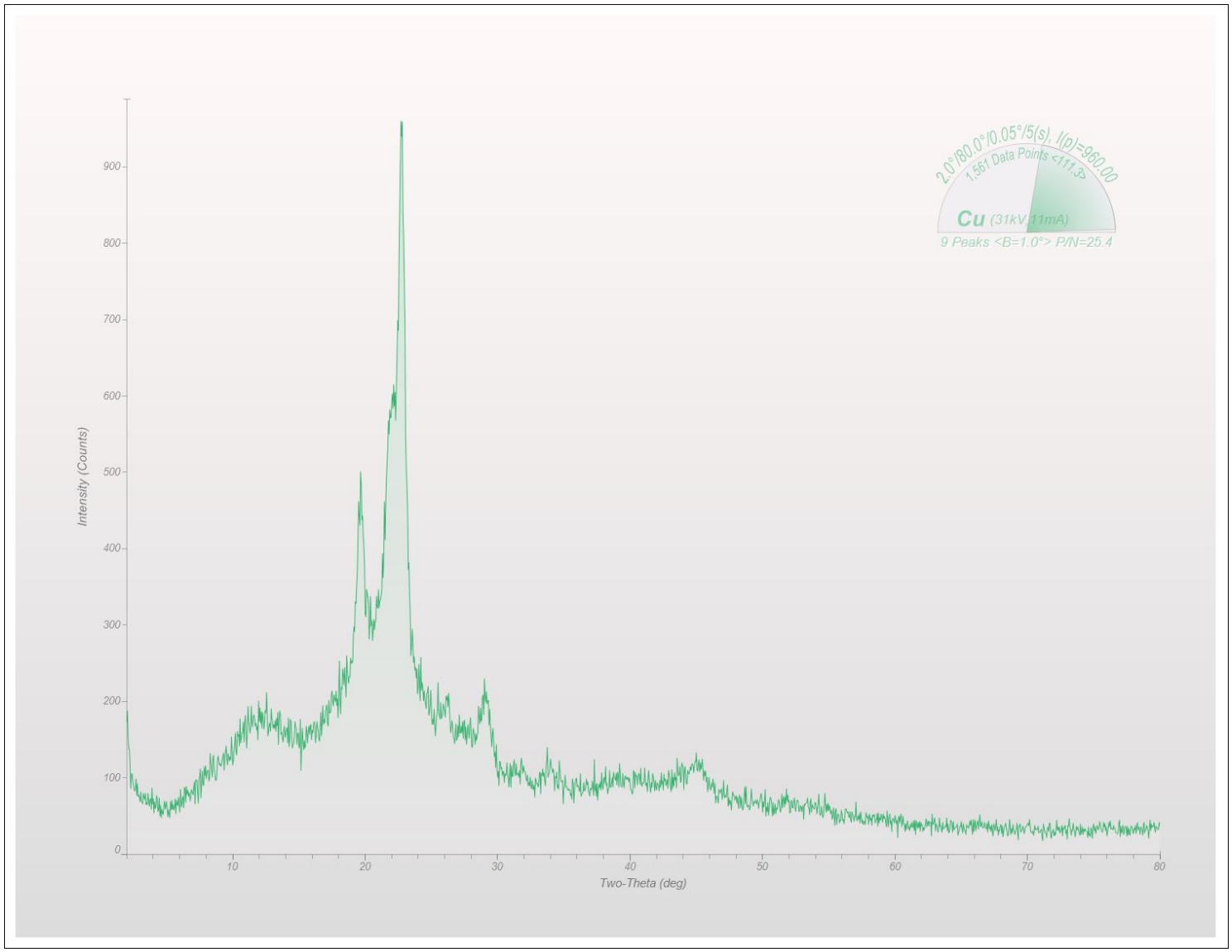

Figure 8.86 SA BD 1 20% lignin XRD diffractogram

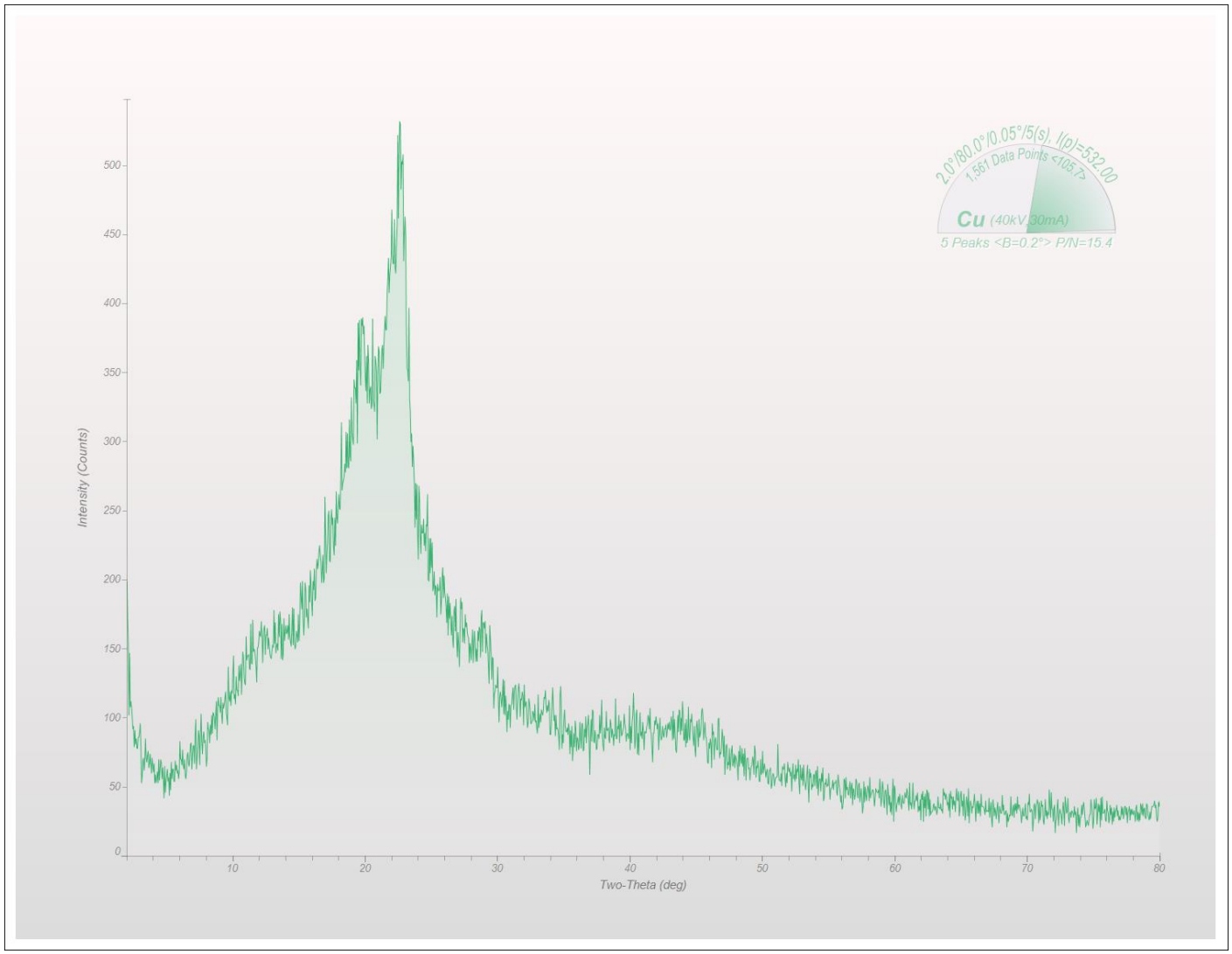

Figure 8.87 SA BD 1 30% lignin XRD diffractogram

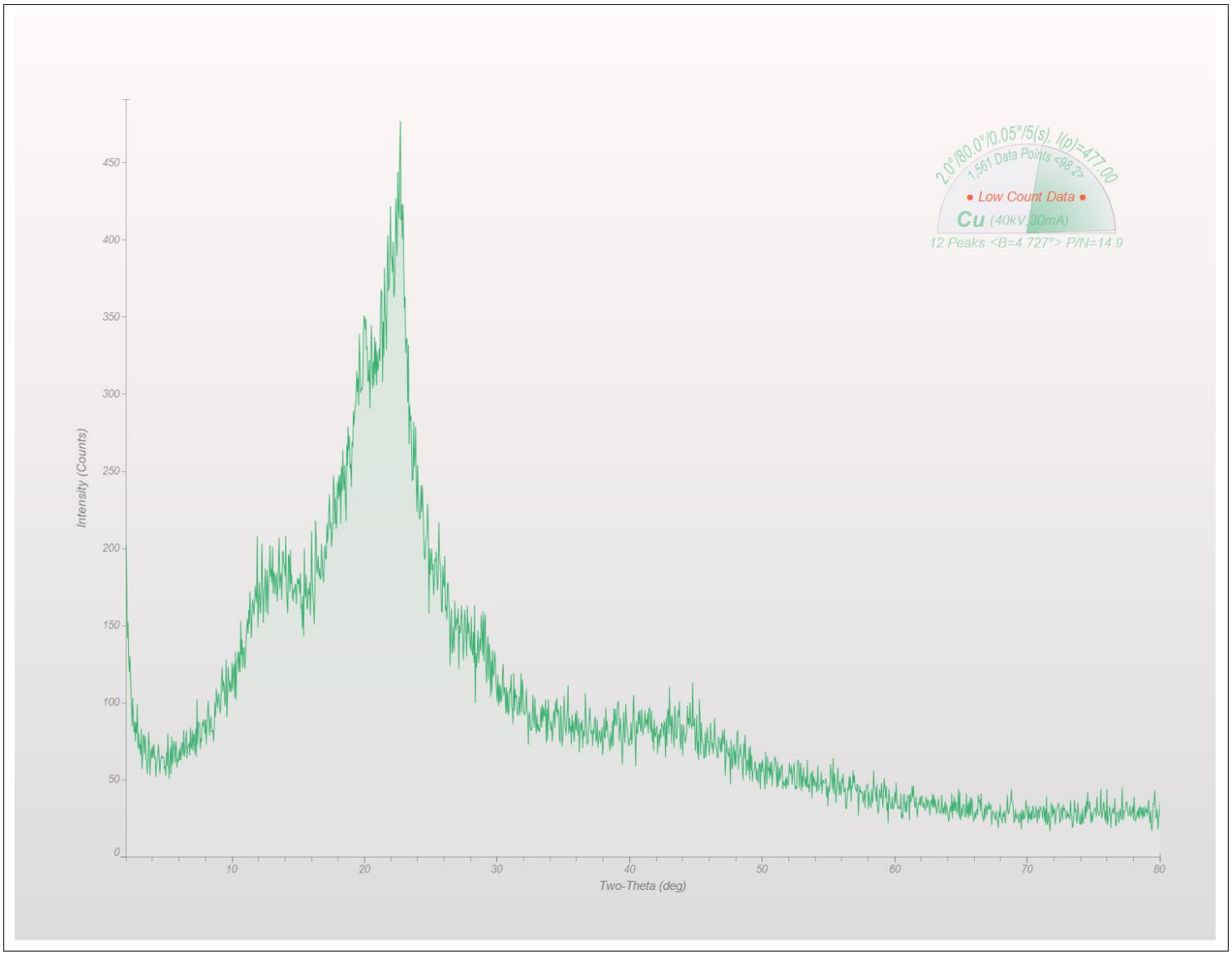

Figure 8.88 SA BD 1 40% lignin XRD diffractogram

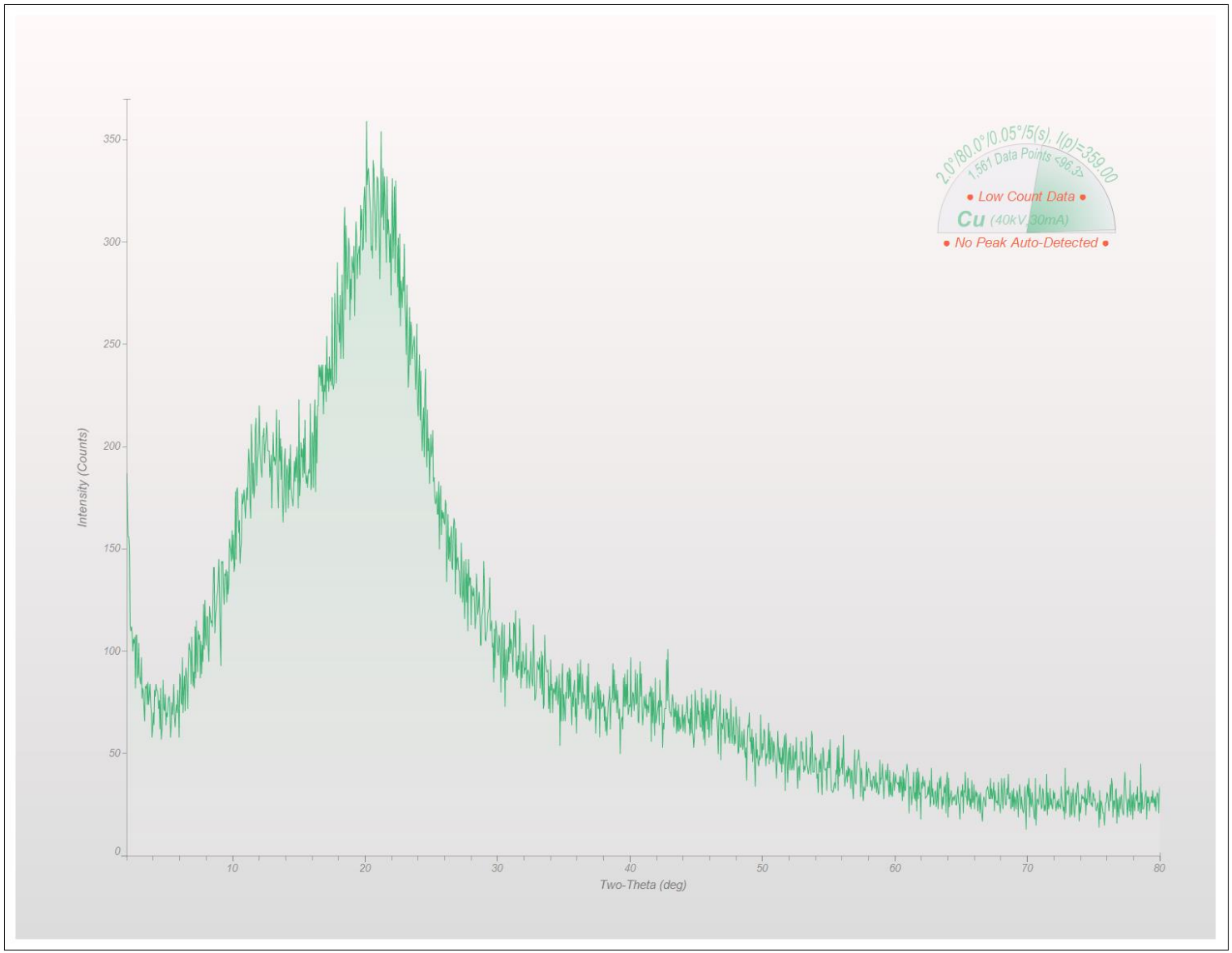

Figure 8.89 SA BD 1 50% lignin XRD diffractogram